



**RESEARCH & DEVELOPMENT**

# **Impact of quarry gradation and material properties on base course aggregate testing and rutting model calibration**

**Erol Tutumluer, PhD**

**Yong-Hoon Byun, PhD**

**Bin Feng**

**Issam Qamhia**

**Maziar Moaveni, PhD, PE**

**Department of Civil and Environmental Engineering  
University of Illinois at Urbana-Champaign**

**NCDOT Project 2015-23**

**FHWA/NC/2015-23**

**July 2018**



# ILLINOIS CENTER FOR TRANSPORTATION

CIVIL ENGINEERING STUDIES  
Illinois Center for Transportation Series No. 18-xxx  
UILU-ENG-2018-xxxx  
ISSN: xxx-xxxx

## **IMPACT OF QUARRY GRADATION AND MATERIAL PROPERTIES ON BASE COURSE AGGREGATE TESTING AND RUTTING MODEL CALIBRATION**

Prepared By

Erol Tutumluer  
Yong-Hoon Byun  
Bin Feng  
Issam Qamhia  
Maziar Moaveni

University of Illinois at Urbana-Champaign

Research Report ICT-18-xxx

Prepared for  
North Carolina Department of Transportation  
Contract / Agreement #2015-23  
/ UI Grant #B8488

Illinois Center for Transportation

July 2018

## Technical Report Documentation Page

1. Report No. <b>FHWA/NC/2015-23</b>	2. Government Accession No.	3. Recipient's Catalog No.	
4. Title and Subtitle <b>Impact of Quarry Gradation and Material Properties on Base Course Aggregate Testing and Rutting Model Calibration</b>		5. Report Date <b>July 2018</b>	
		6. Performing Organization Code	
7. Author(s) <b>Erol Tutumluer, Yong-Hoon Byun, Bin Feng, Issam Qamhia, and Maziar Moaveni</b>		8. Performing Organization Report No.	
9. Performing Organization Name and Address <b>Department of Civil and Environmental Engineering University of Illinois at Urbana-Champaign 205 North Mathews Avenue Urbana, IL 61801, USA</b>		10. Work Unit No. (TRAIS)	
		11. Contract or Grant No.	
12. Sponsoring Agency Name and Address <b>North Carolina Department of Transportation Research and Development Unit  104 Fayetteville Street Raleigh, North Carolina 27601</b>		13. Type of Report and Period Covered <b>Final Report May 2015 – March 2018</b>	
		14. Sponsoring Agency Code <b>2015-23</b>	
Supplementary Notes:			
16. Abstract This research effort, conducted at the Illinois Center for Transportation (ICT), evaluated the rutting potentials of unbound aggregate materials commonly used in the state of North Carolina (NC) for pavement subbase and base applications. Tests were conducted on different crushed aggregate materials at quarry source gradations to determine moisture-density, resilient modulus, shear strength and permanent deformation responses, and predict field rutting performances of base courses constructed with these materials. This study serves as a continuation of the Phase I study, which tested sixteen NC aggregate materials at one engineered gradation, and a pilot Phase II study, that tested four of those sixteen materials at the source gradations. The Phase I study successfully developed an improved rutting model (known as the University of Illinois at Urbana-Champaign rutting model or UIUC rutting model). The ability of the UIUC rutting model to accurately predict permanent strain accumulation at different gradations was investigated by evaluating the rutting performance of fifteen of the original materials at their source gradations. To accomplish the overall objective of re-evaluating the performance of the UIUC rutting model at different gradations, this study focused on: (1) performing modified Proctor type moisture-density and resilient modulus tests to establish maximum dry densities and optimum moisture contents as well as the resilient modulus response characterization, (2) conducting a full suite of shear strength and permanent deformation characterizations to determine the permanent deformation trends influenced by aggregate material properties, shear strength, applied stress states and stress to strength ratios, and (3) developing the UIUC rutting damage model for all the aggregate materials tested at both the engineered and source gradations. The final product of this project was a materials testing and characterization procedure to account for gradation and aggregate property effects in assigning the UIUC rutting damage model parameters in order to predict realistic rutting potentials of base course aggregate materials in NC. A comprehensive database was established for all 16 NC aggregate materials characterized at both original source and engineered gradations. The use of forced regression, to force the model parameters within specified pre-determined ranges, resulted in reasonable predictions of permanent strains for the aggregate materials at different gradations, while producing reasonably controlled values of the model parameters. Next, a stepwise regression approach was used to identify the most significant gradation and material properties which influenced the values of the UIUC rutting model parameters. The model parameters were then expressed as functions of these material properties. Finally, a practical design approach was recommended for the improved predictions of field pavement aggregate base rutting potentials using the UIUC rutting model.			
17. Key Words <i>Aggregate, Gradation, Permanent Deformation, Plastic Deformation, Triaxial Shear Tests, Shear Strength, Shear Stress Ratio, Rutting Model Development, Stepwise Regression Analysis, Constrained Regression Analysis</i>		18. Distribution Statement	
19. Security Classif. (of this report) Unclassified	20. Security Classif. (of this page) Unclassified	21. No. of Pages 78	22. Price

Form DOT F 1700.7 (8-72)

Reproduction of completed page authorized

## **ACKNOWLEDGEMENTS**

This publication is a deliverable of the Contract/Agreement #2015-23 and UI Grant #B8488 between North Carolina Department of Transportation and the University of Illinois. The research described in this publication was conducted at the Illinois Center for Transportation (ICT) with financial support provided by the North Carolina Department of Transportation (NCDOT).

Research team members would like to thank ICT staff, particularly James Meister, Aaron Coenen, Greg Renshaw, Michael A. Johnson and Marc Killion, for their assistance with the laboratory efforts at the Advanced Transportation Research and Engineering Laboratory (ATREL). Research team members also want to thank Dr. Judith B. Corley-Lay and Clark S. Morrison from the NCDOT for their cooperation and help with providing test data for this research study. Aggregate producers in North Carolina graciously provided the aggregate materials used in the experimental test matrix. Liang Chern Chow and Dr. Debakanta Mishra worked on the first phase of this project and contributed greatly to the development of the UIUC aggregate rutting model. Finally, the authors would like to thank the members and visiting scholars of the UIUC Transportation Geotechnics Research Group; namely, Hasan Kazmee, Pengcheng Wang, Ilhan Cetin, Scott Schmidt, Chao Fu, Jiayi Luo, for their assistance and contributions to various parts of the project. Lastly, thanks to Osman Erman Gungor for his help with developing the MATLAB code used for forced regression (optimization).

## **DISCLAIMER**

The contents of this report reflect the views of the authors and not necessarily the views of the University. The authors are responsible for the facts and the accuracy of the data presented herein. The contents do not necessarily reflect the official views or policies of either the North Carolina Department of Transportation or the Federal Highway Administration at the time of publication. This report does not constitute a standard, specification, or regulation.

Trademark or manufacturers' names appear in this report only because they are considered essential to the object of this document and do not constitute an endorsement of product by the Illinois Center for Transportation and the North Carolina Department of Transportation.

## EXECUTIVE SUMMARY

This research study aims to evaluate the rutting potentials of unbound aggregate materials commonly used in the state of North Carolina (NC) for pavement subbase and base applications. All the testing and characterization tasks completed by the University of Illinois research team were conducted at the Illinois Center for Transportation (ICT), which is housed in the Advanced Transportation Research and Engineering Laboratory (ATREL) facility. Tests were conducted on sixteen different crushed aggregate materials at their engineered and quarry source gradations to determine moisture-density, resilient modulus, shear strength and permanent deformation properties and predict field rutting performances of base courses constructed with these materials.

Although the first phase of the study documented in the final report by Chow et al. (2014) successfully developed an improved rutting model (known as the University of Illinois at Urbana-Champaign rutting model or UIUC rutting model), all test results used in model development and the corresponding rutting model parameters were obtained for an engineered gradation used for the sixteen aggregate materials. The ability of the UIUC rutting model to accurately predict permanent strain accumulation at different gradations was not studied during the first phase. This is particularly important as aggregate materials used for constructing pavement base and subbase layers are usually placed at their respective source gradations. Thus, the main goal of the current study including the results reported in a pilot study (Phase II) was to re-evaluate the performance of the newly developed rutting model at different aggregate source gradations. Accordingly, fifteen of the original sixteen aggregate materials, obtained from quarries in North Carolina, were also tested at the source gradations.

To accomplish the overall objective of re-evaluating the performance of the UIUC rutting model at different gradations, this study focused on: (1) performing modified Proctor type moisture-density and resilient modulus tests to establish maximum dry densities and optimum moisture contents as well as the resilient modulus response characterization, (2) conducting a full suite of shear strength and permanent deformation characterizations to determine the permanent deformation trends influenced by aggregate material properties, shear strength, applied stress states and stress to strength ratios, and finally, (3) developing the UIUC rutting damage model for all the aggregate materials tested at both the engineered and source gradations. The final product of this project includes a materials testing and characterization procedure to account for gradation and aggregate property effects in assigning the UIUC rutting damage model parameters for predicting realistic rutting potentials of base course aggregate materials in North Carolina.

Mohr-Coulomb failure envelopes were established for each tested material, and the concept of Shear Stress Ratio (SSR) was used to evaluate the permanent deformation behavior at different stress states. Rutting model parameters established from the laboratory data at the source gradations were compared with those established at the engineered gradations in the 'Phase I' study to assess their sensitivities to gradation and other material property changes. Clearly, the permanent deformation responses of the aggregate materials correlated better with shear strength than the resilient modulus properties. For all the sixteen aggregate materials tested at both

engineered and source gradations, the accumulated permanent strains were found to steadily increase with applied stress levels and SSR in a linear fashion.

The main goal of this Phase III study was to highlight the significant effects of gradation and other material properties on the performances of the sixteen NC aggregate materials by comparing their shear strength and repeated load triaxial test results at the source and engineered gradations. Generally, the permanent deformations at the source gradations (SG) were different from those at the engineered gradation (EG). Since permanent strain accumulation between SG and EG could not be distinguished by a sole variable, variations in the permanent deformation behavior between EG and SG specimens can result from the combined effects of gradation and material properties as well as the achieved densities and moisture contents of as-constructed unbound aggregate layers. When plastic fines existed in the aggregate gradation, the permanent deformation potential was drastically higher; for example, plastic fines (i.e., plasticity Index or PI = 6) produced undesirable high permanent deformations for one of the aggregate materials. The effects of gradation on aggregate permanent deformation behavior was more significant as the applied stress levels approached the corresponding shear strength values of the materials.

Based on the findings of current study, a comprehensive database was established for all the 16 NC aggregate materials characterized at both original source and engineered gradations and a practical design approach was recommended for the improved prediction of aggregate base rutting potentials using the developed UIUC rutting damage model. The UIUC model considers new performance based specifications including strength criteria for unbound aggregate layers. The use of forced regression to force the model parameters within specified pre-determined ranges was shown to result in reasonable predictions of permanent strains for the aggregate materials at different gradations, while producing reasonably controlled values of the model parameters that do not vary widely and can be assigned as a function of applied stress and strength variables and material properties. The forced regression results and the correlations of model parameters properly established with material properties following a stepwise regression approach are presented in this report. Finally, a methodology is presented on how to determine the UIUC rutting model parameters from aggregate gradation, compaction, shear strength and image-based shape properties through different sets of developed regression equations. This simple methodology can be implemented to determine field rutting damage potentials of unbound aggregate layers through the use of the UIUC rutting damage model in mechanistic based flexible pavement design and hence correct rutting damage computations currently generated by the Pavement ME software.

## Table of Contents

EXECUTIVE SUMMARY .....	v
CHAPTER 1: INTRODUCTION .....	1
1.1 General Overview .....	1
1.2 Recent NCDOT Project Accomplishments.....	2
1.3 Purpose and Objectives .....	4
1.4 Report Organization .....	5
CHAPTER 2: LITERATURE REVIEW .....	7
2.1 Introduction .....	7
2.2 Factors Influencing Permanent Deformation in Unbound Layers .....	7
2.3 Available Permanent Deformation Predictive Models.....	8
CHAPTER 3: MATERIALS AND LABORATORY TESTS.....	10
3.1 Introduction .....	10
3.2 Materials Description .....	10
3.3 Laboratory Characterization and Testing.....	11
3.3.1 Grain Size Distribution.....	11
3.3.2 Atterberg Limits .....	12
3.3.3 Moisture-Density Relationships .....	12
3.3.4 Imaging Based Properties (Shape, Angularity, and Surface Texture).....	13
3.3.5 Triaxial Shear Strength Testing.....	14
3.3.6 Repeated Load Triaxial Testing for Permanent Deformation .....	16
3.3.7 Resilient Modulus Testing.....	18
CHAPTER 4: TEST RESULTS .....	19
4.1 Introduction .....	19
4.2: Results from Laboratory Testing and Characterization .....	19
4.2.1 Grain Size Distribution.....	19
4.2.2 Moisture-Density Relationship.....	20
4.2.3 Imaging Based Properties (Shape, Angularity and Surface Texture).....	22
4.2.4 Triaxial Shear Strength Testing.....	24
4.2.5 Repeated Load Triaxial Testing for Permanent Deformation .....	28
4.2.6 Resilient Modulus Testing.....	35
CHAPTER 5: UIUC PERMANENT DEFORMATION MODEL.....	37

5.1 Introduction .....	37
5.2 UIUC Rutting Model Results .....	38
5.3 Recommended Aggregate Base Design using the UIUC Rutting Model .....	42
5.4 Forced Regression (Optimization) Results for UIUC Model Parameters .....	50
5.5 Stepwise Regression Results for UIUC Model Parameters .....	54
CHAPTER 6: SUMMARY AND CONCLUSIONS .....	70
6.1 Effects of Gradation on Shear Strength and Permanent Deformation Properties .....	71
6.3 Recommendations for Future Research .....	74
REFERENCES .....	75
APPENDIX A Sieve Analysis Results .....	79
APPENDIX B Moisture-Density and CBR Test Results .....	87
APPENDIX C Monotonic Shear Strength Test Results .....	95
APPENDIX D Repeated Load Permanent Deformation Test Results .....	103
APPENDIX E Resilient Modulus Test Results .....	111
APPENDIX F Material Properties for Stepwise Regression Analysis .....	122
APPENDIX G Comparison of Forced and Stepwise Regression Results .....	124
APPENDIX H Permanent Deformation Predictions with Forced Regression and Stepwise Regression (Excluding Goldhill) .....	125

# CHAPTER 1: INTRODUCTION

## 1.1 General Overview

Rutting or accumulation of permanent deformation is the primary damage/distress mechanism of unbound granular base/subbase layers in pavements. Accordingly, rutting resistance is a major performance measure for designing pavements with granular base/subbase layers. Granular base/subbase permanent deformation may contribute significantly to the overall flexible pavement surface ruts. Low strength granular materials are generally more susceptible to undesirable permanent deformation accumulation. A properly compacted good quality aggregate base and subbase, on the other hand, adequately prevents settlement and any lateral movement in the layer through high shearing resistance and contributes significantly to dissipation of wheel load stresses. Indeed, the NCHRP 4-23 study identified shear strength of unbound aggregates as one of the most significant mechanistic properties influencing pavement performance (Saeed et al. 2001). Moreover, shear strength property rather than resilient modulus ( $M_R$ ) was shown to better correlate with unbound aggregate permanent deformation behavior for predicting field rutting performance (Thompson 1998; Tao et al. 2010; Xiao et al. 2012).

The influence of stress state on  $M_R$  of unbound materials is well known (e.g., Hicks and Monismith 1971; Rada and Witczak 1981; Thompson and Elliott 1985; Uzan 1985). Increased confining stress can substantially increase the resilient modulus of unbound pavement materials, particularly for coarse grained granular base materials, while increased shear stress can substantially decrease the resilient modulus, particularly for fine grained subgrade soils. The incorporation of stress state influences on the resilient modulus of unbound granular base and subbase layers was explicitly included in the AASHTO's empirical pavement design procedure beginning in 1986.

Although the influence of stress state on unbound resilient modulus is relatively well understood, its influence on the actual performance (rutting, cracking, roughness) of flexible pavements has not been thoroughly investigated. The design domains in which the influence of stress state is significant are also poorly defined. This issue has taken on more significance with the release of the AASHTO's Pavement ME Design Guide implementation of the mechanistic-empirical (M-E) pavement design procedure. Whereas the earlier implementation of the M-E pavement design procedure in the public domain MEDPG software explicitly included stress dependency of unbound resilient moduli as Level 1 inputs, this capability was removed from the AASHTO Pavement ME software implementation. This is arguably a step backwards for the pavement design profession.

Road pavements in North Carolina (NC) have a long history of good performance of unbound base courses often constructed with granite type aggregate materials. The new AASHTO mechanistic-empirical (M-E) pavement design guide Pavement ME software does not credit the contribution of the unbound aggregate base sufficiently for it to be cost competitive. To properly account for

aggregate quality impacting performance of pavements with unbound aggregate bases, the first challenge is to be able to incorporate aggregate shear strength or rutting potential into materials characterization through the inputs required by M-E design procedures such as Pavement ME.

## **1.2 Recent NCDOT Project Accomplishments**

Recent North Carolina Department of Transportation (NCDOT) research project, entitled, “Base Course Aggregate Testing and Rutting Model Calibration,” by Chow et al. (2014), herein referred to as Phase I study, was aimed at evaluating rutting potentials of unbound aggregate materials commonly used in the state of North Carolina (NC) for pavement subbase/base construction. Shear strength and permanent deformation tests were conducted at the University of Illinois on sixteen different crushed aggregate materials to predict field rutting performances of base courses constructed with these materials. The original intent was to properly factor them into M-E pavement design approaches such as the MEPDG or AASHTO’s Pavement ME Design procedure through calibration of the rutting damage models built into the design procedure based on the work of Tseng and Lytton (1989). To accomplish the overall objective, the project specific goals linked to the proposed tasks were as follows: (1) identify and select local base course aggregates from quarries in NC, (2) conduct triaxial monotonic shear strength and repeated load permanent deformation tests, (3) investigate the effects of shear strength, applied stress states and material properties on plastic shakedown behavior of the aggregate materials to determine the most damaging field loading conditions through permanent deformation testing, (4) based on the newly established laboratory database, calibrate the rutting damage model used in the MEPDG or Pavement ME Design software, or propose new improved rutting prediction models, and finally, (5) prepare a set of recommendations for developing new performance-based specifications including strength criteria for these unbound aggregate layers.

The laboratory phase considered a target engineered gradation within the lower and upper limits of NCDOT dense-graded base course specification bands; laboratory-established compaction curves for the sixteen aggregate materials were used to prepare specimens for shear strength and permanent deformation testing. The complete suite of laboratory characterization tests included imaging-based aggregate particle shape analyses, moisture-density tests, resilient modulus, shear strength, and permanent deformation tests. The concept Shear Strength Ratio (SSR), defined as the ratio between the wheel load applied shear stress and the material’s shear strength (or stress/strength), was introduced based on the shear strength test results, and later on used to properly examine the effects of varying proportions of stress/strength on the permanent deformation behavior of unbound materials. Clearly, the permanent deformation responses of the aggregate materials correlated better to shear strength than the resilient modulus properties. The accumulated permanent strains were found to steadily increase with applied stress levels in a linear fashion. When plastic fines existed in the aggregate gradation, the permanent deformation potential was drastically higher. Since all aggregate materials were quarry crushed, no clear trends were

observed between the imaging based aggregate shape, texture and angularity properties and the permanent deformation behavior.

The experimental results established a consistent database to investigate the permanent deformation trends influenced by aggregate material properties, shear strength, applied stress states and stress/strength ratios, and to develop a new University of Illinois at Urbana-Champaign (UIUC) rutting model. Case studies compared the model predictions with those from the MEPDG or Pavement ME Design procedure and evaluated the adequacy of the proposed model. Based on the findings, a practical design approach was recommended for better prediction of aggregate base rutting potentials.

Recognizing the need to investigate impact of quarry gradation and material properties on base course aggregate rutting behavior for the developed UIUC rutting model calibration, a pilot (Phase II) study first selected four of the sixteen NC aggregate materials at source properties; these were Fountain, Nash, Rougemont and Goldhill quarry materials. Tests were conducted on these four crushed aggregate materials at their quarry source gradations to investigate the significant effect of gradation on permanent deformation behavior by comparing their shear strength and repeated load triaxial test results at the source and engineered gradations. Based on the study findings, a practical design approach was recommended for the improved prediction of aggregate base rutting potentials. Additionally, the use of forced regression to force the model parameters within specified pre-determined ranges was shown to result in reasonable predictions of permanent strains for the aggregate materials at different gradations, while producing reasonably controlled values of the model parameters that do not vary widely and can be assigned as a function of applied stress and strength variables and material properties.

Preliminary good results on forced regression analyses and model parameter variations with material properties clearly substantiated the need to test the other 12 aggregate materials from the Phase I engineered gradation study at their source properties. Accordingly, the current scope focused on evaluating moisture-density, shear strength and resilient modulus characteristics and the rutting potentials of the other 12 NC aggregate sources, specifically Arrowood, Belgrade, Franklin, Hendersonville, Jamestown, Lemon Spring, Moncure, North Wilkesboro, Princeton, Raleigh, Rockingham, and Rocky Point quarry materials, at their original quarry or source gradations. Note that the amount of aggregate material from Franklin quarry was not sufficient to conduct the suite of tests at the source gradation. It was found that Franklin quarry operations had shifted to a new location, a new aggregate source being mined had a different geology; i.e., different specific gravity and aggregate properties, and furthermore, there was also a change of crushers used at the Franklin quarry locations and the neighboring quarries. Accordingly, it was decided not to conduct tests on a new material from Franklin quarry. The new aggregate material would provide bad data in the project database since it would not meet any of the parameters established for the original Franklin material. Therefore, altogether the original 15 materials, except from Franklin quarry, were studied at their source properties.

### 1.3 Purpose and Objectives

Road pavements in North Carolina (NC) have a long history of good performance of unbound base courses often constructed with good quality aggregate materials. However, the new AASHTO mechanistic-empirical (M-E) pavement design guide Pavement ME software does not credit the contribution of the unbound aggregate base sufficiently for it to be cost competitive. To properly quantify performance trends of unbound aggregate base courses in flexible pavements constructed in NC, the researchers aimed to complete an extensive suite of shear strength and permanent deformation tests on fifteen different quarry materials at the original quarry gradations including the four quarry materials reported in the Phase II study. Among the properties determined were gradation, aggregate angularity, fines content, plasticity index (PI), and moisture-density characteristics. The ultimate goal was to prepare a set of recommendations for developing new performance based rutting evaluations including strength criteria and the proper assignment of the UIUC model parameters for these unbound aggregate layers.

The research scope included four main tasks as follows:

- Task 1: Conduct modified Proctor type moisture-density and resilient modulus tests to establish optimum moisture contents and resilient modulus response characterizations, respectively.
- Task 2: Conduct shear strength and permanent deformation tests to determine the permanent deformation trends influenced by aggregate material source properties, shear strength, applied stress states and stress/strength ratios.
- Task 3: In accordance with the laboratory findings, develop the corresponding UIUC rutting damage models for the fifteen aggregate materials so that gradation and material property effects on the model parameters can be identified for predicting realistic rutting potentials of NCDOT base course aggregate materials and accordingly, correcting rutting damage computations by Pavement ME software.
- Task 4: Provide a final report to include all of the research findings. The laboratory study will develop a comprehensive database for all the NC aggregate materials that will be characterized at both original source and engineered gradations. This will establish a better methodology for the use of forced regression so that the rutting model parameters can be confidently determined from both the applied stress states and the gradation as well as other material property effects in the pavement design implementation of the developed rutting damage model. This will result in an approach to correct rutting damage computations currently generated by the Pavement ME software. The study findings will also highlight recommendations for developing new performance based specifications including strength criteria for unbound aggregate layers.

## 1.4 Report Organization

The current study builds on the Phase I research (Chow et al. 2014) framework which had the goal to develop and calibrate the UIUC rutting model to better predict rutting accumulations of in-service unbound aggregate pavement layers. The *Research Methodology* follows the same approach adopted for the Phase I and II studies. Material characterization tasks start with determining the source gradations and followed by studying the compaction characteristics. The next step is to conduct the full suite of monotonic shear strength testing and permanent deformation triaxial tests, accounting for the effects of shear strength properties and SSR on rutting accumulation. The model parameters for the UIUC rutting model are then determined by regression analyses and fine-tuned into more appropriate ranges with forced regression optimization. Further, the stepwise regression analysis is used to correlate the model parameters assigned in the UIUC rutting model with aggregate material properties and image-based shape properties. Finally, a procedure is established to determine the model parameters as function of material properties.

This report contains six chapters as follows:

- Chapter 1** Provides a general introduction to the research need, purpose, and objectives.
- Chapter 2** Provides a brief literature review of pavement rutting mechanisms and material properties affecting the performances of flexible pavements constructed with unbound aggregate base/subbase layers. This chapter also provides a summary of the permanent deformation/strain models and factors that were extensively researched during Phase I and II studies.
- Chapter 3** Describes the laboratory test equipment, sample preparation and the test procedures used to test the aggregate materials and lists the source properties.
- Chapter 4** Summarizes and discusses the laboratory tests conducted on and material characterizations performed for the aggregate materials. Results from sieve analyses, moisture-density studies, shear strength and repeated load triaxial tests are presented in this chapter.
- Chapter 5** Lists and discusses the research tasks undertaken to re-evaluate the proposed UIUC rutting model at the source gradations, compares and contrasts the model parameters at source gradations and the engineered gradation, investigates forced regression analyses to obtain more robust model parameters, establishes relationships between the model parameters and material properties, and

accordingly, recommends unbound layer design methodology using the UIUC routing model.

**Chapter 6** Summarizes the major findings of the research study and lists recommendations for future research.

## **CHAPTER 2: LITERATURE REVIEW**

### **2.1 Introduction**

This chapter provides a concise literature review of the currently available and commonly utilized models for predicting permanent deformation accumulation in unbound aggregate layers. A more comprehensive discussion of these rutting models was presented earlier in the Phase I report of the project by Chow et al. (2014). Aggregate characteristics and the factors that significantly contribute to permanent deformation are also discussed.

### **2.2 Factors Influencing Permanent Deformation in Unbound Layers**

The main factors identified by past studies (Barksdale 1972, Thom et al. 1988, Brown et al. 1996, and Lekarp et al. 2000) to significantly affect the permanent deformation accumulation in unbound aggregate materials include: applied stress and material strength, moisture content or degree of saturation, dry density, fines content and plasticity, mineralogy, grain size distribution, principal stress orientation under moving wheel, and stress history.

Several widely used permanent deformation predictive models, including the one used by the Pavement ME Design software by AASHTO, use the resilient strains levels to predict the permanent deformation accumulation in unbound aggregate layers. However, past research studies (Tao et al 2010, Thompson 1972, and Chow et. al 2014) have clearly established that aggregate shear strength plays a significant effect on the amount of rutting accumulated in unbound aggregates under loading. They reported that aggregate materials with relatively high shear strength properties generally exhibit lower tendencies for accumulate lateral and vertical deformations under loading conditions compared to aggregate materials with relatively low shear strength under similar loading conditions.

The effect of changing the gradation on the mechanical behavior of aggregate materials, such as shear strength properties and resilient properties under repeated loading, was intensively studied. Grain size distribution or gradation has been identified as one of the main factors that influence the permanent deformation accumulation in unbound aggregate materials. Cunningham et al. (2013) studied the effects of particle size distribution on the mechanical behavior (shear strength and resilient properties) of aggregates by testing the same unbound materials at five different gradations satisfying typical gradation bands specified by the North Carolina DOT (NCDOT). A wide variety of laboratory tests were conducted, and the researchers concluded that the Optimum Moisture Content (OMC), Maximum Dry Density (MDD), and other index properties such as Atterberg limits were not significantly influenced by changing grain size distribution of the aggregate materials. However, an adverse effect on the mechanical response of the specimens was reported as the fines content (material passing No. 200 sieve or finer than 0.076 mm) approached 8-12% by weight.

In a similar study, Ghabchi et al. (2013) tested different aggregate types at gradations corresponding to the upper and lower limits of a specified gradation band for Oklahoma Department of Transportation (ODOT). They observed that the specimens blended at gradations that correspond to the upper limit had higher densities and OMC values compared to specimens blended at gradations near the lower limit of the specification band. They also observed that specimens with finer gradations exhibited higher stability and resilient moduli due to better packing.

Recent research efforts at the University of Illinois (Tutumluer et al. 2009, Mishra et al. 2012, and Mishra 2012) studied the effect of grain size distribution on aggregate behavior, and compared relative impacts of moisture content, amount and type of fines (plastic versus nonplastic) on the permanent deformation behavior of both crushed and uncrushed aggregate materials. A significant reduction in aggregate shear strength and resistance to permanent deformation was observed when excess moisture was introduced in uncrushed gravel specimens comprising high amounts of plastic fines.

### **2.3 Available Permanent Deformation Predictive Models**

Deformation under repeated loading can be the result of the following mechanisms: densification/dilation, distortion, and attrition. The densification/dilation mechanism is the process of volume change through reorientation and rearrangement of particles resulting from compressing the soil structure. Distortion is the motion due to bending, sliding and rolling of individual particles. Particle bending is governed by the particle shape properties, whereas sliding and rolling are characterized by interparticle friction resistance. Attrition, on the other hand, is the crushing and breakdown of particles when applied contact load exceeds strength limit of the single particles. Particle crushing is governed by particle shape, size, mineralogy, strength of individual aggregate particles and effective pressure. Volumetric strains are mainly associated with densification/dilation and attrition, whereas shear strains are mainly contributed through distortion.

Several predictive models have been proposed by researchers to predict the permanent deformation accumulation in unbound aggregate base/subbase layers. The most important ones were discussed in detail by Chow et al. (2014) in the Phase I report. Some of these models in chronological order are mentioned hereafter. Barksdale (1972) proposed a linear relationship between permanent strain and the logarithm of number of load applications. Monismith et al. (1975) proposed the widely used log-log relationship between permanent strain and number of load applications (also known as the phenomenological model). Other common models developed in the 1970s and 1980s include those proposed by Pappin (1979), El-Mitiny (1980), Khedr (1985), and Tseng and Lytton (1989). Several additional models proposed in the 1990s also include those developed by Wolff (1992), Thompson and Nauman (1993), van Niekerk and Huurman (1998), Paute et al. (1996), Huurman (1997), and Ullidtz (1997). Additionally, Lekarp and Dawson (1998) state that the failure of granular materials under repeated loading is a gradual process dependent on applied stress states

and number of load applications. Gidel et al. (2001) also proposed a stress dependent permanent deformation model based on the laboratory data.

In the context of mechanistic-empirical (M-E) pavement design or Pavement ME by AASHTO, permanent deformation ( $\delta$ ) of an unbound aggregate base/subbase layer is estimated using Equation (2.1) as a function of traffic repetitions ( $N$ ), sublayer thickness ( $h$ ), and vertical resilient strain computed for sublayer ( $\epsilon_v$ ). The ratio  $\epsilon_0/\epsilon_r$ ,  $\beta$ ,  $\rho$  are material properties and model parameters, which are computed as a function of moisture content, resilient modulus ( $M_R$ ) and state of stress according to the original Tseng and Lytton (1989) rutting model. Note that the Pavement ME Design eliminated the stress state dependence and therefore changed this equation of permanent deformation to assess rutting potential during construction through field measurement of moisture content only –  $M_R$  is typically obtained from the California Bearing Ratio (CBR).

$$\delta(N) = \beta_1 \left( \frac{\epsilon_0}{\epsilon_r} \right) e^{-\left(\frac{\rho}{N}\right)^\beta} \epsilon_v h \quad (2.1)$$

where  $\delta(N)$  is permanent deformation corresponding to  $N$ -load application;

$\beta_1$  is field calibration parameter;

$\epsilon_0$ ,  $\beta$ ,  $\rho$  are material parameters;

$\epsilon_r$  is resilient strain imparted in the laboratory to determine material properties;

$\epsilon_v$  is vertical resilient strain computed from sublayer; and

$h$  is thickness of sublayer.

One limitation of the Pavement ME Design program is that it does not credit the contribution of the unbound aggregate base sufficiently for it to be cost competitive. Thus, to properly account for granular material quality impacting performance of pavements with unbound aggregate bases, the first challenge is to be able to incorporate shear strength or rutting potential into materials characterization. Most recently, Chow et al. (2014) proposed a framework for predicting permanent deformation (also known as the UIUC Rutting Model) as a function of applied wheel load stress levels and aggregate shear strength under applied confinement (or ratio of the two defined as the shear stress ratio) along with the number of load applications.

## CHAPTER 3: MATERIALS AND LABORATORY TESTS

### 3.1 Introduction

This chapter presents the material characterization and testing techniques required to pursue the scientific approach adopted in this research study to develop a laboratory test matrix for studying rutting performances of the 15 unbound aggregate materials used in pavement base/subbase layers in the State of North Carolina at their respective source gradations. Relevant technical features of the laboratory equipment used to test the aggregates are discussed in this chapter. The results from characterization and testing of the fifteen unbound materials are presented in Chapter 4.

### 3.2 Materials Description

Fifteen different crushed aggregate materials, commonly used for unbound base and subbase applications in the state of North Carolina, were received from different quarries across the state to be tested and evaluated in this study. The corresponding quarry, county and supplier of each material are alphabetically listed in Table 3.1. Compared to the Phase I study, the aggregate material from Franklin quarry, due to not having an adequate quantity of the original material shipped to UIUC, was excluded in the current study.

**Table 3.1** List of the fifteen crushed stone materials studied

Quarry	County	Supplier
Arrowood	Mecklenburg	Martin Marietta
Belgrade	Onslow	Martin Marietta
Fountain	Pitt	Martin Marietta
Goldhill	Cabarrus	Vulcan Materials
Hendersonville	Henderson	Vulcan Materials
Jamestown	Guilford	Martin Marietta
Lemon Spring	Lee	Martin Marietta
Moncure	Lee	Wake Stone Corp.
Nash County	Nash	Wake Stone Corp.
North Wilkesboro	Wilkes	Vulcan Materials
Princeton	Johnston	Hanson Aggregates
Raleigh	Wake	Hanson Aggregates
Rockingham	Richmond	Vulcan Materials
Rocky Point	Pender	Martin Marietta
Rougemont	Durham	Hanson Aggregates

### 3.3 Laboratory Characterization and Testing

#### 3.3.1 Grain Size Distribution

To control the gradation of an individual aggregate sample, sieving and separation of the aggregate materials by size was deemed to be a priority task. The stockpiles of the fifteen materials received from different quarries were processed through a set of sieves following the practice of ASTM C136 in Phase I study. Accordingly, the material retained on each sieve size was stored in seven separated buckets with individual particle sizes as shown in Figure 3.1.

As one of the first and most important steps, the grain size distribution of the materials received from each of the fifteen quarries was determined based on dry sieving method of representative samples from the aggregate stockpiles. Coarse-grained aggregate sizes from 1.0 in. (25.4-mm) and 0.5 in. (12.7 mm) sieve sizes were separated on Gilson Testing Screen following the best practices for quality control and manufacturer's recommendations. The materials passing No. 4 sieve (sizes corresponding to No. 10, No. 40, No. 200 sieves and fines retained on pan) were separated on the DuraShake™ sieve shaker. Any oversize granular particles larger than 1.5-in. were discarded from the sieve operation and not used in this study.



**Figure 3.1** Size separation of each aggregate material batched at the source gradation determined from sieve analysis. From left to right and top to bottom: materials retained on sieve sizes 1.0 in., 0.5 in., No.4, No. 10, No. 40, No. 200 and pan.

To ensure uniform gradations for all samples prepared later for moisture-density, repeated load permanent deformation, and monotonic shear strength tests, the samples were engineered to the source gradations by batching and mixing the materials from the seven different sizes indicated in Figure 3.1 so that the gradations exactly matched the source gradations reported. This step was

deemed important to reduce any source of error coming from variable gradations, and is more accurate than other methods such as quartering or using a splitter. The results for dry sieve analysis are presented and discussed in Chapter 4.

### 3.3.2 Atterberg Limits

The Atterberg limit tests of the fifteen aggregate materials were provided by NCDOT Material and Tests Unit during the Phase I of the project. Atterberg limits tests are conducted on the fraction of material finer than 0.425 mm (passing No. 40 sieve), following the standard practice for ASTM 4318. The liquid limit and plasticity index test results are presented in Table 3.3.

**Table 3.3** Atterberg limits of the fifteen crushed stone materials studied

<b>Quarry</b>	<b>Plasticity Index (%)</b>	<b>Liquid Limit (%)</b>
Arrowood	Nonplastic	18
Belgrade	Nonplastic	16
Fountain	Nonplastic	19
Goldhill	6	23
Hendersonville	Nonplastic	21
Jamestown	Nonplastic	23
Lemon Spring	Nonplastic	17
Moncure	Nonplastic	17
Nash County	Nonplastic	18
N. Wilkesboro	Nonplastic	24
Princeton	Nonplastic	18
Raleigh	Nonplastic	22
Rockingham	Nonplastic	22
Rocky Point	Nonplastic	17
Rougemont	Nonplastic	18

### 3.3.3 Moisture-Density Relationships

The compaction characteristics of the fifteen aggregate materials at their source gradations were initially provided by NCDOT Material and Tests Unit. As part of Task 1 in the project deliverables, moisture-density studies were also conducted at ATREL for all the fifteen materials. Following the standard practice of NCDOT engineers, the compaction method followed a procedure similar to the modified compaction test (AASHTO T-180) but with additional 30 blows (total of 86 blows) applied to each layer with a 10-lb. (4.54-kg) hammer and an 18-in. (457-mm) drop height.

Aggregate specimens were prepared at different moisture contents, ranging from 3% to 9%, or as required, and compacted in the standard 6 in. (152 mm) by 7 in. (178 mm) mold in five (5) equal

lifts at 86 blows per lift. The resulting dry densities at different moisture contents were plotted against moisture content. As a minimum, four tests were performed and used to draw the modified compaction effort moisture-density curves to establish the maximum dry density (MDD) and optimum moisture content (OMC) values. MDD and OMC values for all the fifteen materials at the source gradations are presented in Chapter 4.

Given that the compaction characteristics were investigated with the modified compaction effort using the standard California bearing Ratio (CBR) mold, each of the prepared aggregate specimens at the different moisture contents was tested to determine the unsoaked CBR for each specimen. CBR is the ratio of force per unit area required to penetrate a soil mass to that required for the corresponding penetration of a standard material. The testing was carried out immediately after the sample was compacted and weighted, using a Humboldt Master Loader HM-300 loading frame, with the standard 2-in. (50-mm) diameter circular piston at the rate of 0.05 in/min (1.25 mm/min).

### 3.3.4 Imaging Based Properties (Shape, Angularity, and Surface Texture)

Aggregate morphological properties, such as shape, angularity and surface texture, are recognized to highly influence the engineering behavior of unbound aggregate materials under loading. These morphological indices of aggregate particles were determined during the Phase I study using the Enhanced-University of Illinois Aggregate Image Analyzer (E-UIAIA) housed in ATREL (Figure 3.2). The device is equipped with three high resolution ( $1292 \times 964$  pixels) Charge Coupled Device (CCD) progressive scan color cameras to capture three orthogonal views (front, top and side) of aggregate particles. More details on the features of the E-UIAIA can be found elsewhere (Moaveni et al. 2013).

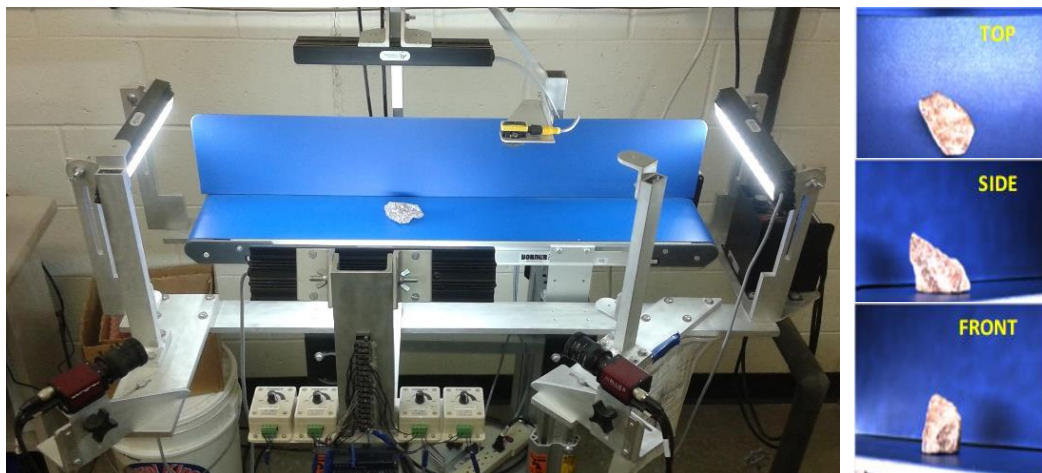


**Figure 3.2** Enhanced University of Illinois Aggregate Image Analyzer (E-UIAIA)

E-UIAIA is capable of quantifying shape properties of aggregate particles as imaging based indices for Angularity Index (AI), Surface Texture Index (STI), and Flat and Elongated Ratio (FER).

These imaging based shape indices have been validated by successfully measuring aggregate properties and linking results to corresponding laboratory strength data and field rutting performances (Rao et al. 2002; Pan et al. 2004). More detailed description of the shape indices measured by E-UIAIA can be found elsewhere (Tutumluer et al. 2000; Rao et al. 2001; Rao et al. 2002; Pan and Tutumluer 2007; Moaveni et al. 2013).

In this study, fifty (50) particles corresponding to two particle sizes, 1 in. (25.4 mm) and 0.5 in. (12.7 mm), were randomly collected from each of the fifteen aggregate materials, and scanned using the E-UIAIA through three replicate tests. Results from the E-UIAIA image analyses are presented and discussed in Chapter 4. All of the collected aggregate particles were washed thoroughly using clean water and oven dried before conducting image analyses.

### **3.3.5 Triaxial Shear Strength Testing**

The first step involved testing the fifteen aggregate materials for shear strength properties at their source gradations. Triaxial monotonic shear strength tests were performed to establish the shear strength properties (friction angle,  $\phi$ ; and cohesion intercept,  $c$ ) for each aggregate material. Cylindrical test specimens, 6 in. (152 mm) in diameter and 12 in. (305 mm) in nominal height, were prepared by compacting in six equal lifts. The OMC and MDD obtained from the moisture-density tests were targeted during sample preparation, and the achieved moisture content was measured after each shear strength test was conducted.

The sample preparation involved using an aluminum split-mold lined with a 31-mil (0.79-mm) neoprene membrane assembled on the triaxial cell base plate. Each sample was compacted in six (6) successive lifts using a 10-lb. (4.54-kg) drop hammer. Prior to removing the split-mold, an internal vacuum was applied to the specimen at the drainage port to support it upon removal of the mold. A second 25-mil (0.64-mm) thick membrane was externally placed on the specimen as the first neoprene membrane was frequently punctured by the larger aggregates during the compaction process. The membranes were finally tightened using two rubber O-rings at both ends. Finally, the triaxial chamber and top platen were placed and the specimen was positioned in the loading frame.

Prior to applying confining pressure, a vertical seating load corresponding to a pressure level of 1-2 psi (6.89-13.8 kPa) was applied. Next, the confining pressure was applied manually through an air valve and the gage reading was recorded to the nearest 0.5 psi (3.4 kPa). Subsequently, the vacuum was removed from the drainage port. A minimum of three tests were conducted for each material at target confining pressure levels of around 35 kPa (5 psi), 69 kPa (10 psi), and 103 kPa (15 psi) to establish the Mohr-Coulomb failure envelopes. An axial strain rate of 1% per minute (3 mm/min or 0.12 in./min) was applied to shear the specimens. After the completion of each test, the specimen was weighed and oven-dried for achieved moisture content measurement. More details regarding sample preparation and the testing procedure were given in the Phase I report

(see Chow et al. 2014). Figure 3.3 shows the sample preparation and part of the setup of the triaxial shear strength apparatus, known as the TX-12.



**Figure 3.3** Sample preparation for shear strength test and the TX-12 shear strength setup

### Shear Stress Ratio Calculations:

In addition to establishing the shear strength properties (friction angle,  $\phi$ ; and cohesion intercept,  $c$ ), knowing the shear strength allows the calculation of the Shear Stress Ratio (SSR). SSR is defined as the ratio between the induced shear stress to the shear strength ( $\tau_f$ ) of a particular aggregate material. The concept originates from the Mohr-Coulomb failure envelope and is clearly shown in Figure 3.4. For any particular combination of confining pressure ( $\sigma_3$ ) and deviator stress ( $\sigma_d$ ) applied during triaxial testing, the mobilized normal pressure ( $\sigma_n$ ) and the mobilized shearing resistance ( $\tau_n$ ) can be computed on the potential shear failure surface using Equations 3.1-3.2. The failure surface is oriented at an angle of  $45^\circ + \phi/2$  to the horizontal. The shear strength can then be computed using Equation 3.3. Finally, the SSR is computed as the ratio of the shear resistance to the shear strength (Equation 3.4 and Figure 3.5). More details about the concept of SSR and its calculation can be found in the Phase I report (see Chow et al. 2014). The following equations are used to compute the SSR as follows:

$$\sigma_n = \sigma_3 + \frac{\sigma_d (1 - \sin \phi)}{2} \quad (3.1)$$

$$\tau_n = \frac{\sigma_d \cos \phi}{2} \quad (3.2)$$

$$\tau_f = c + \sigma_n \tan(\phi) \quad (3.3)$$

$$\text{Shear Stress Ratio (SSR)} = \frac{\text{Mobilized Shearing Resistance}}{\text{Shear Strength}} = \frac{\tau_n}{\tau_f} \quad (3.4)$$

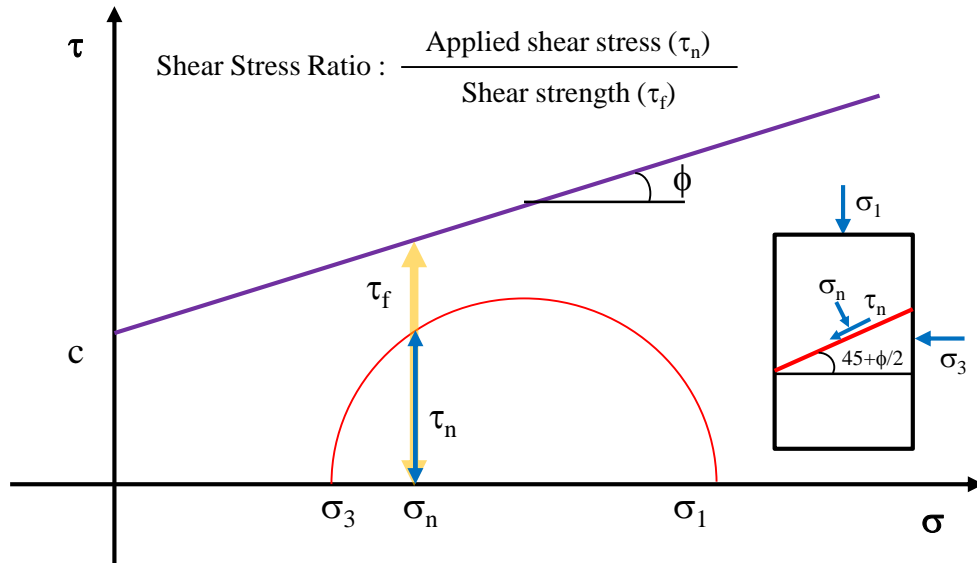


**Figure 3.4** Mohr-Coulomb envelope and the concept of shear stress ratio (SSR)

### 3.3.6 Repeated Load Triaxial Testing for Permanent Deformation

The main objective of this study is to evaluate and predict the permanent deformation trends in commonly used North Carolina aggregate materials at their source gradations. Thus, conducting repeated load laboratory test is a critical evaluation step. The performed tests correlate permanent deformation accumulation to strength properties, and the results from the shear strength tests are essentially used to calculate the applied stress states at predefined SSR values of 0.25, 0.50, and 0.75 for each material. A confining pressure level of 5 psi (34.5 kPa) was selected for the repeated load permanent deformation tests to ensure that deviator stress values required for achieving the target SSR values remained within the equipment limits. Additionally, this assumption closely simulates typical confining pressure levels in the field, considering typical residual compaction stresses locked-in the granular base during pavement construction and subsequent trafficking.

All the repeated load permanent deformation tests in this study were conducted using an advanced triaxial testing device, referred to as the University of Illinois FastCell (UI-FastCell). The FastCell presents unique capabilities for independent pulsing in the vertical and horizontal directions (Tutumluer and Seyhan 1999). A detailed explanation of the UI-FastCell and its advanced capabilities can be found in the Phase I report (Chow et al. 2014) and elsewhere (Tutumluer and Seyhan, 1999).

The specimen preparation for permanent deformation tests is similar to the triaxial shear strength test specimen preparation procedure described previously. However, the cylindrical permanent deformation test specimens is smaller and have the dimensions of 6 in. (150 mm) height and 6 in. (150 mm) diameter. Aggregate specimens were prepared using a customized split-mold

manufactured with the UI-FastCell, with a 25-mil (0.64-mm) thick membrane lined to the interior of the split-mold. A vacuum line was attached to the drainage port of the bottom platen of the mold to hold the membrane tight against the mold. A nonwoven geotextile was placed on top of the bottom platen to prevent the drainage port from being clogged. Aggregate mixture with target moisture content was compacted in three equal lifts, with a 10-lb. (4.54-kg) hammer from an 18-in. (457-mm) drop height, following the exact specimen preparation procedure as triaxial shear strength test. The target density and moisture content were the MDD and OMC, respectively.

Following compaction, the specimen was carefully moved to UI-FastCell loading frame for testing. Internal vacuum was switched from mold to the bottom port to maintain specimen stability. The top platen was then placed on top of the specimen before the split-mold was taken apart. A second 25-mil (0.64-mm) thick membrane was placed on the specimen because first membrane often punctured during the compaction procedure. Next, the specimen was placed in the UI-FastCell loading frame, and the loading plate was lowered to make contact with top platen. Finally, the UI-FastCell confining cell was lowered down, and confining pressure was applied before internal vacuum was removed. Figure 3.5 shows some steps from specimen preparation as well as the UI-FastCell triaxial equipment.

All the permanent deformation tests were performed by applying 10,000 cycles at each stress level using a haversine-shaped load pulse with a load pulse duration of 0.1 seconds and a rest period of 0.9 seconds. For each aggregate material at the source gradation, tests were conducted at the three SSR values of 0.25, 0.50 and 0.75; corresponding to the stress levels of low, medium and high, respectively. Only single-stage loading permanent deformation tests were carried out. After the completion of each test, the specimen was weighed and oven dried for achieved moisture content measurement.



**Figure 3.5** University of Illinois FastCell showing a sample inserted inside the cell (left) and the cell lowered around the sample prior to starting the test (right)

### 3.3.7 Resilient Modulus Testing

Resilient modulus ( $M_R$ ) tests were conducted on all the fifteen aggregate materials at the source gradations. The elimination of stress dependency from the original Tseng and Lytton (1989) equation has resulted in permanent deformation predictions of unbound granular layers to be solely predicted from the moisture content and resilient modulus values. Accordingly, the stress dependent resilient modulus, if used, would be a primary input parameter for the design of unbound aggregate base/subbase layers in pavement structures. Thus, resilient modulus tests were performed with the intent to link the results with the strength-based UIUC rutting model and the current Pavement ME permanent deformation model.

The resilient modulus testing followed the procedure and the loading sequence listed in the AASHTO T307-99 (2012) standard. All the repeated load permanent deformation tests in this study were conducted using the UI-FastCell. The sample preparation is similar to that for the repeated load permanent deformation tests, and was described in detail in the previous section. Each material was weighed according to its MDD and OMC, then was compacted in three (3) equal layers. Similar to the sample preparation for permanent deformation tests, it was assumed that the target density (MDD) was achieved when the total weighed amount of materials were all compacted to a predetermined layer height. Therefore, there was no specified blow count for each layer during compaction. Prior to conducting a resilient modulus test, 1,000 loading cycles were applied for a conditioning phase.

## **CHAPTER 4: TEST RESULTS**

### **4.1 Introduction**

This chapter presents results from the various testing and characterizations performed on the fifteen aggregate materials at the quarry source gradations, including the results of the four materials reported in the pilot Phase II study. The test results of each material are compared to those of the same material tested at the engineered gradation in the Phase I study. For convenience, the materials tested at the source gradations will be referred to as SG (Source Gradation) in the Phase II and current Phase III studies, while the same materials tested at the engineered gradation in the Phase I study will be referred to with EG (Engineered Gradation). Also, for simplicity, the terms ‘Phase I’, ‘Phase II’, and ‘Phase III’ will be used throughout this chapter to refer to the testing performed in the three phases of this project.

This chapter presents the results of the sieve analysis, moisture-density and CBR tests conducted on all the fifteen materials including imaging-based particle shape characterization. In addition, the results of the triaxial tests, which consist of (i) monotonic shear strength and (ii) repeated load permanent deformation tests, are presented along with the analyses of the test data. The laboratory study findings are described for certain behavior trends, and possible reasons for any discrepancies in the aggregate material behavior are discussed.

### **4.2: Results from Laboratory Testing and Characterization**

#### **4.2.1 Grain Size Distribution**

Figure 4.1 shows the gradation curves for the fifteen materials along with the NCDOT base course material specification bands. The fixed engineered gradation used in the ‘Phase I’ study is also plotted in Figure 4.1, which represents the average gradation of the upper and lower bounds for the NCDOT base course gradation specification bands. The individual gradation curves based on dry sieving for each aggregate material are presented in Appendix A. The source gradations were determined in Phase I by dry-sieving several 5-gallon buckets containing representative samples from each material. In the early stages of Phase II and III studies, all samples were engineered to the SG by dry sieving and prepared to the predetermined source gradation.

Comparing the source gradations with the engineered gradation, the source gradation for Fountain material is almost similar to the engineered gradation. Although certain portions of the source gradation curves for Belgrade, N. Wilkesboro, Hendersonville, Princeton, Rockingham, and Rocky Point materials differ from the engineered gradation curve, their source gradation curves resemble the engineered gradation. For Nash material, the fines content of the SG passing the No. 200 sieve is higher than the engineered gradation one. The other fourteen materials at SG have lower fines contents compared to the engineered gradation value. Especially for Goldhill material,

the fines content is even smaller than the lower bound of NCDOT specification band. It should be noted that although Arrowood, Goldhill, Jamestown, Lemon Spring, Moncure and Rougemont materials are commonly used by NCDOT for pavement base/subbase applications, parts of the source gradation curves were found to lie outside the agency-specified gradation band.

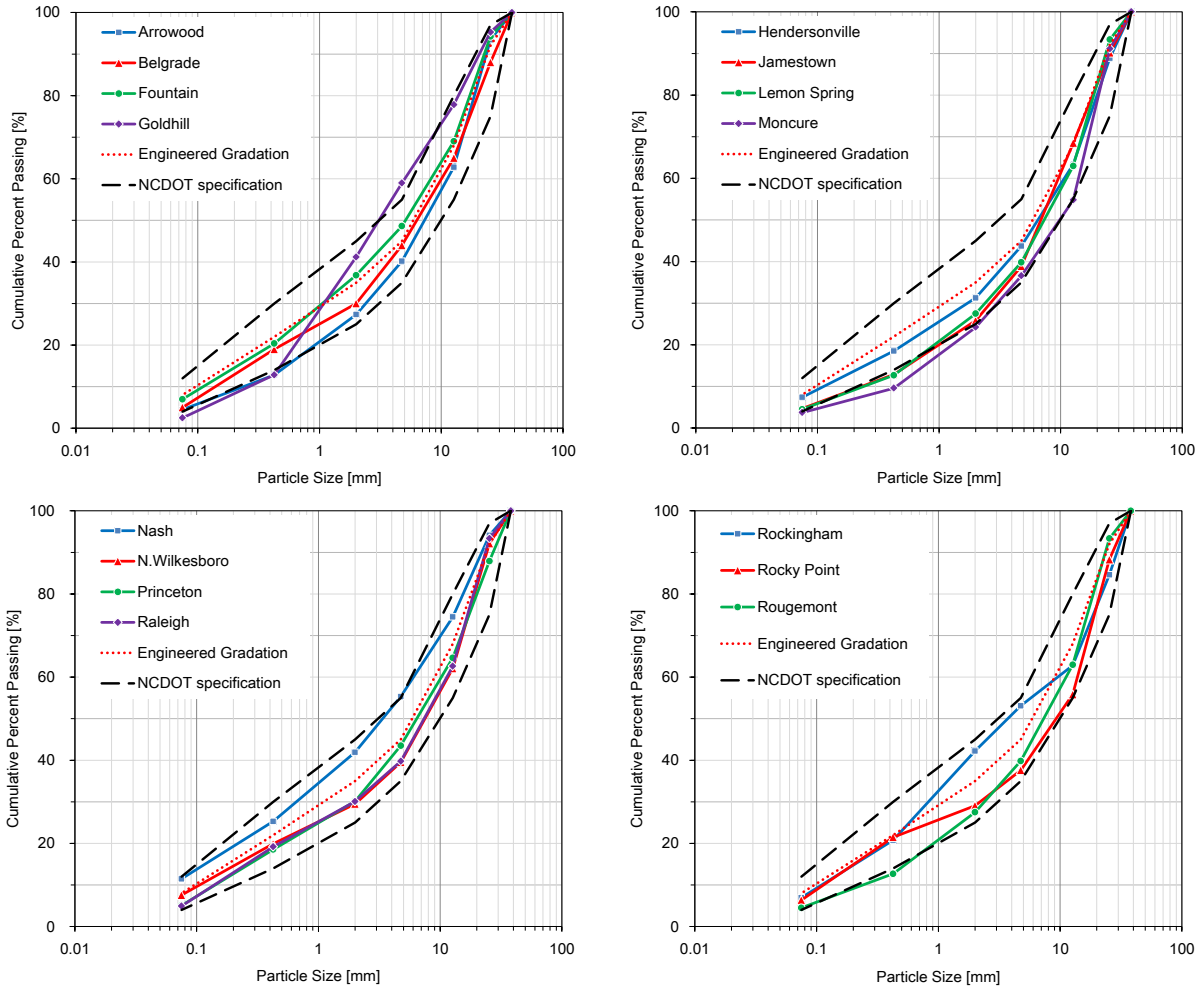


**Figure 4.1** The source gradations (SG) of the tested aggregate materials shown plotted with the engineered gradation (EG) and the NCDOT gradation specification band

#### 4.2.2 Moisture-Density Relationship

Table 4.1 presents the MDD and OMC results for the fifteen aggregate materials. The compaction characteristics at the engineered gradations were reported earlier by the NCDOT Material and Tests Unit and published in the Phase I study report. The compaction characteristics at the source gradations were determined at the University of Illinois through the Phase II and III research tasks. The individual moisture-density curves graphed at the source gradations for each of the fifteen materials along with the CBR results are presented in Appendix B.

Table 4.1 lists the MDDs of specimens tested at UIUC at the source gradations, while the MDDs for the specimens prepared at engineered gradation were reported by NCDOT. Except for Goldhill and Rockingham, the MDDs obtained from the moisture-density tests conducted at UIUC are slightly higher (within 5.4 pcf) than those obtained by the NCDOT. Considering the wide range of MDD values determined from 131 to 159 pcf, the maximum densities generally agree with each other. Overall, the aggregate materials are densely packed at source gradations, showing higher maximum dry densities. Arrowood has the highest density at source gradation, while Belgrade has the lowest density. The OMCs at source gradations are generally similar to those at engineered gradations, except for Arrowood, Belgrade, Hendersonville, and Rockingham, which have OMCs are slightly different (by 1.2%) from those at engineered gradations. Note that all the samples prepared for further testing were compacted at the OMCs and the MDDs obtained at source gradations.

According to the CBR results, presented in Appendix B, all the fifteen materials can be considered as high quality aggregates. Only Goldhill, Hendersonville, and Jamestown materials show CBR values less than 100% and as low as 63% at the OMC, while the other twelve materials indicate CBR values exceeding 100% at the OMC, as shown in Appendix B.

**Table 4.1** Aggregate compaction characteristics

Material	Source gradation		Engineered gradation	
	MDD	OMC	MDD	OMC
	$\gamma_{d,max}$ pcf	$\omega_{opt}$ (%)	$\gamma_{d,max}$ pcf	$\omega_{opt}$ (%)
Arrowood	158.9	5.4	153.5	4.2
Belgrade	134.5	6.8	131.3	7.4
Fountain	142.4	6.1	141.2	6.1
Goldhill	141.6	5.9	142.2	6.4
Hendersonville	143.2	6.3	139.3	5.5
Jamestown	142.7	5.9	141.6	5.8
Lemon Spring	145.4	5.2	140.9	5.5
Moncure	150.0	5.6	148.2	5.2
Nash	143.6	5.7	142.3	5.7
N. Wilkesboro	145.3	4.9	142.5	5.0
Princeton	145.7	5.6	141.3	5.1
Raleigh	141.5	6.4	139.6	6.1
Rockingham	140.5	5.4	141.4	6.1
Rocky Point	139.6	6.0	134.7	5.9
Rougemont	144.7	6.0	144.0	6.1

### 4.2.3 Imaging Based Properties (Shape, Angularity and Surface Texture)

The use of the Enhanced-University of Illinois Aggregate Image Analyzer (E-UIAIA), was pursued for the sixteen NCDOT aggregate materials as part of Phase I of the project to give timely consideration to imaging based shape, angularity and surface texture property determinations. Basic components of the imaging equipment and its principle of operation were introduced in Chapter 3. The E-UIAIA based imaging indices for the fifteen coarse aggregate materials studied at SG fall into the following two categories: (1) particle sizes, which include maximum, intermediate and minimum dimensions, and volume of the aggregate particle (Tutumluer et al. 2000; Rao 2001); (2) particle morphological or shape indices, which include the Flat and Elongated Ratio (FER) (Rao et al. 2001), Angularity Index (AI) (Rao et al. 2002), and Surface Texture Index (STI) (Rao et al. 2003; Pan et al. 2004).

For quantifying the shape and angularity aspects of the fifteen aggregate materials tested at SG, fifty (50) particles of each material were analyzed using the E-UIAIA. The Surface Texture Index (STI) and the Angularity Index (AI) were computed using the automated algorithms by Rao et al. (2002 and 2003). Tables 4.2, 4.3 and 4.4 list the average values of AI, STI and FER, respectively, based on selected 50 particles having average sizes of 1.0 in. (25.4 mm) and 0.5 in. (12.5 mm). This information was shown and discussed in more detail for the sixteen aggregate materials studied in Phase I (Chow et al. 2014), and they are summarized again here for the fifteen aggregate materials studied in Phase II and III studies at the source gradations.

**Table 4.2** Imaging based Angularity Index (AI) Properties

Quarry	Average AI in Degrees (Particle Size)				
	AI (0.5-in.)	Std. Dev.	AI (1.0-in.)	Std. Dev.	AI for All Sizes
Arrowood	384	70	431	96	408
Belgrade	557	113	560	90	558
Fountain	457	91	430	69	444
Goldhill	464	89	463	88	464
Hendersonville	484	91	496	100	490
Jameston	456	80	412	66	434
Lemon Spring	430	73	418	66	424
Moncure	444	88	432	74	438
N. Wilkesboro	439	95	394	73	416
Nash	421	72	389	90	405
Princeton	467	83	458	72	462
Raleigh	426	75	401	81	414
Rockingham	451	77	524	71	488
Rocky Point	497	89	526	114	511
Rougemont	552	85	481	78	516

**Table 4.3** Imaging based Surface Texture Index (STI) for Roughness

<b>Quarry</b>	<b>Average STI (Particle Size)</b>				
	<i>STI</i> <i>(0.5-in.)</i>	<i>Std. Dev.</i>	<i>STI</i> <i>(1.0-in.)</i>	<i>Std. Dev.</i>	<i>STI for All Sizes</i>
Arrowood	1.710	0.520	2.722	0.969	2.216
Belgrade	1.966	0.572	1.799	0.487	1.883
Fountain	2.794	1.291	1.992	0.857	2.393
Goldhill	2.381	0.914	2.072	0.775	2.226
Hendersonville	2.588	0.866	2.769	0.871	2.678
Jameston	2.306	0.751	1.597	0.535	1.951
Lemon Spring	1.698	0.501	1.847	0.955	1.773
Moncure	1.899	0.721	1.471	0.408	1.685
N. Wilkesboro	2.382	1.032	1.611	0.546	1.997
Nash	2.179	0.644	1.636	0.808	1.908
Princeton	2.468	0.883	2.229	0.789	2.348
Raleigh	2.684	1.022	2.035	0.710	2.360
Rockingham	1.877	0.498	2.401	0.724	2.139
Rocky Point	1.960	0.575	1.906	0.686	1.933
Rougemont	2.805	1.297	2.686	1.113	2.746

**Table 4.4** Imaging based Flatness and Elongation Ratio (FER)

<b>Quarry</b>	<b>Average FER (Particle Size)</b>				
	<i>FER</i> <i>(0.5-in.)</i>	<i>Std. Dev.</i>	<i>FER</i> <i>(1.0-in.)</i>	<i>Std. Dev.</i>	<i>FER for All Sizes</i>
Arrowood	2.470	0.730	2.628	0.731	2.549
Belgrade	1.884	0.399	1.834	0.392	1.859
Fountain	3.001	0.975	2.667	0.956	2.834
Goldhill	2.442	0.867	2.307	0.581	2.375
Hendersonville	2.528	0.702	2.479	0.807	2.504
Jameston	2.336	0.626	2.239	0.471	2.287
Lemon Spring	2.557	0.896	2.355	0.631	2.456
Moncure	2.340	0.608	2.049	0.581	2.194
N. Wilkesboro	2.767	0.900	2.519	0.786	2.643
Nash	2.792	0.825	2.343	0.668	2.567
Princeton	2.484	0.901	2.299	0.789	2.392
Raleigh	2.897	0.862	2.580	0.784	2.739
Rockingham	2.103	0.527	1.876	0.471	1.990
Rocky Point	2.119	0.564	1.829	0.386	1.974
Rougemont	2.478	0.848	2.667	0.855	2.573

The STI and AI can be directly linked to shear strength and permanent deformation properties of the studied aggregates to be discussed in the following sections. Considering the imaging properties with the shear strength results shown in the next section, Rougemont is one of the aggregate materials with the highest AI and STI as well as the highest friction angle. Higher STI results are usually linked to higher shearing resistance due to rougher surface texture. Note that **more** detailed interpretation of the effect of shape properties on shear strength properties and permanent deformation should also be accompanied with the hardness of the particles and the mineralogy of the material. Further, the shear strength properties are not only related to the particle shape effect but also to other factors, e.g. dry density and water content.

#### 4.2.4 Triaxial Shear Strength Testing

Monotonic shear strength tests were conducted on the fifteen (15) aggregate materials by compacting specimens at their MDD and OMC values at their quarry source gradations to establish the Mohr Coulomb envelopes and the shear strength properties (friction angle,  $\phi$ ; and cohesion intercept,  $c$ ). The procedure was described in Chapter 3. At each confining pressure, the stress-strain relationship was recorded, and the peak deviator stress values recorded at specimen failure were used as an indicator to evaluate the shear strength behavior of an aggregate sample.

The shear strength results are compared to the results of the same fifteen (15) aggregate materials previously tested in the same manner at the engineered gradation established during the Phase I study. The significant trends observed in the strength behavior of the studied granular materials and the discrepancies between results at the EG and SG are reported in this section. The stress-strain plots established from shear strength testing of the fifteen aggregate materials at the source gradations are presented in Appendix C. The stress-strain plots for the same aggregate materials at the engineered gradation were presented by Chow et al. (2014). For all tests performed at the SG and most of the tests performed at the EG, the stress-strain curves are qualitatively similar in shape to those for dense sand, which exhibits a well-defined peak value and then a typical decrease after the peak (post-peak softening).

#### *Shear Strength Properties ( $\phi$ and $c$ )*

In this study, the Mohr-Coulomb yield criteria were based on the overall development of the permanent deformation model. Note that the dilatational behavior of granular soils under triaxial states of stress results in a nonlinear Mohr-Coulomb failure envelope. However, in this study, as in the previous Phase I & II studies, the validity of a linear Mohr-Coulomb failure envelope was assumed. The Mohr-Coulomb failure criteria therefore assume a simplified linear relationship between shear and normal stresses

$$\tau_f = c + \sigma_n \tan \phi \quad (4.1)$$

where  $\tau_f$  is maximum shear stress or shear strength of material; and  
 $\sigma_n$  is normal stress at failure.

The friction angle ( $\phi$ ) and cohesion intercept ( $c$ ) are presented in Table 4.5, and are computed by establishing a linear regression relation following Equation 4.2 below

$$\sigma_1 = a + b \sigma_3 \quad (4.2)$$

where  $\sigma_{1,f}$  is major principal stress at failure;  
 $\sigma_3$  is confining pressure, or minor principal stress at failure; and  
 $a$  and  $b$  are the constant and slope from the regression line.

The values of  $a$  and  $b$  constants are used to determine  $\phi$  and  $c$  of granular material following Equations 4.3 and 4.4.

$$c = \frac{a}{2\sqrt{b}} \quad (4.3)$$

$$\phi = \sin^{-1} \left( \frac{b-1}{b+1} \right) \quad (4.4)$$

To obtain accurate results from the linear regression relation presented in Equation 4.2, a minimum of three test results at different confining pressures (around 5, 10 and 15 psi in this study) are plotted. The values of coefficient of determination ( $R^2$ ) were found to fall within the range of 0.86 to 1 for the fifteen aggregate materials studied.

In addition to friction angle ( $\phi$ ), the secant friction angle ( $\phi_{sec}$ ) is alternatively used to establish the relationship of shear strength in granular soils. The primary advantage of using  $\phi_{sec}$  is to better evaluate friction angles of different granular materials without the influence of linearly interpolated cohesion intercept. The secant friction angles are reported in Table 4.5 for the fifteen materials tested at both SG and EG for comparison purposes. These values are based on triaxial shear strength test results at the ~5psi (34.5 kPa) confining pressure.

As listed in Table 4.5, the shear strength properties for the majority of aggregate materials varied according to their gradations. Belgrade, Lemon Spring, Moncure, Rocky Point, and Rougemont materials have higher shear strength properties ( $c$ ,  $\phi$ , and  $\phi_{sec}$ ) at the SG compared to the values at the EG. To account for the difference in shear strength properties between two gradations, the  $D_{60}$  is also summarized in Table 4.5. The five aggregate materials have higher  $D_{60}$  values at SG compared to those at EG. This means that the increase in particle size contributed to the improvement of shear strength properties. In contrast, Arrowood, Hendersonville, Rockingham materials have significantly lower shear strength properties at SG compared to the values at EG. For Rockingham, the shear strength properties and  $D_{60}$  at SG are smaller than those at EG. However, contrary to the previously mentioned materials, the  $D_{60}$  values at SG for Arrowood and Hendersonville are greater than those at EG. Especially for Hendersonville, the friction angle was

unacceptably low, and thus, additional shear tests were performed at a moisture content of 5.5%, smaller than the OMC of Hendersonville. From the test results, it was found that the friction angle of Hendersonville at SG significantly increased from 23.6° to 57.8°. This means for Arrowood and Hendersonville, their higher OMCs at SG compared to EG and the susceptibility of their CBR values to varying moisture conditions may have contributed to the lower shear strength values. For the other materials, the variation in shear strength properties between two gradations is trivial.

The effects of dry density and moisture content on the shear strength properties were also observed from the test results. For example, the increase in dry density and decrease in moisture content of Lemon Spring at SG compared to EG caused a significant increase in cohesion which influenced the secant friction angle. However, the increases in dry density and moisture content of Arrowood at SG resulted in shear strength properties to increase. Therefore, several factors including dry density, moisture content, and gradation may affect the shear strength properties.

**Table 4.5** Shear strength properties of the fifteen aggregate materials at the SG and EG

Material	Source Gradation (SG)				Engineered Gradation (EG)			
	D <sub>60</sub>	Secant Friction Angle, $\phi_s$	Friction Angle, $\phi$	Cohesion, $c$	D <sub>60</sub>	Secant Friction Angle, $\phi_s$	Friction Angle, $\phi$	Cohesion, $c$
	mm	Degree	Degree	kPa (psi)	mm	Degree	Degree	kPa (psi)
Arrowood	11.2	47.7	35.4	24.2 (3.5)	9.0	65.2	50.2	85.1 (12.4)
Belgrade	10.2	60.4	50.6	49.0 (7.1)	9.0	42.5	41.8	6.5 (0.9)
Fountain	8.0	56.9	39.4	55.2 (8.0)	9.0	66.9	39.3	160.6 (23.3)
Goldhill	4.8	56.2	40.3	49.0 (7.1)	9.0	50.5	37.7	43.4 (6.3)
Hendersonville	10.1	50.5	23.6	60.7 (8.8)	9.0	59.4	45.3	59.4 (8.6)
Jamestown	9.4	53.5	30.4	61.4 (8.9)	9.0	49.4	41.2	23.3 (3.4)
Lemon Spring	11.8	63.4	41.5	121.4 (17.6)	9.0	46.6	41.4	11.3 (1.6)
Moncure	14.4	62.9	54.4	40.7 (5.9)	9.0	47.1	50.6	1.1 (0.2)
Nash	5.7	50.8	40.0	21.4 (3.1)	9.0	51.2	41.4	19.1 (2.8)
N. Wilkesboro	11.6	55.8	46.7	31.1 (4.5)	9.0	58.0	46.0	48.0 (7.0)
Princeton	10.2	49.2	40.0	20.0 (2.9)	9.0	45.3	49.1	7.1 (1.0)
Raleigh	11.1	47.0	48.6	0 (0)	9.0	51.1	42.3	17.9 (2.6)
Rockingham	8.8	51.5	37.4	29.0 (4.2)	9.0	54.3	41.7	35.7 (5.2)
Rocky Point	13.7	64.3	44.1	93.2 (13.5)	9.0	42.4	44.9	2.4 (0.3)
Rougemont	12.0	55.8	48.1	13.1 (1.9)	9.0	51.3	48.8	3.7 (0.5)

### ***Mohr-Coulomb Envelope***

Based on the shear strength properties (friction angle,  $\phi$  and cohesion intercept,  $c$ ) for each material, the linear regression relations following Equation 4.2 was established. The plots for the linear estimation of the Mohr-Coulomb envelopes for the materials at SG and EG are shown in Figures 4.2(a) and 4.2(b), respectively. Figure 4.2 shows the comparison of the Mohr-Coulomb

envelopes obtained at the SG with those previously plotted for the same materials at the EG from the Phase I project. At EG, Fountain exhibits the highest shear strength below a normal stress of 30 psi, whereas Arrowwood exhibits the highest shear strength above a normal stress of 30 psi. At SG, Lemon Spring exhibits the highest shear strength below a normal stress of 23 psi, whereas Moncure exhibits the highest shear strength above a normal stress of 23 psi. Considering that the typical confining pressure of 5 psi applied on all the aggregate materials tested corresponded to the range of a normal stress from 9 to 24 psi at failure (refer to Table 3.5 in Phase I report), Fountain at EG and Lemon Spring at SG have the highest shearing resistance capacity in the typical normal stress range at failure. Note that the linearly interpolated  $c$  and  $\phi$  may not be definite in representing the strength properties of the test aggregate materials, especially for the low confining pressure range. As mentioned before,  $\phi_{sec}$  values may also be used to represent the strength characteristics.

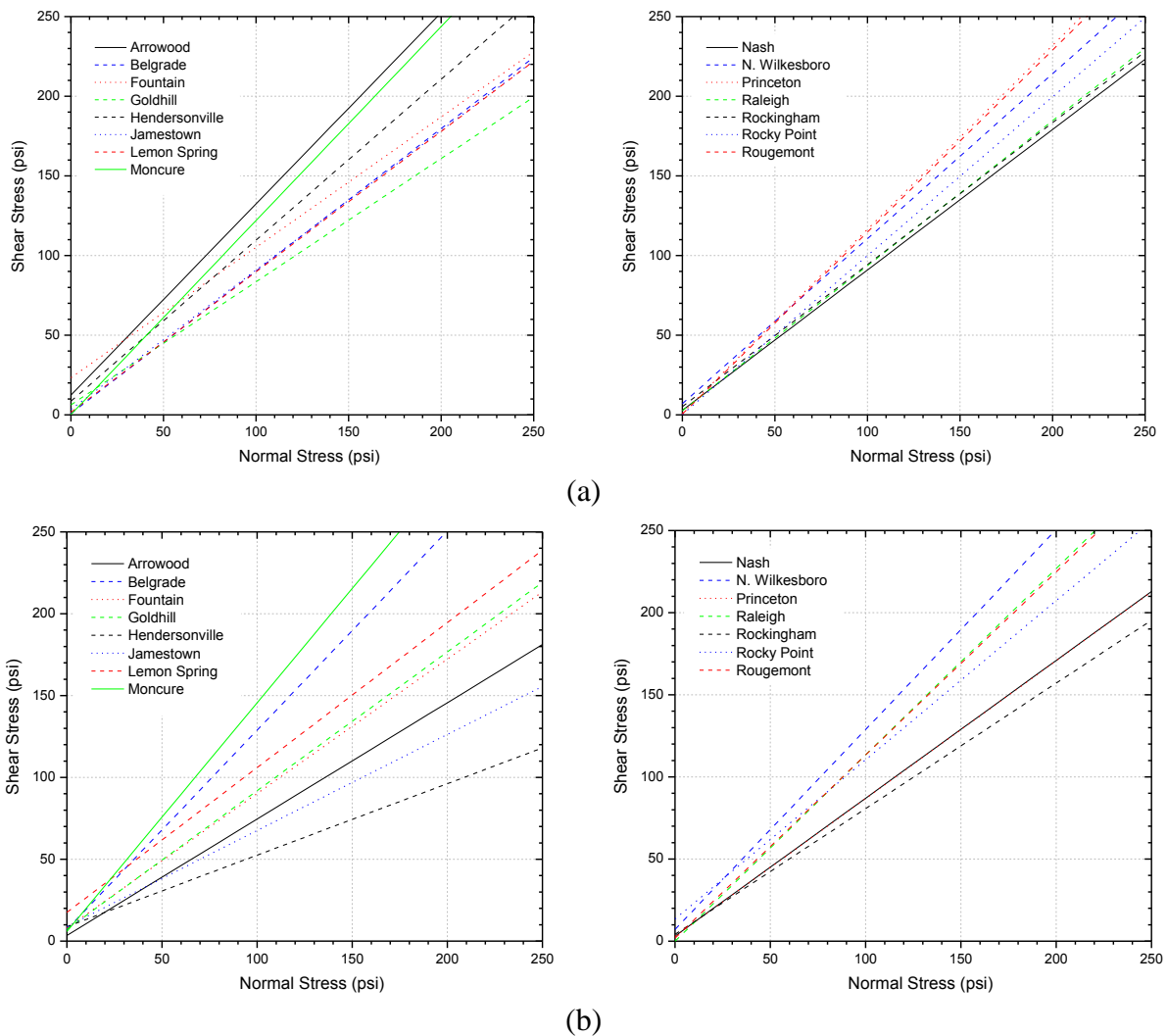


**Figure 4.2** Mohr-Coulomb envelopes for the fifteen aggregate materials: (a) EG and (b) SG

#### 4.2.5 Repeated Load Triaxial Testing for Permanent Deformation

This section presents the results from single-stage repeated load triaxial testing performed on the fifteen aggregate materials. All the materials were tested at their source gradations at selected SSR levels according to wheel load deviator stress levels. The permanent deformation tests were performed at a confining pressure of 5 psi (34.5 kPa), which closely simulates typical low confining pressure levels in the field and also considers the residual compaction stresses locked-in the granular base. For each test, 10,000 load cycles were applied at each stress level using a haversine type dynamic load pulse with a 0.1-second pulse duration and 0.9-second rest period. The loading condition and the number of load cycles are considered to capture the first two stages in the shakedown theory. Werkmeister et al. (2014) suggested three ranges for stress-strain response of unbound aggregate materials based on the magnitude of stress levels: (a) plastic shakedown; (b) plastic creep; and (c) incremental collapse.

The current permanent deformation tests were compared to those performed at the engineered gradation (EG) during Phase I of the project. The full set of permanent deformation accumulations plotted against load cycles is presented in Appendix D for all the fifteen materials tested at the SG. The results clearly indicate that the accumulation of permanent deformation increases as the applied stress to strength ratios increase. Table 4.6 lists the SSR values and the corresponding stress states for each test, and compares the stress states required to achieve the SSR at both gradations (SG and EG). For some of the aggregate materials (Lemon Spring and Rocky Point at SG, and Arrowood and Fountain at EG), the highest SSR levels achieved during testing were under 0.75 due to the high shear strength properties of these materials and the limiting equipment capacity.

The full set of permanent deformation test results at both SG and EG are shown in Figure 4.3. The results corresponding to the SG are plotted using solid lines. As shown in Figure 4.3 and Appendix D, the higher SSR levels consistently resulted in the higher permanent strain accumulations for all material types and gradations. The permanent strain accumulations for Arrowood and Rocky Point materials at SG were greater than those at their EG, while for the other materials, the permanent strain accumulations at SG were smaller than those at their EG. Considering that the results of dry density, moisture content, and shear strength at SG were different from those at EG as reported in the previous sections, the trends of permanent strain accumulation between SG and EG cannot be explained by a sole variable. Thus, in the following Chapter, the multiple linear regression analysis adopted to study those variables will be discussed. Nevertheless, Goldhill material at the 0.75 SSR accumulated the highest permanent strain at both EG and SG. This may be attributed to the existence of plastic fines in this material, because Goldhill is the only material which contains plastic fines among all the aggregate materials studied in this project. The presence of the plastic fines weakened the aggregate matrix significantly, leading to high permanent strain accumulations. Note that the same material at SG accumulated significantly lower amounts of permanent strain, compared to EG. This result is in good agreement with the recent findings about the effect of plastic fines on rutting resistance by Mishra and Tutumluer (2012). Interestingly, only for 0.75

SSR of Rocky Point at SG, the permanent strain curve showed the permanent strain rate not decreasing, which reached to the plastic creep stage, while the other materials remain at the plastic shakedown stage.

**Table 4.6** Achieved stress states and SSR for FastCell permanent deformation tests at SG & EG

Material	Source Gradation (SG)			Engineered Gradation (EG)		
	SSR	Confining pressure, $\sigma_3$	Deviator stress, $\sigma_d$	SSR	Confining pressure, $\sigma_3$	Deviator stress, $\sigma_d$
	-	psi	psi	-	psi	psi
Arrowood	0.25	5	4.8	0.25	5	16.0
	0.50	5	10.6	0.50	5	36.0
	0.75	5	17.9	0.69	5	54.8
Belgrade	0.25	5	11.7	0.25	5	4.4
	0.50	5	26.6	0.50	5	9.4
	0.75	5	46.4	0.75	5	16.0
Fountain	0.25	5	8.8	0.25	5	17.5
	0.50	5	19.6	0.50	5	37.9
	0.75	5	33.7	0.67	5	54.9
Goldhill	0.25	5	8.6	0.25	5	7.5
	0.50	5	19.9	0.50	5	16.2
	0.75	5	33.1	0.75	5	27.3
Hendersonville	0.25	5	6.7	0.25	5	11.1
	0.50	5	13.9	0.50	5	24.4
	0.75	5	22.9	0.75	5	40.0
Jamestown	0.25	5	7.5	0.25	5	5.9
	0.50	5	16.5	0.50	5	12.9
	0.75	5	27.7	0.75	5	22.0
Lemon Spring	0.25	5	17.0	0.25	5	4.7
	0.50	5	38.3	0.50	5	10.1
	0.62	5	50.0	0.75	5	17.0
Moncure	0.25	5	12.5	0.25	5	5.9
	0.50	5	28.2	0.50	5	13.2
	0.75	5	45.9	0.75	5	22.6
Nash	0.25	5	5.5	0.25	5	5.4
	0.50	5	12.2	0.50	5	12.1
	0.75	5	20.4	0.75	5	20.2
N. Wilkesboro	0.25	5	8.0	0.25	5	9.94
	0.50	5	18.1	0.50	5	22.2
	0.75	5	31.4	0.75	5	37.8
Princeton	0.25	5	5.1	0.25	5	6.0
	0.50	5	11.5	0.50	5	13.3
	0.75	5	19.9	0.75	5	23.1
Raleigh	0.25	5	5.8	0.25	5	5.5
	0.50	5	13.1	0.50	5	12.1
	0.75	5	22.7	0.75	5	20.6
Rockingham	0.25	5	5.6	0.25	5	7.5
	0.50	5	12.5	0.50	5	16.5
	0.75	5	21.2	0.75	5	28.1
Rocky Point	0.25	5	15.0	0.25	5	4.6
	0.50	5	33.9	0.50	5	9.8
	0.67	5	50.0	0.75	5	16.6
Rougemont	0.25	5	6.3	0.25	5	5.7

	0.50	5	14.5	0.50	5	12.6
	0.75	5	24.5	0.75	5	21.4

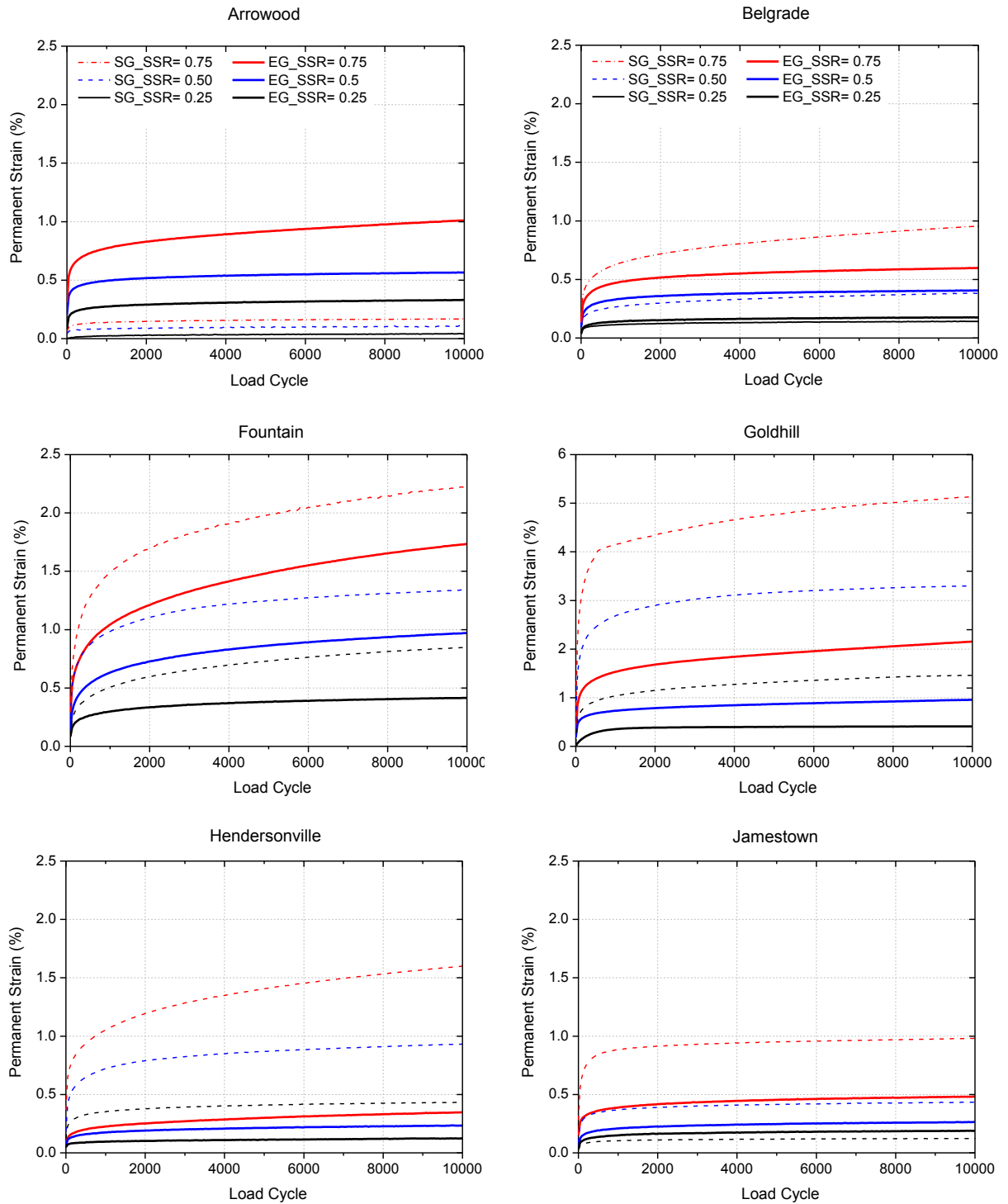


**Figure 4.3** Permanent strain accumulations in the fifteen aggregate materials at different SSR levels and gradations

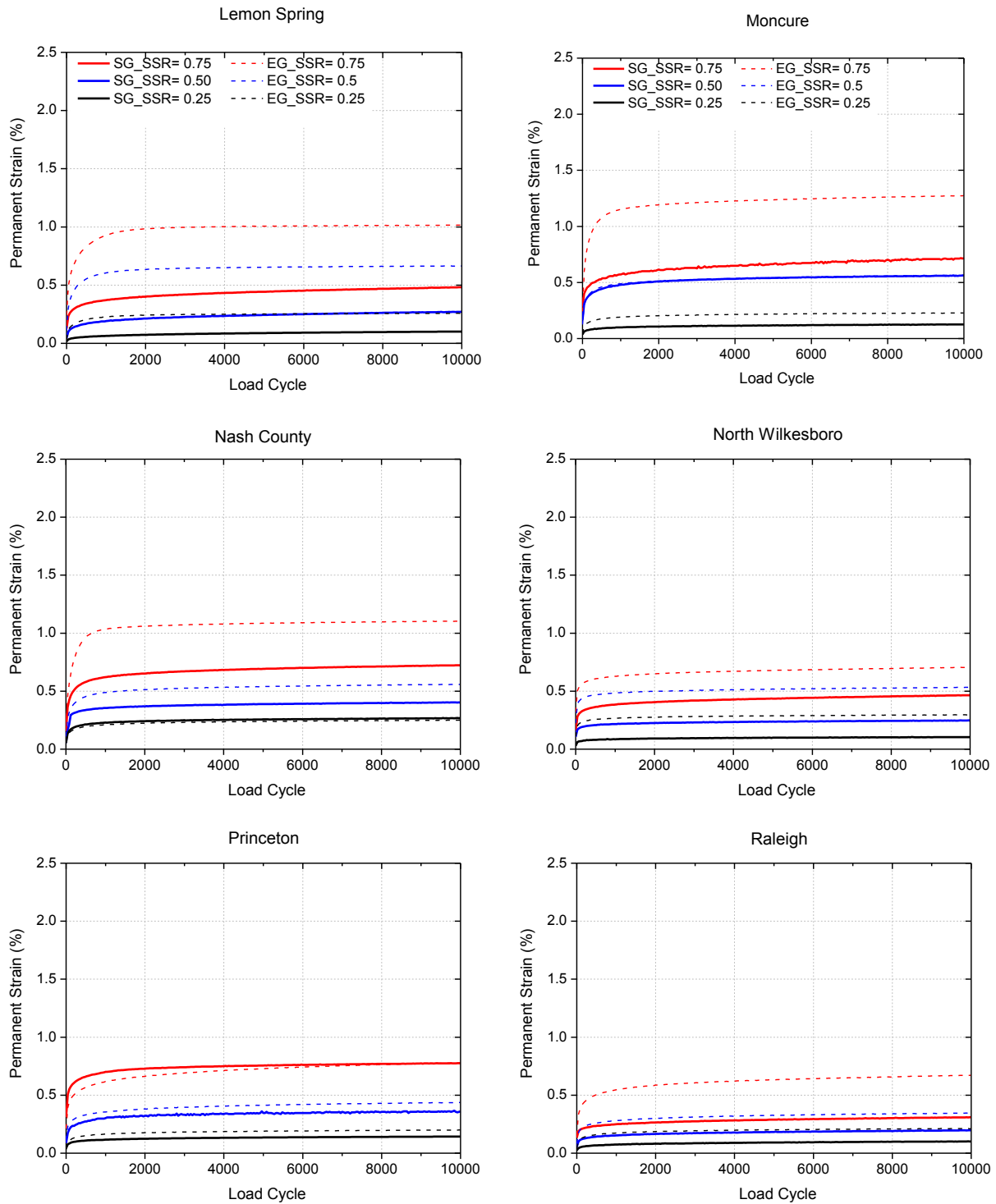


**Figure 4.3** Permanent strain accumulations in the fifteen aggregate materials at different SSR levels and gradations (cont'd)

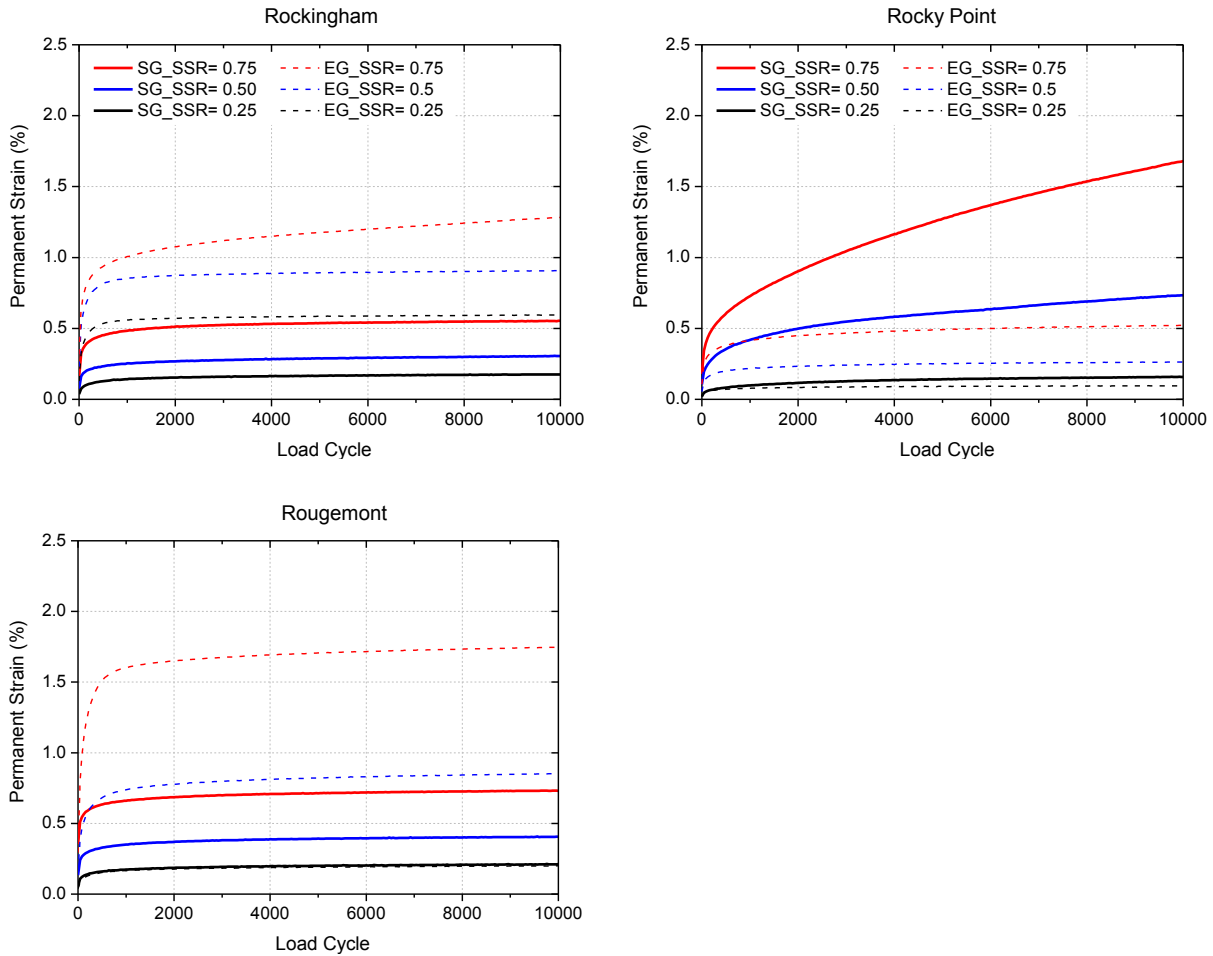


**Figure 4.3** Permanent strain accumulations in the fifteen aggregate materials at different SSR levels and gradations (cont'd)

Considering that Fountain material grain size distributions at SG and EG are almost identical, the difference in the permanent strain accumulations between EG and SG specimens for this material can be mainly influenced by the variation in the applied stress levels to achieve the different SSR values during permanent deformation testing. In general, the differences in accumulated permanent strains between the EG and SG specimens were the highest at the SSR of 0.75, and the lowest at the SSR of 0.25. This clearly implies that the effect of gradation on permanent deformation behavior of aggregates becomes more significant as the applied stress levels approach the corresponding shear strength values of the materials.

Figure 4.4 shows the permanent strains accumulated at 10,000 loading cycles for the fifteen materials tested at EG along with the deviator stress and the SSR. In general, it was found that higher values of deviator stress or SSR produce higher permanent deformations, and the relationships between permanent deformation and deviator stress/SSR were matched well with a linear approximation. It should be noted that since the materials at the same SSR level can be

assigned to different deviator stress, both the SSR and the magnitude of deviator stress need to be considered together for the permanent deformation accumulation. In Figure 4.4, the lower rate of permanent strain increase along the deviator stress/SSR levels can be linked to the improved rutting resistance of the materials. For all the aggregate materials tested at EG, the rate of permanent strain increase along the deviator stress/SSR levels is quite different from each other. In particular, the rate of permanent strain increase along the deviator stress/SSR levels for Goldhill is much higher than the other materials, which still implies the significant effect of plastic fines on permanent deformation. It should be careful to use a base aggregate material which has low permanent deformation at the low SSR level, but high permanent deformation at the high SSR level. For example, Jamestown material shows lower permanent deformation at the 0.25 SSR than those for Belgrade, Princeton, N. Wilkesboro, and Raleigh. However, at the 0.75 SSR, the permanent deformation of Jamestown is higher than those of the four materials.

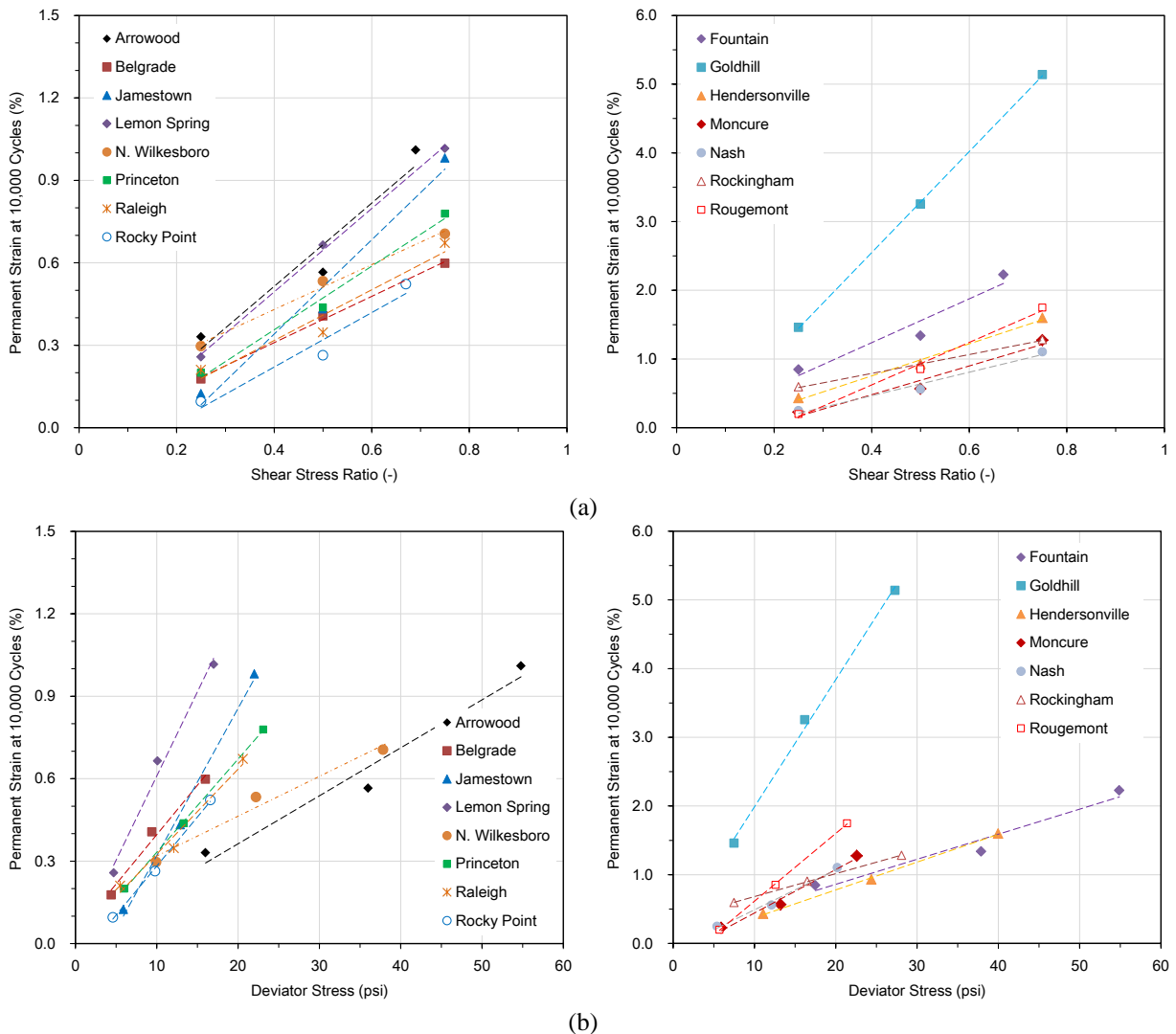


**Figure 4.4** Permanent strain values after 10,000 cycles for the fifteen materials at EG graphed with (a) applied deviator stress levels and (b) SSR values ( $\sigma_3 = 5 \text{ psi} = 34.5 \text{ kPa}$ )

Note that y-axis scales are different for the left and right graphs

Figure 4.5 shows the permanent strain accumulation at SG varying with the deviator stress and the SSR. Similar to the results at EG, the rate of increase in permanent strain with increasing deviator stress levels for Goldhill is the highest compared to other materials, but decreases compared to that of EG specimens. The result might be related to the reduction in the amount of plastic fine of SG specimens for Goldhill compared to the EG specimens. In contrast, Arrowood shows the lowest permanent strain in the low deviator stress level. However, it should be noted that Arrowood material at SG under low stress state can reach to failure, because it has a lower shear strength at SG. In fact, Arrowood material at EG also represented the best rutting resistance over the wide range of stress states showing the lowest rate of increase in permanent strain.

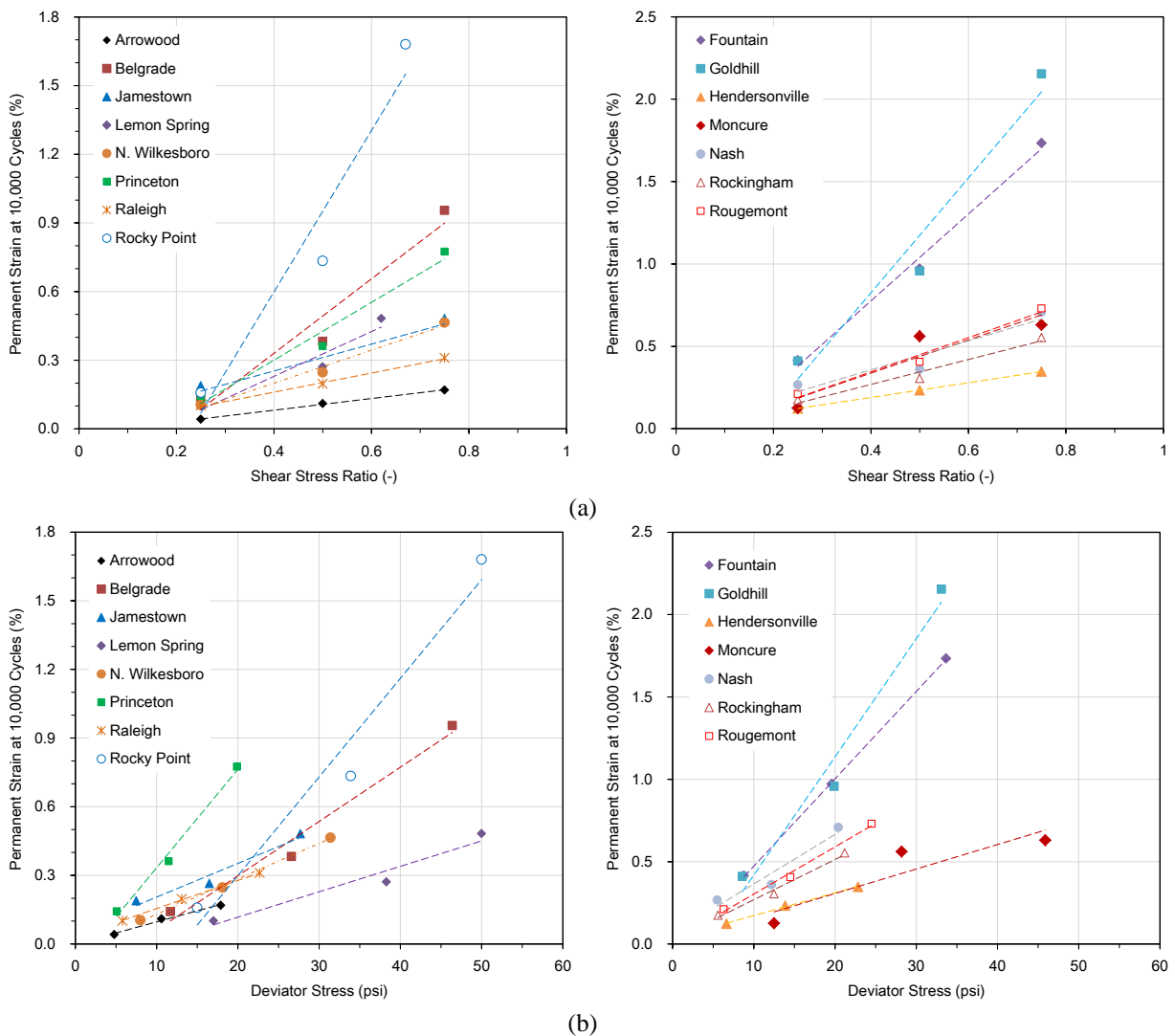


**Figure 4.5** Permanent strain values after 10,000 cycles for the fifteen materials at SG graphed with (a) applied deviator stress levels and (b) SSR values ( $\sigma_3 = 5 \text{ psi} = 34.5 \text{ kPa}$ )  
 Note that y-axis scales are different for the left and right graphs

#### 4.2.6 Resilient Modulus Testing

Resilient modulus ( $M_R$ ) tests were performed using the advanced triaxial test equipment (UI-FastCell). The test sequence of AASHTO T307-99 procedure was followed, and all materials were tested at their source gradations and compacted at MDD-OMC conditions. For each material, two samples were tested, and the results reported herein are based on the average of both samples. Resilient modulus test results, as provided in Appendix E, were fitted with the three commonly used resilient modulus models: (1) K- $\theta$  Model (Hicks and Monismith 1971), (2) Uzan Model (Uzan and Witczak 1998) and (3) MEPDG Model (Ayres 2002; NCHRP 1-37A study), to compare the differences in model performances:

$$\text{K-}\theta \text{ Model:} \quad M_R = K \theta^n \quad (4.5)$$

$$\text{Uzan Model:} \quad M_R = K_1 p_a \left( \frac{\theta}{p_a} \right)^{K_2} \left( \frac{\sigma_3}{p_a} \right)^{K_3} \quad (4.6)$$

$$\text{MEPDG Model:} \quad M_R = K_4 p_a \left( \frac{\theta}{p_a} \right)^{K_5} \left( \frac{\tau_{\text{oct}}}{p_a} + 1 \right)^{K_6} \quad (4.7)$$

where bulk stress  $\theta = \sigma_1 + \sigma_2 + \sigma_3$  ;

$\sigma_d$  is deviator stress;

$\sigma_3$  is confining pressure;

$p_a$  is atmospheric pressure (14.7 psi or 101.3 kPa);

octahedral stress,  $\tau_{\text{oct}} = \sqrt{2/3} * \sigma_d$ ; and

$n$ ,  $K$ ,  $K_1$ ,  $K_2$ ,  $K_3$ ,  $K_4$ ,  $K_5$  and  $K_6$  are model parameters obtained from regression.

The resulting model parameters for the three resilient modulus models are listed in Table 4.7. The Phase I study (Chow et al. 2014) also presented resilient modulus test results and the characterization models for the fifteen materials tested and reported by the NCDOT Material and Tests Unit. However, the results are not shown here as the samples were tested at different gradations from those studied in this project. Instead, Figure 4.6 shows the resilient modulus results varying with the bulk stress at SG for all the fifteen materials. Rocky Point material has the highest resilient modulus ( $M_R$ ) values over the whole range of bulk stresses. The difference in  $M_R$  values between Rocky Point and the other materials is more obvious at the high bulk stress. In contrast, the  $M_R$  values were the lowest for Goldhill material over the whole bulk stress levels. The difference between Goldhill and the other materials becomes much more noticeable for the higher bulk stress values due to the presence of plastic fines.

For each aggregate material, an average resilient modulus is calculated from the two laboratory  $M_R$  tests. In Chapter 5, the  $M_R$  values of the fifteen aggregate materials (fitted with the commonly used K- $\theta$  Model) will be used as a base layer property in the analysis using the ILLI-PAVE program. Note that the UIUC permanent deformation model, to be discussed in Chapter 5, incorporates both shear strength properties and applied stress states for predicting rutting in an

unbound aggregate base course, whereas the Pavement ME Design program rutting prediction model currently utilizes the resilient modulus properties.

**Table 4.7** Resilient modulus (at SG) model parameters obtained from regression analyses

Quarry	K-θ Model		Uzan Model			MEPDG 1-37A Model		
	K	n	K <sub>1</sub>	K <sub>2</sub>	K <sub>3</sub>	K <sub>4</sub>	K <sub>5</sub>	K <sub>6</sub>
Arrowood	2.04E+03	0.649	1.79E+03	0.790	-0.154	8.34E+02	0.748	-0.385
Belgrade	2.91E+03	0.580	2.60E+03	0.703	-0.135	9.76E+02	0.652	-0.282
Fountain	2.47E+03	0.589	2.30E+03	0.662	-0.080	8.37E+02	0.637	-0.188
Goldhill	2.01E+03	0.604	1.74E+03	0.763	-0.172	7.38E+02	0.720	-0.451
Hendersonville	4.08E+03	0.467	2.51E+03	0.638	-0.083	8.26E+02	0.637	-0.210
Jamestown	1.18E+03	0.742	1.04E+03	0.877	-0.146	6.30E+02	0.864	-0.473
Lemon Spring	4.07E+03	0.488	2.39E+03	0.676	-0.091	8.52E+02	0.683	-0.239
Moncure	5.14E+03	0.464	2.94E+03	0.661	-0.096	1.01E+03	0.659	-0.240
Nash County	1.72E+03	0.677	1.53E+03	0.809	-0.143	7.66E+02	0.792	-0.449
N. Wilkesboro	2.35E+03	0.606	1.99E+03	0.786	-0.196	8.70E+02	0.734	-0.499
Princeton	3.53E+03	0.534	1.65E+03	0.801	-0.130	7.78E+02	0.803	-0.331
Raleigh	2.59E+03	0.581	2.30E+03	0.710	-0.140	8.80E+02	0.671	-0.351
Rockingham	3.49E+03	0.572	3.06E+03	0.716	-0.157	1.17E+03	0.684	-0.435
Rocky Point	3.58E+03	0.566	3.22E+03	0.686	-0.131	1.16E+03	0.635	-0.267
Rougemont	2.21E+03	0.624	2.02E+03	0.724	-0.110	8.39E+02	0.704	-0.312

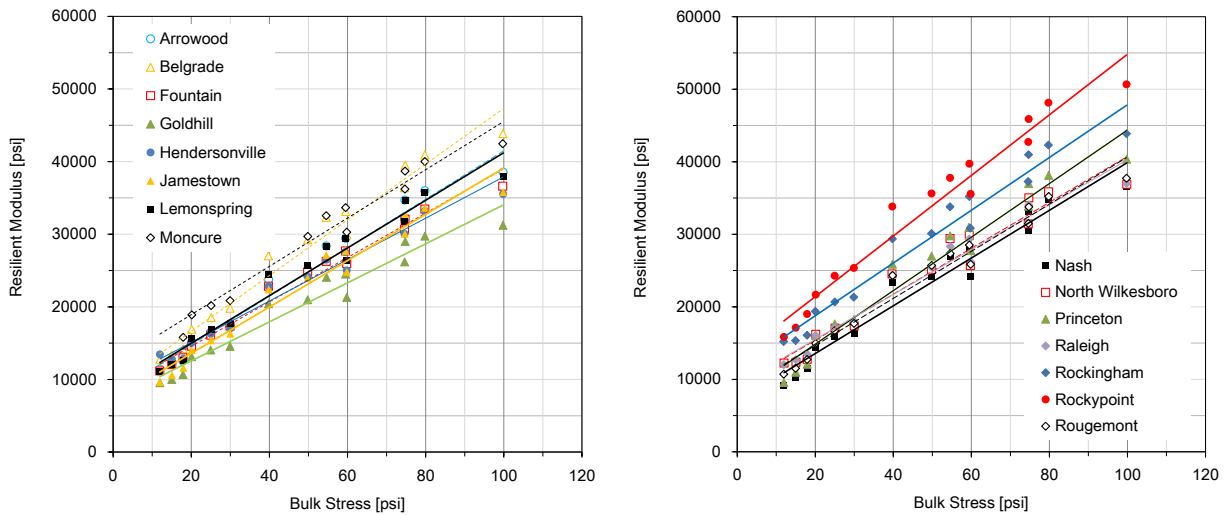


**Figure 4.6** Resilient moduli plotted at different bulk stress conditions for the fifteen aggregate materials tested at source gradations

## CHAPTER 5: UIUC PERMANENT DEFORMATION MODEL

### 5.1 Introduction

After the comprehensive laboratory characterization of the fifteen materials at the source gradations (SG), the permanent deformation accumulation trends of the fifteen materials were fitted with the UIUC rutting model previously developed in the Phase I of the project (Chow et al. 2014). The UIUC rutting model is represented as follows.

$$\varepsilon_p(N) = AN^B \sigma_d^C SSR^D \quad (5.1)$$

where

$SSR$	Shear Stress Ratio = $\frac{\tau_n}{\tau_f} = \frac{\tau_n}{c + \sigma_n \tan \phi}$
$\varepsilon_p(N)$	Permanent strain (in %) corresponding to $N$ -load application;
$\sigma_d$	Applied deviator stress;
$\tau_n$	Shear stress acting on failure plane;
$\tau_f$	Available shear strength at a normal stress (confinement);
$c$	Apparent cohesion intercept;
$\phi$	Friction angle;
$\sigma_n$	Normal stress acting on specimen failure plane; and
$A, B, C, D$	Regression parameters.

In the Phase I study, the UIUC rutting model was developed and validated using laboratory results obtained from shear strength tests and repeated load triaxial tests on the sixteen (16) North Carolina aggregate materials commonly used in base/subbase applications. The UIUC rutting model was able to predict the permanent deformation accumulation trends of the sixteen unbound aggregate materials at the engineered gradation. The model consists of three primary components: the number of load cycles, applied deviator stress level, and Shear Stress Ratio (SSR). The four different model parameters (A, B, C and D) for each material were determined.

The primary advantages of the UIUC rutting model are that (1) the stress levels applied on the specimens are effectively reflected to predict the permanent strain accumulation and (2) the shear strength properties of the materials are properly considered by incorporating the SSR ( $\tau_f/\tau_{max}$ ) term. All of the permanent deformation testing is performed at one confining pressure (5 psi = 34.5 kPa), properly considering the typical low confining pressure levels in the field and the residual compaction stresses locked-in the granular base. Note that since all the shear strength and permanent deformation tests were conducted at OMC-MDD conditions, any effect of moisture content on permanent deformation accumulation was not considered in the model parameter assignment in the Phase I study.

## 5.2 UIUC Rutting Model Results

The model parameters (*A* through *D*) for the fifteen aggregate materials are determined from a multiple linear regression analysis. After determining these model parameters, the permanent deformation can be calculated at any deviator stress level and load cycles considering that the 5-psi confining stress is the most critical low confinement experienced in a base course. Comparing the measured and predicted values of permanent strains, the accuracy of the UIUC rutting model in predicting the permanent deformation was validated in the Phase I study. This section presents the accuracy of the model in predicting permanent strains for the fifteen aggregate materials at the source gradation, including the results reported in the recent Phase II study.

Table 5.1 lists the UIUC rutting model parameters (*A* through *D*) for the fifteen aggregate materials established from the repeated load triaxial testing at the SG. The values of the four different model parameters vary widely from -15.8 to 9.4. Note that the model parameters are essentially coefficients corresponding to the least square errors between measured and predicted values of permanent strains. Nevertheless, the parameters of UIUC rutting model lead to the accurate prediction of permanent deformations, showing the high coefficient of determination ( $R^2$ ) values. The values of  $R^2$  for most aggregate materials are higher than 0.99, except for three materials: Arrowood, Goldhill, and Nash. The regression model parameters for the fifteen aggregate materials at both SG and EG are summarized in Table 5.2. Even for the same material, the model parameters obtained from multiple linear regression analyses can vary based on the changes in gradation.

**Table 5.1** UIUC rutting model parameters for the fifteen aggregate materials at source gradations

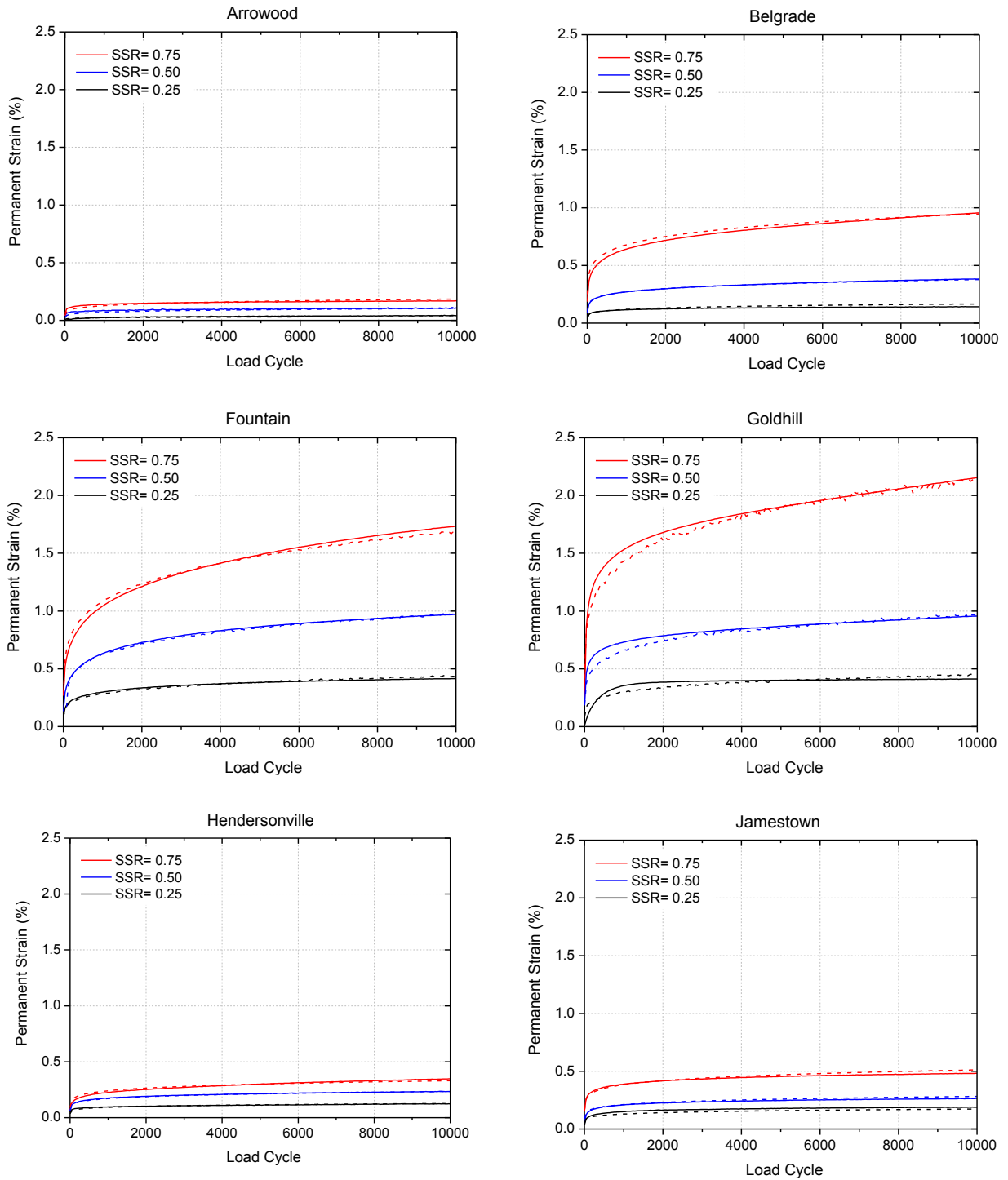
Material	Gradation	A	B	C	D	$R^2$
Arrowood	SG	9.4123	0.16261	-1.5403	3.4239	0.971
Belgrade	SG	5.086E-12	0.1446	6.0075	-5.7746	0.998
Fountain	SG	4.187E-3	0.1954	1.1840	-0.2034	0.998
Goldhill	SG	8.1828E-10	0.17715	5.3655	-5.1513	0.974
Hendersonville	SG	8.031E-01	0.1381	-0.5604	1.4849	0.992
Jamestown	SG	7.606E-15	0.1255	8.4525	-9.1565	0.991
Lemon Spring	SG	4.905E-30	0.1659	14.91	-15.8440	0.998
Moncure	SG	3.362E+17	0.1059	-9.6436	13.7790	0.999
Nash County	SG	5.1081E-12	0.0967	7.4817	-8.2813	0.981
N. Wilkesboro	SG	3.701E-03	0.0873	1.1664	-0.0568	0.998
Princeton	SG	4.160E-06	0.0959	3.5126	-2.7747	0.997
Raleigh	SG	1.000E-02	0.1188	0.8093	0.0779	0.997
Rockingham	SG	9.859E-09	0.1106	5.0550	-5.0382	0.993
Rocky Point	SG	7.128E-16	0.2620	7.8131	-7.1077	0.996
Rougemont	SG	2.1531E-6	0.0857	3.4715	-3.1729	0.996

**Table 5.2** UIUC rutting model parameters for the fifteen aggregate materials tested both at the source gradation (SG) and engineered gradation (EG)

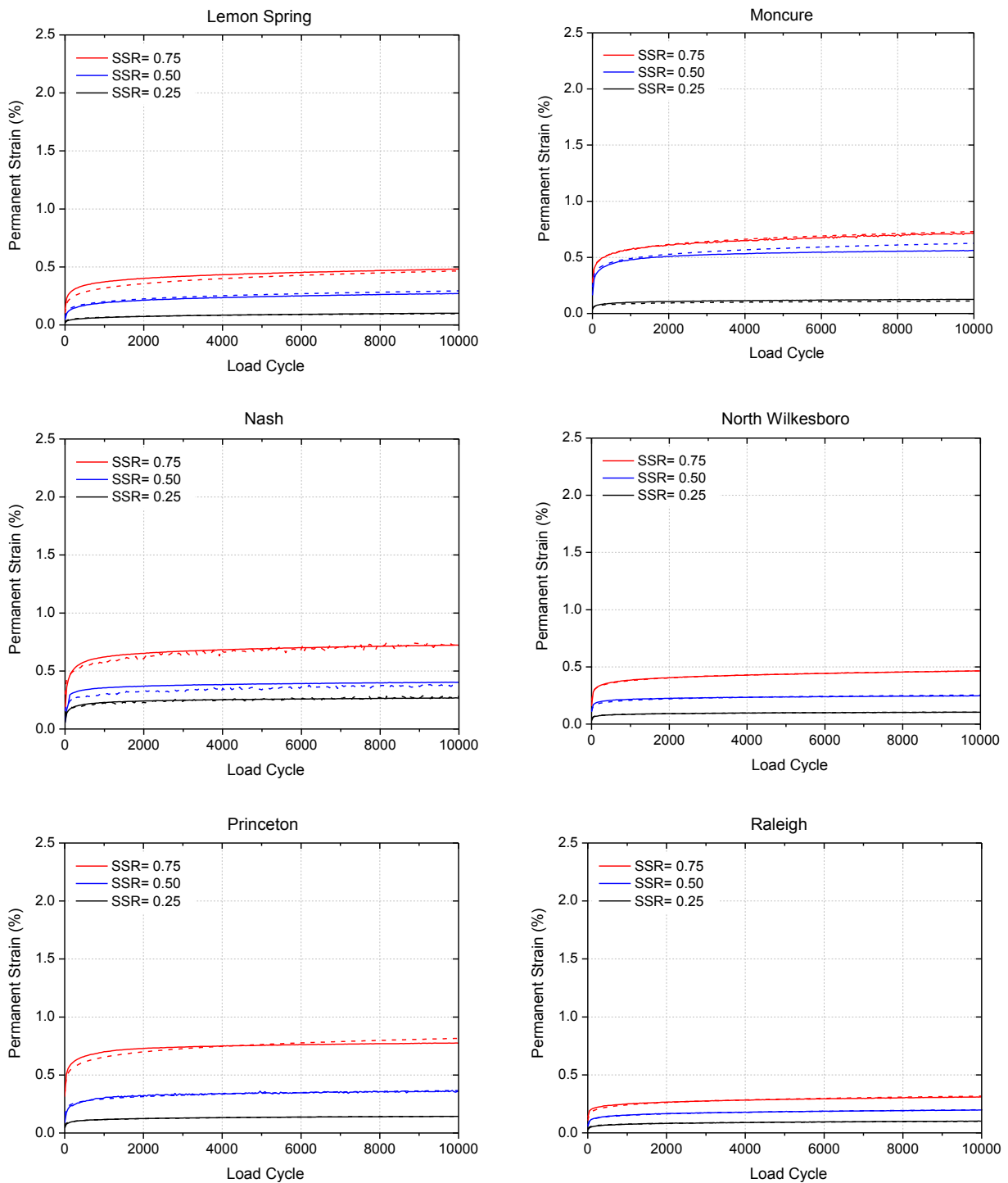
Material	Gradation	A	B	C	D	R <sup>2</sup>
Arrowood	EG	1.652E-12	0.0988	5.9649	-6.2489	0.996
	SG	9.4123	0.16261	-1.5403	3.4239	0.971
Belgrade	EG	6.460E+02	0.1227	-2.5291	4.2775	0.993
	SG	5.086E-12	0.1446	6.0075	-5.7746	0.998
Fountain	EG	3.778E-14	0.1959	6.7787	-6.9203	0.991
	SG	4.187E-3	0.1954	1.1840	-0.2034	0.998
Goldhill	EG	5.551E+00	0.1659	-0.3291	1.6501	0.982
	SG	8.1828E-10	0.17715	5.3655	-5.1513	0.974
Hendersonville	EG	1.392E-02	0.1392	0.9248	0.0085	0.995
	SG	8.031E-01	0.1381	-0.5604	1.4849	0.992
Jamestown	EG	3.422E-03	0.0994	1.5569	0.0611	0.997
	SG	7.606E-15	0.1255	8.4525	-9.1565	0.991
Lemon Spring	EG	6.050E+02	0.1220	-2.2506	4.0630	0.986
	SG	4.905E-30	0.1659	14.91	-15.8440	0.998
Moncure	EG	1.925E-06	0.1017	3.7611	-3.0862	0.994
	SG	3.362E+17	0.1059	-9.6436	13.7790	0.999
Nash County	EG	2.838E-06	0.1045	3.7036	-3.1253	0.99
	SG	5.1081E-12	0.0967	7.4817	-8.2813	0.981
N. Wilkesboro	EG	2.985E+01	0.0632	-1.0292	2.0756	0.995
	SG	3.701E-03	0.0873	1.1664	-0.0568	0.998
Princeton	EG	3.015E-03	0.1180	1.3897	-0.4778	0.996
	SG	4.160E-06	0.0959	3.5126	-2.7747	0.997
Raleigh	EG	5.639E-10	0.1169	6.0100	-6.3182	0.994
	SG	1.000E-02	0.1188	0.8093	0.0779	0.997
Rockingham	EG	1.814E-01	0.0925	0.3418	0.2204	0.965
	SG	9.859E-09	0.1106	5.0550	-5.0382	0.993
Rocky Point	EG	1.352E-02	0.1266	0.9338	0.4428	0.996
	SG	7.128E-16	0.2620	7.8131	-7.1077	0.996
Rougemont	EG	2.771E+02	0.1250	-1.6669	4.1391	0.994
	SG	2.1531E-6	0.0857	3.4715	-3.1729	0.996

Figure 5.1 shows the comparisons of the UIUC rutting model-predicted permanent strain values with the laboratory-measured values for the fifteen aggregate materials at different SSR levels at SG. The solid lines indicate the permanent strain accumulations obtained from the laboratory tests at different SSR values, and the dashed lines are those obtained from the model predictions at the corresponding SSR values. After obtaining the four model parameters, the same applied deviator stress and SSR values as those used in the laboratory tests were used for the permanent strain prediction. Using the assumed model input variables, the UIUC model predicts the permanent strains quite reasonably. As for the wide range of model parameters, the appropriate range determination based on typical aggregate behavior and forced regression analysis were recommended to improve the engineering significance of the model parameters. Based on this

recommendation, the attempts to make the forced regression analyses and furthermore, the stepwise regression analyses will be discussed next in the following sections.



**Figure 5.1** Permanent strain accumulations for the fifteen aggregate materials of SG at different SSR levels. *Solid lines represent experimental data. Dashed lines represent model predictions.*



**Figure 5.1** Permanent strain accumulations for the fifteen aggregate materials of SG at different SSR levels. *Solid lines represent experimental data. Dashed lines represent model predictions.*  
(cont'd)

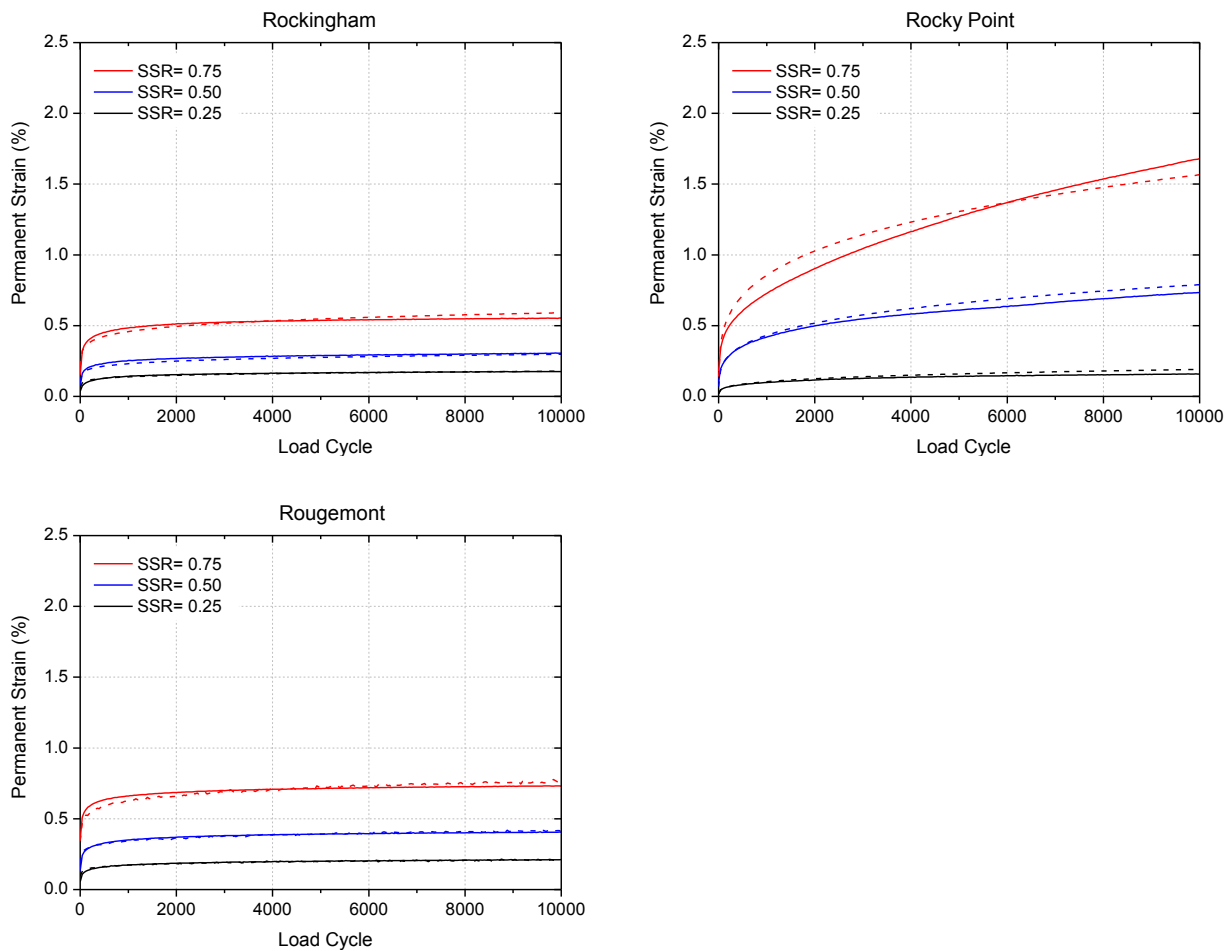


**Figure 5.1** Permanent strain accumulations for the fifteen aggregate materials of SG at different SSR levels. *Solid lines represent experimental data. Dashed lines represent model predictions.*  
(cont'd)

### 5.3 Recommended Aggregate Base Design using the UIUC Rutting Model

This section presents a recommended implementation of the UIUC rutting model to predict the in-service permanent deformation trends of unbound base/subbase layers in flexible pavements. Figure 5.2 shows the design procedure of flexible pavements with unbound aggregate layers using the UIUC rutting model. Three different scenarios of conventional flexible pavement road sections carrying low, moderate and high traffic volumes are considered with the intended evaluations of the corresponding SSR values of 0.25, 0.50 and 0.75. To estimate typical stress states at mid-depths of the aggregate base layers, the structural analyses of flexible pavements are performed by using ILLI-PAVE. For each road scenario, the typical thicknesses and material properties of three different layers are summarized in Figure 5.3. To investigate the effect of gradation on model predictions, the structural analysis using ILLI-PAVE was conducted for six different cases for each

material at both SG and EG. After running ILLI-PAVE, the mid-depth stress states in the unbound base layers under the centerline of the wheel were determined.

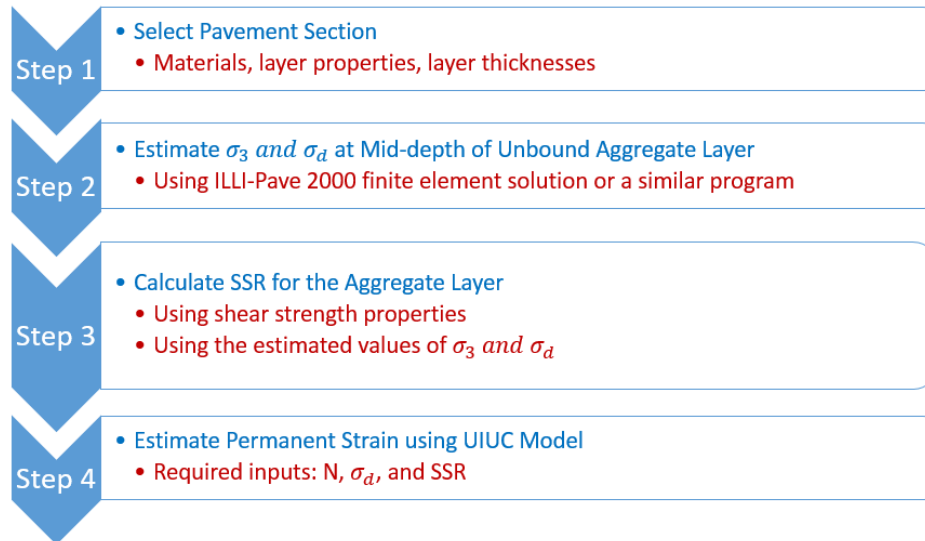


**Figure 5.2** Flowchart for using UIUC rutting model in designing conventional flexible pavements unbound aggregate layers

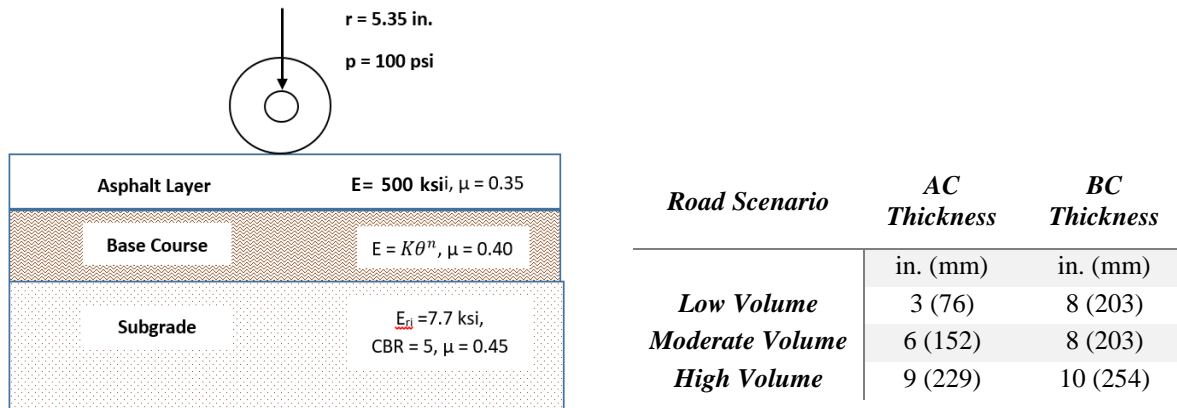


**Figure 5.3** Geometry and layer properties for the conventional flexible pavement scenarios analyzed (AC: asphalt concrete; BC: base course)

For the base course (BC) layer, the stress dependent resilient modulus properties (K and n) obtained from the laboratory resilient modulus tests were used as inputs of the structure analysis. To reflect the stress-dependent resilient modulus behavior, the K and n values previously determined for the K- $\theta$  model given in Table 4.7 were used. The K and n values are listed in Table 5.3 for the fifteen NC aggregate materials tested at the source gradations. Since the fifteen materials at EG lack the resilient modulus information, the same model fitting parameters for SG were consistently used in conducting the structural analyses of aggregate materials at EG. Also, the shear strength properties determined for each aggregate material at the SG and EG from the laboratory tests were assigned to the base course layer in the ILLI-PAVE runs.

The SSR values were calculated from the shear strength properties (see Table 5.3) for each aggregate material, using the mid-depth deviator stress in the unbound base layer determined from ILLI-PAVE analyses. Although the values of confining pressure computed from ILLI-PAVE were different for each case, the confining pressure of 34.5-kPa (5-psi) was assumed for the SSR calculation. The 34.5-kPa (5-psi) confining pressure assumption closely simulates typical confining pressure levels in the field considering typical residual compaction stresses locked-in the granular base during pavement construction and subsequent trafficking. Using the SSR values and deviator stresses determined from ILLI-PAVE and the four model parameters obtained from the multiple regression, the permanent strains at 10,000 load repetitions were predicted with the UIUC rutting model. Figure 5.4 shows the permanent strains predicted at 10,000 load repetitions and SSR values for the six different cases. The LVR, MVR, and HVR in Figure 5.4 indicate the low, medium and high volume road scenarios, respectively.

The accumulated permanent strain for each material tested at the EG and SG varied according to the road scenarios. Overall, the highest permanent strain accumulation occurred at the low volume roads, regardless of the gradation of an aggregate material. Note that at the low volume roads, the deviator stress calculated at mid-depth of the base course layer and the corresponding SSR values were the highest due to the lowest asphalt concrete (AC) thickness of 3 in. (see Figure 5.3). In addition, it was found that the computed SSRs and rutting accumulations are influenced by the shear strength properties ( $c$  and  $\phi$ ). For Belgrade, Goldhill, Moncure, and Rougemont materials, the rutting accumulations increase with an increase in the computed SSR. These materials show that the increase in the shear strength properties at SG leads to the reduction of their rutting accumulation, compared to EG. Especially for Belgrade material at EG for the low volume road, the shear stress was higher than its shear strength based on the computed SSR of 1.03, indicating premature failure. In contrast, Belgrade material at SG can survive more load repetitions due to the SSR of 0.88. On the other hand, for Arrowood, Fountain, Hendersonville, N. Wilkesboro, and Rockingham materials, the increase in the rutting accumulations with the computed SSR interestingly depended on the gradation. In fact, for these materials, the reduction of the shear strength properties at SG leads to the reduction of their rutting accumulation. In these materials, the effect of gradation, and especially  $D_{60}$  value, on the rutting accumulation seems to be more dominant than the shear strength properties. There is a combined effect of both the material properties and the applied stress states and shear strength. In fact, the  $D_{60}$  is one of the most important aggregate material properties used for correlating the rutting model parameters in section 5.5 of the report. Therefore, the assumption of resilient modulus properties at EG governing the structural analysis might be far from actual field conditions where aggregates are delivered and constructed at the SG condition. Nevertheless, the results caution that even at the low permanent strain accumulation, the higher SSR may result in a premature movement into the incremental collapse (Zone C), or failure, of the material based on the shakedown concept for unbound aggregate materials (Werkmeister et al. 2004). Thus, the SSR level estimation for design alternatives with different materials at a stress state will be required to realistically evaluate the field rutting accumulation and prevent premature failure.

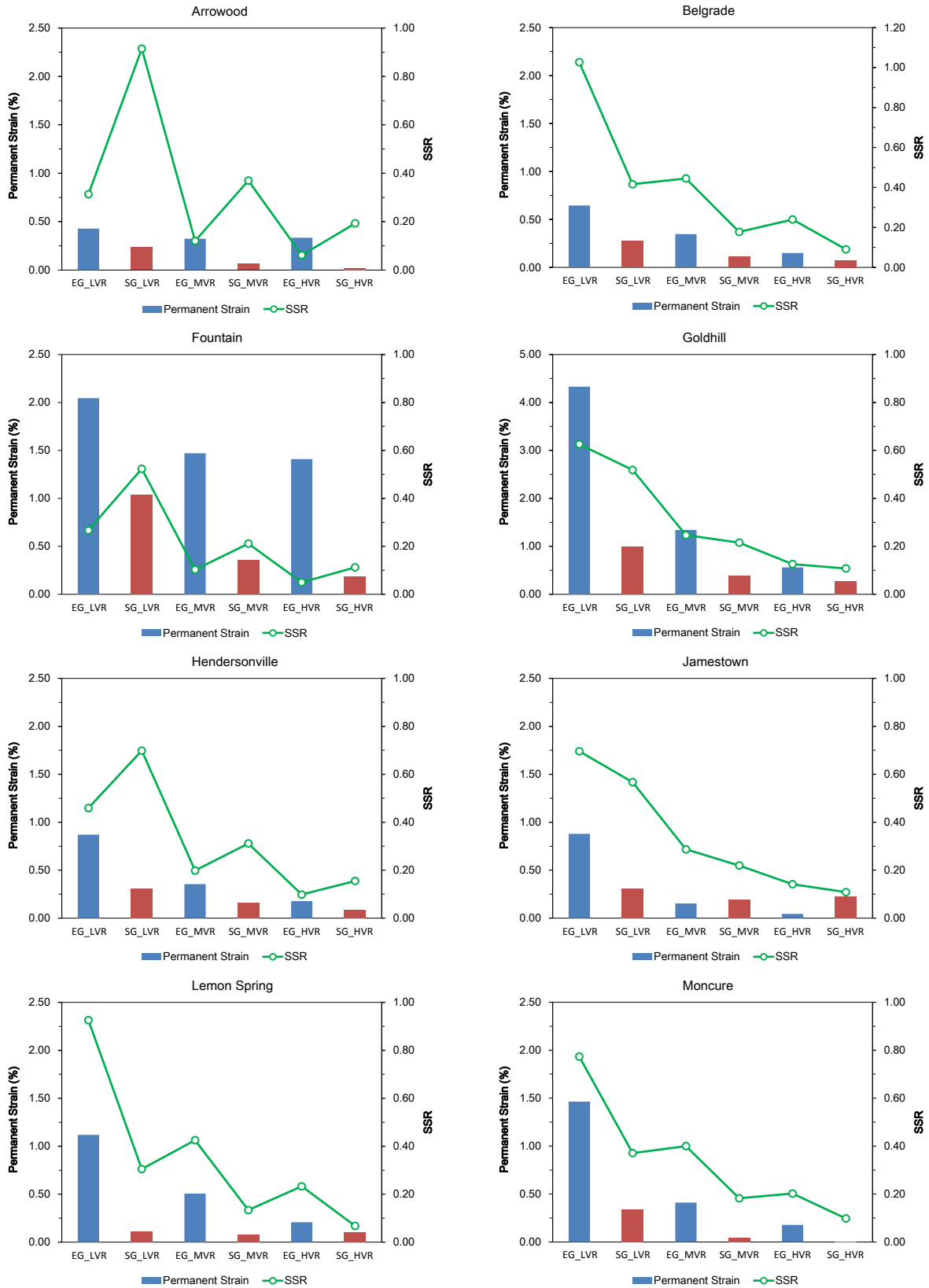
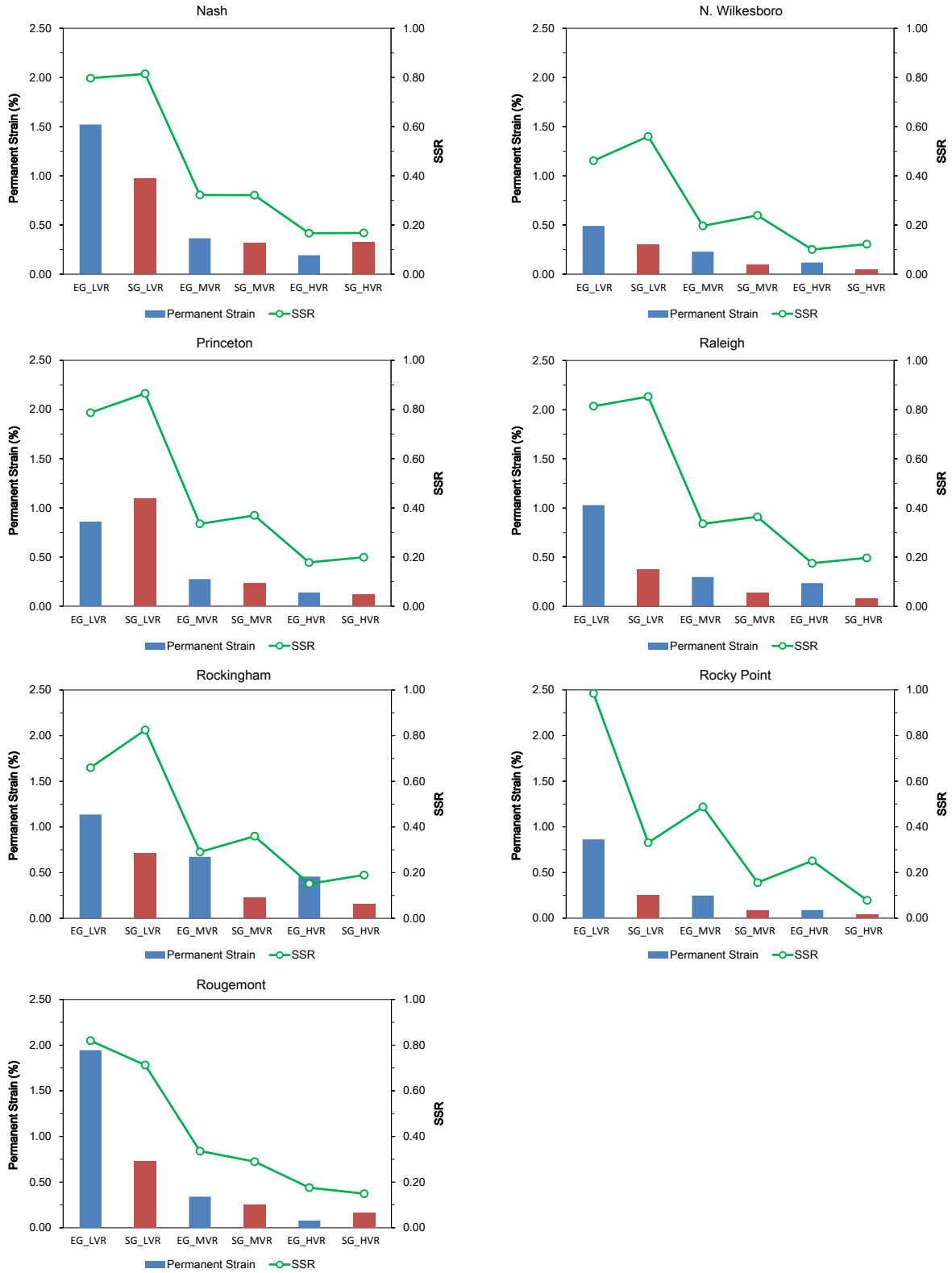


Figure 5.4 UIUC model predicted permanent deformations for the three road scenarios at the engineered (EG) and source gradations (SG) [N = 10,000 load cycles]



**Figure 5.4** UIUC model predicted permanent deformations for the three road scenarios at the engineered (EG) and source gradations (SG) [N = 10,000 load cycles] (cont'd)

**Table 5.3** Summary of resilient modulus model parameters, mid-layer stress states from ILLI-PAVE, shear strength properties and UIUC model-predicted strains for the three road scenarios

<b>Low Volume Roads (LVR)</b>									
Material / Gradation		$M_R$ ( $K - \theta$ Model)		Mid-Layer Stress States		Shear Strength Properties		SSR	Predicted strain
		K (psi)	n	$\sigma_d$ (psi)	$\sigma_3$ (psi)	$\phi$ (degree)	C (psi)		Strain (%)
Arrowood	EG	2035	0.649	20.85	0.695	50.2	12.4	0.31	0.43
	SG	2035	0.649	23.82	0.655	35.4	3.5	0.91	0.23
Belgrade	EG	2909	0.580	25.11	0.305	41.8	0.9	1.03	0.65
	SG	2909	0.580	21.13	0.165	50.6	7.1	0.42	0.28
Fountain	EG	2467	0.589	21.12	0.805	39.4	23.3	0.27	2.04
	SG	2467	0.589	20.53	0.795	39.3	8	0.52	1.03
Goldhill	EG	2011	0.604	21.08	1.665	37.7	6.3	0.63	4.33
	SG	2011	0.604	19.36	1.755	40.3	7.1	0.52	0.99
Hendersonville	EG	4081	0.467	22.03	0.225	45.3	8.6	0.46	0.87
	SG	4081	0.467	20.93	0.185	23.6	8.8	0.70	0.31
Jamestown	EG	1181	0.742	19.88	2.105	41.2	3.4	0.70	0.88
	SG	1181	0.742	19.22	2.075	30.4	8.9	0.57	0.31
Lemon Spring	EG	4075	0.488	23.48	0.325	41.4	1.6	0.93	1.12
	SG	4075	0.488	20.4	0.765	41.5	17.6	0.30	0.11
Moncure	EG	5144	0.464	23.12	1.495	50.6	0.2	0.77	1.46
	SG	5144	0.464	19.69	1.505	54.4	5.9	0.37	0.34
Nash	EG	1717	0.677	22.44	1.075	41.4	2.8	0.80	1.52
	SG	1717	0.677	22.77	0.985	40	3.1	0.81	0.97
N. Wilkesboro	EG	2349	0.606	20.05	0.685	46.0	7.0	0.46	0.49
	SG	2349	0.606	20.97	0.71	46.7	4.5	0.56	0.30
Princeton	EG	3532	0.534	24.62	0.605	49.1	1.0	0.79	0.86
	SG	3532	0.534	24.23	0.44	40.0	2.9	0.87	1.10
Raleigh	EG	2587	0.581	23.4	0.61	42.3	2.6	0.81	1.03
	SG	2587	0.581	23.07	0.63	48.6	0	0.85	0.37
Rockingham	EG	3492	0.572	23.18	1.18	41.7	5.2	0.66	1.14
	SG	3492	0.572	24.21	1.49	37.4	4.2	0.82	0.71
Rocky Point	EG	3583	0.566	24.78	1.62	44.9	0.3	0.98	0.86
	SG	3583	0.566	19.57	1.34	44.1	13.5	0.33	0.25
Rougemont	EG	2211	0.624	23.85	0.91	48.8	0.5	0.82	1.94
	SG	2211	0.624	22.92	0.83	48.1	1.9	0.71	0.73

**Table 5.3** Summary of resilient modulus model parameters, mid-layer stress states from ILLI-PAVE, shear strength properties and UIUC model-predicted strains for the three road scenarios (cont'd)

**Medium Volume Roads (MVR)**

Material / Gradation		$M_R$ ( $K - \theta$ Model)		Mid-Layer Stress States		Shear Strength Properties		SSR	Predicted strain
		K (psi)	n	$\sigma_d$ (psi)	$\sigma_3$ (psi)	$\phi$ (degree)	C (psi)		Strain (%)
Arrowood	EG	2035	0.649	7.3	2.1	50.2	12.4	0.12	0.32
	SG	2035	0.649	7.4	2.1	35.4	3.5	0.37	0.06
Belgrade	EG	2909	0.580	7.8	1.7	41.8	0.9	0.45	0.35
	SG	2909	0.580	8.0	1.7	50.6	7.1	0.18	0.11
Fountain	EG	2467	0.589	7.6	2.0	39.4	23.3	0.10	1.47
	SG	2467	0.589	7.2	2.0	39.3	8	0.21	0.36
Goldhill	EG	2011	0.604	7.0	2.4	37.7	6.3	0.25	1.34
	SG	2011	0.604	7.0	2.4	40.3	7.1	0.22	0.39
Hendersonville	EG	4081	0.467	8.4	1.5	45.3	8.6	0.20	0.35
	SG	4081	0.467	8.2	1.5	23.6	8.8	0.31	0.16
Jamestown	EG	1181	0.742	6.7	2.8	41.2	3.4	0.29	0.15
	SG	1181	0.742	6.5	2.8	30.4	8.9	0.22	0.19
Lemon Spring	EG	4075	0.488	8.2	1.4	41.4	1.6	0.43	0.51
	SG	4075	0.488	8.3	1.4	41.5	17.6	0.13	0.08
Moncure	EG	5144	0.464	9.6	0.9	50.6	0.2	0.40	0.41
	SG	5144	0.464	8.8	1.0	54.4	5.9	0.18	0.05
Nash	EG	1717	0.677	7.1	2.3	41.4	2.8	0.32	0.36
	SG	1717	0.677	7.0	2.3	40	3.1	0.32	0.32
N. Wilkesboro	EG	2349	0.606	7.5	2.0	46.0	7.0	0.20	0.23
	SG	2349	0.606	7.6	2.1	46.7	4.5	0.24	0.10
Princeton	EG	3532	0.534	8.1	1.5	49.1	1.0	0.34	0.28
	SG	3532	0.534	8.0	1.5	40.0	2.9	0.37	0.24
Raleigh	EG	2587	0.581	7.5	2.0	42.3	2.6	0.34	0.30
	SG	2587	0.581	7.4	2.0	48.6	0	0.36	0.14
Rockingham	EG	3492	0.572	8.5	1.3	41.7	5.2	0.29	0.67
	SG	3492	0.572	8.4	1.3	37.4	4.2	0.36	0.22
Rocky Point	EG	3583	0.566	9.1	1.2	44.9	0.3	0.49	0.25
	SG	3583	0.566	8.5	1.2	44.1	13.5	0.16	0.08
Rougemont	EG	2211	0.624	7.4	2.1	48.8	0.5	0.34	0.34
	SG	2211	0.624	7.4	2.1	48.1	1.9	0.29	0.25

**Table 5.3** Summary of resilient modulus model parameters, mid-layer stress states from ILLI-PAVE, shear strength properties and UIUC model-predicted strains for the three road scenarios (cont'd)

<b>High Volume Roads (HVR)</b>									
Material / Gradation		$M_R$ ( $K - \theta$ Model)		Mid-Layer Stress States		Shear Strength Properties		SSR	Predicted strain
		K (psi)	n	$\sigma_d$ (psi)	$\sigma_3$ (psi)	$\phi$ (degree)	C (psi)		Strain (%)
Arrowood	EG	2035	0.649	3.64	1.845	50.2	12.4	0.06	0.33
	SG	2035	0.649	3.59	1.88	35.4	3.5	0.19	0.02
Belgrade	EG	2909	0.580	3.82	1.665	41.8	0.9	0.24	0.15
	SG	2909	0.580	3.91	1.645	50.6	7.1	0.09	0.07
Fountain	EG	2467	0.589	3.62	1.805	39.4	23.3	0.05	1.41
	SG	2467	0.589	3.67	1.8	39.3	8	0.11	0.18
Goldhill	EG	2011	0.604	3.4	1.94	37.7	6.3	0.13	0.56
	SG	2011	0.604	3.35	1.945	40.3	7.1	0.11	0.26
Hendersonville	EG	4081	0.467	3.99	1.54	45.3	8.6	0.10	0.18
	SG	4081	0.467	3.89	1.605	23.6	8.8	0.16	0.08
Jamestown	EG	1181	0.742	3.1	2.095	41.2	3.4	0.14	0.04
	SG	1181	0.742	3.09	2.14	30.4	8.9	0.11	0.23
Lemon Spring	EG	4075	0.488	4.11	1.49	41.4	1.6	0.23	0.21
	SG	4075	0.488	4.1	1.51	41.5	17.6	0.07	0.10
Moncure	EG	5144	0.464	4.39	1.275	50.6	0.2	0.20	0.18
	SG	5144	0.464	4.55	1.24	54.4	5.9	0.10	0.01
Nash	EG	1717	0.677	3.43	1.95	41.4	2.8	0.17	0.19
	SG	1717	0.677	3.42	1.95	40	3.1	0.17	0.32
N. Wilkesboro	EG	2349	0.606	3.67	1.815	46.0	7.0	0.10	0.12
	SG	2349	0.606	3.68	1.795	46.7	4.5	0.12	0.04
Princeton	EG	3532	0.534	3.99	1.57	49.1	1.0	0.18	0.14
	SG	3532	0.534	4	1.57	40.0	2.9	0.20	0.12
Raleigh	EG	2587	0.581	3.65	1.775	42.3	2.6	0.18	0.24
	SG	2587	0.581	3.69	1.755	48.6	0	0.20	0.08
Rockingham	EG	3492	0.572	4.16	1.5	41.7	5.2	0.15	0.46
	SG	3492	0.572	4.12	1.5	37.4	4.2	0.19	0.15
Rocky Point	EG	3583	0.566	4.18	1.455	44.9	0.3	0.25	0.09
	SG	3583	0.566	4.14	1.46	44.1	13.5	0.08	0.04
Rougemont	EG	2211	0.624	3.58	1.85	48.8	0.5	0.18	0.08
	SG	2211	0.624	3.57	1.82	48.1	1.9	0.15	0.16

## 5.4 Forced Regression (Optimization) Results for UIUC Model Parameters

As previously presented in Section 5.2, using multiple linear regression to determine the UIUC rutting model parameters (A through D) for the tested aggregate materials can result in model parameters that vary over a wide range, as these model parameters are essentially coefficients that produce the least sum of square errors between the measured and predicted values of permanent strains. This section and the following section discuss an approach to improve the engineering significance of these model parameters; using forced regression and stepwise regression statistical techniques. In this approach, the values of the UIUC model parameters (A through D) will be forced to assume values within appropriate ranges that correspond to commonly observed aggregate behavior trends. Forced regression is then followed by stepwise regression to determine the most significant gradation and material properties that influence the values of the UIUC model parameters.

The goal of using forced regression is to control the values of the model parameters, obtained from multiple linear regression, within more confined ranges that permit predicting those reasonably using shear strength properties, stress variables, and other material properties that include: gradation, compaction characteristics, particle shape properties and index properties. This approach is primarily needed to eliminate any negative or unreasonably small/large model parameters previously presented in Section 5.2 that minimized the sum of errors for regression but are not indicative of unbound material behavior from an engineering point of view.

The approach used for forced regression was initiated after a pilot study in Phase II with four of the materials (Fountain, Goldhill, Nash, and Rougemont) tested at the source gradation in order to determine reasonable range values of the model parameters A, B, C, and D (Qamhia et al. 2016, Qamhia et al. 2017). The approach comprised of the following steps:

1. First, the permanent deformation results for twelve materials tested during Phase I at the EG and those for the four materials tested at the SG in Phase II were divided into groups based on the accumulated levels of permanent deformations after 10,000 load applications. Primarily, twelve of the sixteen materials tested at the EG (Chow et al. 2014) and the four materials tested at the SG (Qamhia et al., 2016, Qamhia et al., 2017) were bundled into groups with permanent deformation levels in the vicinity of 0.5%, 1.0% and 2.0% at SSR = 0.75, as shown in Figure 5.5. Multiple linear regression analyses were then performed using all the individual permanent deformation results at different SSR levels for all the materials in the same group. The results for the regression are shown in Table 5.4 below. This grouping was found to successfully eliminate any negative or excessively large/small model parameters.

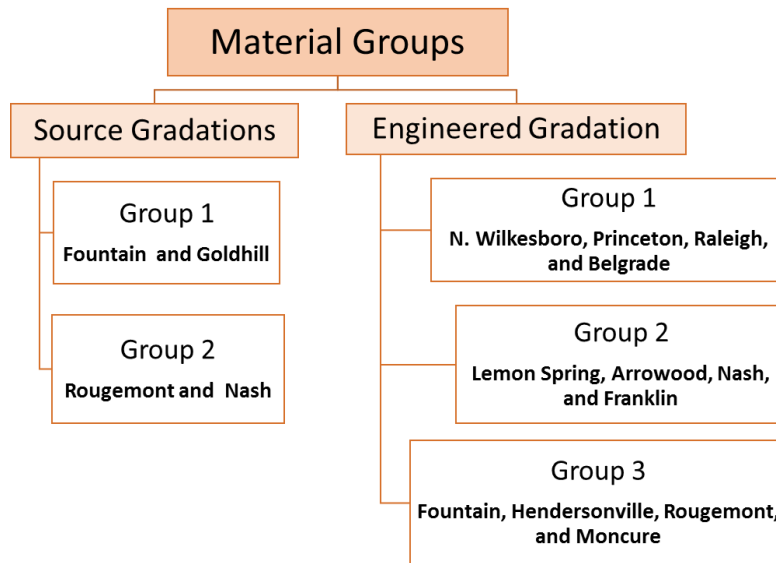


**Figure 5.5** Material grouping based on similar permanent strain levels after 10,000 load cycles at the SSR of 0.75, following Phase II study (Qamhia et al. 2016, Qamhia et al. 2017)

**Table 5.4** UIUC rutting model parameters obtained using forced regression (optimization)

<b>Source Gradations</b>	<b>UIUC Rutting Model Parameters</b>				<b>R<sup>2</sup></b>
Material	A	B	C	D	
Rougemont and Nash	0.2160	0.0922	0.1697	0.8183	0.9178
Goldhill and Fountain	0.0290	0.1866	0.7295	0.4488	0.9644
<b>Engineered Gradation</b>	<b>UIUC Rutting Model Parameters</b>				<b>R<sup>2</sup></b>
Material	A	B	C	D	
N. Wilkesboro, Princeton, Raleigh, and Belgrade	0.0694	0.1050	0.4652	0.4936	0.9569
Lemon Spring, Arrowood, Nash, and Franklin	0.3545	0.1064	0.1086	1.1157	0.9180
Fountain, Hendersonville, Rougemont, and Moncure	0.0499	0.1406	0.6951	0.6236	0.9138

- Secondly, based on the model parameters obtained from the first step from the regression analyses of multiple materials in each, appropriate ranges were selected for the UIUC rutting model parameters for forced regression parameters. The upper and lower bounds for the ranges selected for the UIUC rutting model parameters are shown in Table 5.5. Note that the ranges for B, C, and D cover the entire range of parameters obtained from step 1. For the A parameter, however, the chosen range was confined to include the most probable range achieved from step 1. This was found to significantly reduce the boundary values for the other model parameters when each material is considered separately by forced regression. Additionally, for material groups producing higher values for the ‘A’ parameter, more variations were seen between the individual results of the materials at the lower SSR values (0.25 and 0.50), which

supports using the more confined range in order to have a better control over the model parameters and their engineering significance.

**Table 5.5** UIUC rutting model parameters obtained using forced regression (optimization)

<b>Model Parameter</b>	<b>Lower Bound</b>	<b>Upper Bound</b>
A	0.02	0.09
B	0.08	0.20
C	0.10	0.90
D	0.30	1.20

3. The third and final step was to use the proposed ranges for the model parameters (shown in Table 5.5) to predict the accumulation of permanent strains for all the tested materials at the SG and EG, individually.

The results of the forced regression are shown in Table 5.6, which shows that the computed model parameters predicted the permanent deformations reasonably well, as indicated by the relatively high values obtained for the coefficient of determination ( $R^2$ ). Note that for the 32 tested materials / gradations (Franklin material at SG is missing, however, Hendersonville material was evaluated twice at OMC and  $w=5.5\%$ ), either the lower or upper bounds of the chosen forced regression range were picked up eight times for parameter ‘A’, four times for parameter ‘C’, and 15 times for parameter ‘D’. The achieved  $R^2$  values are also summarized in Figure 5.6, and the plots for the experimental and model-predicted permanent strain curves at the different SSR values are presented in Appendix H for all the 32 tested materials and gradations. As indicated by these plots, all the tested materials show that the computed model parameters predict permanent deformations reasonably well. The computed  $R^2$  values from forced regression (optimization) exceed 0.95 for 28 out of the 32 tested materials, and exceeds 0.9 for all materials, except for Nash material at the SG, which had the lowest  $R^2$  value of 0.8864.

**Table 5.6** UIUC rutting model parameters obtained from forced regression optimization for all the materials tested in Phases I, II and III of this project

<b>Gradation</b>	<b>Number</b>	<b>Material</b>	<b>A</b>	<b>B</b>	<b>C</b>	<b>D</b>	<b>R<sup>2</sup></b>
<b>Source Gradations</b>	1	Arrowood	0.0297	0.1621	0.2460	1.2000	0.9685
	2	Belgrade	0.0200	0.1411	0.7139	0.8057	0.9806
	3	Fountain	0.0203	0.1954	0.7715	0.3000	0.9969
	4	Goldhill	0.0200	0.1747	0.8846	0.3494	0.9588
	5	Hendersonville	0.0794	0.1388	0.1141	0.7375	0.9914
	6	Hendersonville (w=5.5%)	0.0200	0.1717	0.5801	0.5206	0.9969
	7	Jamestown	0.0336	0.1255	0.4605	0.3000	0.9137
	8	Lemon Spring	0.0200	0.1634	0.5838	1.1908	0.9768
	9	Moncure	0.0794	0.1205	0.4129	1.1408	0.9099
	10	Nash County	0.0687	0.0981	0.4739	0.3000	0.8864
	11	N. Wilkesboro	0.0200	0.0870	0.7218	0.4947	0.9979
	12	Princeton	0.0247	0.0959	0.9000	0.4445	0.9914
	13	Raleigh	0.0200	0.1186	0.5995	0.3400	0.9966
	14	Rockingham	0.0293	0.1107	0.6537	0.3000	0.9712
	15	Rocky Point	0.0200	0.1797	0.7737	1.2000	0.9858
	16	Rougemont	0.0368	0.0862	0.7119	0.3000	0.9861
<b>Engineered Gradation</b>	1	Arrowood	0.0367	0.0978	0.6072	0.3000	0.9705
	2	Belgrade	0.0794	0.1244	0.4021	0.6795	0.9856
	3	Fountain	0.0341	0.1981	0.6098	0.3000	0.9748
	4	Franklin	0.0794	0.1068	0.4693	0.6397	0.9760
	5	Goldhill	0.0794	0.1854	0.8099	0.3000	0.9765
	6	Hendersonville	0.0370	0.1391	0.6822	0.3000	0.9953
	7	Jamestown	0.0318	0.0998	0.9000	0.8669	0.9968
	8	Lemon Spring	0.0794	0.1145	0.6194	0.5669	0.9780
	9	Moncure	0.0319	0.1088	0.9000	0.4864	0.9864
	10	Nash County	0.0300	0.1087	0.9000	0.3048	0.9838
	11	N. Wilkesboro	0.0794	0.0805	0.4381	0.3000	0.9871
	12	Princeton	0.0259	0.1181	0.7641	0.3000	0.9956
	13	Raleigh	0.0369	0.1167	0.6107	0.3000	0.9543
	14	Rockingham	0.0794	0.1815	0.3949	0.3000	0.9359
	15	Rocky Point	0.0200	0.1264	0.8092	0.5972	0.9962
	16	Rougemont	0.0794	0.1194	0.7790	1.1078	0.9912

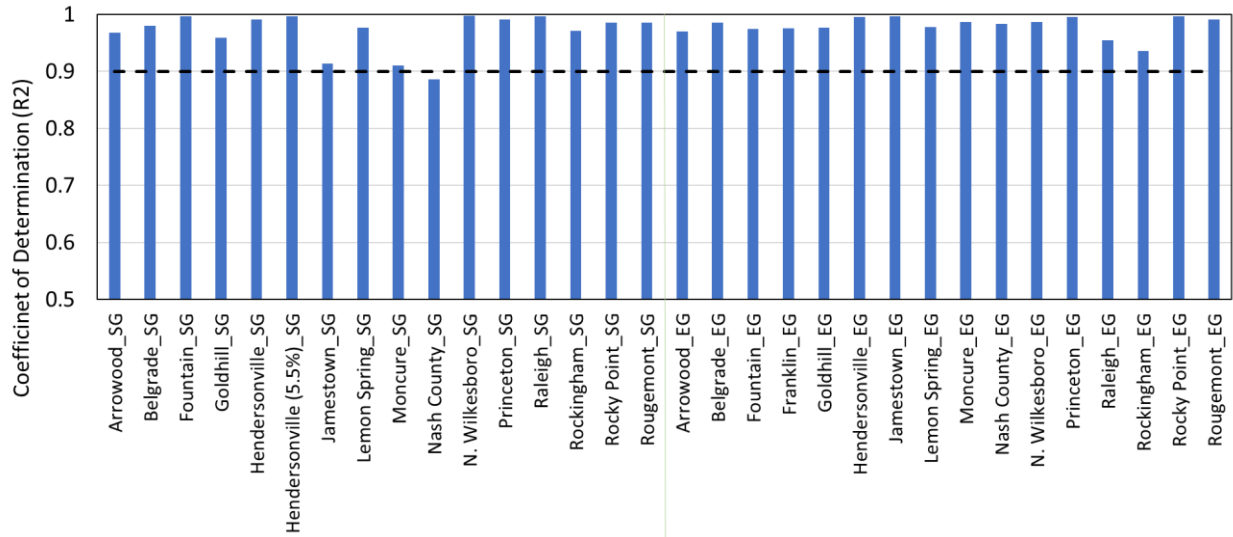


**Figure 5.6** Achieved coefficients of determination ( $R^2$ ) for all the tested materials at EG and SG using the forced regression (optimization) technique

In conclusion, it is clear that using the model parameters obtained by the forced regression (optimization) technique can predict the permanent strain accumulations reasonably well; this is accomplished by comparing the model predictions and the laboratory results for all the materials at the SG and EG at the different SSR levels. Thus, the forced regression optimization technique can be successfully applied to obtain reasonable permanent deformation predictions using the UIUC rutting model, while eliminating any negative or excessively low/high values for the model parameters that do not have engineering significance.

### 5.5 Stepwise Regression Results for UIUC Model Parameters

Stepwise regression which is used in data mining is a method of fitting regression models where the selection of predictive variables is conducted by an automatic procedure. JPM statistical analysis software was used in this study for stepwise regression analysis (Ron Klimberg, B. D. McCullough, “Fundamentals of Predictive Analytics with JMP®, Second Edition”, SAS Institute 2016).

Using stepwise regression, an attempt to correlate the model parameters assigned in the UIUC rutting model with aggregate material properties, such as gradation characteristics, compaction properties, index properties, and morphological particle shape properties was established. The model parameters obtained from the forced regression analysis (optimization) were used in this analysis. Stepwise regression was used to automatically select the most significant variables that influence the magnitude of the UIUC rutting model parameters (A through D) from a multitude of candidate variables such as gradation and material index properties and morphological shape properties. Stepwise regression is a statistical method in which the candidate variables are checked

for significance by adding them incrementally to the model, and removing any variable whose significance is reduced below a specified tolerance, through a cutoff probability for adding and removing variables (Draper and Smith, 1981). The first step for stepwise regression comprised collecting the candidate variables that are expected to influence the magnitude of the UIUC rutting model parameters. In total, 26 variables that are expected to influence model parameters were considered. These 26 variables were divided into gradation properties (14 variables), compaction properties (five variables), index properties (1 variable), shear strength properties (3 variables), and morphological shape properties (3 variables). The 26 variables for each of the 32 materials are summarized in Appendix F. The selected variables are:

- **Selected gradation properties:** Coefficient of uniformity ( $C_c$ ), coefficient of curvature ( $C_u$ ),  $D_{10}$ ,  $D_{30}$ ,  $D_{50}$ ,  $D_{60}$ , percent passing 1.5 in. (38.1 mm) sieve, percent passing 1.0 in. (25.4 mm) sieve, percent passing 0.5 in. (12.7 mm) sieve, percent passing No. 4 (4.75 mm) sieve, percent passing No. 10 (2 mm) sieve, percent passing No. 40 (0.425 mm) sieve, percent passing No. 200 (0.075 mm) sieve, and percent passing No. 200 (0.075 mm) sieve divided by  $\log_{10}(C_u)$ .
- **Selected compaction properties:** Optimum moisture content, achieved moisture content, the ratio of achieved moisture content to optimum moisture content, maximum dry density (MDD) in pcf, and  $MDD^2$  divided by percent passing No. 40 (0.425 mm) sieve.
- **Selected index property:** Plasticity index (PI).
- **Selected shear strength properties:** Friction angle, secant friction angle, and cohesion.
- **Selected imaging based morphological shape properties:** Angularity Index (AI), Surface Texture Index (STI), and Flat and Elongated Ratio (FER)

Three different analyses were conducted using stepwise regression. The first analysis included all 32 tested materials and gradations. One of these materials (Goldhill) has a Plasticity Index (PI) of six, while all other materials are nonplastic. The researchers strongly believe that PI is one of the most significant variables that correlate with the values of the UIUC rutting model parameters. However, since only one of the materials tested was plastic, insufficient data was available to establish a robust correlation between PI and the UIUC model parameters. Thus, the second and third analyses omitted Goldhill from the pool of data and used the remaining 30 tested materials/gradations.

Additionally, the second analysis considered all the aforementioned 26 variables, while the third analysis included only 23 variables when the morphological shape properties were omitted. Generally, DOTs can have limited capabilities in measuring morphological shape properties since these are imaging based quantifications of aggregate particle flatness and elongation, texture and angularity. Reducing the regression coefficients to 23 allows utilizing readily available material properties as inputs into the proposed UIUC model and reasonably estimates the accumulated rutting. Note that quite satisfactory results were obtained in a previous study when model parameters of the MEPDG resilient modulus model were determined from aggregate gradation and shape properties [Xiao and Tutumluer 2012 (<http://www.lrrb.org/pdf/201201.pdf>) and Xiao et

al. 2012]. However, the satisfactory results were obtained with a significantly larger dataset exceeding 375 observations; 115 of which with known imaging-based shape properties.

The results from the three analyses are described in more details below:

### **Analysis 1: Including all 32 tests & considering image-based shape properties**

The first analysis conducted using stepwise regression considered data from all the 32 tests conducted at the source and engineered gradations, and considered all 26 material variables including aggregate shape properties. JMP statistical tool was used to conduct the stepwise regression analyses [[https://www.jmp.com/en\\_us/home.html](https://www.jmp.com/en_us/home.html)] to determine the most significant variables that correlate with each of the model parameters. Table 5.7 shows the most significant variables that correlated with each of the model parameters, along with the P-value for each of the model parameters. Typically, a P-value less than 0.05 indicates a good correlation.

Note that plasticity index was selected as one of the most significant properties that correlated well with parameters B and C for the UIUC rutting model. However, since only one material is plastic (Goldhill), more tests with plastic materials are needed to determine a robust correlation. Additionally, when all 32 materials were considered, none of the image-based shape properties were found to be a significant variable that correlates with the UIUC rutting model parameters.

Figure 5.7 shows the achieved coefficients of determination for the individual materials using the significant variables and the estimate values from Table 5.7 used to compute the model parameters A, B, C and D. The obtained model parameters are listed in Table 5.8. Note that if an  $R^2$  of 0.5 or higher is obtained, the prediction is considered successful. A negative  $R^2$  indicates a poor fitting (i.e. the sum of squared errors between the fitted model and the data are high). The negative  $R^2$  values are indicated in Figure 5.7 for 10 aggregate materials with missing bar chart data. When all 32 tests were considered, the predictions using the estimates obtained from stepwise regression successfully predicted the experimental data for only 17 of the 32 materials (11 at SG and 6 EG), which indicates a 53 % success rate. Also, note that permanent deformations predicted for source gradations had a higher success rate than those predicted for tests at the engineered gradations, partly due to the effect of gradation that is picked up and gradation variables represented as important predictors by the model parameters.

Following this first analysis using data from all 32 tests, a second analysis was carried out omitting Goldhill, and using the remaining 30 tests. The reason for this analysis was to achieve significantly improved correlations between the UIUC rutting model parameters and material properties. Since only one of the tested materials was plastic, more investigation is required to assess the sensitivity of the UIUC model parameters to the plasticity of fines, and achieve a robust correlation.

**Table 5.7:** Significant variables that correlate with the UIUC model parameters when all 32 tests are considered

**Parameter: Log (A),  $R^2 = 0.45$**

Term	P-Value	Estimate	Std Error	t Ratio	Prob> t
Intercept		-0.060895	0.642689	-0.09	0.9252
Cc	0.00228	-0.274559	0.081142	-3.38	0.0023
P_2 mm	0.01119	-0.037667	0.013792	-2.73	0.0112
Achieved Moisture Content	0.24483	0.0682338	0.057343	1.19	0.2448
Friction Angle	0.07109	-0.00975	0.005181	-1.88	0.0711
P_0.075 mm/log (Cu)	0.00533	0.1254312	0.041253	3.04	0.0053

**Parameter: B,  $R^2 = 0.52$**

Term	P-Value	Estimate	Std Error	t Ratio	Prob> t
Intercept		0.0981721	0.082443	1.19	0.2441
OMC	0.03651	0.0174454	0.007928	2.20	0.0365
Cohesion	0.00296	0.00045	0.000138	3.27	0.0030
Achieved Moisture Content/OMC	0.12715	-0.099132	0.062984	-1.57	0.1272
Plasticity Index	0.02327	0.0079867	0.00332	2.41	0.0233

**Parameter: C,  $R^2 = 0.58$**

Term	P-Value	Estimate	Std Error	t Ratio	Prob> t
Intercept		1.6389201	0.434949	3.77	0.0009
P_0.075 mm	0.00047	-0.072984	0.018264	-4.00	0.0005
Achieved Moisture Content	0.07757	-0.085171	0.046347	-1.84	0.0776
Friction Angle	0.00660	0.010972	0.003716	2.95	0.0066
(Max Dry Density) <sup>2</sup> /P_0.425	0.00014	-0.000497	0.000111	-4.46	0.0001
Plasticity Index	0.02454	0.0454225	0.019028	2.39	0.0245

**Parameter: D,  $R^2 = 0.47$**

Term	P-Value	Estimate	Std Error	t Ratio	Prob> t
Intercept		-5.052434	1.830637	-2.76	0.0101
D60	0.00055	0.0935974	0.02399	3.90	0.0005
Max Dry Density	0.03097	0.0244371	0.010756	2.27	0.0310
Achieved Water Content	0.01062	0.2391464	0.087335	2.74	0.0106

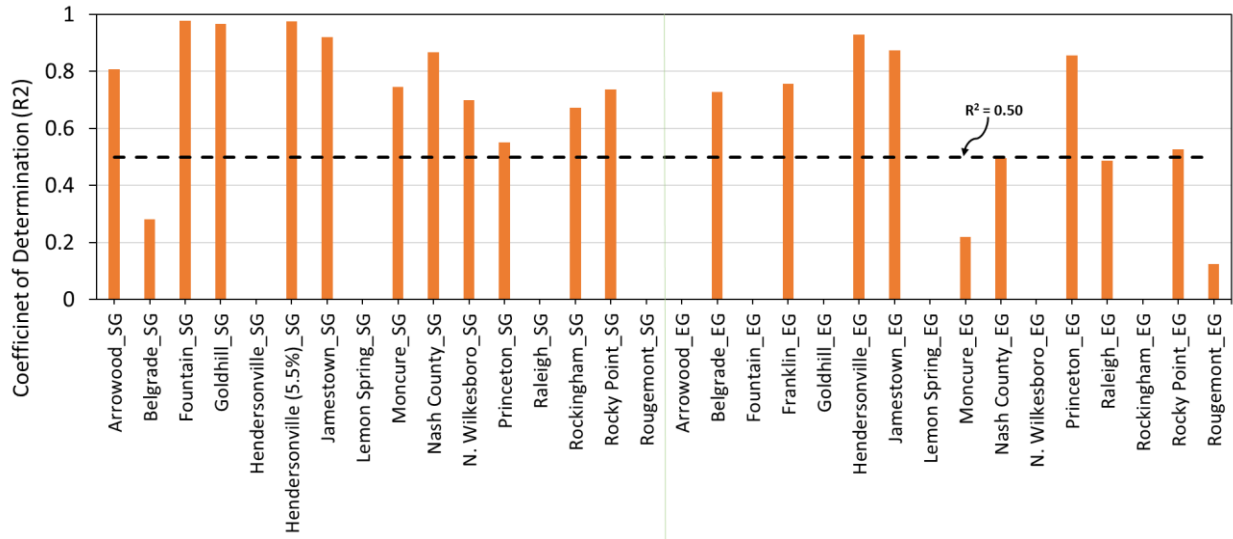


**Figure 5.7** Achieved coefficients of determination ( $R^2$ ) for all the tested materials, using stepwise regression technique and including data from all 32 tests (negative  $R^2$  values for 10 aggregate materials with missing bar chart data)

**Analysis 2: Omitting Goldhill, including 30 tests & considering image-based shape properties**

The second analysis conducted using stepwise regression omitted Goldhill, the only plastic material, and considered data from the remaining 30 tests at the source and engineered gradations. All 25 material variables and shape properties were also considered in this analysis, and plasticity index PI was excluded. JMP statistical tool was used to conduct the stepwise regression to determine the most significant variables that correlate with the UIUC rutting model parameters A, B, C and D. Table 5.9 presents the most significant variables that correlated with each of the four model parameters (A through D), along with the P-value and the estimate for each of the parameters.

Compared to the first analysis, the achieved coefficients of determination ( $R^2$ ) for each of the model parameters are significantly higher and ranging from 0.44 for the ‘B’ parameter to 0.71 for the ‘D’ parameter. Additionally, one of the image-based shape properties, namely angularity index, was picked as one of the most significant variables that correlated well with two of the UIUC rutting model parameters: log (A) and D. Figure 5.8 shows the achieved coefficients of determination for the individual tests, using the significant variables and the estimate values from Table 5.9. Similar to the first analysis, if an  $R^2$  of 0.5 or higher is obtained, the prediction is considered successful. A negative  $R^2$  indicates a poor fitting. When Goldhill was omitted in this analysis, the fitting equations using the estimates obtained from stepwise regression successfully predicted the experimental data for 21 of the 30 materials (13 at SG and 8 EG), which indicates a 70 % success rate. Similarly for this analysis, the permanent deformations predicted for source gradations had a higher success rate than those predicted for tests at the engineered gradations.

**Table 5.8** UIUC rutting model parameters obtained from stepwise regression analysis #1 including imaging properties for all the materials tested in Phases I, II and III of this project

<b>Gradation</b>	<b>Number</b>	<b>Material</b>	<b>A</b>	<b>B</b>	<b>C</b>	<b>D</b>	<b>R<sup>2</sup></b>
<b>Source Gradations</b>	1	Arrowood	0.0440	0.1114	0.2956	1.0725	0.8085
	2	Belgrade	0.0224	0.1429	0.7947	0.7606	0.2804
	3	Fountain	0.0346	0.1509	0.7162	0.3313	0.9788
	4	Goldhill	0.0185	0.1714	0.9233	0.2609	0.9660
	5	Hendersonville	0.0657	0.1586	0.2173	0.4671	-
	6	Hendersonville (w=5.5%)	0.0300	0.1148	0.6011	0.4432	0.9754
	7	Jamestown	0.0370	0.1429	0.4157	0.5377	0.9204
	8	Lemon Spring	0.0467	0.1519	0.5479	0.7593	-
	9	Moncure	0.0618	0.1310	0.4253	1.0880	0.7456
	10	Nash County	0.0692	0.1138	0.4429	0.2745	0.8664
	11	N. Wilkesboro	0.0198	0.0999	0.6314	0.7411	0.6991
	12	Princeton	0.0199	0.1235	0.7658	0.5594	0.5506
	13	Raleigh	0.0216	0.1308	0.8491	0.6605	-
	14	Rockingham	0.0392	0.1131	0.6428	0.4114	0.6721
	15	Rocky Point	0.0210	0.1524	0.7476	0.9762	0.7362
	16	Rougemont	0.0196	0.1291	0.6656	0.7595	-
<b>Engineered Gradation</b>	1	Arrowood	0.0302	0.1177	0.7414	0.4737	-
	2	Belgrade	0.0585	0.1378	0.5365	0.6486	0.7279
	3	Fountain	0.0411	0.1974	0.6696	0.2688	-
	4	Franklin	0.0455	0.1095	0.5530	0.4966	0.7564
	5	Goldhill	0.0557	0.1844	0.7734	0.6998	-
	6	Hendersonville	0.0383	0.1361	0.7134	0.3180	0.9299
	7	Jamestown	0.0440	0.1244	0.6283	0.4460	0.8737
	8	Lemon Spring	0.0452	0.1055	0.6179	0.4767	-
	9	Moncure	0.0345	0.0979	0.7052	0.5594	0.2190
	10	Nash County	0.0445	0.1175	0.6175	0.4870	0.4964
	11	N. Wilkesboro	0.0383	0.1118	0.6922	0.4201	-
	12	Princeton	0.0335	0.1048	0.7680	0.2951	0.8556
	13	Raleigh	0.0443	0.1281	0.6360	0.4449	0.4860
	14	Rockingham	0.0442	0.1378	0.6265	0.4650	-
	15	Rocky Point	0.0452	0.1064	0.6523	0.4448	0.5260
	16	Rougemont	0.0377	0.1234	0.6877	0.5285	0.1248

“-“ indicates negative R<sup>2</sup> values for 10 aggregate materials tested at EG and SG.

The obtained model parameters are shown in Table 5.10. The individual test results for all the tested materials at the different SSR values of 0.25, 0.50, and 0.75 are shown in Appendix H. The model parameters listed in Table 5.10 are based on the following model and the individual material properties:

$$\varepsilon_p(N) = AN^B \sigma_d^C SSR^D$$

$$A = 10^{[-6.393 - 0.257C_c + 0.202D_{50} + 0.039P_{12.7mm} - 0.0301\phi + 0.0409\phi_s - 0.009 \text{ Cohesion} + 0.0014AI + 0.106 \frac{P_{0.075mm}}{\log(C_u)}]}$$

$$B = 0.0991 + 0.0175 OMC + 0.00045 \text{ Cohesion} - 0.1006 \frac{AMC}{OMC}$$

$$C = 1.6664 - 0.0752P_{0.075mm} - 0.0869AMC + 0.011\phi - 0.0005 \frac{MDD^2}{P_{0.425mm}}$$

$$D = -8.578 - 0.1162 C_c + 0.149D_{60} + 0.0411 MDD + 0.34 AMC - 0.0199 \phi_s + 0.00476 \text{ Cohesion} + 0.00172AI + 0.1145 \frac{P_{0.075}}{\log(C_u)}$$

where

$C_c$	Coefficient of curvature	AI	Angularity Index
$C_u$	Coefficient of uniformity	OMC	Optimum moisture content
$P_{x \text{ mm}}$	Percent passing sieve size 'x mm'	AMC	Achieved moisture content
$\phi$	Friction angle	MDD	Maximum dry density (pcf)
$\phi_s$	Secant Friction angle	Cohesion	Cohesion in kPa

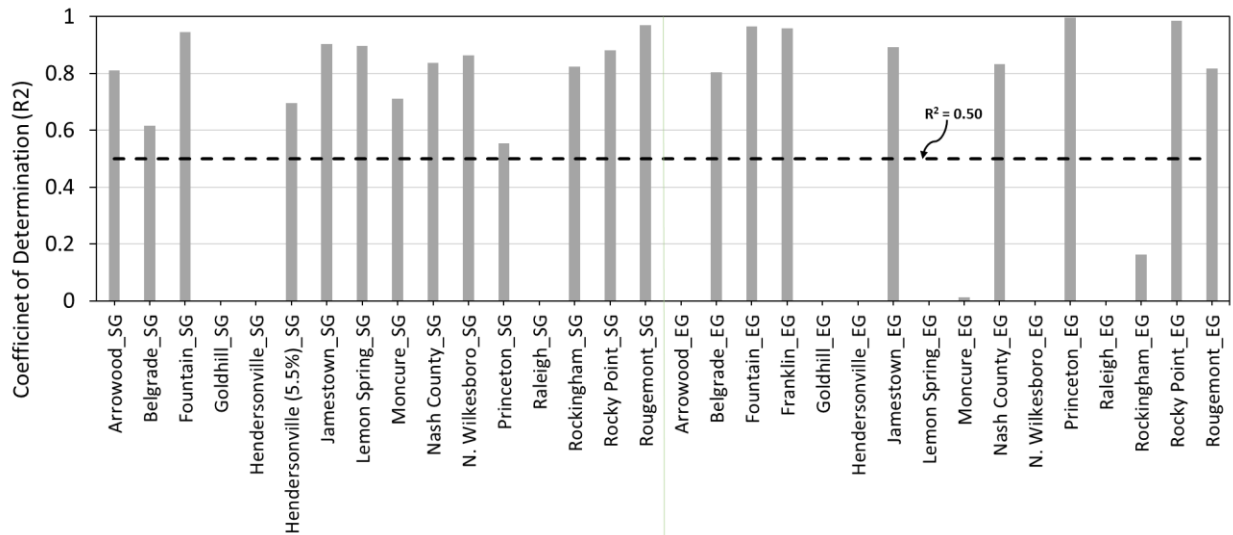


**Figure 5.8** Achieved coefficients of determination ( $R^2$ ) for all the tested materials using stepwise regression, including data from 30 tests (i.e. excluding Goldhill) and considering image-based shape properties (negative  $R^2$  values for 9 aggregate materials with missing bar chart data)

**Table 5.9:** Significant variables that correlate with the UIUC model parameters when 30 tests and image-based shape properties are considered (excluding Goldhill)

**Parameter: Log (A),  $R^2 = 0.65$**

Term	P-Value	Estimate	Std Error	t Ratio	Prob> t
Intercept		-6.392804	1.536086	-4.16	0.0004
Cc	0.00040	-0.256814	0.061038	-4.21	0.0004
D50	0.00098	0.2019945	0.052758	3.83	0.0010
P_12.7 mm	0.01757	0.0390304	0.015145	2.58	0.0176
Friction Angle	0.00027	-0.030058	0.006877	-4.37	0.0003
Secant Friction Angle	0.00341	0.0409298	0.012401	3.30	0.0034
Cohesion	0.00154	-0.008582	0.002359	-3.64	0.0015
AI	0.06524	0.0013854	0.000712	1.95	0.0652
P_0.075 mm/log (Cu)	0.02132	0.1063284	0.042737	2.49	0.0213

**Parameter: B,  $R^2 = 0.44$**

Term	P-Value	Estimate	Std Error	t Ratio	Prob> t
Intercept		0.0991048	0.08419	1.18	0.2498
OMC	0.03969	0.0175148	0.008087	2.17	0.0397
Cohesion	0.00360	0.0004492	0.00014	3.20	0.0036
Achieved Moisture Content/OMC	0.13295	-0.100619	0.064866	-1.55	0.1329

**Parameter: C,  $R^2 = 0.61$**

Term	P-Value	Estimate	Std Error	t Ratio	Prob> t
Intercept		1.6664411	0.447711	3.72	0.0010
P_0.075 mm	0.00069	-0.075229	0.019428	-3.87	0.0007
Achieved Moisture Content	0.07821	-0.08692	0.04733	-1.84	0.0782
Friction Angle	0.00752	0.0109865	0.003778	2.91	0.0075
(Max Dry Density) <sup>2</sup> /P_0.425	0.00018	-0.0005	0.000114	-4.40	0.0002

**Parameter: D,  $R^2 = 0.71$**

Term	P-Value	Estimate	Std Error	t Ratio	Prob> t
Intercept		-8.577984	2.175689	-3.94	0.0007
Cc	0.11679	-0.116213	0.071044	-1.64	0.1168
D60	0.00032	0.1487678	0.034666	4.29	0.0003
Max Dry Density	0.00143	0.0410942	0.011201	3.67	0.0014
Achieved Moisture Content	0.00130	0.3399275	0.091656	3.71	0.0013
Secant Friction Angle	0.09414	-0.019891	0.011345	-1.75	0.0941
Cohesion	0.02801	0.0047566	0.002015	2.36	0.0280
AI	0.14351	0.0017197	0.001132	1.52	0.1435
P_0.075 mm/log (Cu)	0.05161	0.1144787	0.05547	2.06	0.0516

**Table 5.10** UIUC rutting model parameters obtained from stepwise regression analysis #2 with imaging properties for all the materials tested in Phases I, II and III of this project

Gradation	Number	Material	A	B	C	D	R <sup>2</sup>
Source Gradations	1	Arrowood	0.0313	0.1113	0.2989	1.2334	0.8094
	2	Belgrade	0.0195	0.1428	0.7974	0.6822	0.6153
	3	Fountain	0.0366	0.1510	0.7194	0.2023	0.9460
	4	Goldhill	0.0253	0.1233	0.6603	-0.1327	-
	5	Hendersonville	0.0735	0.1588	0.2084	0.8142	-
	6	Hendersonville (w=5.5%)	0.0232	0.1149	0.5928	0.4890	0.6948
	7	Jamestown	0.0370	0.1429	0.4195	0.3925	0.9027
	8	Lemon Spring	0.0198	0.1517	0.5526	0.9500	0.8956
	9	Moncure	0.0684	0.1310	0.4297	1.1761	0.7104
	10	Nash County	0.0633	0.1138	0.4357	0.3327	0.8370
	11	N. Wilkesboro	0.0207	0.0997	0.6301	0.5769	0.8638
	12	Princeton	0.0183	0.1236	0.7713	0.3783	0.5546
	13	Raleigh	0.0173	0.1310	0.8540	0.4084	-
	14	Rockingham	0.0274	0.1130	0.6435	0.5075	0.8238
	15	Rocky Point	0.0265	0.1523	0.7497	1.1116	0.8802
	16	Rougemont	0.0324	0.1292	0.6741	0.5129	0.9693
Engineered Gradation	1	Arrowood	0.0303	0.1175	0.7416	0.4877	-
	2	Belgrade	0.0486	0.1378	0.5323	0.9308	0.8047
	3	Fountain	0.0290	0.1976	0.6695	0.4046	0.9659
	4	Franklin	0.0570	0.1094	0.5525	0.5489	0.9576
	5	Goldhill	0.0488	0.1365	0.4977	0.9285	-
	6	Hendersonville	0.0531	0.1361	0.7128	0.3103	-
	7	Jamestown	0.0469	0.1244	0.6270	0.4377	0.8924
	8	Lemon Spring	0.0436	0.1054	0.6163	0.4583	-
	9	Moncure	0.0309	0.0978	0.7041	0.5879	0.0131
	10	Nash County	0.0543	0.1175	0.6159	0.3948	0.8334
	11	N. Wilkesboro	0.0438	0.1116	0.6913	0.3221	-
	12	Princeton	0.0278	0.1048	0.7678	0.2740	0.9957
	13	Raleigh	0.0532	0.1282	0.6344	0.3296	-
	14	Rockingham	0.0668	0.1379	0.6250	0.5178	0.1633
	15	Rocky Point	0.0363	0.1063	0.6501	0.5643	0.9850
	16	Rougemont	0.0634	0.1235	0.6862	0.5803	0.8160

“-“ indicates negative R<sup>2</sup> values for 9 aggregate materials tested at EG and SG.

**Analysis 3: Omitting Goldhill, including 30 tests & excluding image-based shape properties**

The third analysis conducted using stepwise regression omitted Goldhill, the only plastic material, and considered data from the remaining 30 tests. Only 22 material variables were considered in this analysis; plasticity index PI and the three image-based shape properties were omitted. Image-based shape properties can be hard to obtain if the required equipment is not available, e.g. in a DOT laboratory. Thus, this analysis presents a method to estimate permanent strains using the UIUC rutting model and the more readily measurable material and compaction properties. Table 5.11 presents the most significant variables that correlated with each of the four model parameters A, B, C and D, along with the P-value and the estimates for each of the parameters.

Compared to the second analysis, the achieved coefficients of determination ( $R^2$ ) for each of the model parameters are slightly lower and ranging from 0.44 for the 'B' parameter to 0.68 for the 'D' parameter. This indicates that the model parameters estimated with this analysis can properly estimate permanent deformation of the tested materials. Figure 5.9 shows the achieved coefficients of determination for the individual tests, using the significant variables and the estimate values from Table 5.11. Similar to the other two analyses, if an  $R^2$  of 0.5 or higher is obtained, the prediction is considered successful. A negative  $R^2$  indicates a poor fitting. When Goldhill and the image-based shape properties were omitted in this analysis, the fitting equations using the estimates obtained from stepwise regression successfully predicted the experimental data for 18 of the 30 materials (12 at SG and 6 EG), which indicates a 60% success rate, which is lower than the second analysis. Again, the permanent deformations predicted for source gradations had a higher success rate than those predicted for tests at the engineered gradations.

The obtained model parameters are listed in Table 5.12. The individual test results for all the tested materials at the different SSR values of 0.25, 0.50, and 0.75 are shown in Appendix H. Note that the individual predictions are the closest to the experimental data using forced regression followed by analysis #2 (stepwise regression including shape properties), and then, followed by analysis #3 (stepwise regression excluding shape properties). The model parameters shown in Table 5.12 are based on the following model/equations and the material properties for the tested materials:

$$\varepsilon_p(N) = AN^B \sigma_d^C SSR^D$$

$$A = 10^{[-4.972 - 0.228C_c + 0.1703D_{50} + 0.0306P_{12.7mm} - 0.0266\phi + 0.0366\phi_s - 0.0079 \text{ Cohesion} + 0.09885 \frac{P_{0.075mm}}{\log(C_u)}]}$$

$$B = 0.0991 + 0.0175 OMC + 0.00045 \text{ Cohesion} - 0.1006 \frac{AMC}{OMC}$$

$$C = 1.6664 - 0.0752P_{0.075mm} - 0.0869AMC + 0.011\phi - 0.0005 \frac{MDD^2}{P_{0.425mm}}$$

$$D = -6.991 - 0.112 C_c + 0.1597D_{60} + 0.0331 MDD + 0.366 AMC - 0.01787\phi_s + 0.00432 \text{ Cohesion} + 0.1163 \frac{P_{0.075}}{\log(C_u)}$$

where

$C_c$	Coefficient of curvature	OMC	Optimum moisture content
$C_u$	Coefficient of uniformity	AMC	Achieved moisture content
$P_{x\text{ mm}}$	Percent passing sieve size 'x mm'	MDD	Maximum dry density (pcf)
$\phi$	Friction angle	Cohesion	Cohesion in kPa
$\phi_s$	Secant Friction angle		

Based on the above equation, the model parameter D is related to a term of  $D_{60}$ , regardless of including the image properties in the regression analysis. Interestingly, the  $D_{60}$  values of several tested aggregate materials (Belgrade, Lemon Spring, Moncure, Rocky Point, and Rougemont) could be used to better explain the increases in shear strength properties at SG compared to those values at EG.

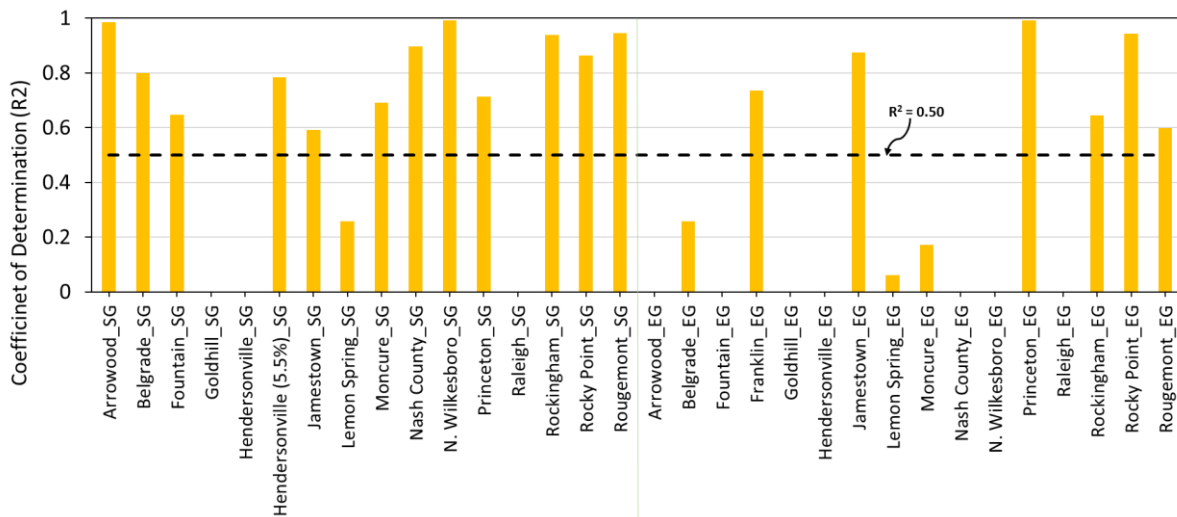


**Figure 5.9** Achieved coefficients of determination ( $R^2$ ) for all the tested materials using stepwise regression, including data from 30 tests (i.e. excluding Goldhill) and excluding image-based shape properties (negative  $R^2$  values for 10 aggregate materials with missing bar chart data)

**Table 5.11:** Significant variables that correlate with the UIUC model parameters when 30 tests are considered and image-based shape properties are excluded (excluding Goldhill)

**Parameter: Log (A),  $R^2 = 0.59$**

Term	P-Value	Estimate	Std Error	t Ratio	Prob> t
Intercept		-4.972319	1.434426	-3.47	0.0022
Cc	0.00148	-0.228127	0.062867	-3.63	0.0015
D50	0.00416	0.1702874	0.053258	3.20	0.0042
P_12.7 mm	0.05970	0.0305715	0.015398	1.99	0.0597
Friction Angle	0.00105	-0.0266	0.007051	-3.77	0.0010
Secant Friction Angle	0.00982	0.0366066	0.01295	2.83	0.0098
Cohesion	0.00419	-0.007912	0.002477	-3.19	0.0042
P_0.075 mm/log (Cu)	0.03958	0.098847	0.045177	2.19	0.0396

**Parameter: B,  $R^2 = 0.44$**

Term	P-Value	Estimate	Std Error	t Ratio	Prob> t
Intercept		0.0991048	0.08419	1.18	0.2498
OMC	0.03969	0.0175148	0.008087	2.17	0.0397
Cohesion	0.00360	0.0004492	0.00014	3.20	0.0036
Achieved Moisture Content/OMC	0.13295	-0.100619	0.064866	-1.55	0.1329

**Parameter: C,  $R^2 = 0.55$**

Term	P-Value	Estimate	Std Error	t Ratio	Prob> t
Intercept		1.6664411	0.447711	3.72	0.0010
P_0.075 mm	0.00069	-0.075229	0.019428	-3.87	0.0007
Achieved Moisture Content	0.07821	-0.08692	0.04733	-1.84	0.0782
Friction Angle	0.00752	0.0109865	0.003778	2.91	0.0075
(Max Dry Density) <sup>2</sup> /P_0.425	0.00018	-0.0005	0.000114	-4.40	0.0002

**Parameter: D,  $R^2 = 0.68$**

Term	P-Value	Estimate	Std Error	t Ratio	Prob> t
Intercept		-6.990505	1.964478	-3.56	0.0018
Cc	0.13958	-0.112006	0.073072	-1.53	0.1396
D60	0.00015	0.1597419	0.034899	4.58	0.0001
Max Dry Density	0.00366	0.033097	0.010178	3.25	0.0037
Achieved Moisture Content	0.00068	0.3659155	0.092687	3.95	0.0007
Secant Friction Angle	0.13757	-0.017872	0.011597	-1.54	0.1376
Cohesion	0.04718	0.0043157	0.002053	2.10	0.0472
P_0.075 mm/log (Cu)	0.05381	0.1163067	0.057084	2.04	0.0538

**Table 5.12** UIUC rutting model parameters obtained from stepwise regression analysis #3 without imaging properties for all the materials tested in Phases I, II and III of this project

<b>Gradation</b>	<b>Number</b>	<b>Material</b>	<b>A</b>	<b>B</b>	<b>C</b>	<b>D</b>	<b>R<sup>2</sup></b>
<b>Source Gradations</b>	1	Arrowood	0.0366	0.1113	0.2989	1.0972	0.9865
	2	Belgrade	0.0156	0.1428	0.7974	0.4216	0.7998
	3	Fountain	0.0374	0.1510	0.7194	-0.0352	0.6478
	4	Goldhill	0.0240	0.1233	0.6603	-0.3831	-
	5	Hendersonville	0.0626	0.1588	0.2084	0.4743	-
	6	Hendersonville (w=5.5%)	0.0236	0.1149	0.5928	0.4342	0.7853
	7	Jamestown	0.0371	0.1429	0.4195	0.1624	0.5909
	8	Lemon Spring	0.0220	0.1517	0.5526	0.4625	0.2572
	9	Moncure	0.0692	0.1310	0.4297	1.0352	0.6921
	10	Nash County	0.0699	0.1138	0.4357	0.3840	0.8975
	11	N. Wilkesboro	0.0252	0.0997	0.6301	0.5260	0.9912
	12	Princeton	0.0196	0.1236	0.7713	0.2572	0.7128
	13	Raleigh	0.0216	0.1310	0.8540	0.5165	-
	14	Rockingham	0.0282	0.1130	0.6435	0.3357	0.9390
	15	Rocky Point	0.0233	0.1523	0.7497	0.7039	0.8642
	16	Rougemont	0.0279	0.1292	0.6741	0.3760	0.9449
<b>Engineered Gradation</b>	1	Arrowood	0.0344	0.1175	0.7416	0.0869	-
	2	Belgrade	0.0356	0.1378	0.5323	0.8556	0.2578
	3	Fountain	0.0288	0.1976	0.6695	-0.2042	-
	4	Franklin	0.0640	0.1094	0.5525	0.3825	0.7360
	5	Goldhill	0.0456	0.1365	0.4977	0.7440	-
	6	Hendersonville	0.0455	0.1361	0.7128	0.0133	-
	7	Jamestown	0.0486	0.1244	0.6270	0.3779	0.8739
	8	Lemon Spring	0.0472	0.1054	0.6163	0.4780	0.0622
	9	Moncure	0.0337	0.0978	0.7041	0.5643	0.1713
	10	Nash County	0.0603	0.1175	0.6159	2.6270	-
	11	N. Wilkesboro	0.0477	0.1116	0.6913	0.1808	-
	12	Princeton	0.0285	0.1048	0.7678	0.2217	0.9918
	13	Raleigh	0.0578	0.1282	0.6344	0.3545	-
	14	Rockingham	0.0568	0.1379	0.6250	0.3203	0.6451
	15	Rocky Point	0.0314	0.1063	0.6501	0.5308	0.9438
	16	Rougemont	0.0512	0.1235	0.6862	0.4600	0.5985

“-“ indicates negative R<sup>2</sup> values for 10 aggregate materials tested at EG and SG.

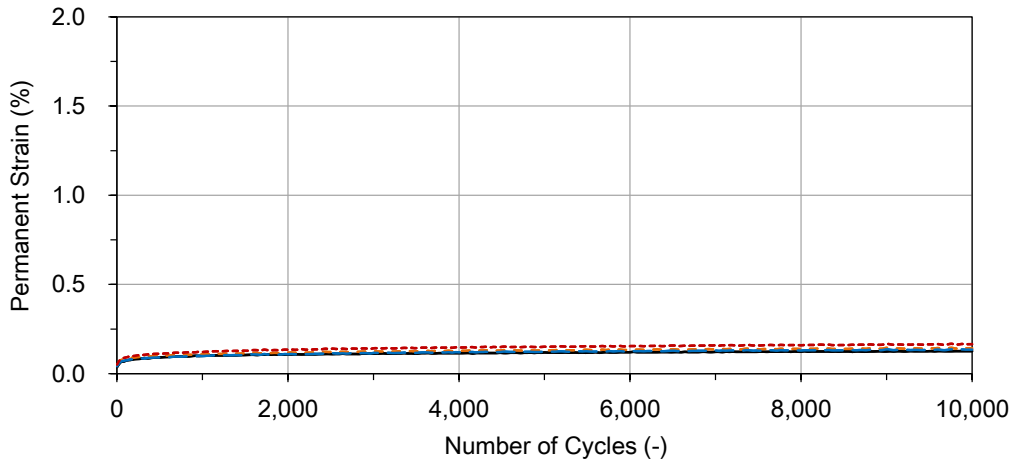
In summary, forced regression proved to be an effective technique to estimate the rutting potentials of unbound aggregate base materials using the UIUC rutting model, while eliminating any values

of the model parameters that do not have engineering significance (i.e. too low/high or negative). Forced regression, followed by stepwise regression, was successfully implemented to determine the UIUC rutting model parameters (A through D) as a function of gradation, compaction, shear strength and the image-based shape properties. From the three analyses performed using stepwise regression, the UIUC model with computed model parameters A, B, C and D could reasonably estimate permanent deformation characteristics of the 16 aggregate materials used in the State of North Carolina, especially those nonplastic materials (Analysis #2 and #3). More research and investigation is needed to consider plastic materials properly in the UIUC rutting model framework. Alternatively, aggregate materials with plastic fines may be cautioned for field applications due to their considerably higher rutting potentials. The success rate for the stepwise analysis was the highest when image-based shape properties were considered. The analysis results presented including the number of observations and success rates are summarized in Table 5.13.

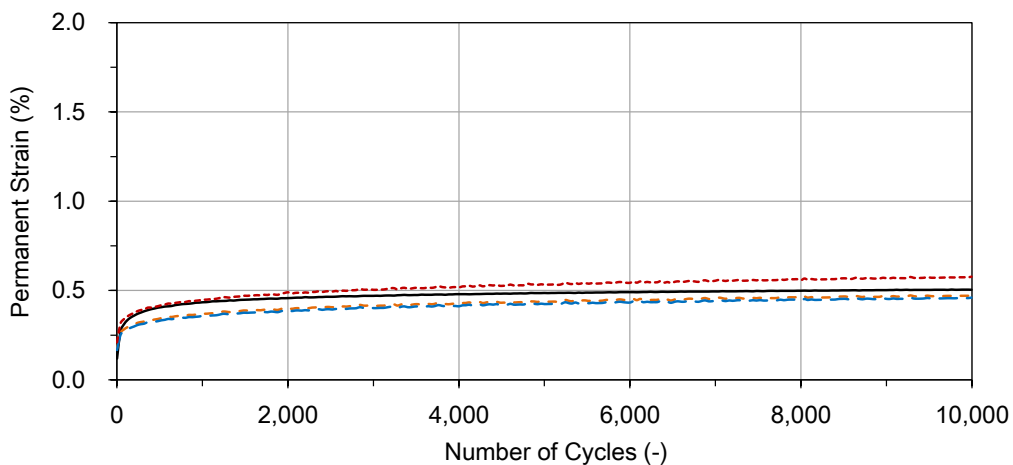
**Table 5.13** Summary of the proposed statistical analysis techniques and their success rates

<b>Method</b>	<b>Used Data Points</b>	<b>No. of Good Correlations</b>	<b>Success Rate (%)</b>	<b>Good Correlations for</b>
<b>Forced Regression</b>	32	32	100	16 SG & 16 EG
Analysis #1	32	17	53	11 SG & 6 EG
Analysis #2	30	21	70	13 SG & 8 EG
Analysis #3	30	18	60	12 SG & 6 EG

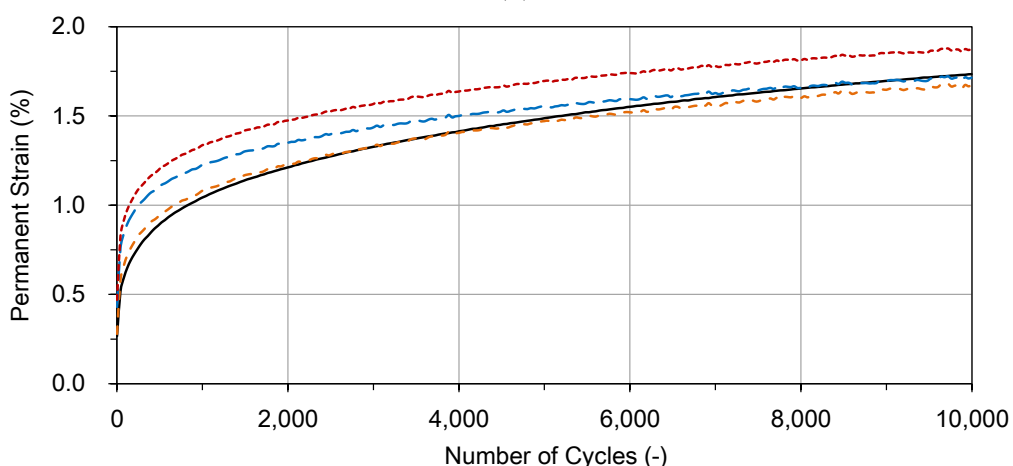
Appendix G presents the overall comparisons of the forced and stepwise regression results for all the statistical analyses undertaken in this chapter. In addition, the full set of experimental permanent strain curves at different SSR values, and the approximations using forced regression, stepwise regression from analysis #2 and analysis #3 are presented and compared in Appendix H. Figures 5.10–5.15 highlight some examples of these individual approximations that showed a good and a poor fitting. Examples are selected to show materials with low, medium, and high levels of permanent strains (left to right respectively). More data points and more materials tested are needed to fine-tune the significant variables and the correlation coefficients, thus improving the approximations of permanent strains using the UIUC rutting model.



(a)



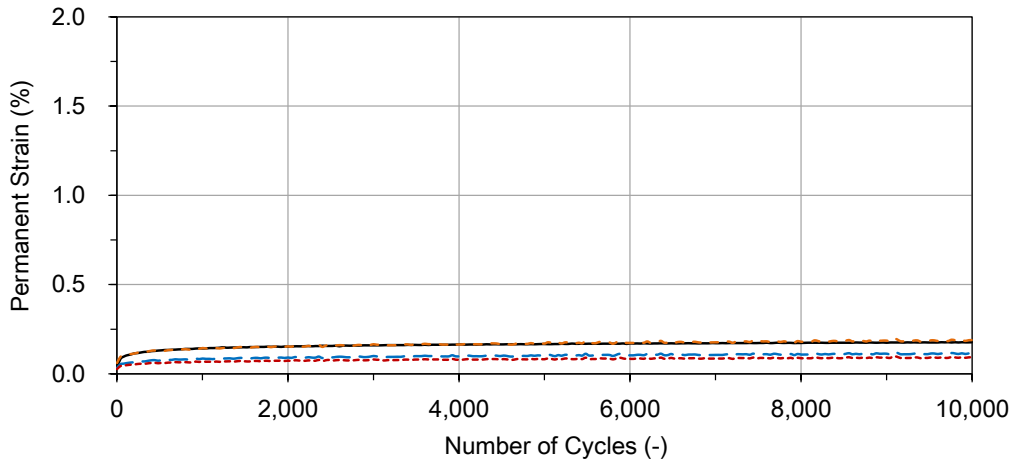
(b)



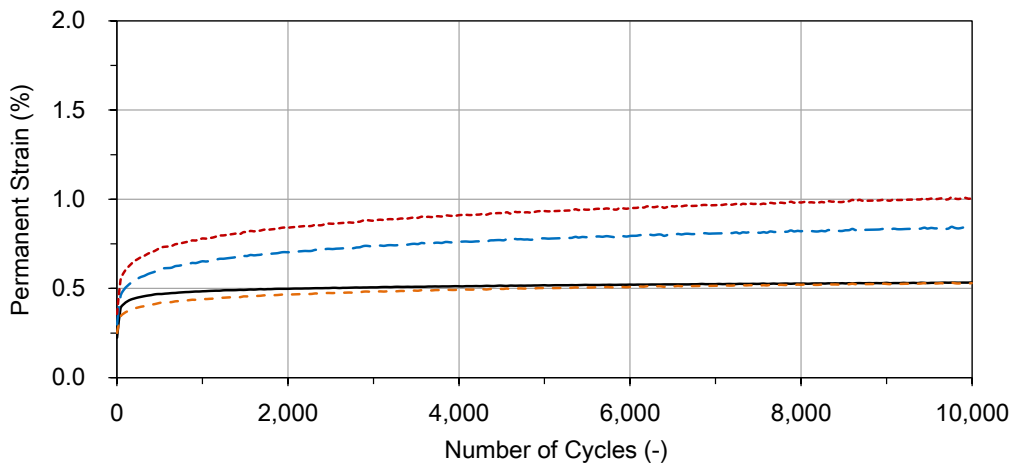
(c)

— Experimental Data                      - - - Forced Regression  
 - - - Stepwise\_Inc. Shape Properties      - - - Stepwise\_Exc. Shape Properties

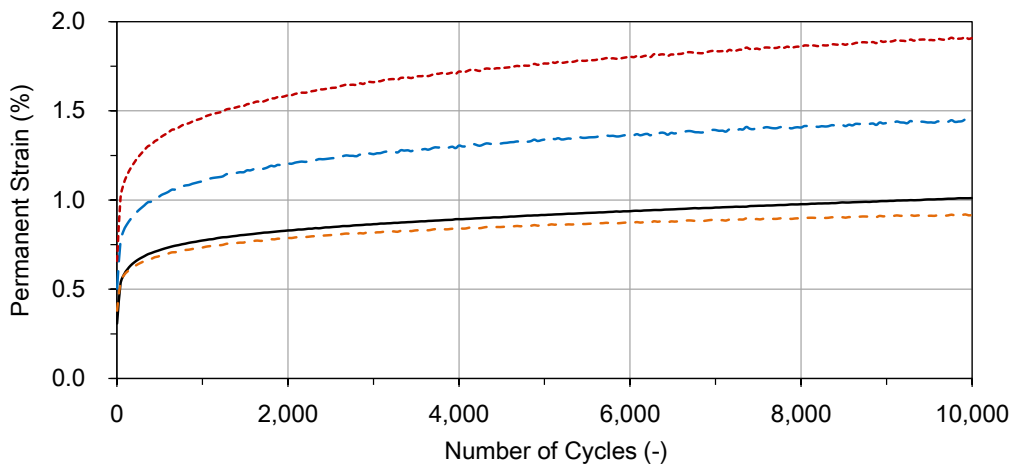
**Figure 5.10:** Example of materials with low, medium, and high levels of permanent strain showing a good fitting with experimental data: (a) Moncure at SG & SSR = 0.25; (b) Franklin at EG & SSR = 0.50; (c) Fountain at SG & SSR = 0.75



(a)



(b)



(c)

— Experimental Data                      - - - Forced Regression  
 - - - Stepwise\_Inc. Shape Properties      - - - Stepwise\_Exc. Shape Properties

**Figure 5.11:** Example of materials with low, medium, and high levels of permanent strain showing a poor fitting with experimental data: (a) Belgrade at EG & SSR = 0.25; (b) N. Wilkesboro at EG & SSR = 0.50; (c) Arrowwood at EG & SSR = 0.75

## CHAPTER 6: SUMMARY AND CONCLUSIONS

The overall objective of the current study (Phase III) was to evaluate the rutting potentials of fifteen different aggregate materials in North Carolina, at their quarry source gradations through laboratory testing and evaluation. To accomplish this overall objective, the project specific goals linked to the work plan tasks were: (1) Perform modified Proctor type moisture-density and resilient modulus tests to establish maximum dry density and optimum moisture contents and resilient modulus response characterizations, respectively, (2) conduct a full suite of shear strength and permanent deformation characterization tests to determine the permanent deformation trends influenced by aggregate material properties, shear strength, applied stress states and stress/strength ratios, and accordingly, (3) develop the UIUC rutting damage model for the NCDOT base course aggregate materials at the source gradations. Also included in the scope was to establish a procedure to account for gradation and material property effects in assigning the UIUC model parameters for predicting realistic rutting potentials of aggregate materials. This would be useful for correcting unbound aggregate layer rutting damage computations by Pavement ME software. The step-by-step procedure for predicting permanent strain accumulation of an unbound aggregate base/subbase layer suggested in this study is summarized in Figure 6.1.

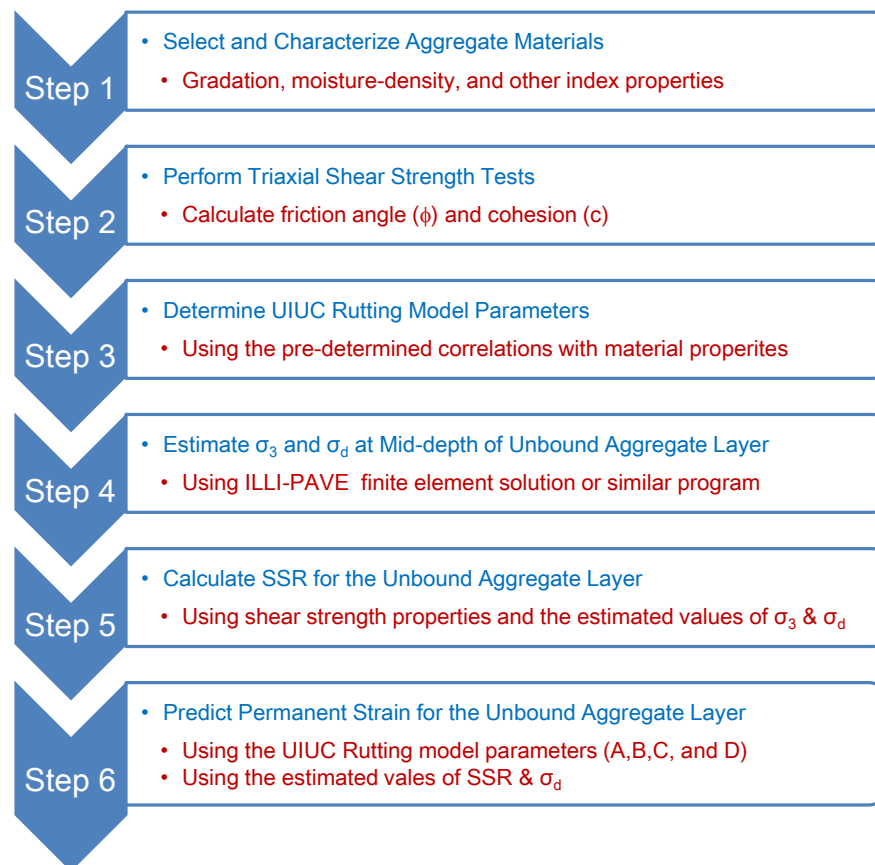


**Figure 6.1** Recommended approach for estimating rut accumulation in pavement base/subbase

Shear strength and permanent deformation tests were conducted at the University of Illinois at Urbana Champaign (UIUC) Illinois Center for Transportation (ICT) laboratories by applying different stress to strength ratios on the fifteen aggregate materials, i.e., Fountain, Nash, Rougemont, Goldhill, Arrowood, Belgrade, Hendersonville, Jamestown, Lemon Spring, Moncure, North Wilkesboro, Princeton, Raleigh, Rockingham, and Rocky Point, at their source gradations. Note that the amount of aggregate material from Franklin quarry was not sufficient to conduct the suite of tests at the source gradation. Accordingly, the framework established in Phase I of this project, entitled “Base Course Aggregate Testing and Rutting Model Calibration,” was again used in the current study to properly consider the strong linkage that exists between the permanent deformations and shear strength characteristics. Laboratory repeated load triaxial testing results of permanent strain accumulations were adequately estimated with the UIUC rutting model, developed by taking into account the applied shear stress levels as certain fractions of the material shear strength under similar confinement conditions.

### **6.1 Effects of Gradation on Shear Strength and Permanent Deformation Properties**

The primary focus of the current study was to present a detailed discussion on the effects of varying grain size distribution on unbound aggregate shear strength and permanent deformation behavior for the four NCDOT materials. The test results for the fifteen different aggregate materials were presented; and their shear strength properties and permanent deformation trends at the quarry source gradations (SG) were compared with the results obtained at the engineered gradations (EG). The study also looked at the effects of shear strength and shear stress ratio on the accumulation trends of permanent strain and the effect of changing the gradation on the accumulated rutting levels. The primary observations are as follows:

- The effects of varying grain size distribution on shear strength of aggregate materials was found to be primarily dominated by the magnitude of  $D_{10}$  and  $D_{60}$  for several aggregate material (Belgrade, Lemon Spring, Moncure, Rocky Point, and Rougemont). However, for Arrowood and Hendersonville, their shear strength properties were more susceptible to moisture content.
- Overall, the effects of gradation on permanent deformation accumulation were more noticeable at the higher shear stress ratio values. Considering that the results of dry density, moisture content, and shear strength at SG were different from those at EG as reported in the previous sections, the trends of permanent strain accumulation between SG and EG could not be explained by a sole variable. Nevertheless, Goldhill material at both EG and SG showed the highest permanent strain accumulation at the 0.75 SSR.
- The model parameters obtained from different gradations were found to work reasonably well given the shear strength properties are similar, regardless of gradation variations.

Shear strength properties (ultimately used in the calculation of SSR) and the applied stress levels clearly dictate the permanent deformation accumulation trends in aggregate materials. Gradation

is also an important material property that contributes the permanent deformation accumulated at a certain level of mobilized shear loading.

## 6.2 Detailed Study Findings

- In most cases of all the fifteen aggregate materials, the permanent deformations at the source gradations (SG) were different from those at the engineered gradation (EG), which was evaluated in Phase I study at the corresponding SSR values of 0.25, 0.5 and 0.75. Since the differences in permanent strain accumulation between SG and EG could not be explained by a single variable, discrepancies in the permanent deformation behavior between EG and SG specimens can result from the combined effects of gradation properties and other material properties, such as image based quantification of particle shape, texture and angularity, compaction (dry density and moisture content; both target and achieved), Atterberg limits, and shear strength properties.
- Higher deviator stress and SSR values produced higher permanent deformations. The effects of gradation on aggregate permanent deformation behavior were more significant as the applied stress levels approached the corresponding shear strength values of the materials at higher SSR values.
- Plastic fines (i.e., PI = 6) produced undesirable high permanent deformations for Goldhill material. The effect of PI on permanent strain accumulation was quite significant and would dominate any statistical analysis for establishing UIUC rutting model parameters as a function of gradation and other property variables.
- A forced regression technique adopted produced a good approximation for predicting permanent strains, while getting regression parameters within reasonable ranges. The ranges for regression parameters were determined by running regression analyses for all the aggregate materials with similar permanent deformation levels combined (grouped regression) and determining the model parameters, then forcing the regression of individual material results to ranges within those obtained by forced regression.
- To correlate the model parameters assigned in the UIUC rutting model with aggregate material properties, stepwise regression was used. Ultimately, these regression parameters can be expressed as functions of the following:

*Excluding the plasticity effect, but considering the image-based shape properties*

- Selected gradation properties: Coefficient of uniformity ( $C_u$ ), coefficient of curvature ( $C_u$ ),  $D_{60}$ ,  $D_{50}$ , percent passing 0.5 in. (12.7 mm) sieve, percent passing No. 40 (0.425 mm) sieve, percent passing No. 200 (0.075 mm) sieve, and percent passing No. 200 (0.075 mm) sieve divided by  $\log_{10}(C_u)$ .
- Selected compaction properties: Optimum moisture content, achieved moisture content, the ratio of achieved moisture content to optimum moisture content,

maximum dry density (MDD) in pcf, and  $MDD^2$  divided by percent passing No. 40 (0.425 mm) sieve.

- Selected shear strength properties: Friction angle, secant friction angle, and cohesion.
- Selected morphological shape properties: Angularity index (AI)

*Excluding the effects of plasticity and image properties*

- Selected gradation properties: Coefficient of uniformity ( $C_u$ ), coefficient of curvature ( $C_u$ ),  $D_{60}$ ,  $D_{50}$ , percent passing 0.5 in. (12.7 mm) sieve, percent passing No. 40 (0.425 mm) sieve, percent passing No. 200 (0.075 mm) sieve, and percent passing No. 200 (0.075 mm) sieve divided by  $\log_{10}(C_u)$ .
  - Selected compaction properties: Optimum moisture content, achieved moisture content, the ratio of achieved moisture content to optimum moisture content, maximum dry density (MDD) in pcf, and  $MDD^2$  divided by percent passing No. 40 (0.425 mm) sieve.
  - Selected shear strength properties: Friction angle, secant friction angle, and cohesion.
- The implementation of the UIUC rutting model in pavement design using analysis results from ILLI-PAVE clearly demonstrates the need to consider both SSR and the levels of rutting in low, medium and high volume roads when choosing the proper material or estimating the accumulation of permanent deformation in unbound aggregate layers.
  - Gradation was found to affect both the levels of stress states and the levels of accumulated permanent strain at any specified value of SSR.
  - Forced regression followed by stepwise regression proved to be an effective technique to express and determine the UIUC rutting model parameters A, B, C, and D as a function of gradation properties and other material properties, such as image based quantification of angularity index, compaction (dry density and moisture content; both target and achieved), and shear strength properties.
  - The success rate for the stepwise analysis was the highest when image-based shape properties were considered.
  - A design flowchart has been established and recommended with the use of SSR concept and representative mid-depth base layer wheel load deviator stress (with a confining pressure of 5 psi assumed) to give conservative base course rutting predictions. This recommendation was also included in the Phase I report (see Chow et al. 2014), and Chapter 5 of this report after validating the suitability of this recommendation to different aggregate gradations.
  - The predictive equations for the UIUC rutting model parameters (A through D) provided in this report are basically the last step of the recommended design flowchart for estimating rut accumulation (see Figure 6.1).

- The overall methodology is therefore readily available for implementation by NCDOT to determine field rutting damage potentials of unbound aggregate layers through the use of the UIUC rutting damage model in mechanistic based flexible pavement design and hence correct rutting damage computations currently generated by the AASHTO's Pavement ME software.

### **6.3 Recommendations for Future Research**

One of the recommendations of the Phase I was to study the sensitivities of the UIUC rutting model predictions to gradations, which focused on the impact of quarry gradation and other material properties on base course aggregate testing and UIUC rutting model calibration. However, some of the assumptions made and the limitations encountered in the course of this research suggest potential improvements that can be made to the UIUC rutting model to further develop the framework of the base course rutting prediction approach. Some of the limitations are that shear strength and permanent deformation tests were conducted mostly on the aggregate materials including nonplastic fines, meaning that the effects of plastic fines on permanent deformation accumulation is not appropriately considered in the model parameters. Additionally, all of the testing was conducted at one confining pressure (5 psi). Thus, the accuracy of the model was only verified at this confining pressure, although it is a conservative value and reasonably takes into account compaction induced residual stresses commonly developed in flexible pavement base courses.

To tackle some of the assumptions and limitations encountered in this research, topics for future research may include the following:

- Additional tests of new aggregate materials including plastic fines will expand the current database and enhance the reliability and accuracy of the permanent deformation model predictions. Note that the plasticity effect on the model parameter determination was excluded in the current study. Further, larger database will provide more robust model parameter correlations to material properties.
- Using ILLI-PAVE or other elastic layered solutions to calculate stress states at the middle of the unbound layer permits using UIUC rutting model for assessing unbound aggregate layer rutting potential when designing conventional flexible pavements. To validate the accuracy of these predictions, the in-situ testing and field measurements of lateral and vertical pressures in the unbound aggregate base layer under traffic loading would establish representative stress states. Additionally, in-situ measurements of the actual field permanent deformation under realistic moving wheel loading can help to validate the suitability of UIUC rutting model predictions.

## REFERENCES

- Ayres, M.J., "Unbound Material Rut Model Modification," *Development of the 2002 Guide for the Design of New and Rehabilitated Pavement Structures, NCHRP 1-37A*, Inter Team Technical Report, 2002.
- Barksdale, R.D., "Laboratory Evaluation of Rutting in Base Course Materials," *Proceedings of the 3<sup>rd</sup> International Conference on Asphalt Pavements*, University of Michigan, Ann Arbor, 1972, pp. 161-174.
- Brown, S.F. and F. Chan, "Reduced Rutting in Unbound Granular Pavement Layers through Improved Grading Design," *Proceedings of the Institution of Civil Engineers, Transport*, No. 117, 1996, pp. 40-49.
- Chow, L. C., Mishra, D., and Tutumluer, E. "Aggregate Base Course Material Testing and Rutting Model Development", *Final Report*, FHWA/NC/2013-18, University of Illinois, Urbana-Champaign, December 2014.
- Chow, L. C., D. Mishra, and E. Tutumluer, "Framework for Improved Unbound Aggregate Base Rutting Model Development for Mechanistic-Empirical Pavement Design". *Transportation Research Record 2401*, Journal of the Transportation Research Board, 2014, pp. 11-21.
- Chow, L. C., "Permanent Deformation Behavior of Unbound Granular Materials and Rutting Model Development". *M.S. Thesis*, Department of Civil and Environmental Engineering, University of Illinois at Urbana-Champaign, Urbana, IL, 2014
- Cunningham, C.N., T. Evans, and A. Akhtar, "Gradation Effects on the Mechanical Response of Crushed Stone Aggregate," *The International Journal of Pavement Engineering*, Vol. 14, pp. 231-41, 2013.
- Draper, N. and Smith, H. "Applied Regression Analysis," 2nd Edition, New York: John Wiley & Sons, Inc., 1981.
- El-Mitiny, M.R., "Material Characterization for Studying Flexible Pavement Behavior in Fatigue and Permanent Deformation," *Ph.D. Thesis*, Ohio State University, Columbus, 1980.
- Ghabchi, R., M. Zaman, N. Khoury, H. Kazmee, and P. Solanki, "Effect of Gradation and Source Properties on Stability and Drainability of Aggregate Bases: A Laboratory and Field Study," *The International Journal of Pavement Engineering*, Vol. 14, pp. 274-90, 2013.
- Gidel G., P. Horny, J.J Chauvin, D. Breyse, and A. Denis, "Nouvelle approche pour l'étude des déformations permanentes des graves non traitées à l'appareil à chargement répétés," *Bulletin des Laboratoire des Ponts et Chaussées*, 2001, pp. 5-21.
- Gray, J. E., "Characteristics of Graded Base Course Aggregates Determined by Triaxial Tests," *Engineering Research Bulletin* No. 12, 1962
- Hicks, R.G. and Monismith, C.L., "Factors Influencing the Resilient Properties of Granular Materials." *Transportation Research Record 345*, TRB, Washington DC, 1971, pp. 15-31.

- Huurman, M., "Permanent Deformation in Concrete Block Pavements," *Ph.D. Thesis*, Delft University of Technology, Delft, the Netherlands, 1997.
- Khedr, S., "Deformation Characteristics of Granular Base Course in Flexible Pavement," *Transportation Research Record 1043*, Transportation Research Board, National Research Council, Washington, D.C., 1985, pp 131-138.
- Lekarp, F., U. Isacsson, and Dawson, A., "State of the Art II: Permanent Strain Response of Unbound Aggregates," *ASCE Journal of Transportation Engineering*, Vol. 126, No. 1, pp. 76-83, 2000.
- Lekarp, F. and A. Dawson, "Modeling Permanent Deformation Behavior of Unbound Granular Materials," *Construction and Building Materials*, Vol. 12, No. 1, 1998, pp 9-18.
- Mishra, D. and E. Tutumluer, "Aggregate Physical Properties Affecting Modulus and Deformation Characteristics of Unsurfaced Pavements," *ASCE Journal of Materials in Civil Engineering*, Vol. 24, No. 9, 2012, pp. 1144-1152.
- Mishra, D., "Aggregate Characteristics Affecting Response and Performance of Unsurfaced Pavements on Weak Subgrades." *Ph.D. dissertation*, University of Illinois at Urbana-Champaign, 2012.
- Moaveni, M., Wang, S., Hart, J.M., Tutumluer, E., and N. Ahuja. "Aggregate Size and Shape Evaluation Using Segmentation Techniques and Aggregate Image Processing Algorithms," *Transportation Research Record 2335*, Journal of the Transportation Research Board, National Research Council, Washington, D.C., 2013, pp 50-59.
- Monismith, C.L., N. Ogawa, and C.R. Freeme, "Permanent Deformation Characteristics of Subgrade Soils Due to Repeated Loading," *Transportation Research Record 537*, Transportation Research Board, National Research Council, Washington, D.C., 1975, pp 1-17.
- Pan, T., E. Tutumluer, and S.H. Carpenter, "Imaging Based Evaluation of Coarse Aggregate used in the NCAT Pavement Test Track Asphalt Mixes," *In Proceedings of the 1<sup>st</sup> International Conference on Design and Construction of Long Lasting Asphalt Pavements*, Auburn, AL, 2004.
- Pan, T., and E. Tutumluer, "Quantification of Coarse Aggregate Surface Texture Using Image Analysis," *ASTM Journal of Testing and Evaluation*, Vol. 35, No. 2, 2007.
- Pappin, J.W., "Characteristics of a Granular Material for Pavement Analysis," University of Nottingham, Nottingham, England, 1979.
- Paute, J.L., P. Hornych, and J.P. Benaben, "Repeated Load Triaxial Testing of Granular Materials in French Network of Laboratories des Ponts et Chaussées," *Flexible Pavements, Proceedings of the European Symposium Euroflex 1993*, A.G. Correia, Ed., Balkema, Rotterdam, the Netherlands, 1996, pp. 53-64.

- Qamhia, I., E. Tutumluer, L.C. Chow, and D. Mishra. "A Framework to Utilize Shear Strength Properties for Evaluating Rutting Potentials of Unbound Aggregate Materials," *Procedia engineering*, 2016, Vol. 143, No. 911-920.
- Qamhia, I.I., L.C. Chow, D. Mishra, and Tutumluer, E. (2017). "Dense-graded aggregate base gradation influencing rutting model predictions," *Transportation Geotechnics*, 2017, Vol. 13, pp. 43-51.
- Rao, C., E. Tutumluer, and I.T. Kim, "Quantification of Coarse Aggregate Angularity based on Image Analysis," *Transportation Research Record 1787*, Transportation Research Board, National Research Council, Washington, D.C., 2002, pp 117-124.
- Rao, C., E. Tutumluer, and J.A. Stefanski, "Flat and Elongated Ratios and Gradation of Coarse Aggregates Using a New Image Analyzer," *ASTM Journal of Testing and Standard*, Vol. 29, No. 5, 2001, pp. 79-89.
- Rada, G., and Witczak, M.W., "Comprehensive Evaluation of Laboratory Resilient Moduli Results for Granular Material," *Transportation Research Record No. 810*, TRB, National Research Council, Washington D.C., 1981, pp. 23-33.
- Saeed, A., Hall J., and Barker W., "Performance-related Tests of Aggregates for Use in Unbound Pavement Layers". *NCHRP Report No.453*, National Academy Press, Washington D.C., 2001.
- Seyhan, U. and E. Tutumluer, "Anisotropic Modular Ratios as Unbound Aggregate Performance Indicators," *ASCE Journal of Materials in Civil Engineering*, Vol. 14, No. 5, 2002, pp. 409-416.
- Tao, M., Louay M.N., Munir N.D., Zhang Z., and Wu Z., "Application of Shakedown Theory in Characterizing Traditional and Recycled Pavement Base Materials," *Journal of Transportation Engineering*, 136(3), 2010, pp. 214-222.
- Thom, N.H. and S.F. Brown, "The Effect of Grading and Density on the Mechanical Properties of a Crushed Dolomitic Limestone," *Proceedings of the 14<sup>th</sup> ARRB Conference*, Part 7. 1988, pp. 94-100.
- Thompson, M.R. and Elliot R.P. (1985). "ILLI-PAVE Based Response Algorithms for Design of Conventional Flexible Pavement," *Transportation Research Record 1043*, TRB, National Research Council, Washington D.C., pp. 50-57.
- Thompson, M.R., "State-of-the-Art: Unbound Base Performance," *Proceedings of the 6<sup>th</sup> Annual Symposium of International Center for Aggregate Research (ICAR)*, Austin, TX. 1998.
- Thompson, M.R. and D. Nauman, "Rutting Rate Analyses of the AASHO Road Test Flexible Pavements," *Transportation Research Record 1384*, Transportation Research Board, National Research Council, Washington, D.C., 1993, pp 36-48.
- Tseng, K.H. and R.L. Lytton, "Prediction of Permanent Deformation in Flexible Pavement Materials," *Implication of Aggregates in the Design, Construction, and Performance of Flexible Pavements*, ASTM STP 1016, ASTM, Philadelphia, PA, 1989, pp. 154-172.

- Tutumluer, E., C. Rao, and J.A. Stefanski, "Video Image Analysis of Aggregates," *Final Project Report, FHWA-IL-UI-278, Civil Engineering Studies UILU-ENG-2000-2015*, University of Illinois at Urbana-Champaign, 2000.
- Tutumluer, E., D. Mishra, and A. Butt, "Characterization of Illinois Aggregates for Subgrade Replacement and Subbase," *Final Report, Illinois Center for Transportation (ICT) R27-1 Project*, University of Illinois, Urbana-Champaign, Sept 2009.
- Tutumluer, E. and U. Seyhan, "Laboratory Determination of Anisotropic Aggregate Resilient Moduli using an Innovative Test Device," *Transportation Research Record 1687*, Transportation Research Board, National Research Council, Washington, D.C., 1999, pp 13-21.
- Tseng, K. and Lytton, R., "Prediction of Permanent Deformation in Flexible Pavement Materials," Implication of Aggregates in the Design, Construction, and Performance of Flexible Pavements. ASTM STP 1016, ASTM, 1989, pp. 154-172.
- Ullidtz, P., "Modeling of Granular Materials Using the Discrete Element Method," *Proceedings of the 8<sup>th</sup> International Conference on Asphalt Pavements*, Seattle, WA, 1997, pp. 757-769.
- Uzan, J., "Characterization of Granular Materials." *Transportation Research Record 1022*, 1985, pp. 52-59.
- van Niekerk, A.A. and M. Huurman, "Establishing Complex Behavior of Unbound Road Building Materials from Simple Material Testing," *Technical Report No. 7-95-200-16*, Delft University of Technology, Delft, the Netherlands, 1995.
- Witczak, M. W., and J. Uzan. *The Universal Airport Design System, Report I of IV: Granular Material Characterization*. Department of Civil Engineering, University of Maryland, College Park, 1988.
- Werkmeister, S., A. R. Dawson, and F. Wellner, "Pavement Design Model for Unbound Granular Materials," *ASCE Journal of Transportation Engineering*, Vol. 130, No. 5, 2004, pp. 665–674.
- Wolff, H., "Elasto-Plastic behavior of Granular Pavement Layers in South Africa," *Ph.D. Thesis*, University of Pretoria, Pretoria, Republic of South Africa, 1992.
- Xiao, Y. and Tutumluer, E. "Best Value Granular Material for Road Foundations," *Final Report, Minnesota Department of Transportation, Final Report 2012-01*, 395 John Ireland Boulevard, St. Paul, MN, January 2012, 167 p. (<http://www.lrrb.org/pdf/201201.pdf>)
- Xiao, Y., Tutumluer, E., Qian, Y. and J. Siekmeier, "Gradation Effects Influencing Mechanical Properties of Aggregate Base and Granular Subbase Materials in Minnesota," *In Transportation Research Record 2267*, Journal of the Transportation Research Board, National Research Council, Washington, D.C., 2012, pp. 14-26.

## APPENDIX A Sieve Analysis Results

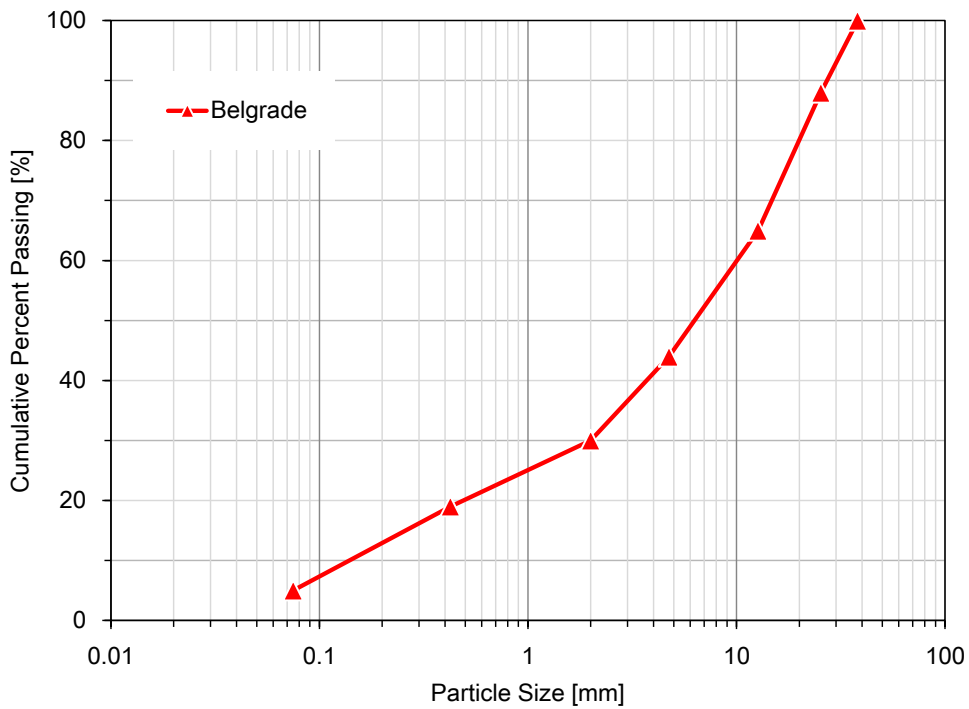
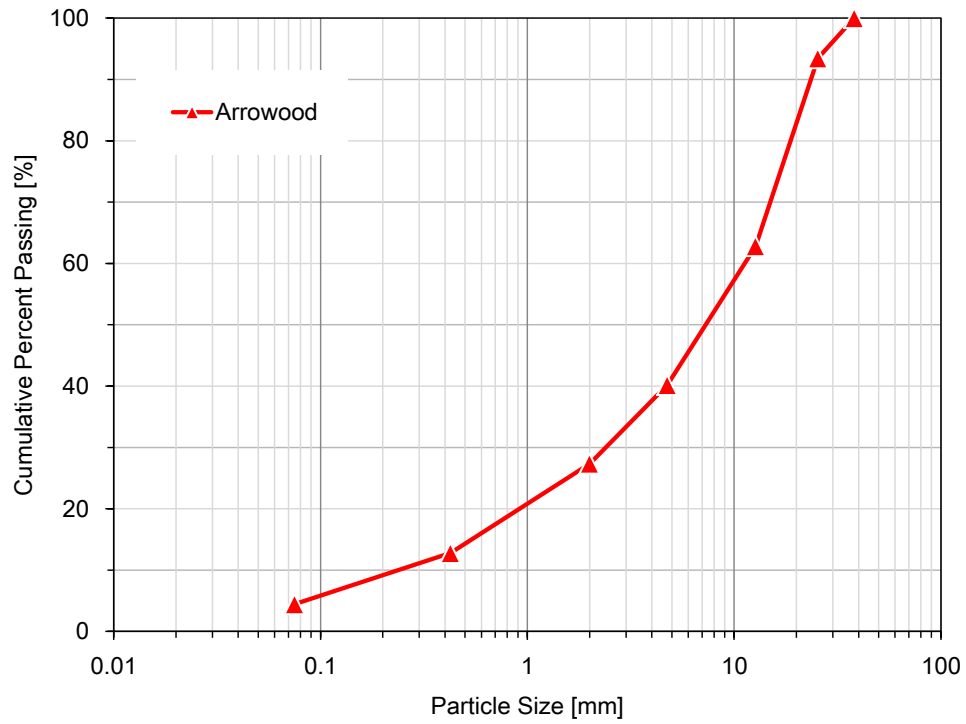


**Figure A.1** Grain size distribution curves obtained from dry sieving of the fifteen aggregate materials at the source gradations

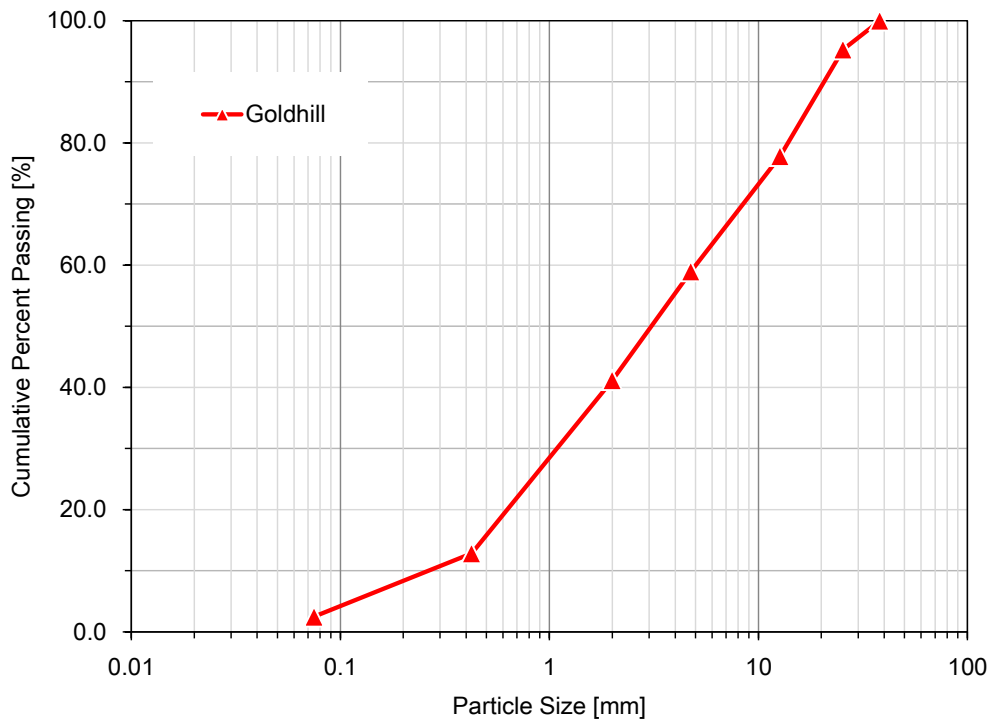
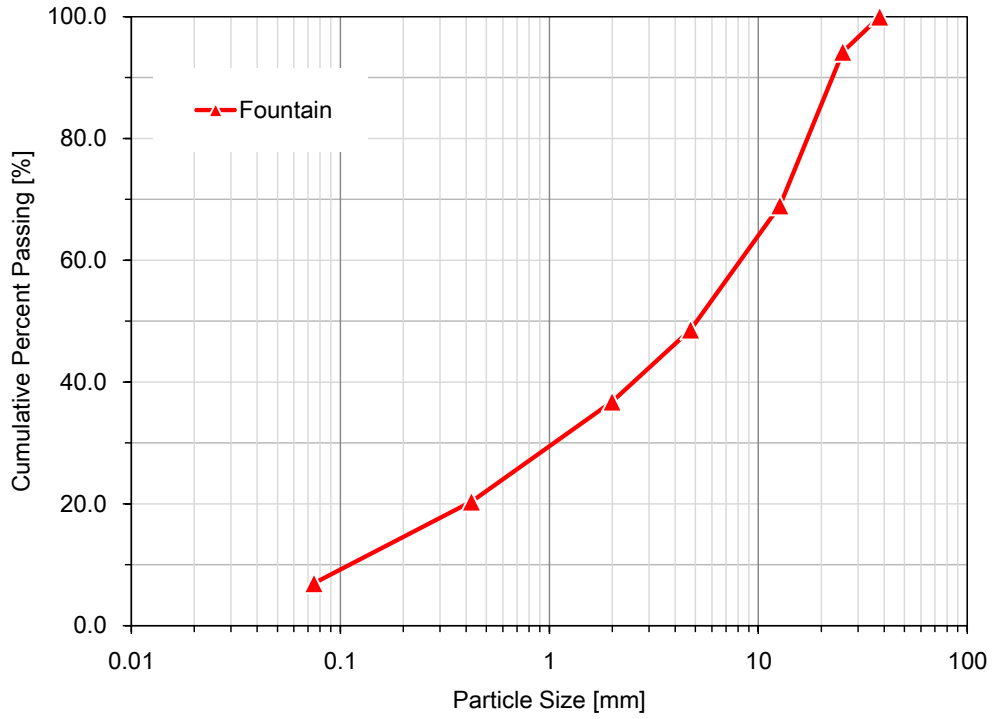


**Figure A.1 (Cont'd)** Grain size distribution curves obtained from dry sieving of the fifteen aggregate materials at the source gradations

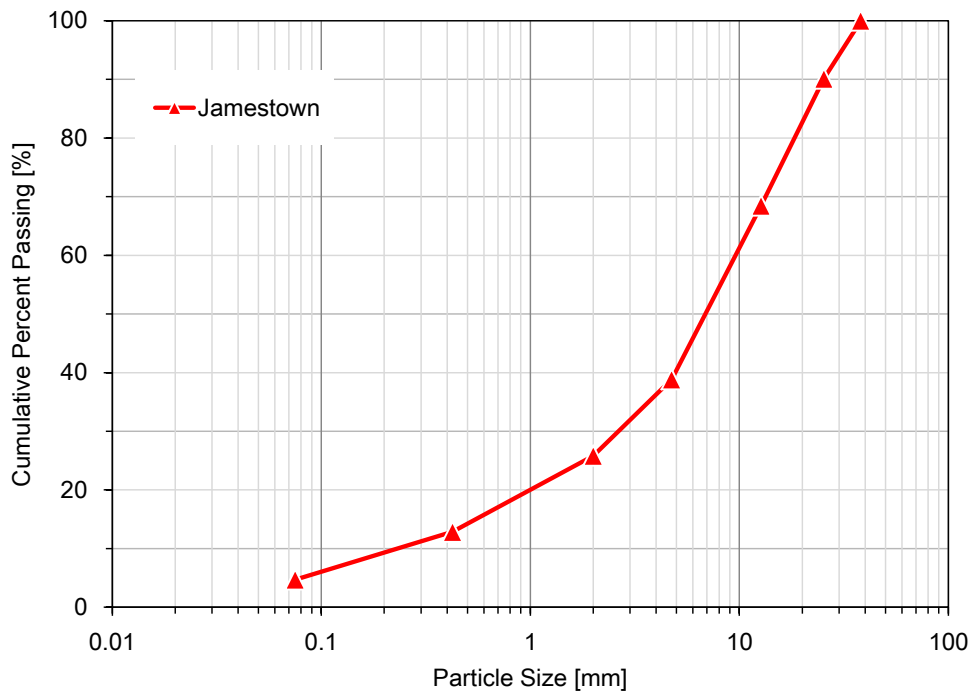
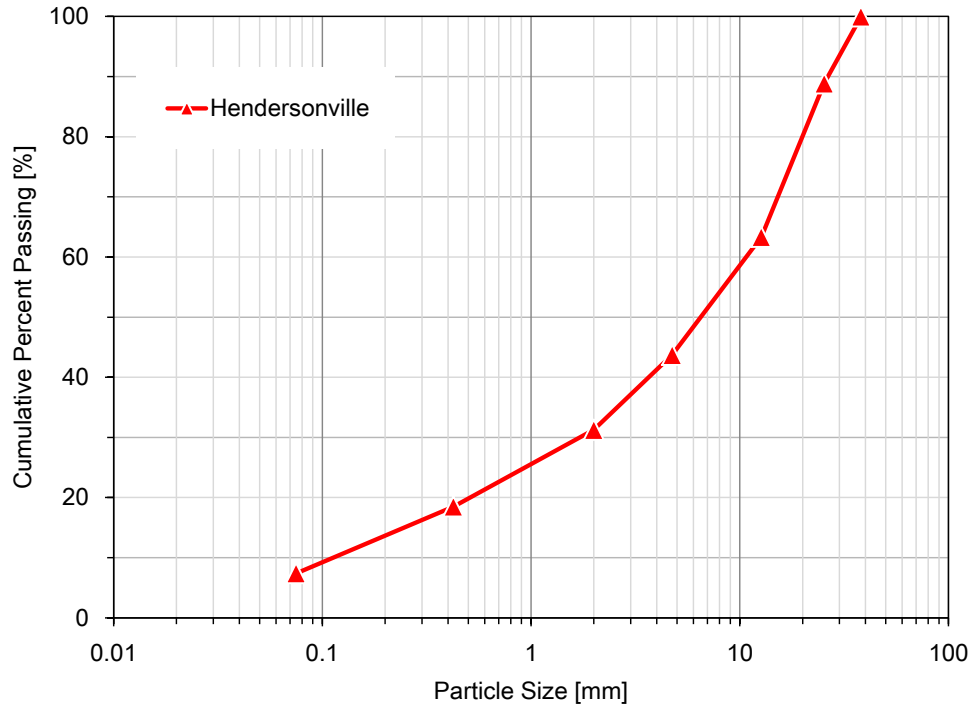


**Figure A.1 (Cont'd)** Grain size distribution curves obtained from dry sieving of the fifteen aggregate materials at the source gradations

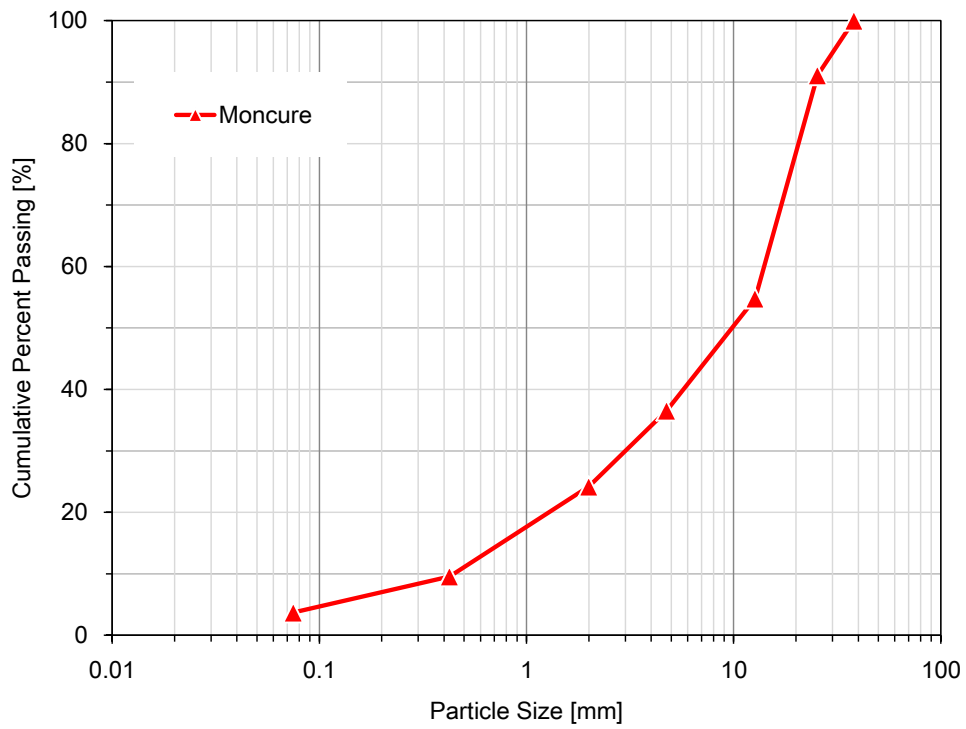
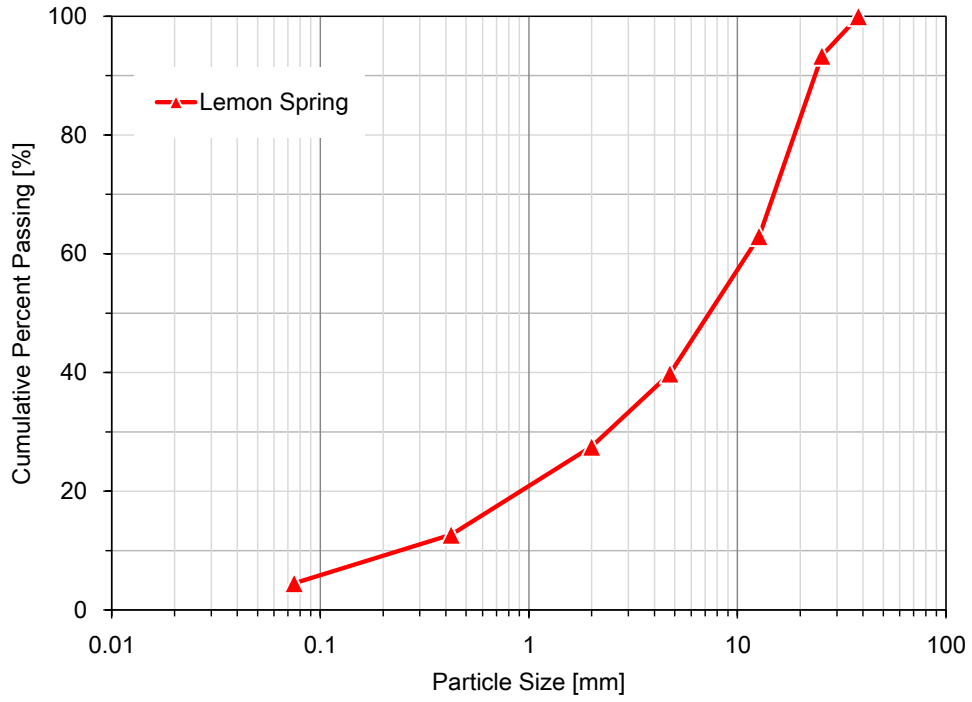


**Figure A.1 (Cont'd)** Grain size distribution curves obtained from dry sieving of the fifteen aggregate materials at the source gradations

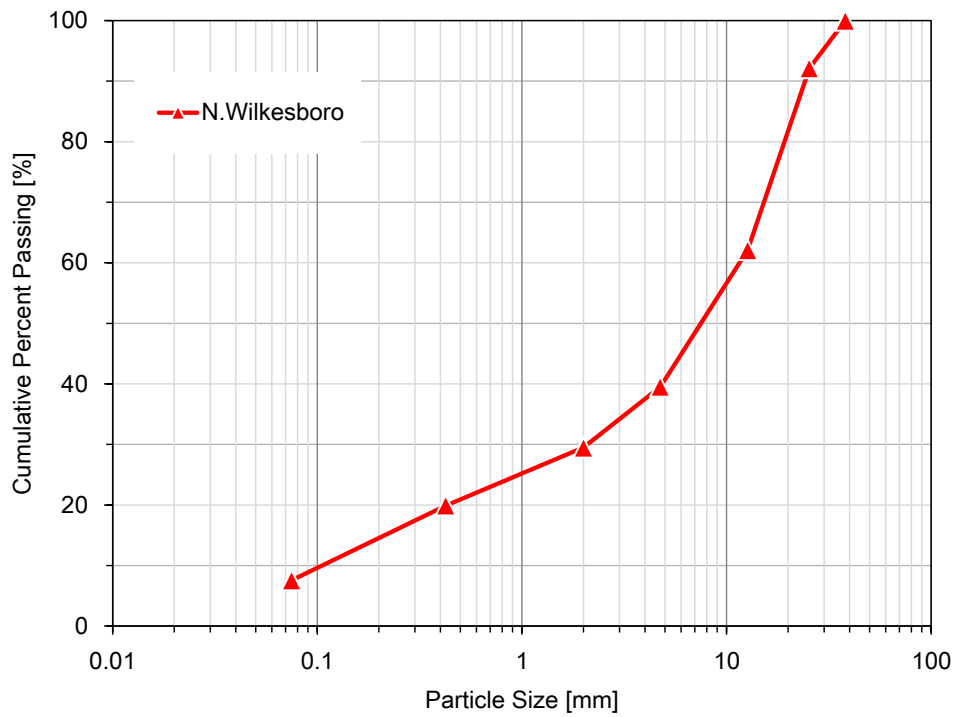
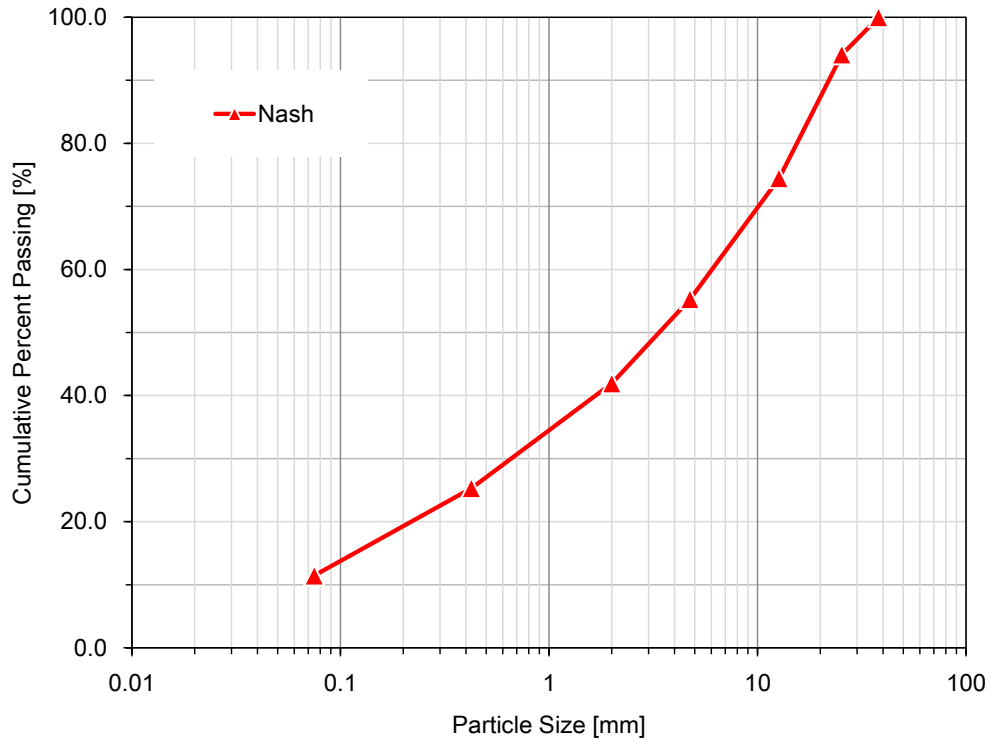


**Figure A.1 (Cont'd)** Grain size distribution curves obtained from dry sieving of the fifteen aggregate materials at the source gradations

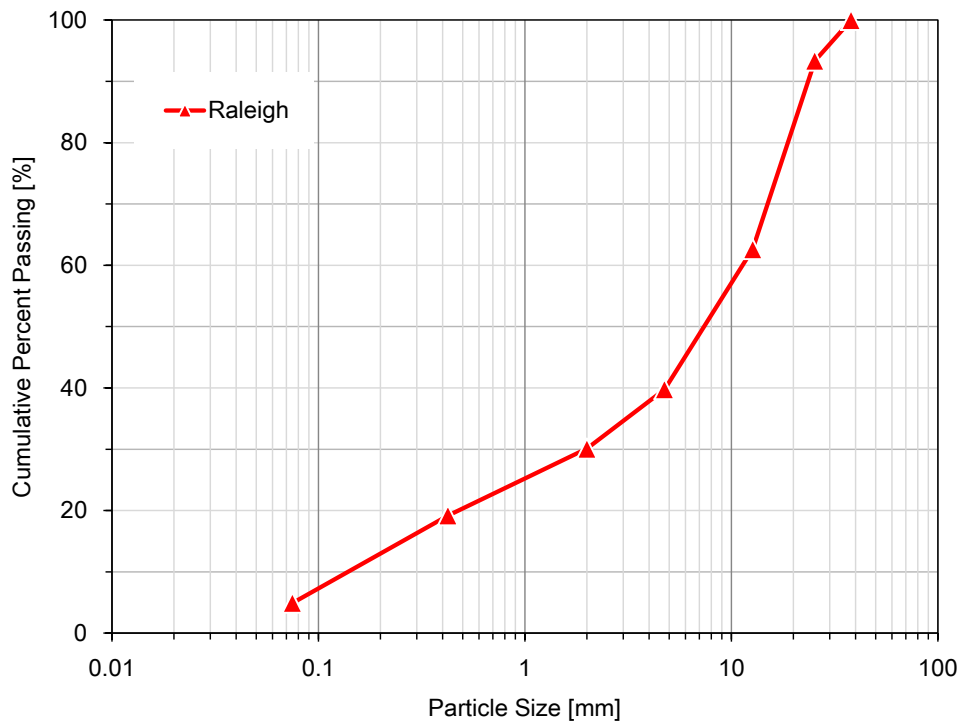
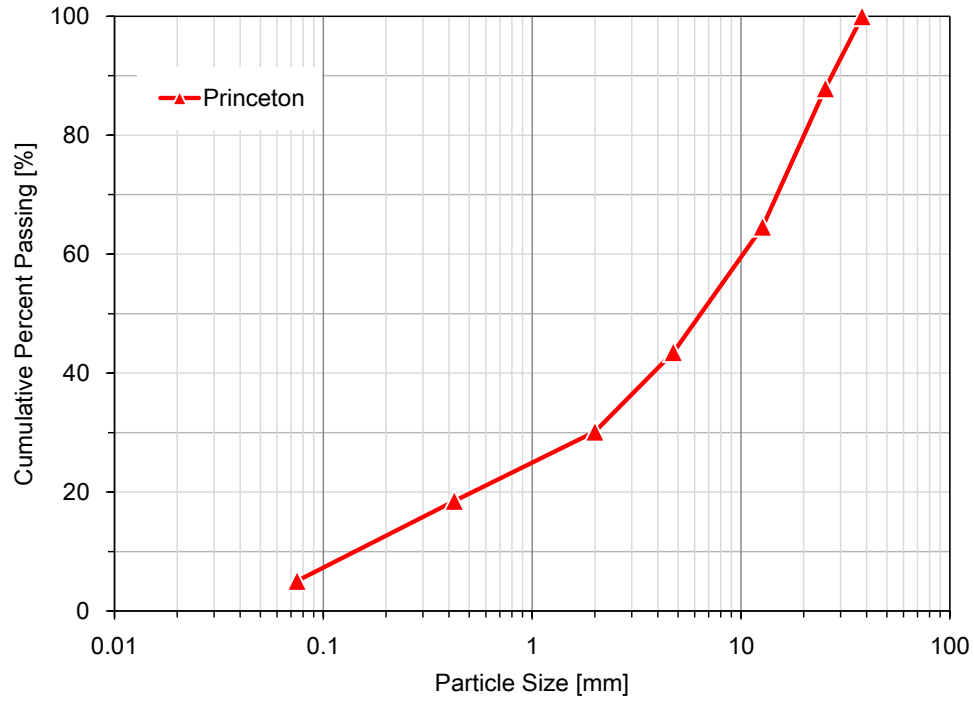


**Figure A.1 (Cont'd)** Grain size distribution curves obtained from dry sieving of the fifteen aggregate materials at the source gradations

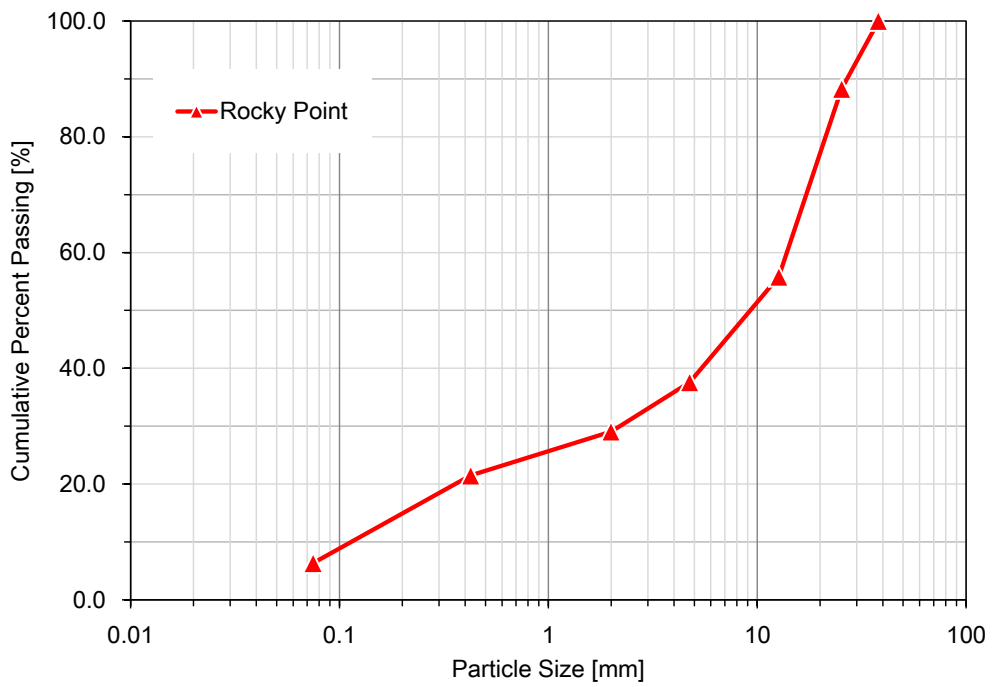
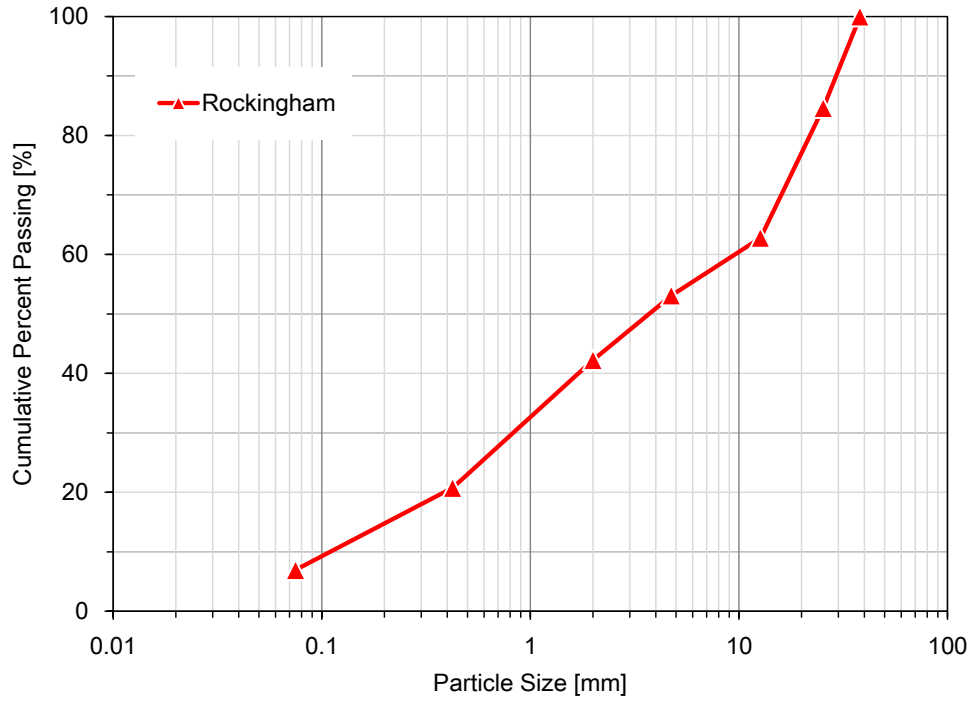


**Figure A.1 (Cont'd)** Grain size distribution curves obtained from dry sieving of the fifteen aggregate materials at the source gradations

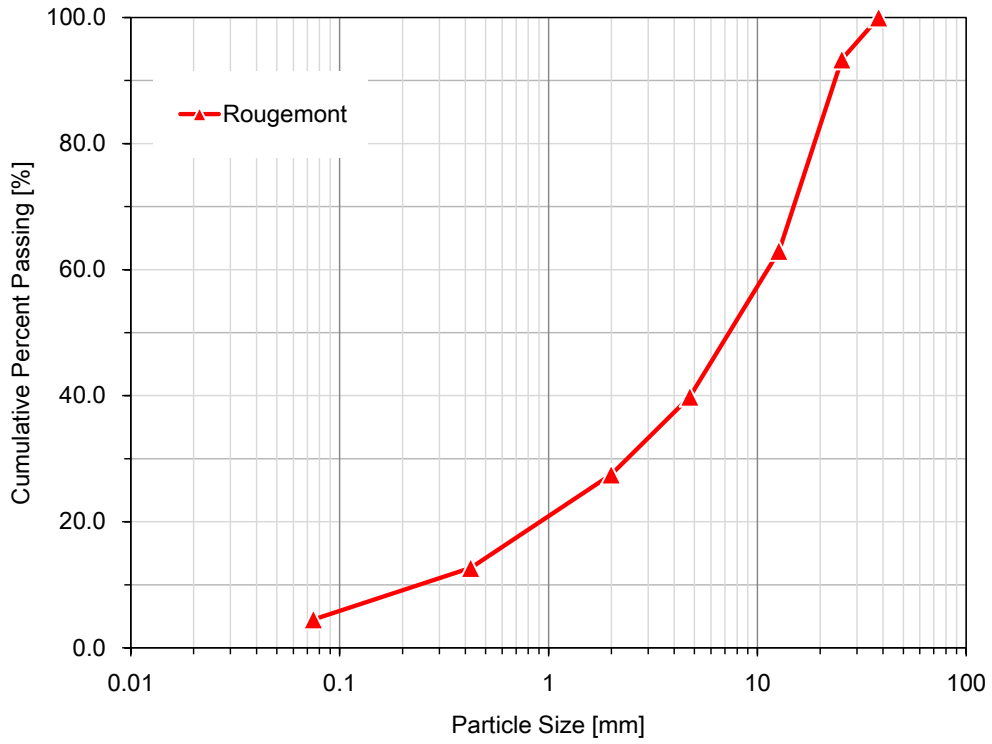


**Figure A.1 (Cont'd)** Grain size distribution curves obtained from dry sieving of the fifteen aggregate materials at the source gradations

## APPENDIX B Moisture-Density and CBR Test Results

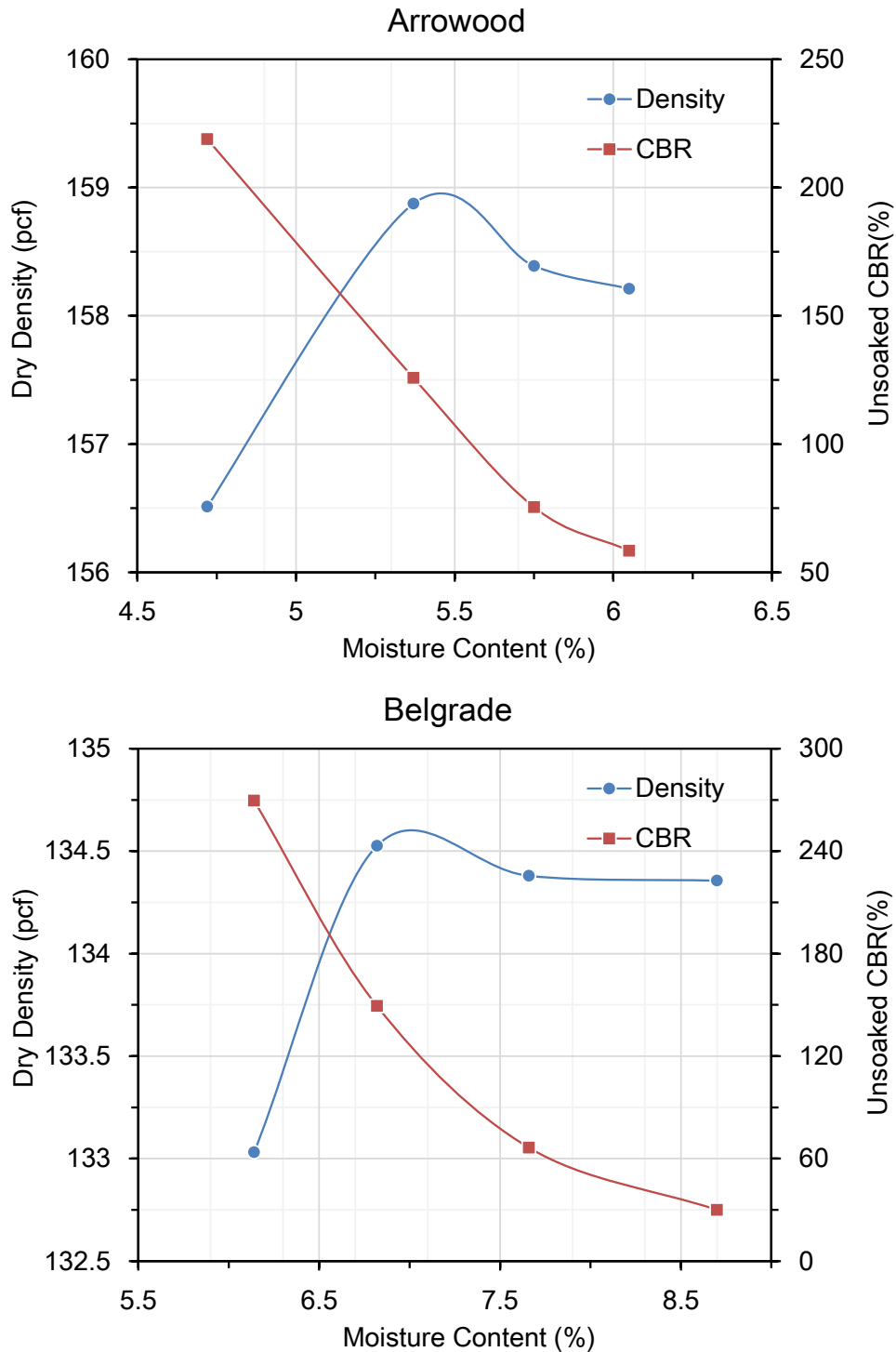


**Figure B.1** Moisture-density and CBR test results for the fifteen aggregate materials at the source gradations (Results from testing at UIUC)

Note: y-axis scales for dry density and unsoaked CBR are different at each material

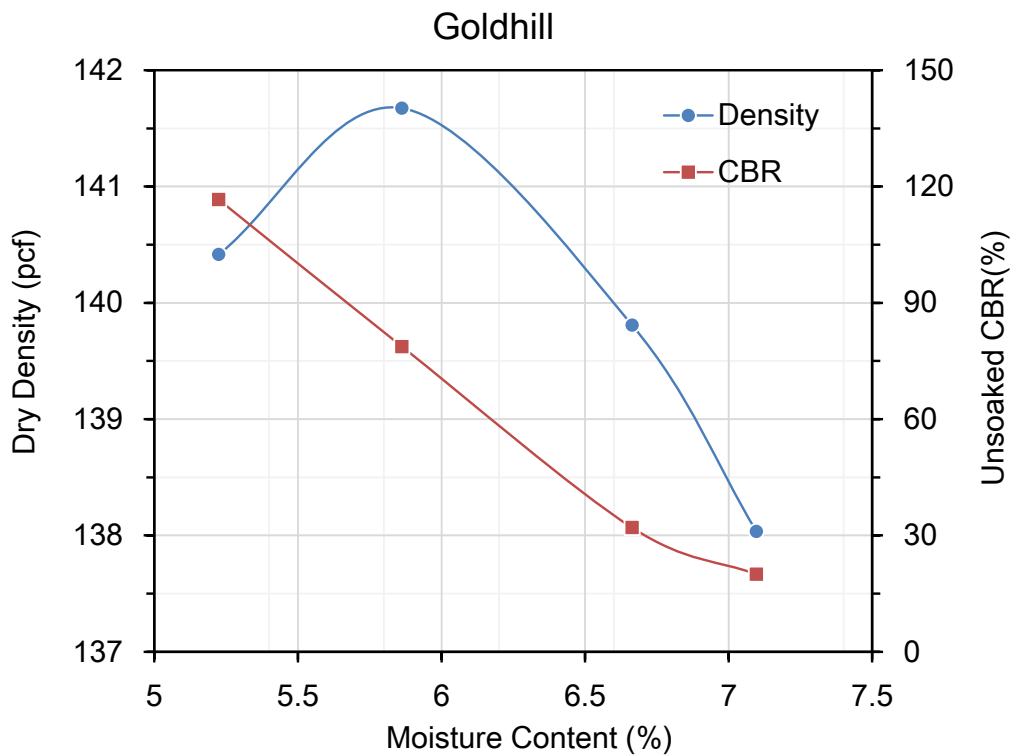
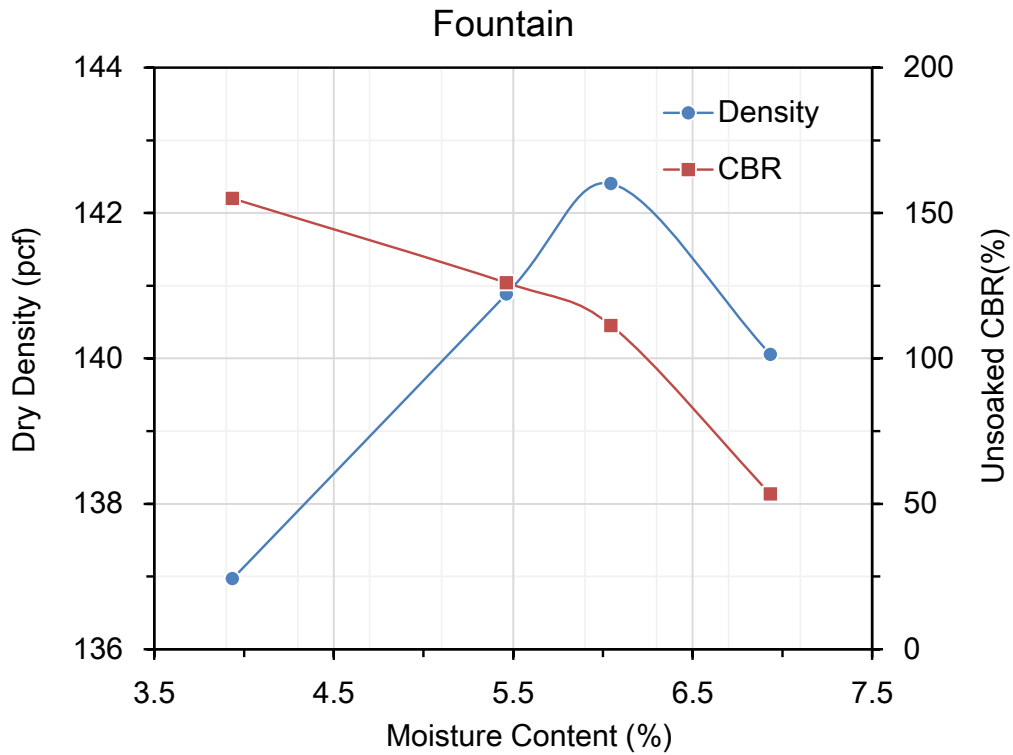


**Figure B.1 (Cont'd)** Moisture-density and CBR test results for the fifteen aggregate materials at the source gradations (Results from testing at UIUC)

Note: y-axis scales for dry density and unsoaked CBR are different at each material

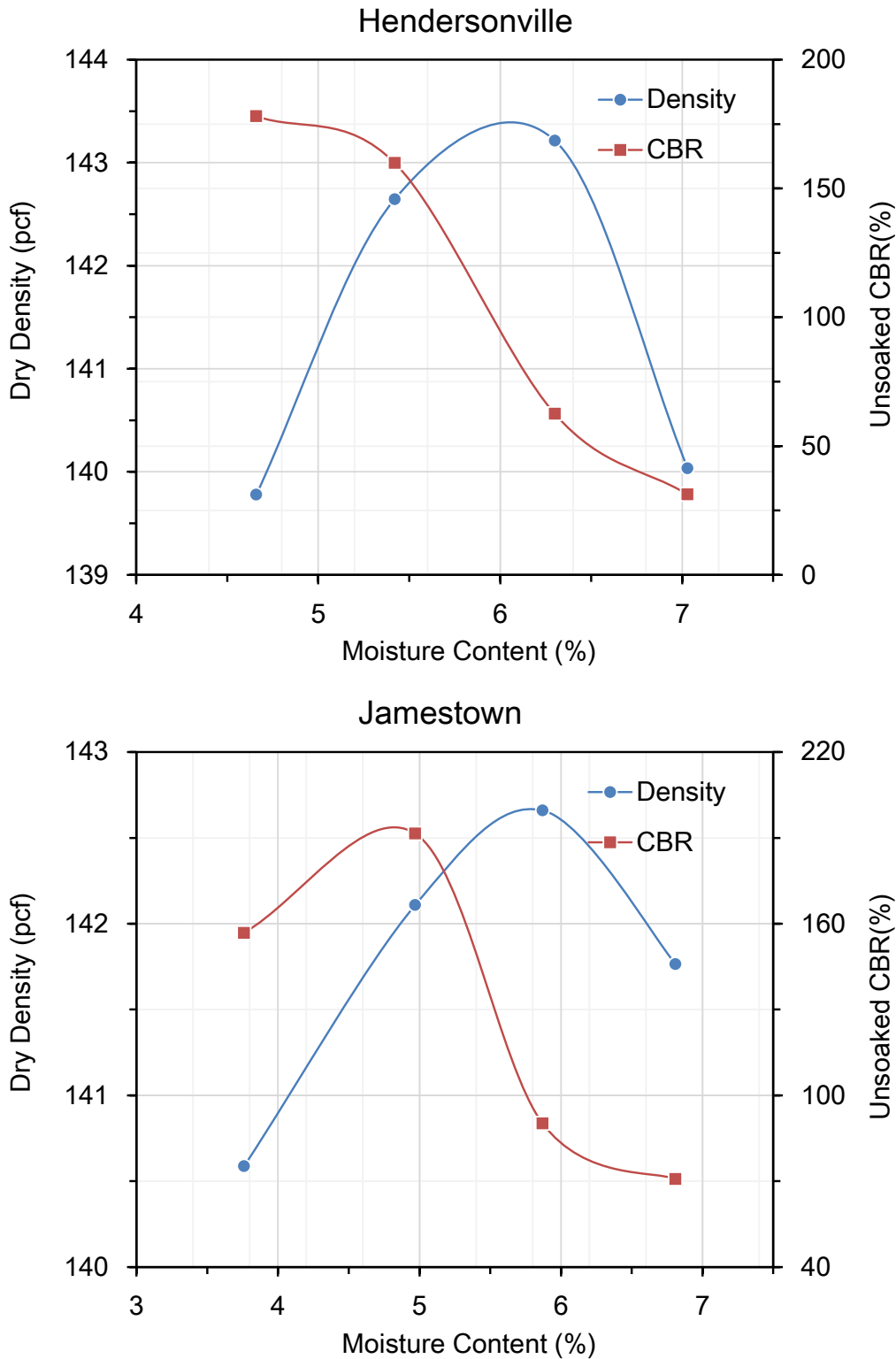


**Figure B.1 (Cont'd)** Moisture-density and CBR test results for the fifteen aggregate materials at the source gradations (Results from testing at UIUC)

Note: y-axis scales for dry density and unsoaked CBR are different at each material

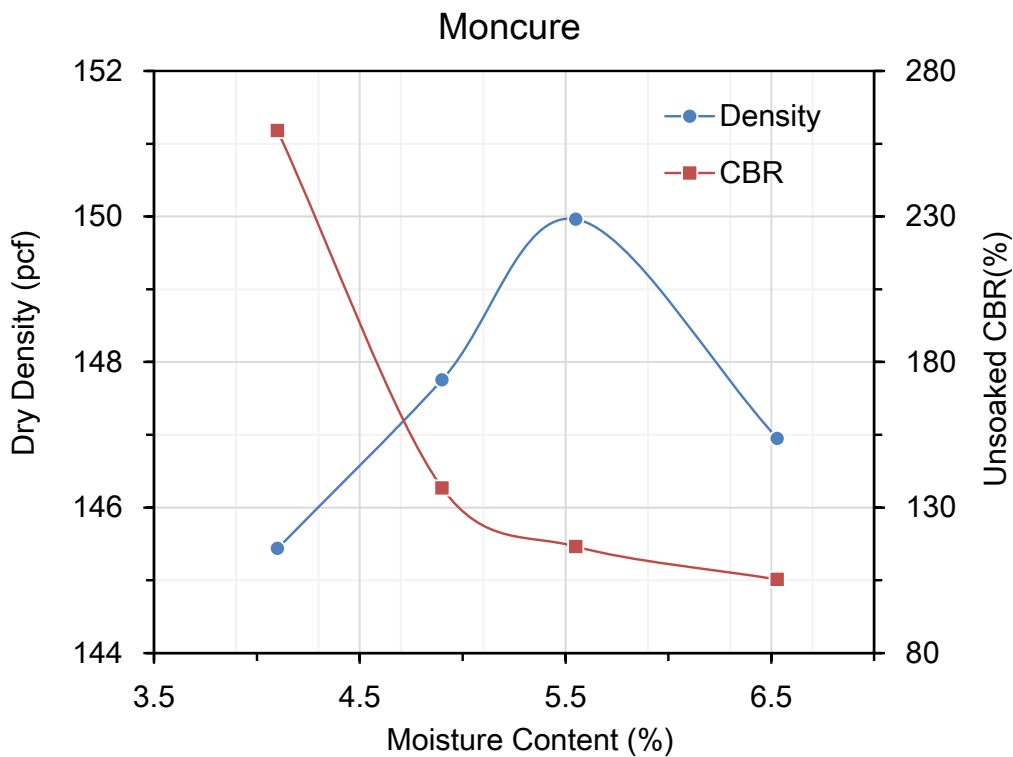
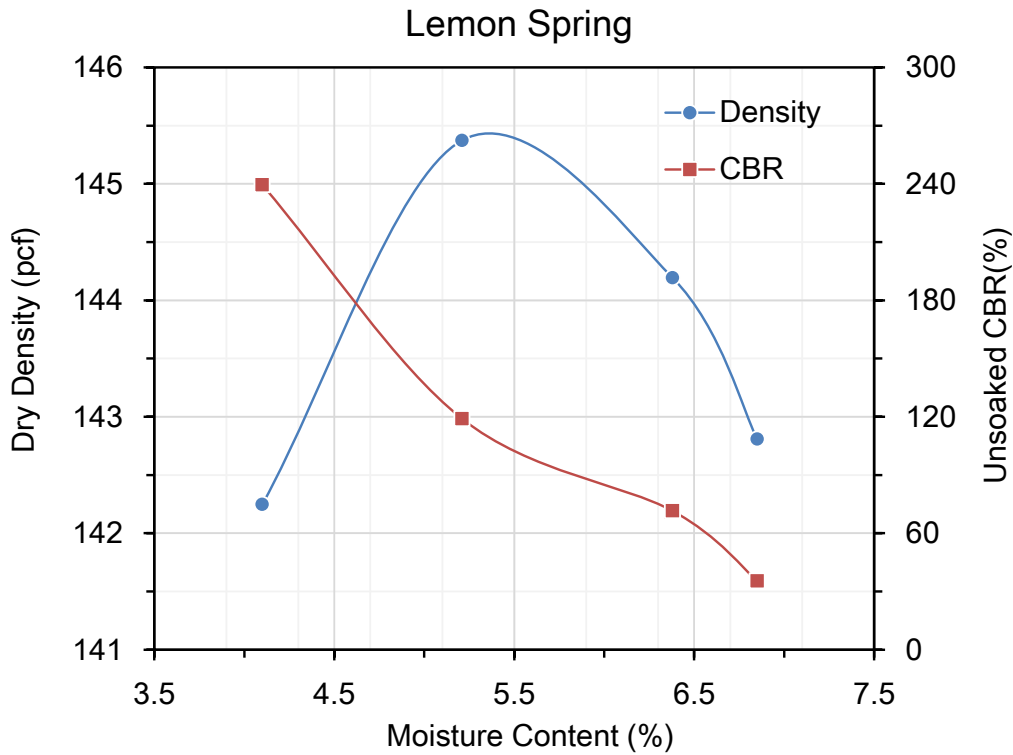


**Figure B.1 (Cont'd)** Moisture-density and CBR test results for the fifteen aggregate materials at the source gradations (Results from testing at UIUC)

Note: y-axis scales for dry density and unsoaked CBR are different at each material

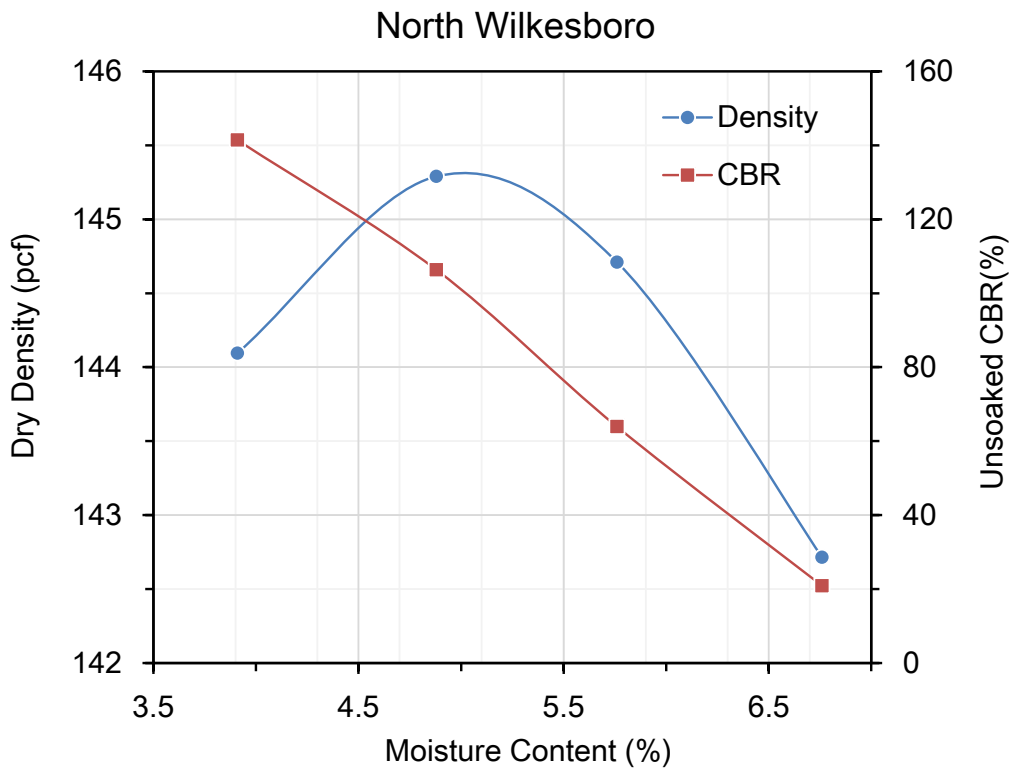
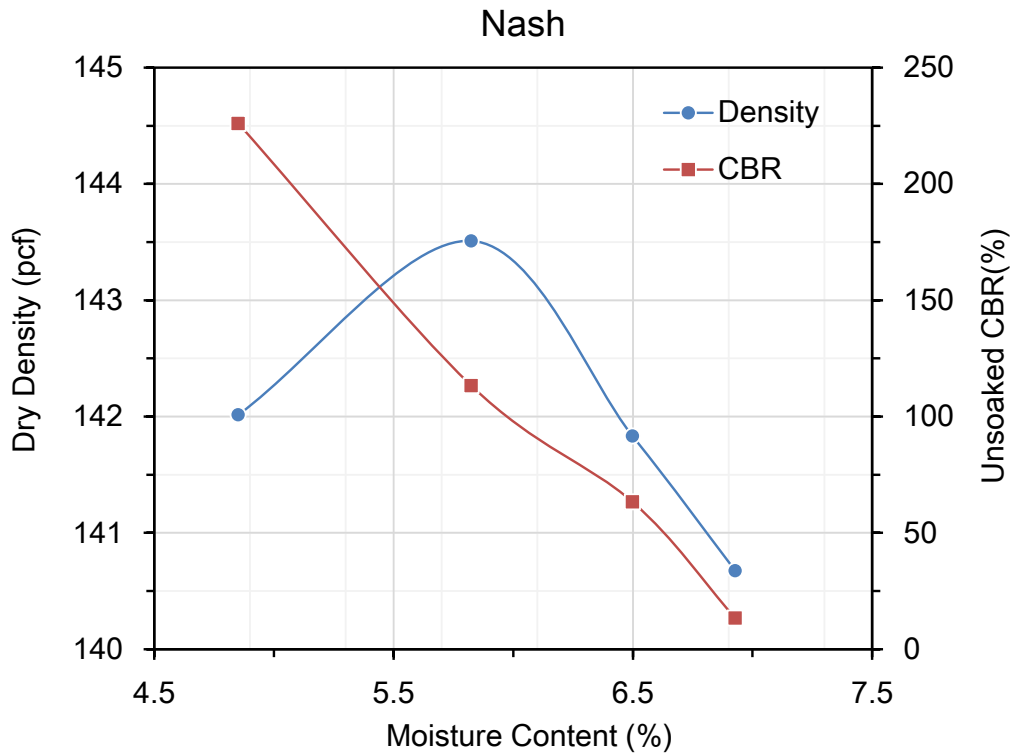


**Figure B.1 (Cont'd)** Moisture-density and CBR test results for the fifteen aggregate materials at the source gradations (Results from testing at UIUC)

Note: y-axis scales for dry density and unsoaked CBR are different at each material

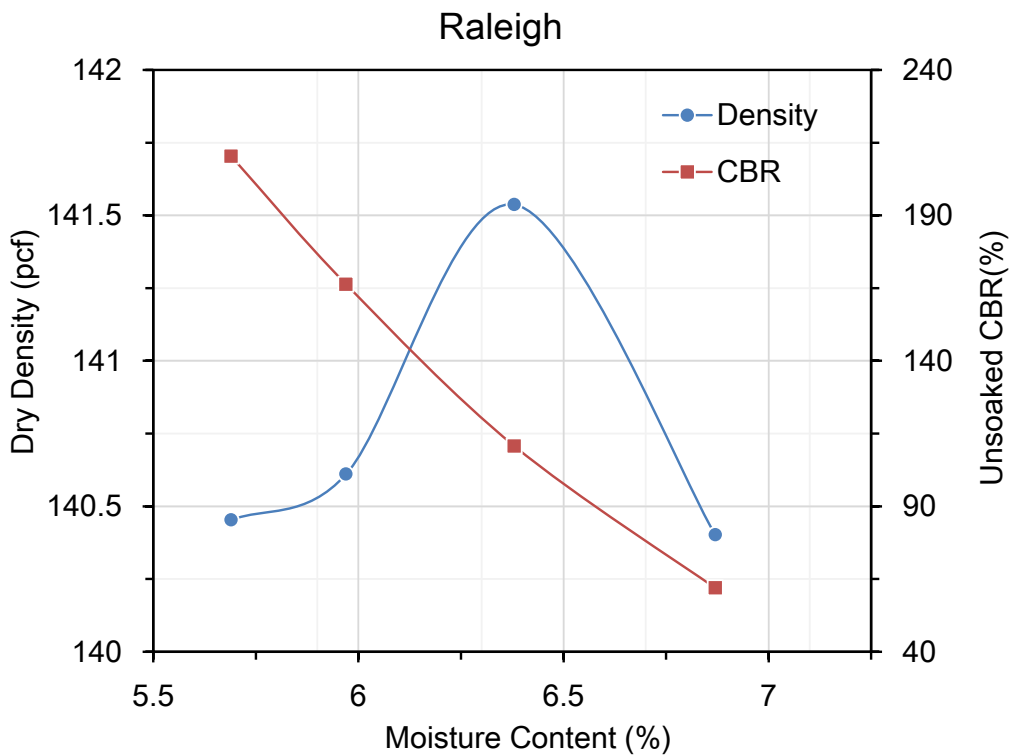
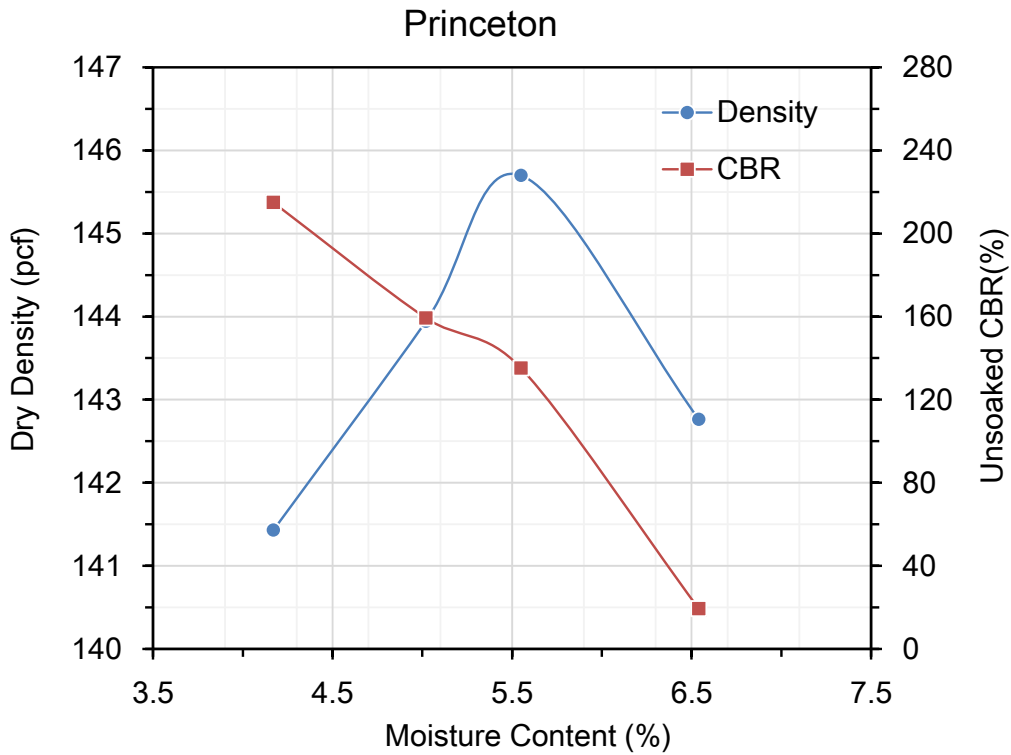


**Figure B.1 (Cont'd)** Moisture-density and CBR test results for the fifteen aggregate materials at the source gradations (Results from testing at UIUC)

Note: y-axis scales for dry density and unsoaked CBR are different at each material

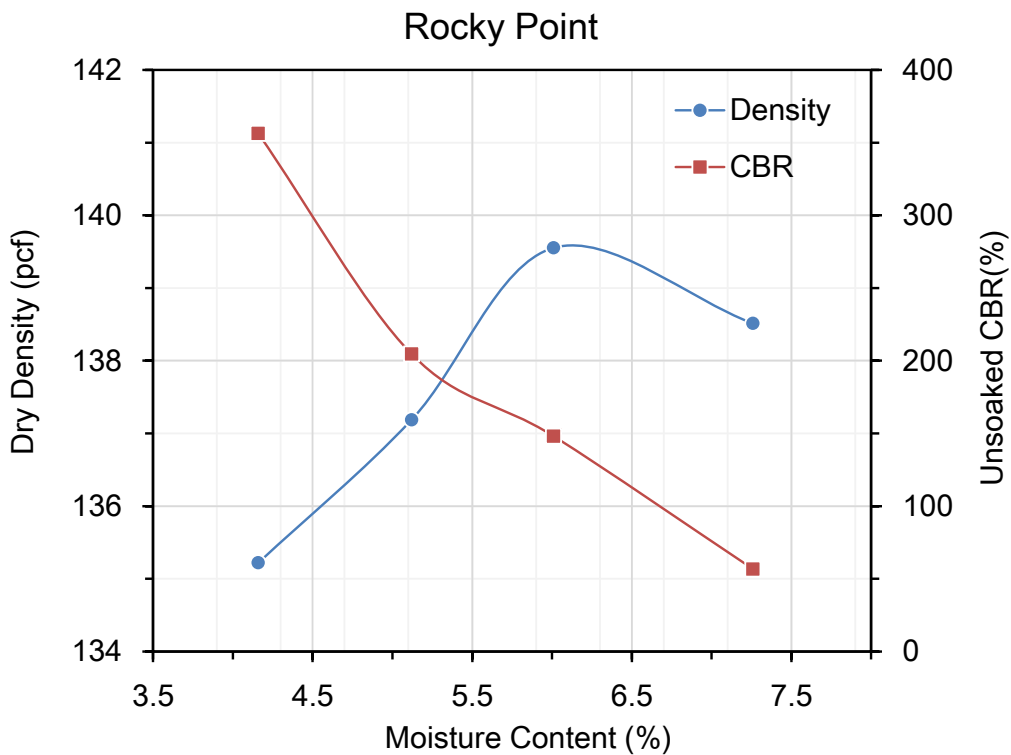
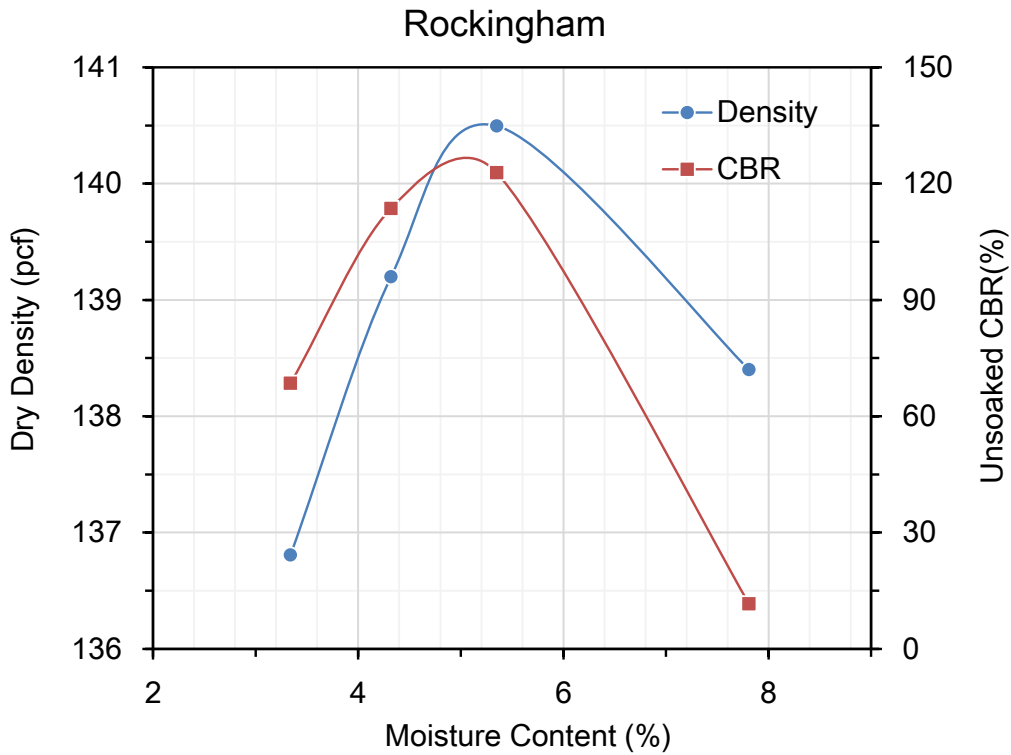


**Figure B.1 (Cont'd)** Moisture-density and CBR test results for the fifteen aggregate materials at the source gradations (Results from testing at UIUC)

Note: y-axis scales for dry density and unsoaked CBR are different at each material

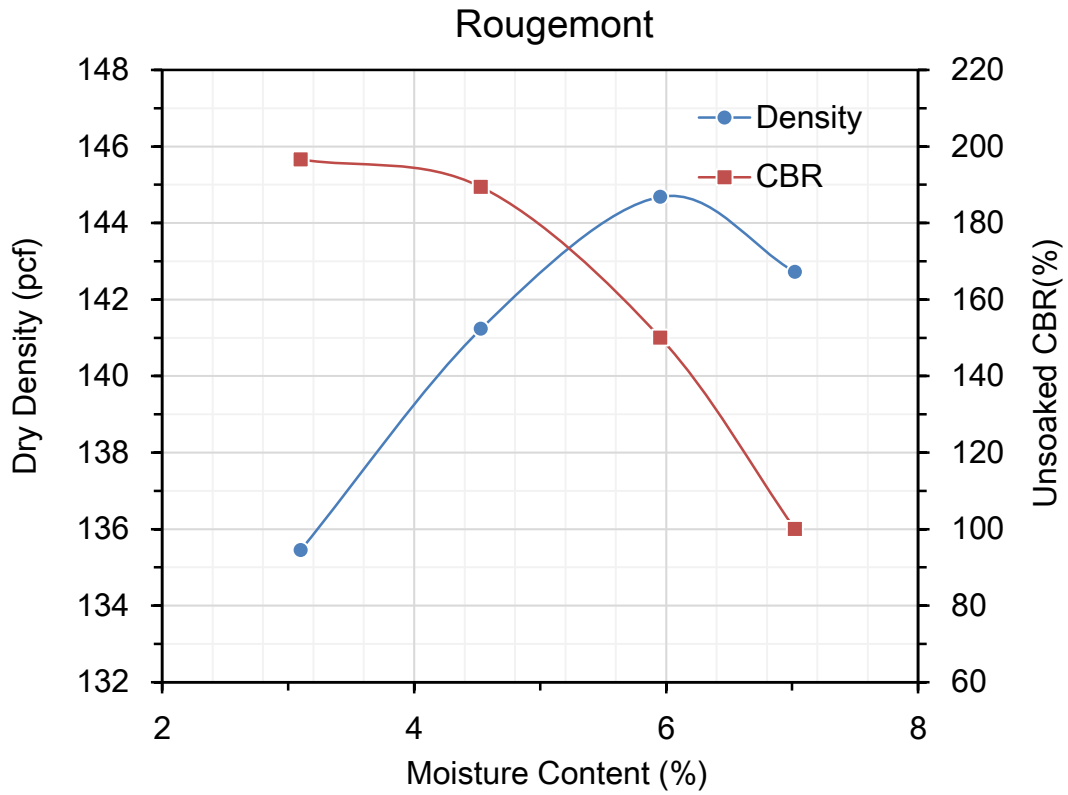


**Figure B.1 (Cont'd)** Moisture-density and CBR test results for the fifteen aggregate materials at the source gradations (Results from testing at UIUC)

Note: y-axis scales for dry density and unsoaked CBR are different at each material

## APPENDIX C Monotonic Shear Strength Test Results

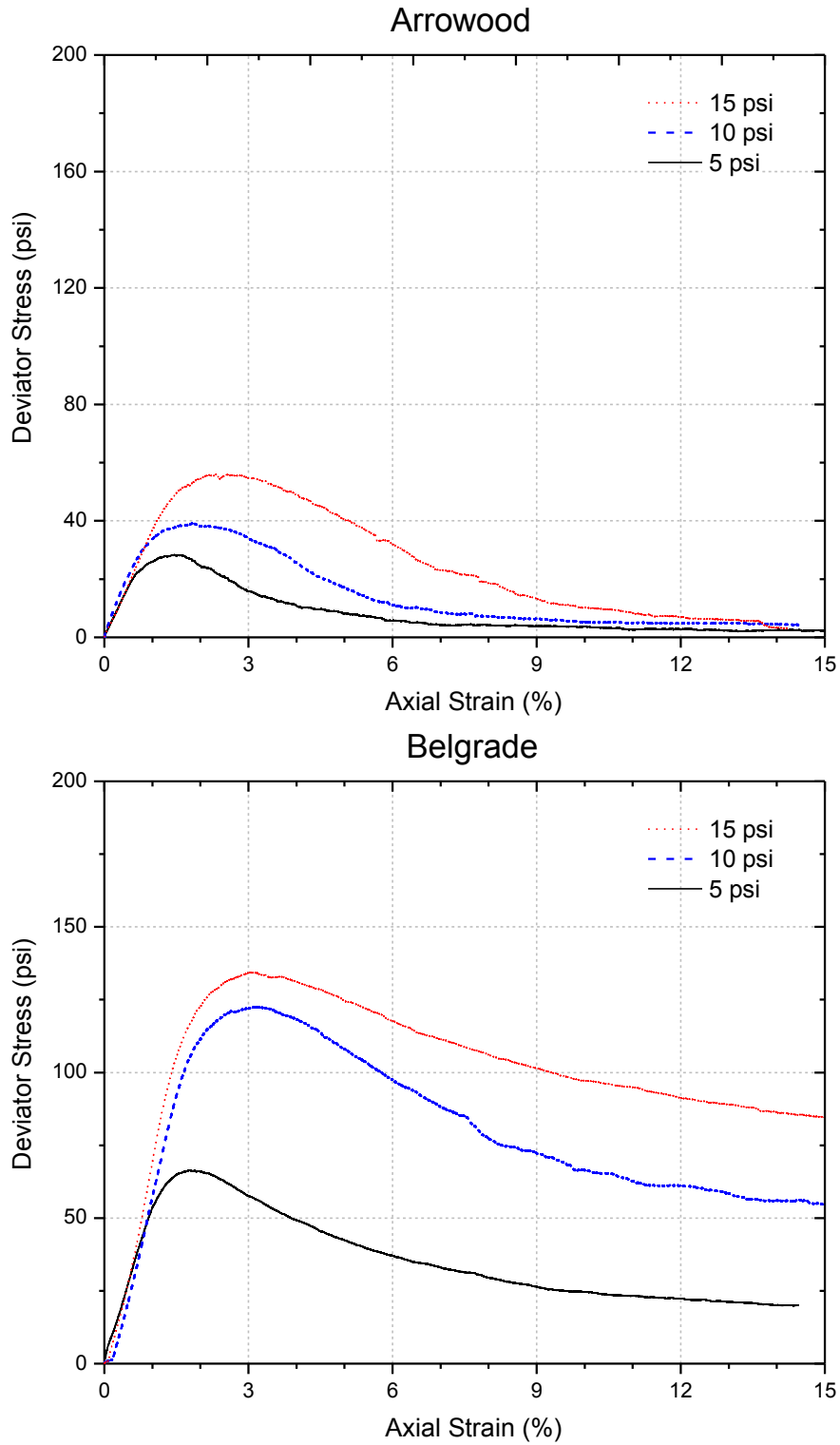


**Figure C.1** Stress-strain diagrams for shear strength tests for the fifteen aggregate materials at the source gradations (SG)

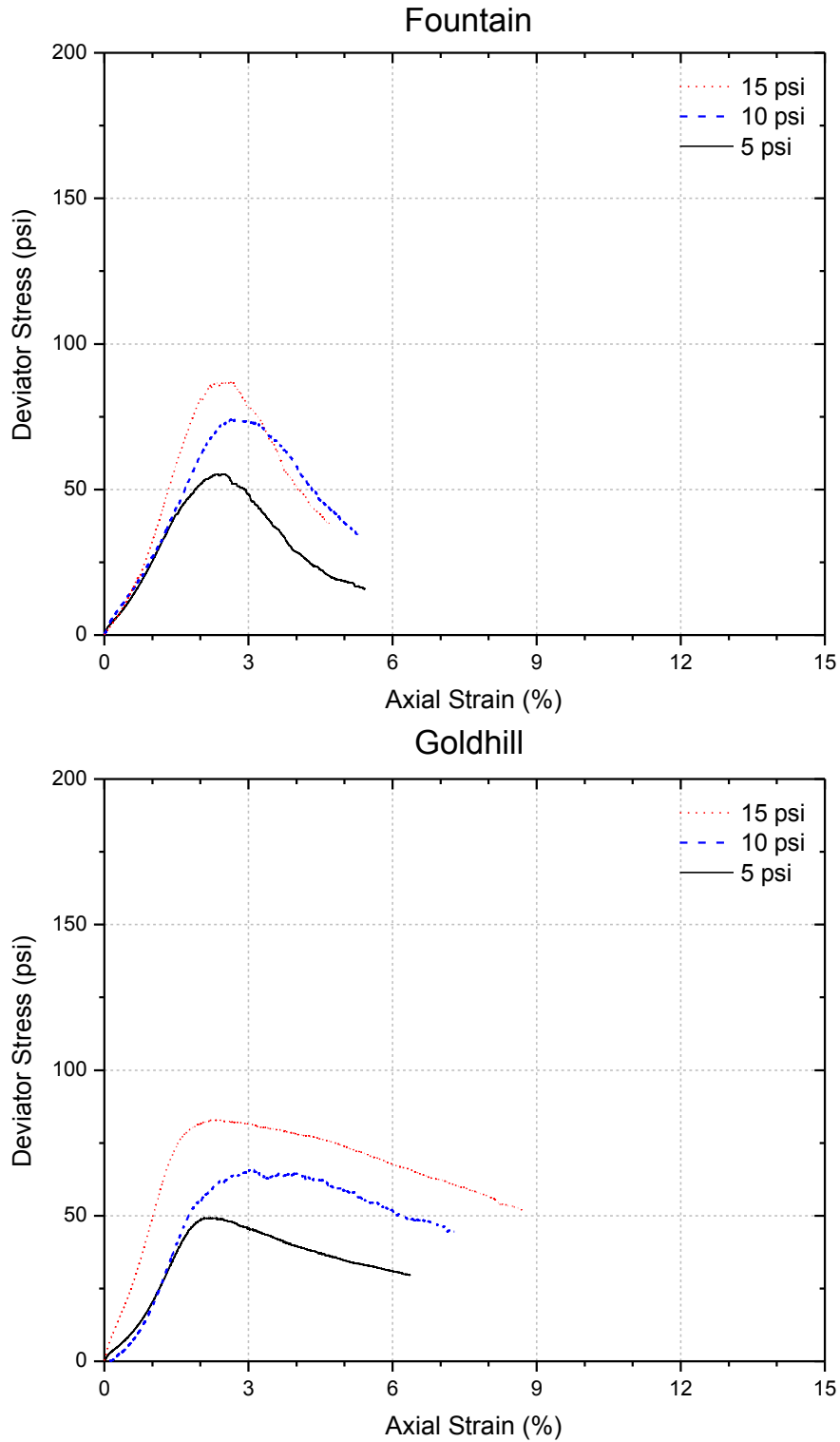


**Figure C.1 (Cont'd)** Stress-strain diagrams for shear strength tests for the fifteen aggregate materials at the source gradations (SG)

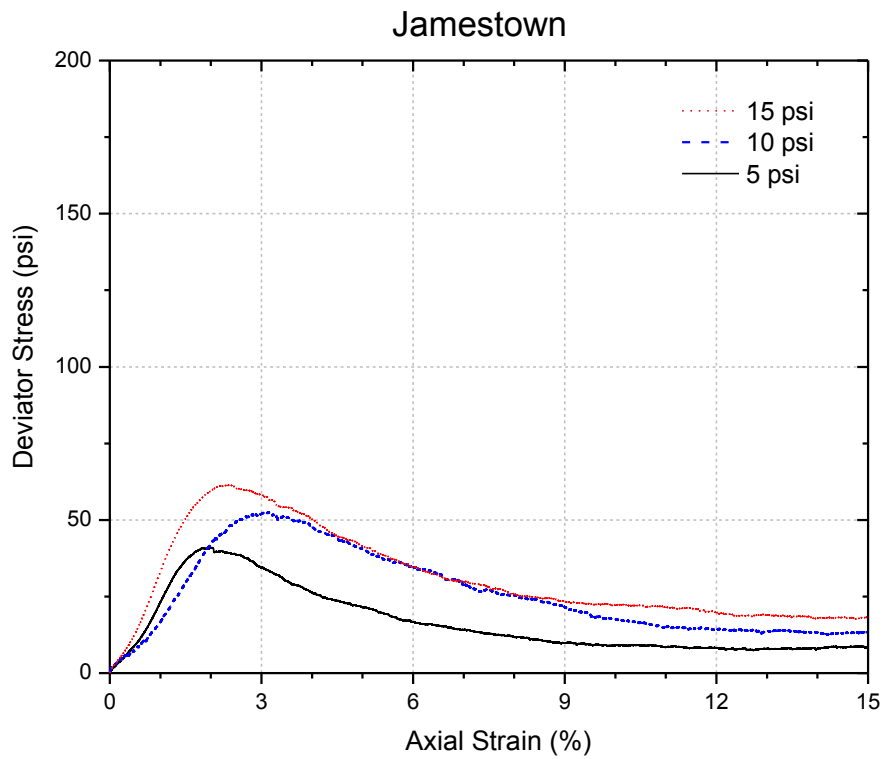
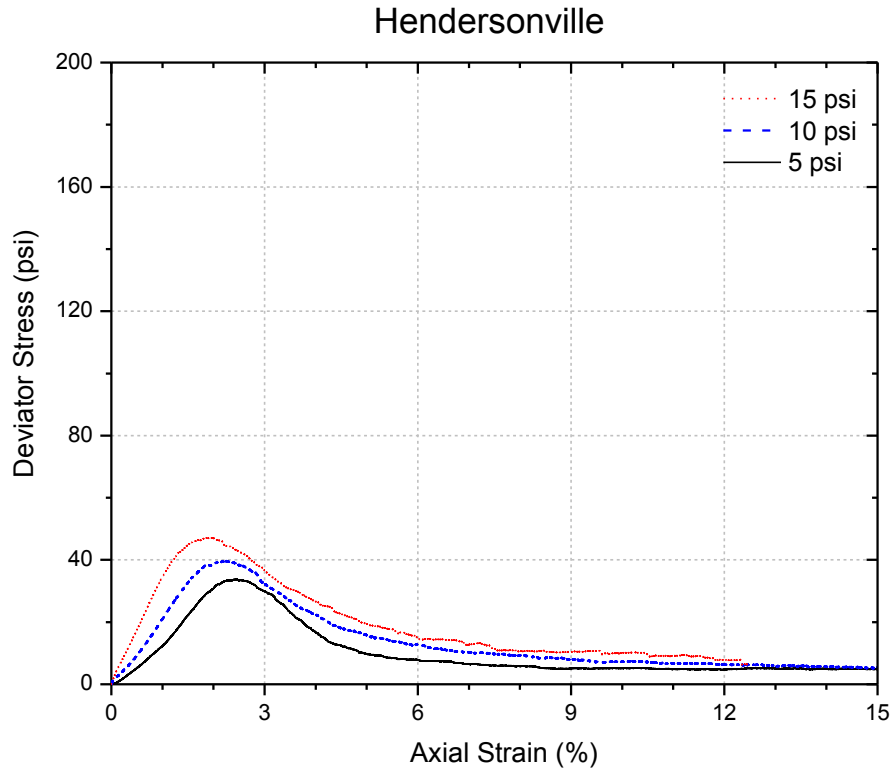


**Figure C.1 (Cont'd)** Stress-strain diagrams for shear strength tests for the fifteen aggregate materials at the source gradations (SG)

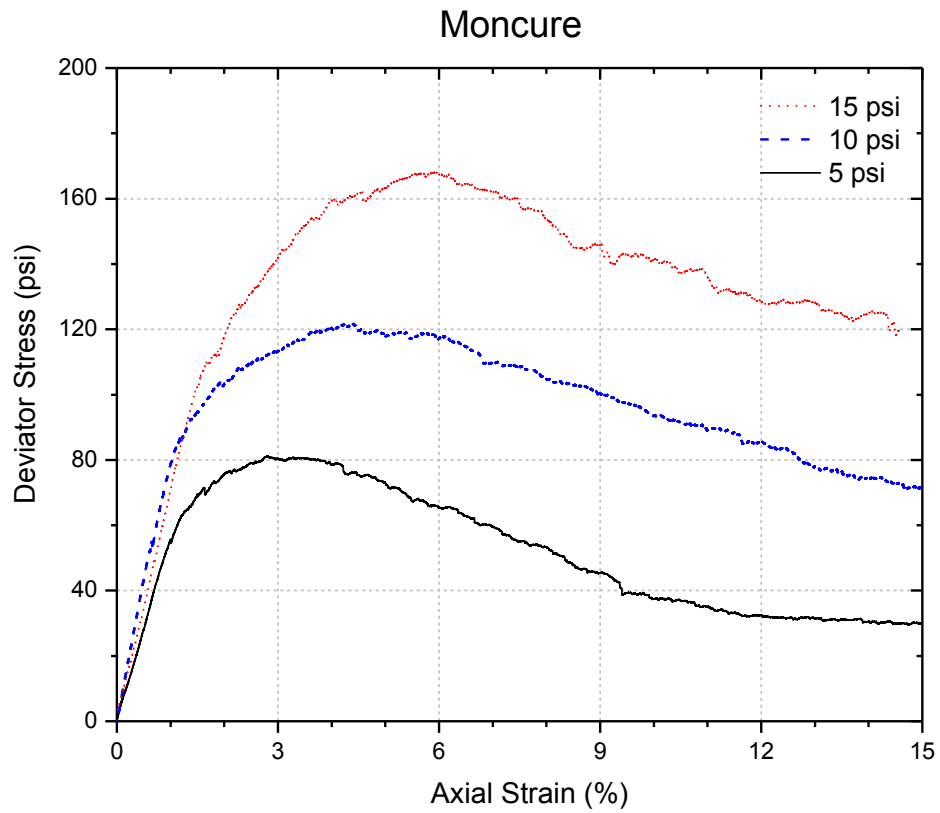
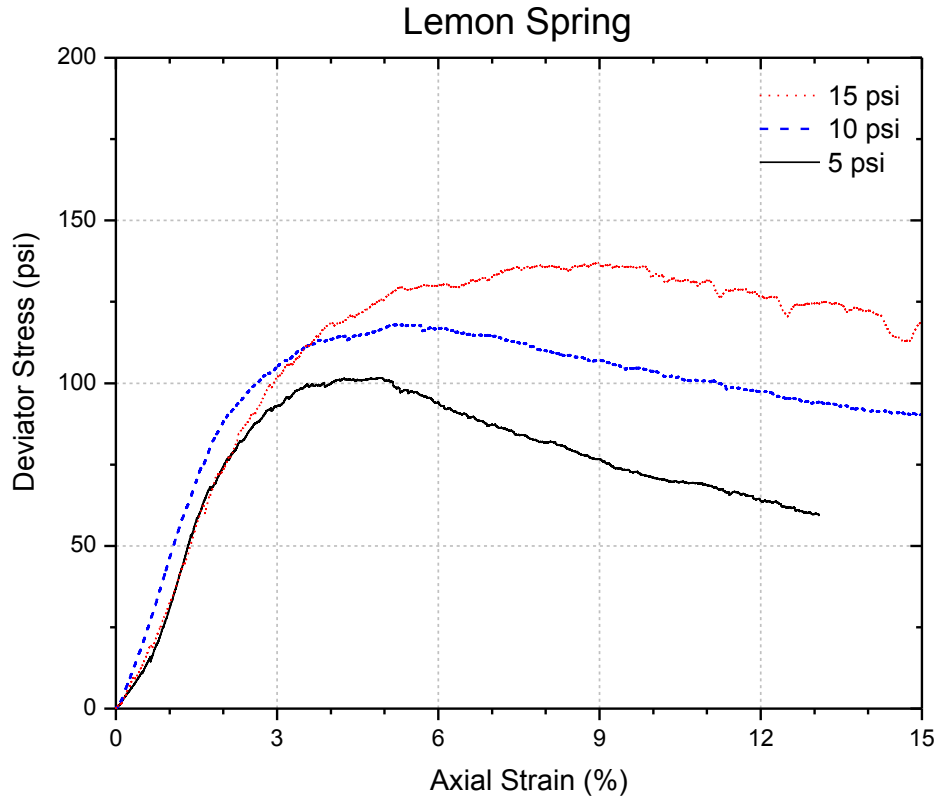


**Figure C.1 (Cont'd)** Stress-strain diagrams for shear strength tests for the fifteen aggregate materials at the source gradations (SG)

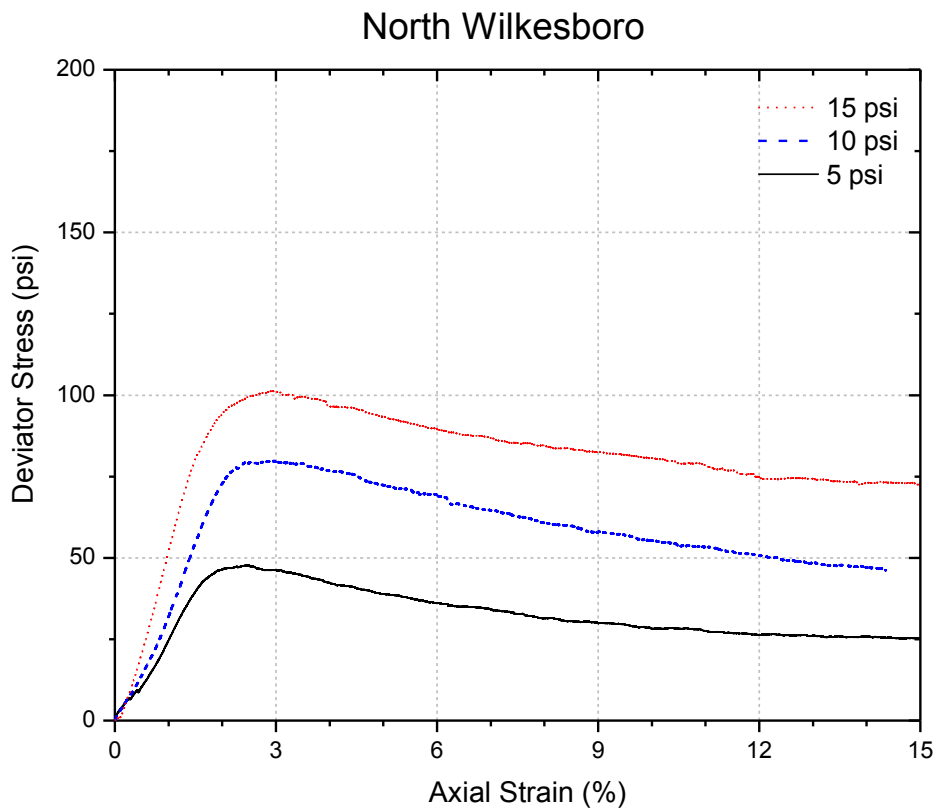
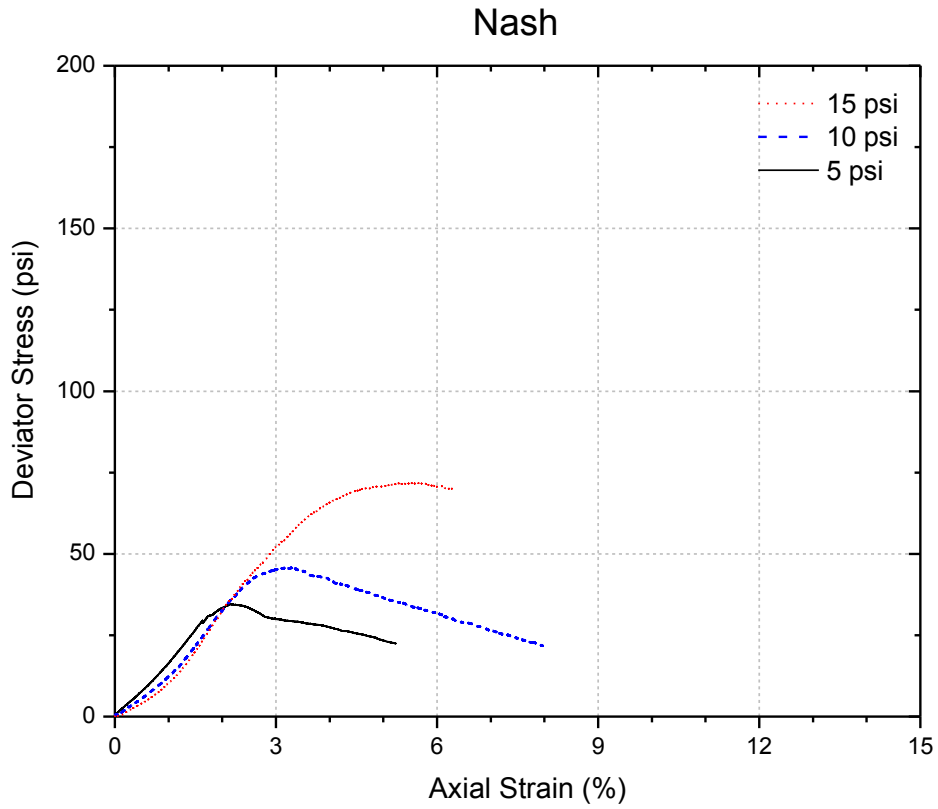


**Figure C.1 (Cont'd)** Stress-strain diagrams for shear strength tests for the fifteen aggregate materials at the source gradations (SG)

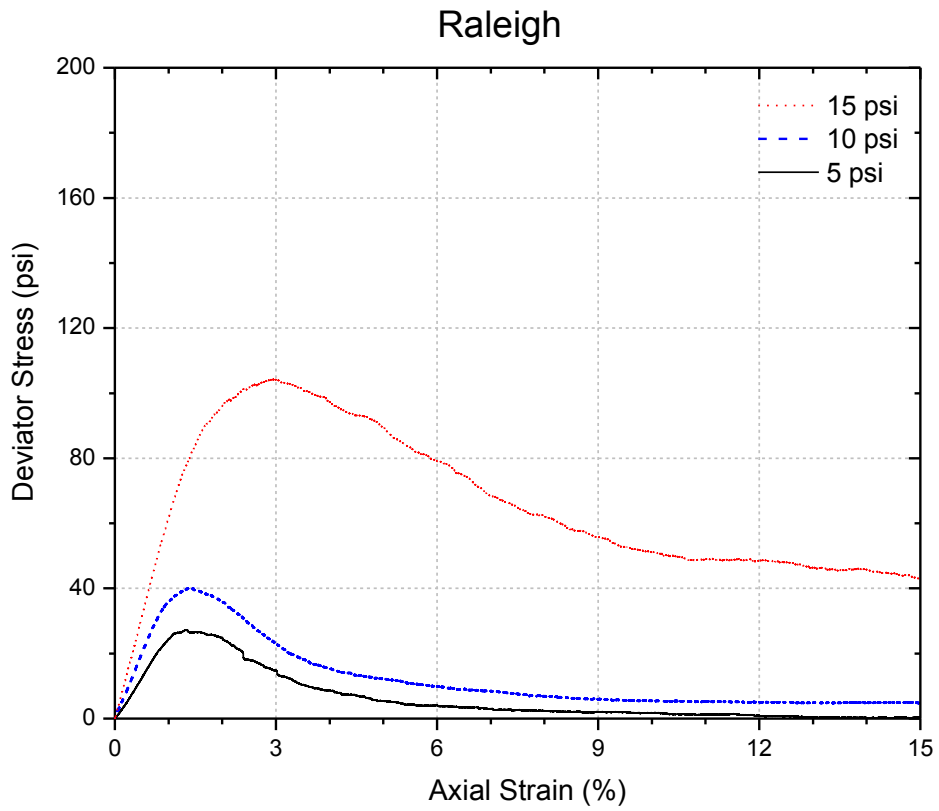
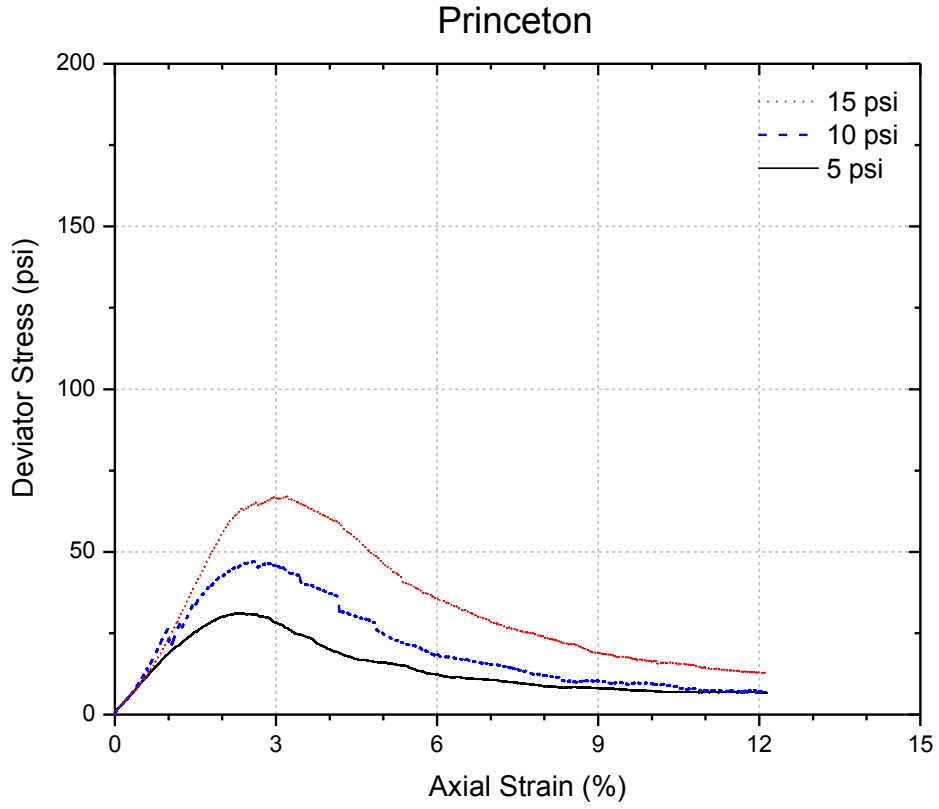


**Figure C.1 (Cont'd)** Stress-strain diagrams for shear strength tests for the fifteen aggregate materials at the source gradations (SG)

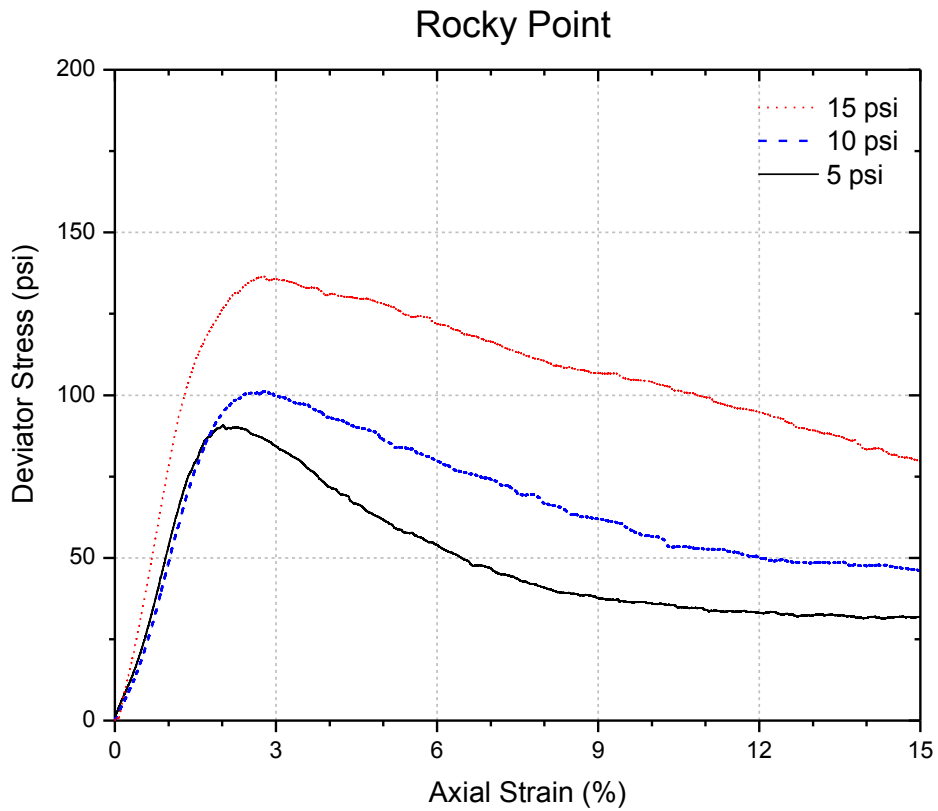
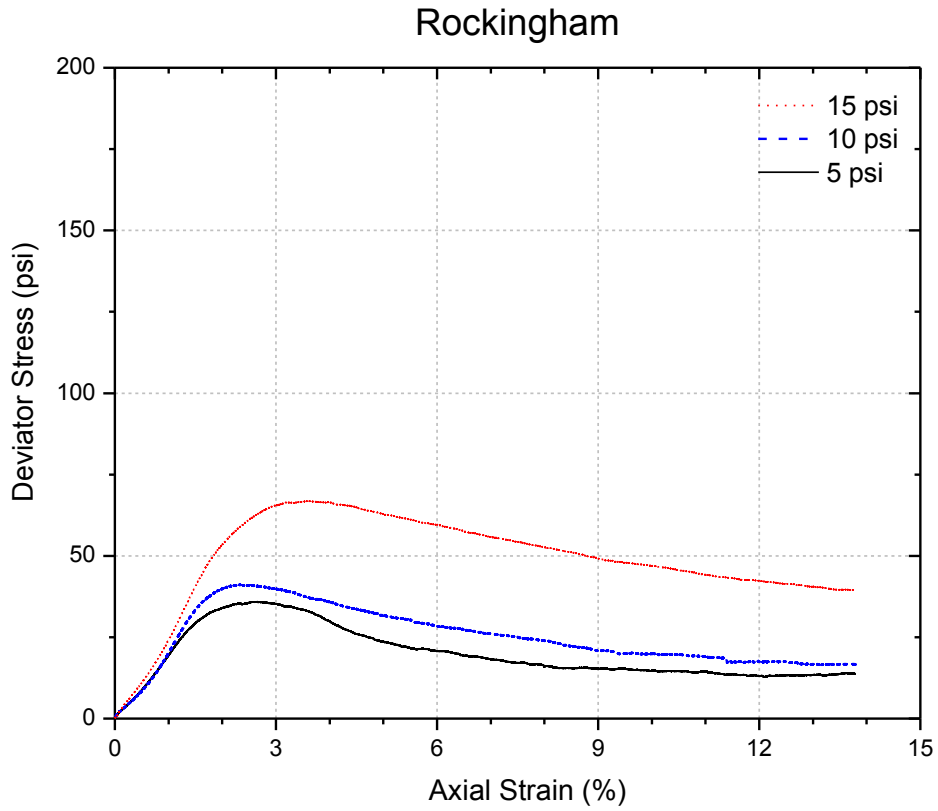


**Figure C.1 (Cont'd)** Stress-strain diagrams for shear strength tests for the fifteen aggregate materials at the source gradations (SG)

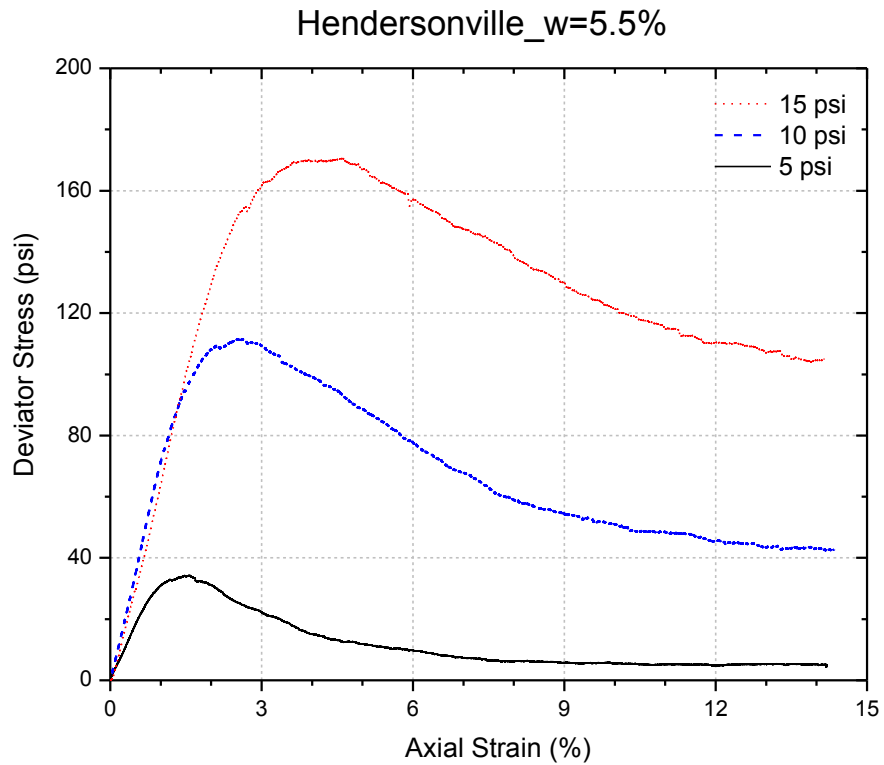
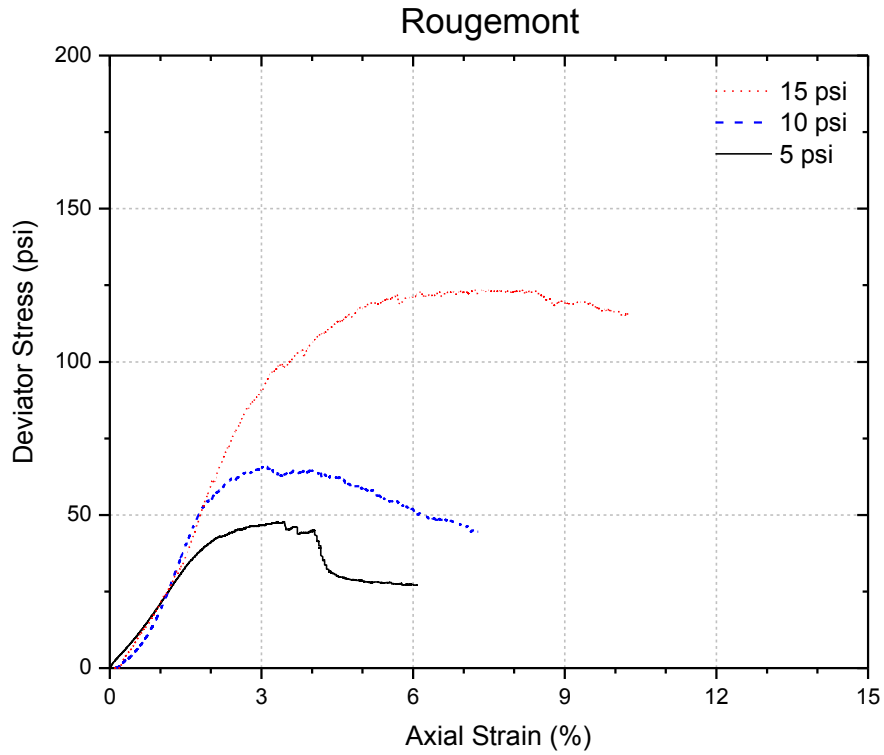


**Figure C.1 (Cont'd)** Stress-strain diagrams for shear strength tests for the fifteen aggregate materials at the source gradations (SG)

## APPENDIX D Repeated Load Permanent Deformation Test Results

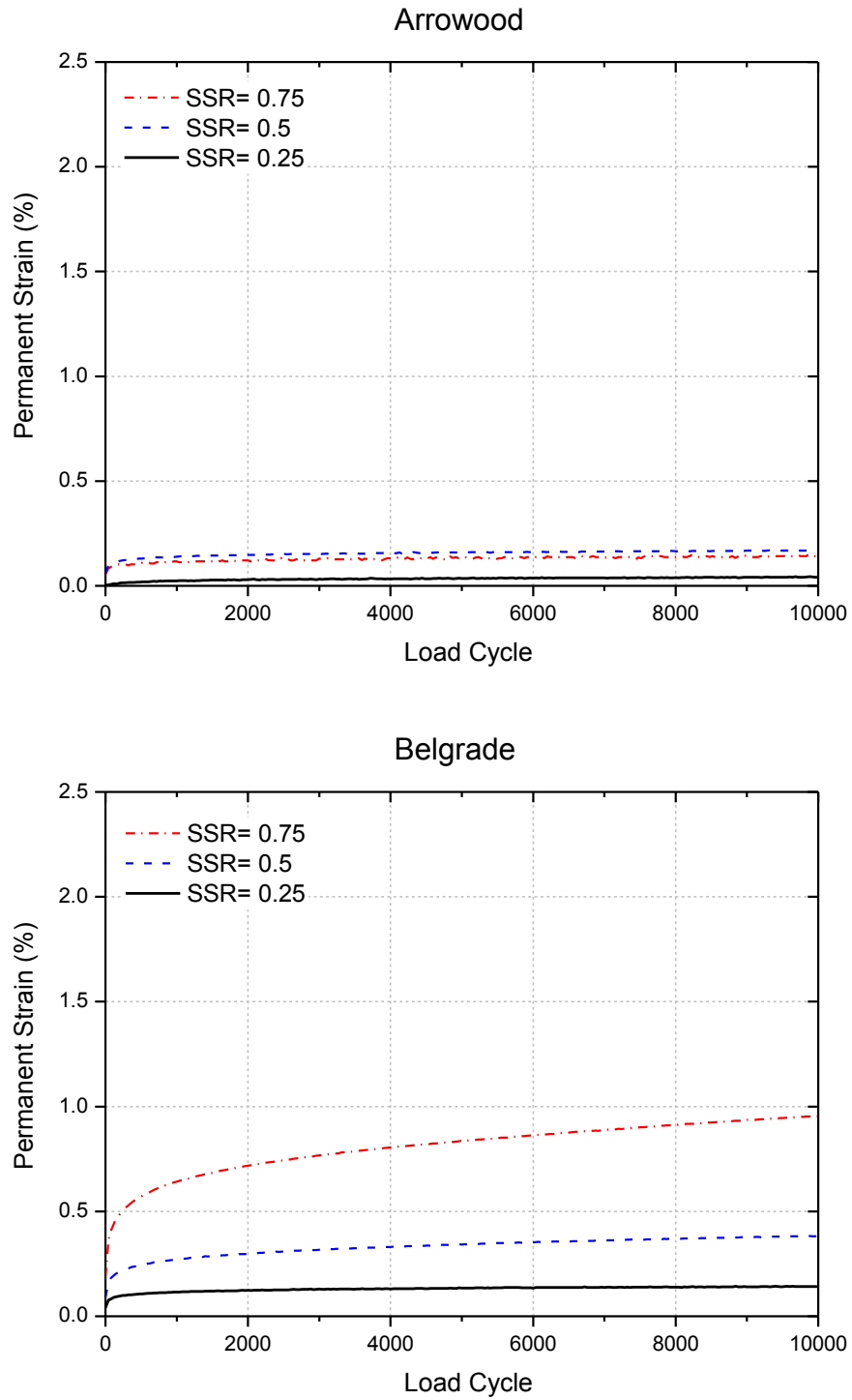


**Figure D.1** Permanent strain accumulations in the fifteen aggregate materials at the source gradations for different SSR levels

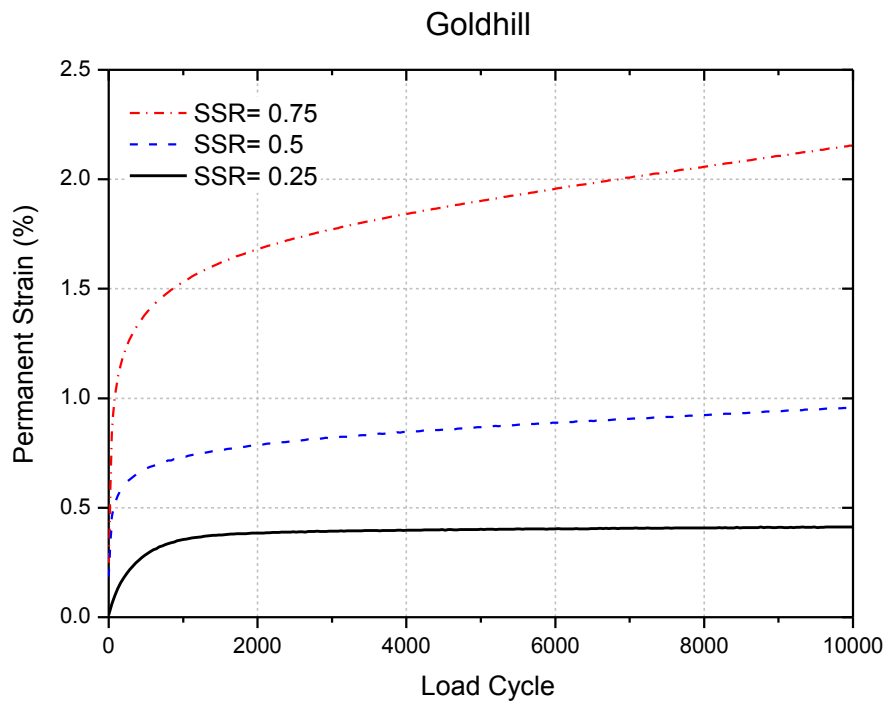
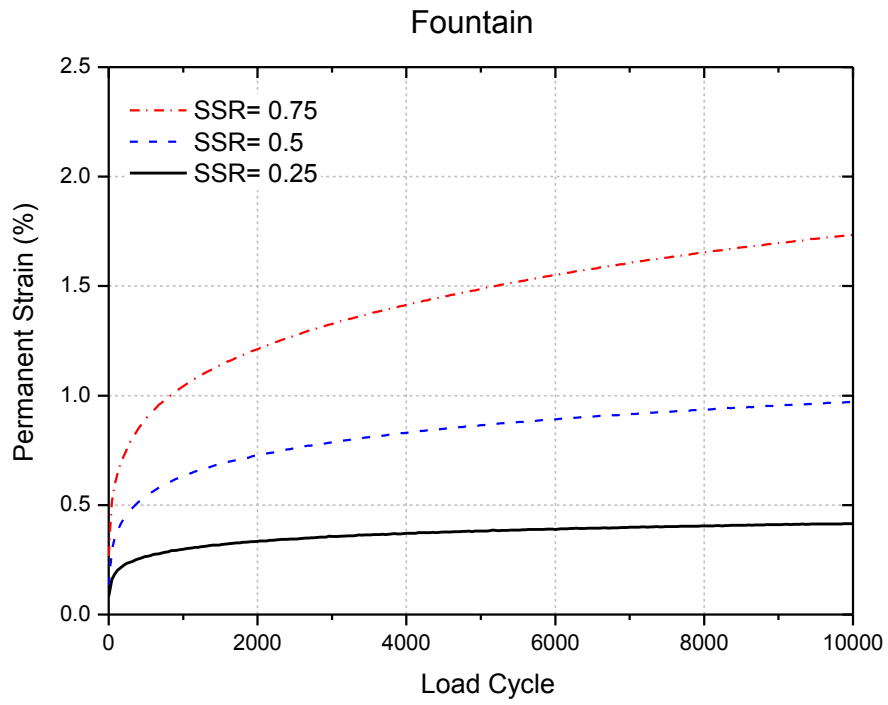


**Figure D.1 (Cont'd)** Permanent strain accumulations in the fifteen aggregate materials at the source gradations for different SSR levels

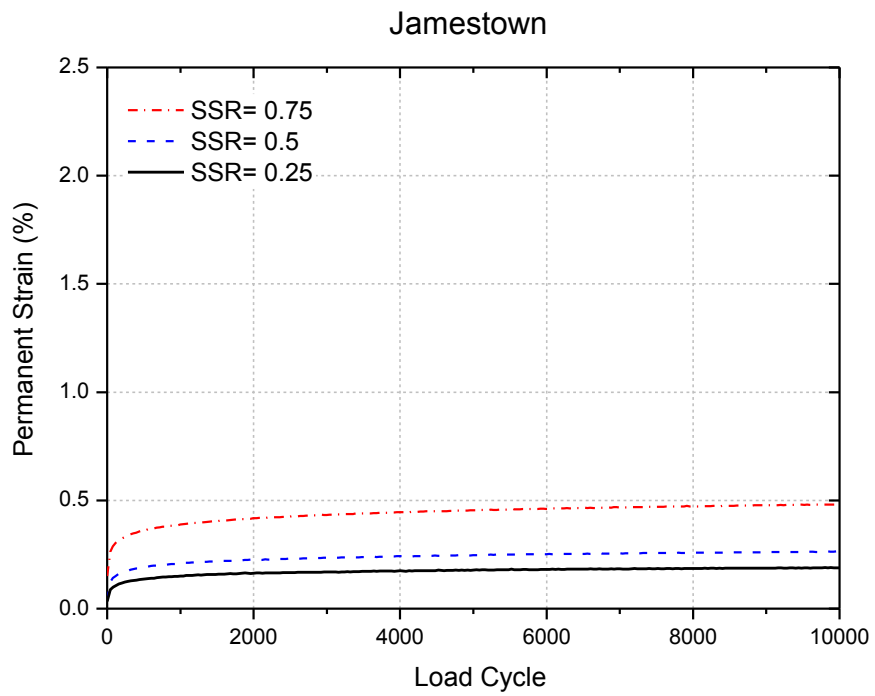
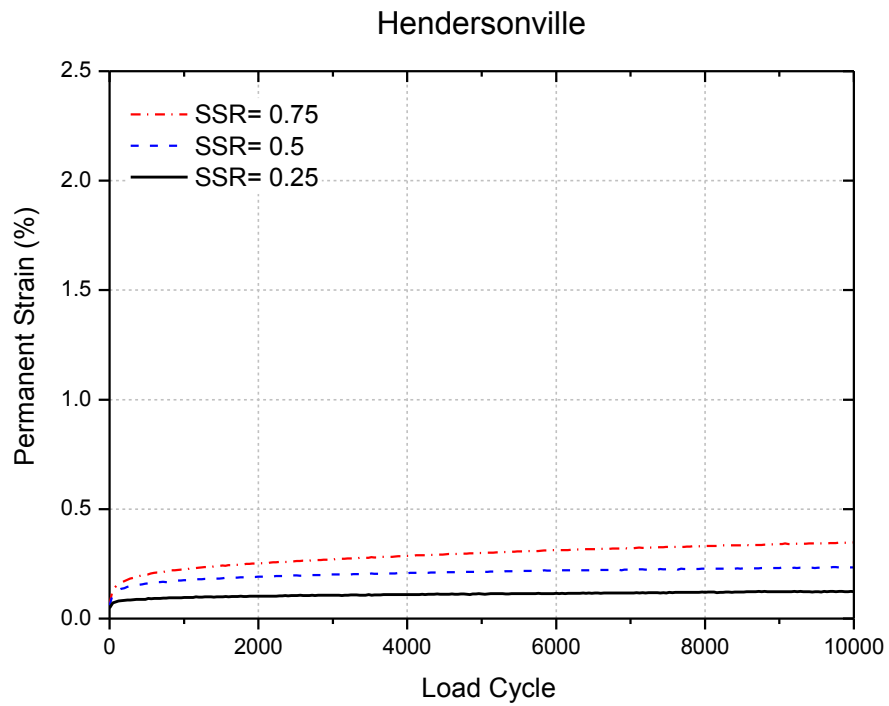


**Figure D.1 (Cont'd)** Permanent strain accumulations in the fifteen aggregate materials at the source gradations for different SSR levels

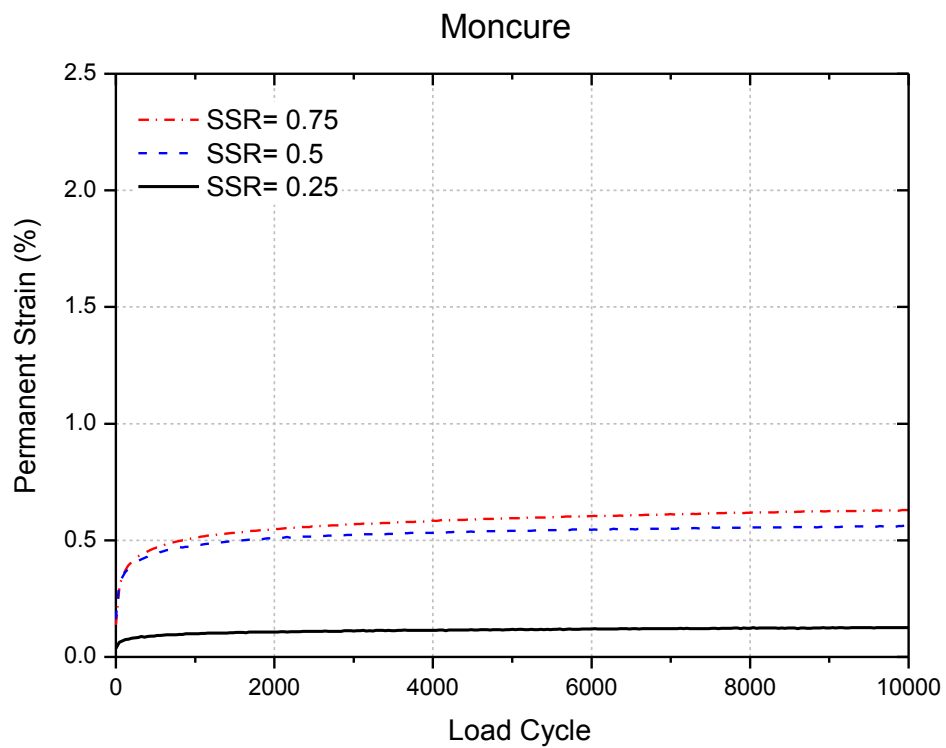
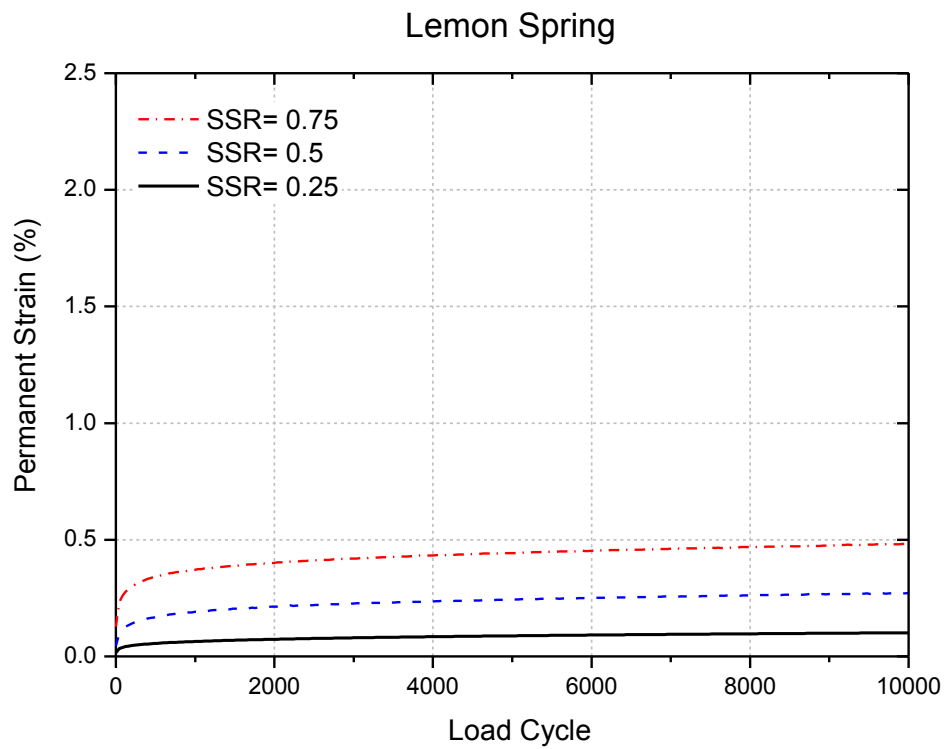


**Figure D.1 (Cont'd)** Permanent strain accumulations in the fifteen aggregate materials at the source gradations for different SSR levels

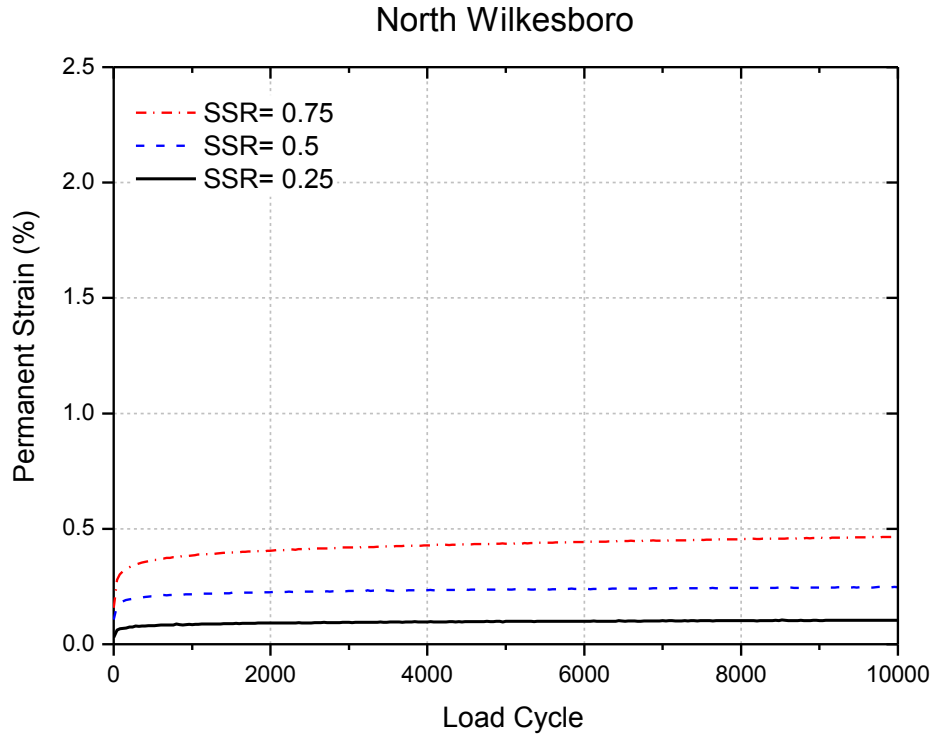
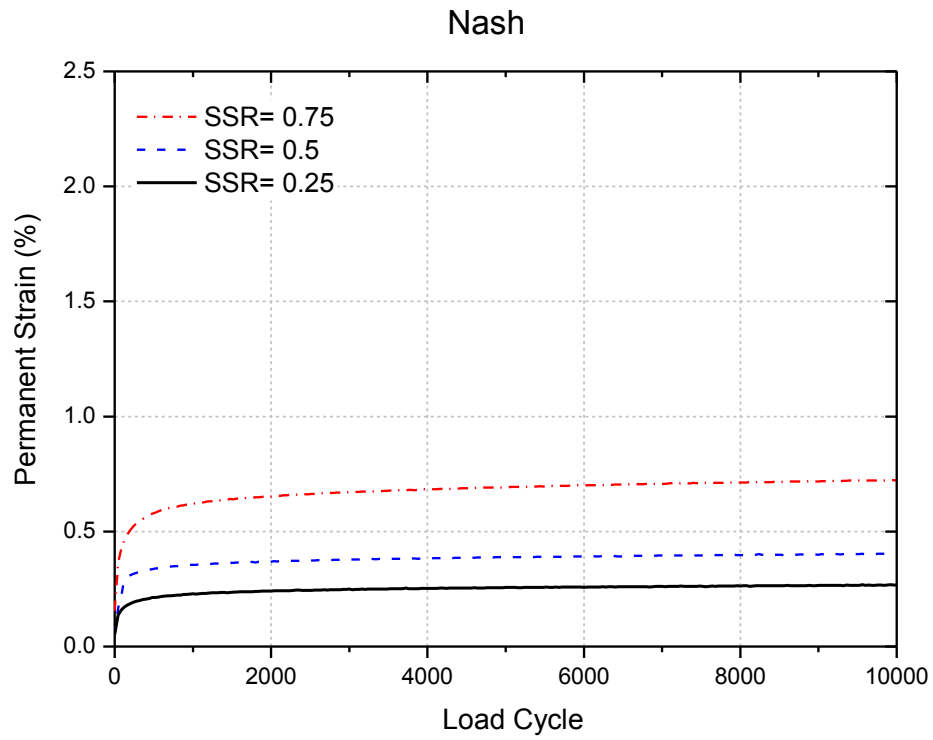


**Figure D.1 (Cont'd)** Permanent strain accumulations in the fifteen aggregate materials at the source gradations for different SSR levels

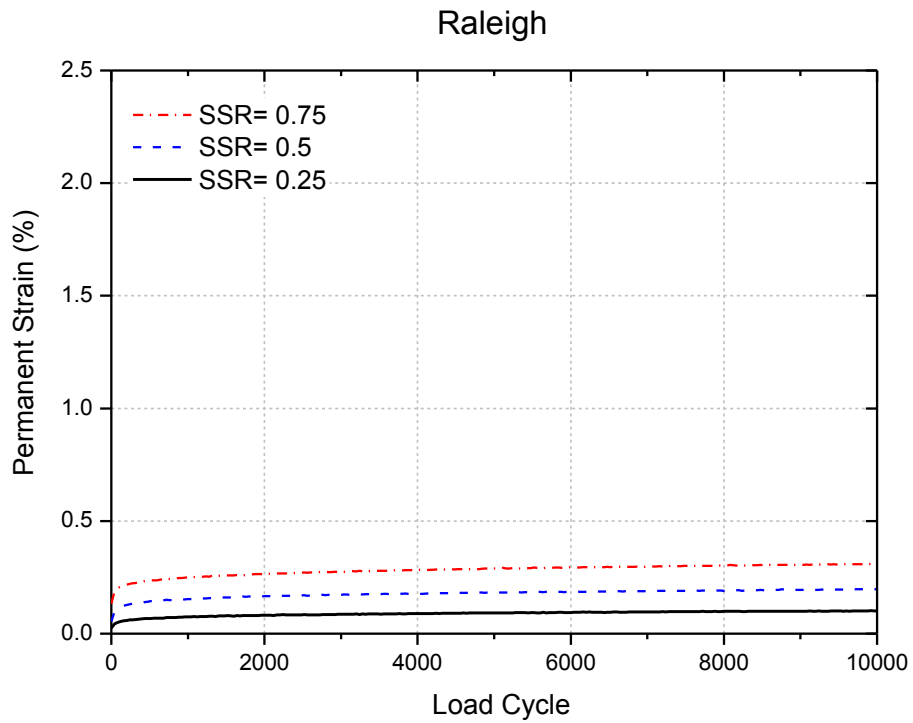
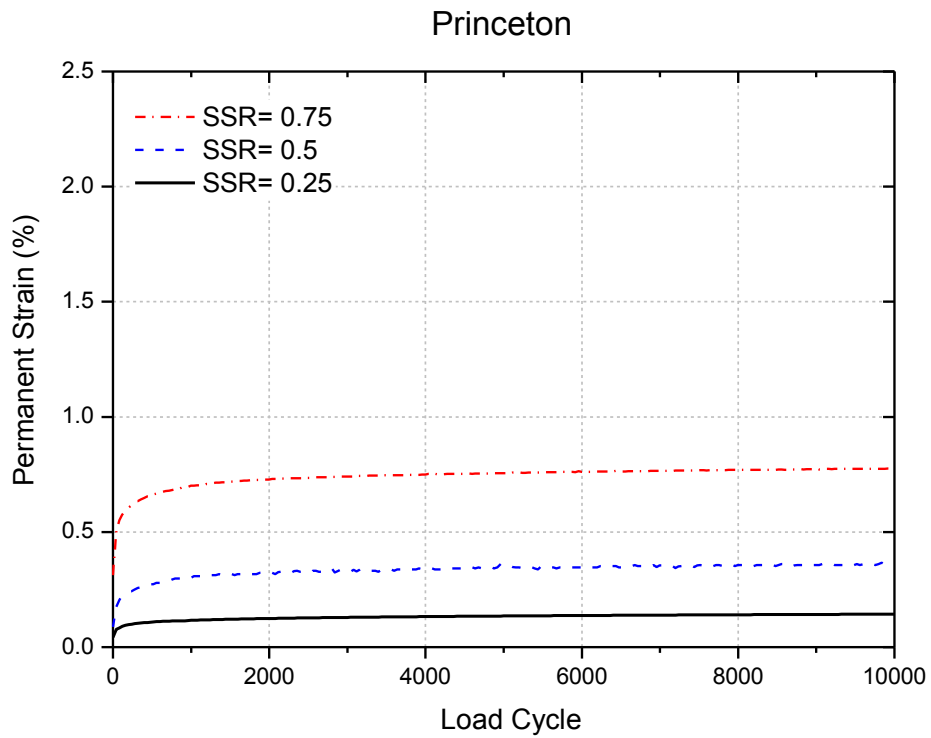


**Figure D.1 (Cont'd)** Permanent strain accumulations in the fifteen aggregate materials at the source gradations for different SSR levels

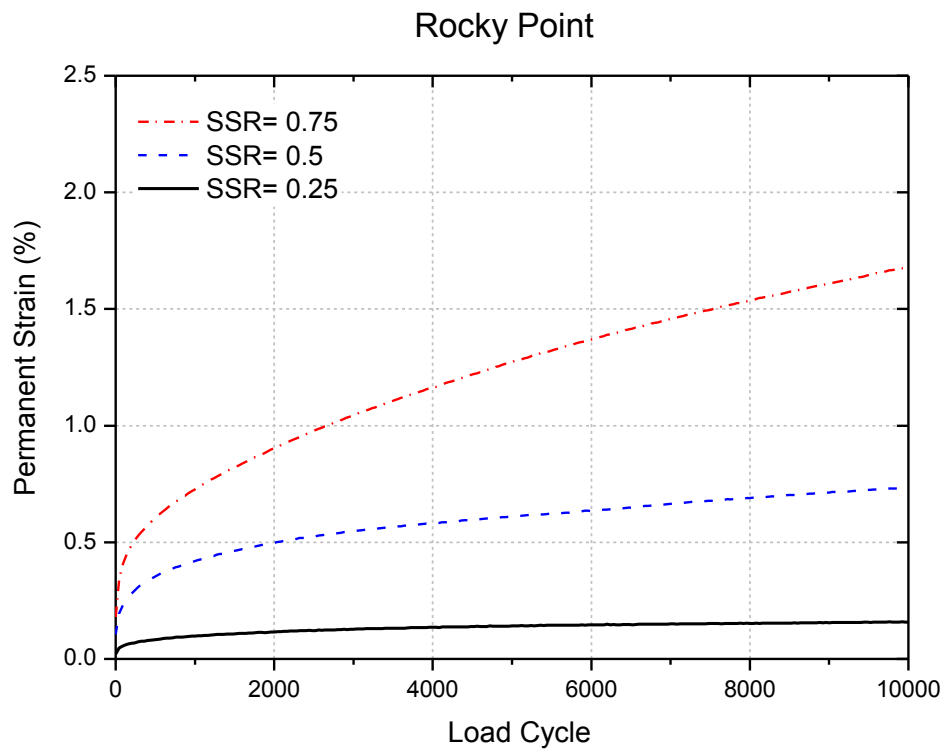
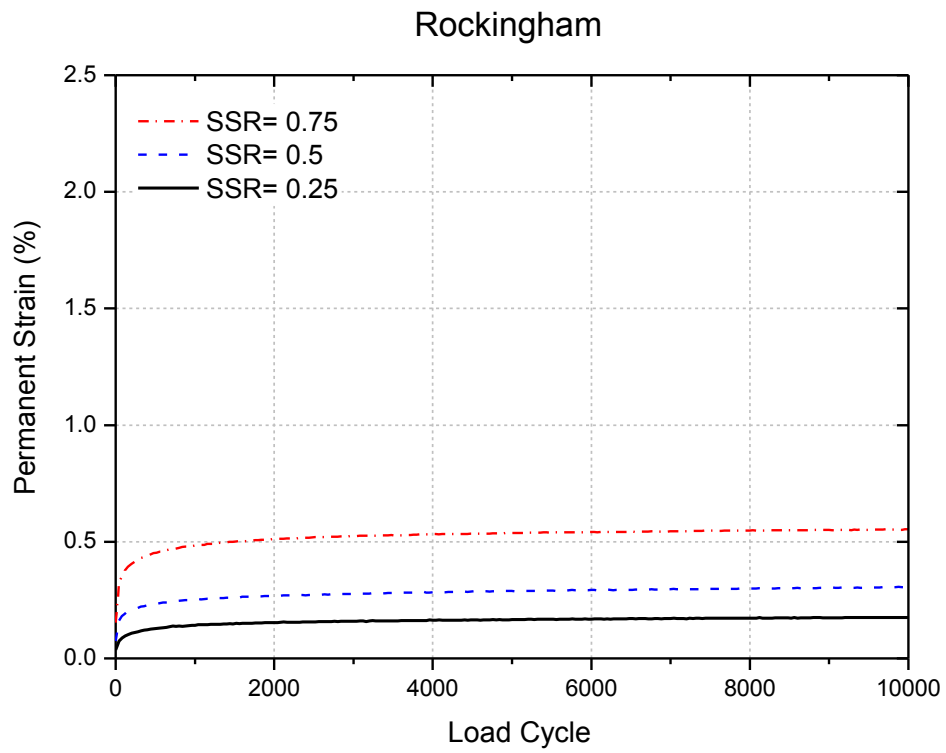


**Figure D.1 (Cont'd)** Permanent strain accumulations in the fifteen aggregate materials at the source gradations for different SSR levels

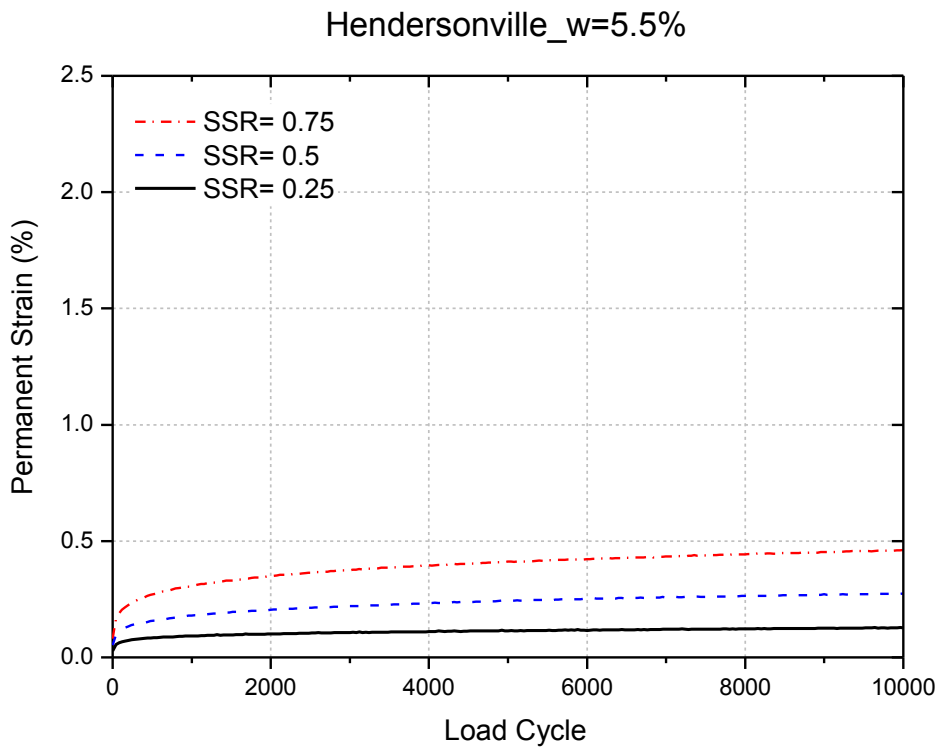
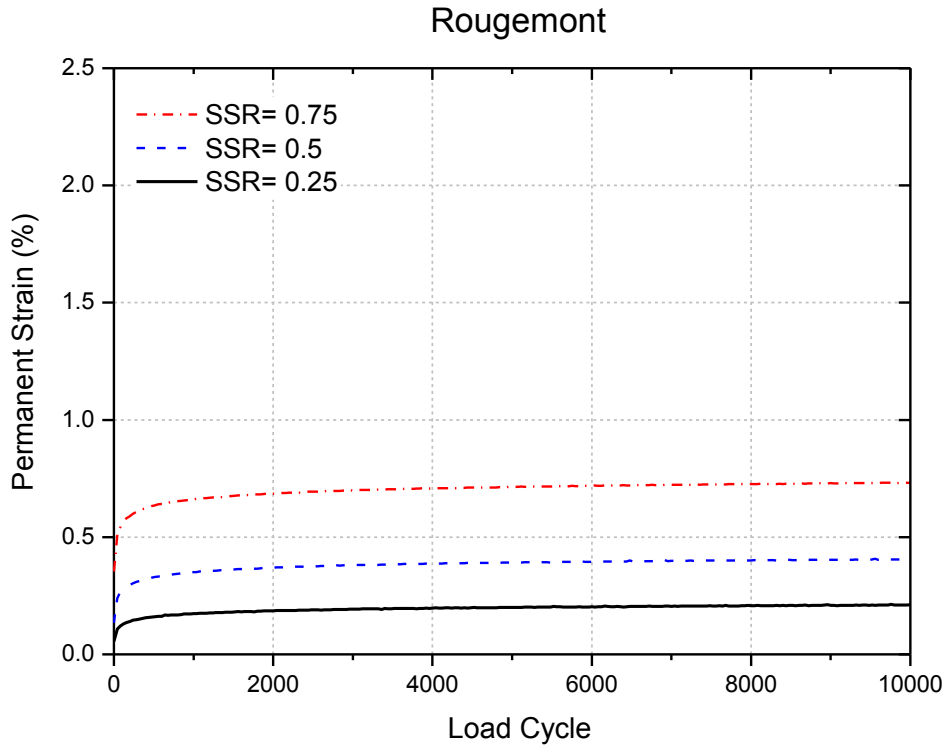


**Figure D.1 (Cont'd)** Permanent strain accumulations in the fifteen aggregate materials at the source gradations for different SSR levels

## APPENDIX E Resilient Modulus Test Results

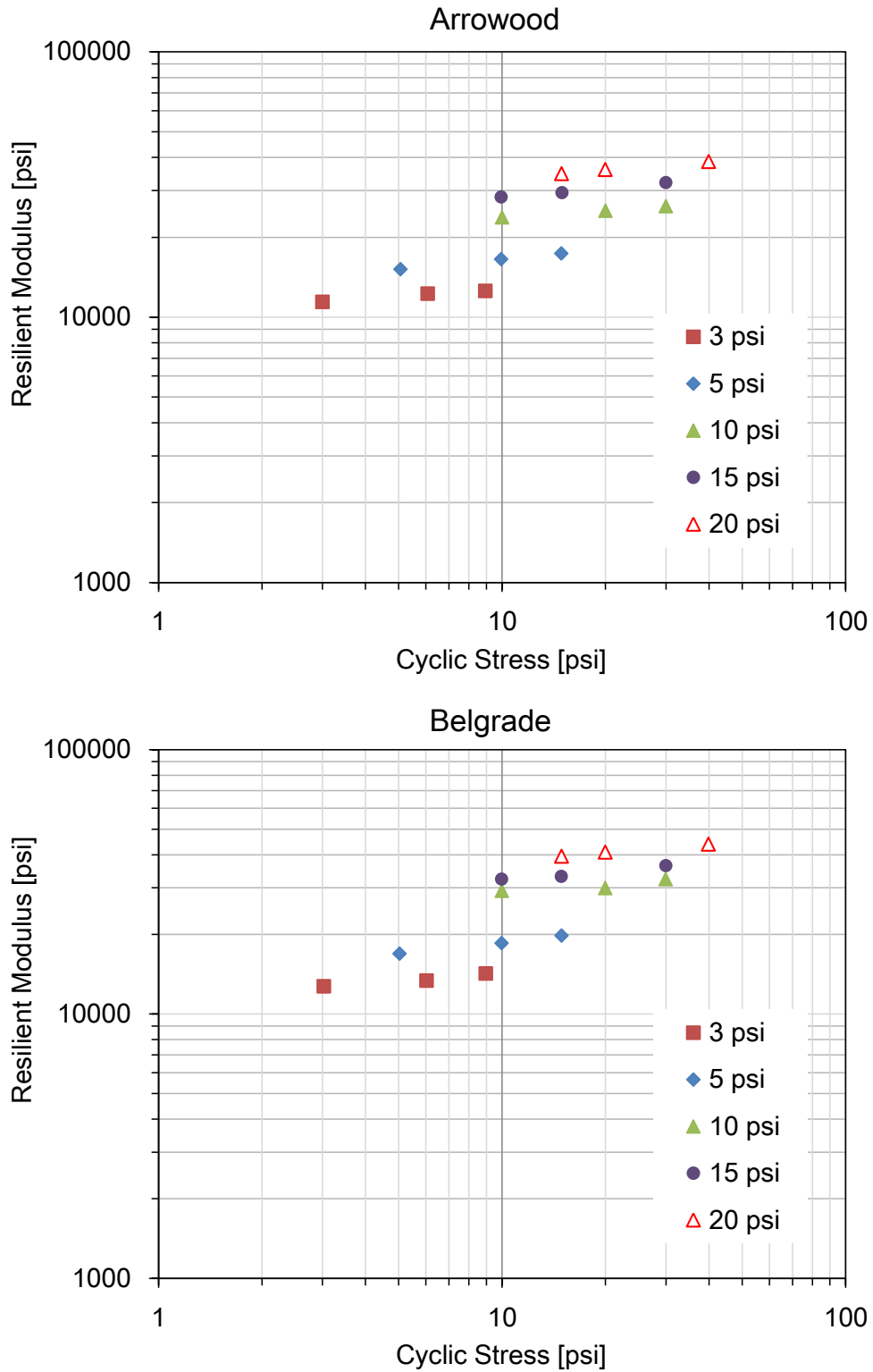


**Figure E.1 (Cont'd)** Resilient Modulus results for the fifteen aggregate materials at the source gradations (Results are for the average of two samples)

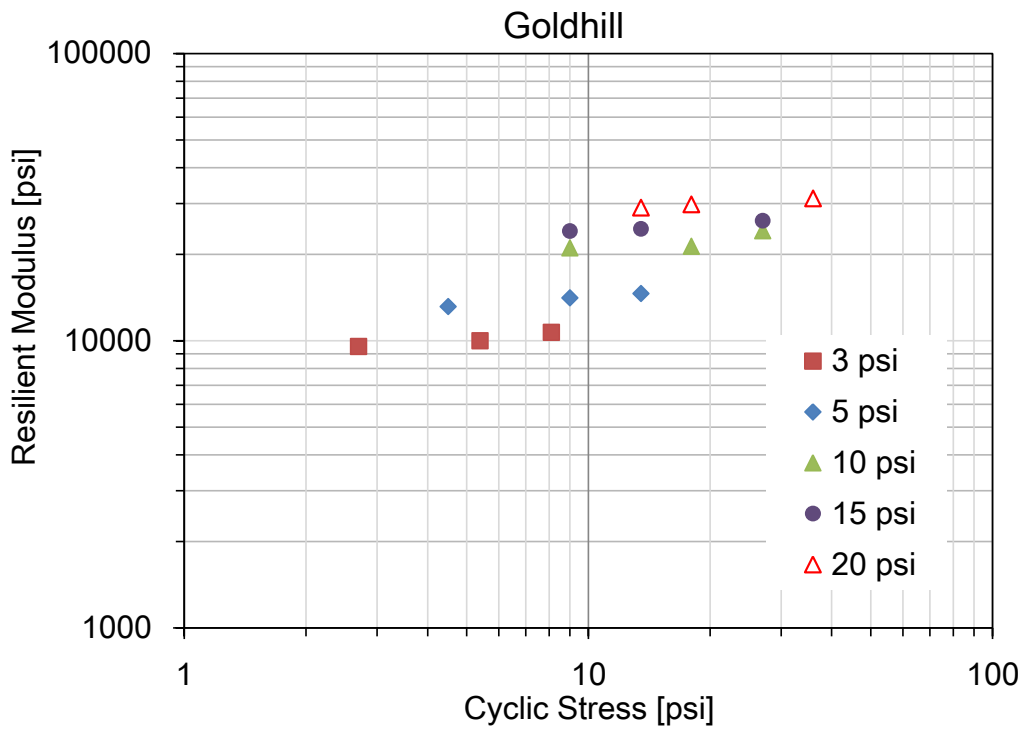
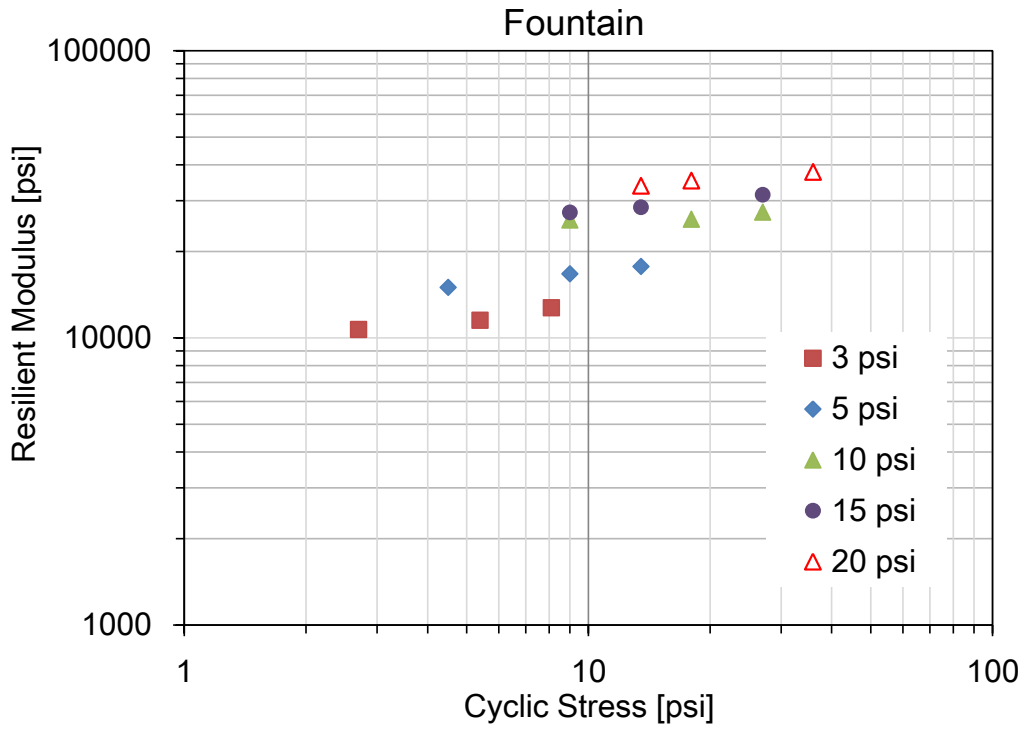


**Figure E.1 (Cont'd)** Resilient Modulus results for the fifteen aggregate materials at the source gradations (Results are for the average of two samples)

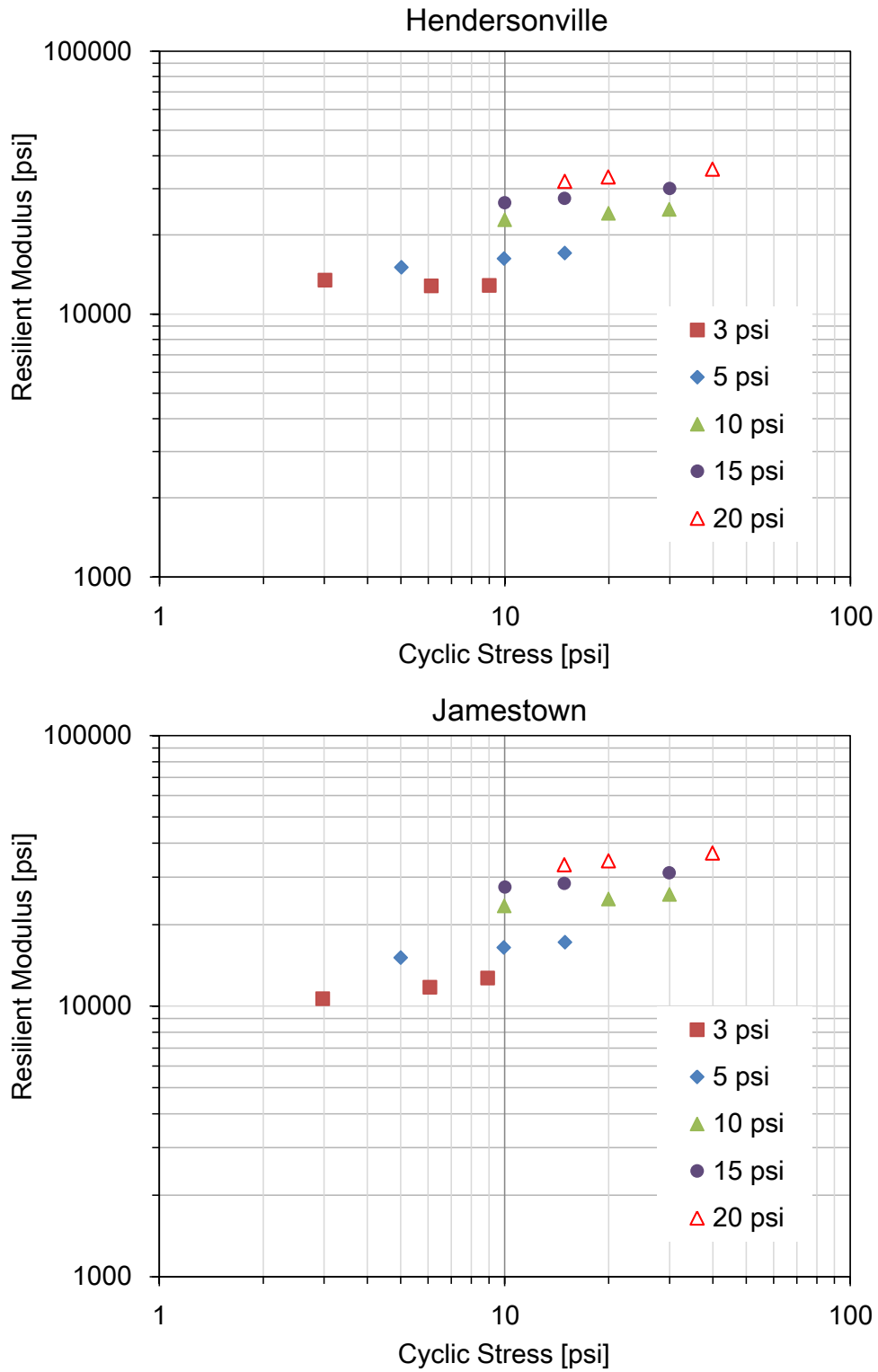


**Figure E.1 (Cont'd)** Resilient Modulus results for the fifteen aggregate materials at the source gradations (Results are for the average of two samples)

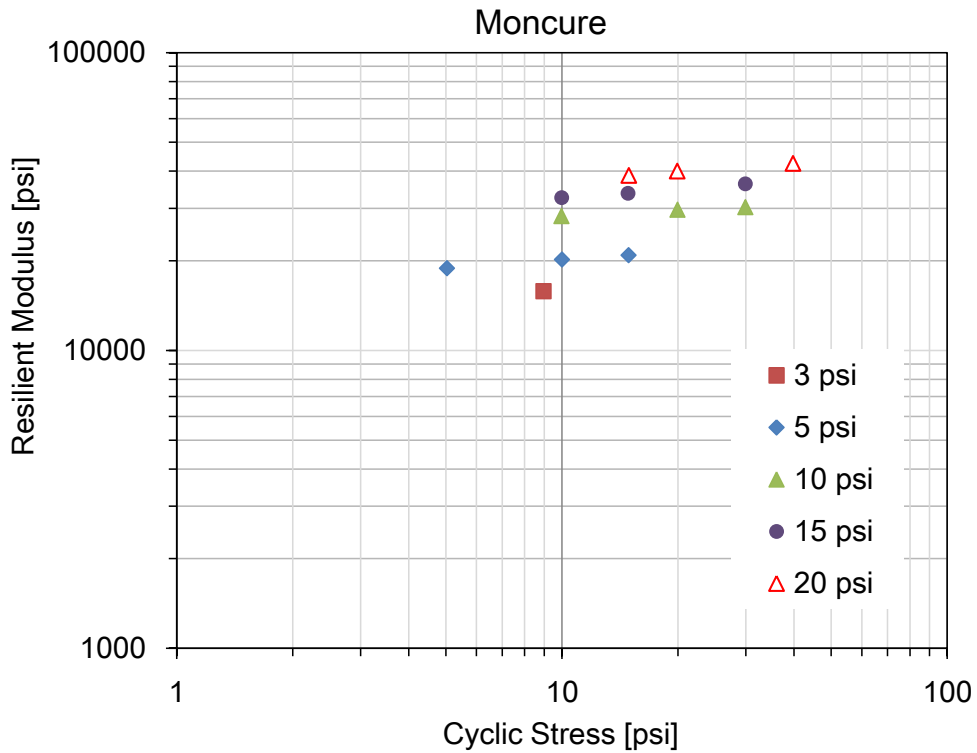
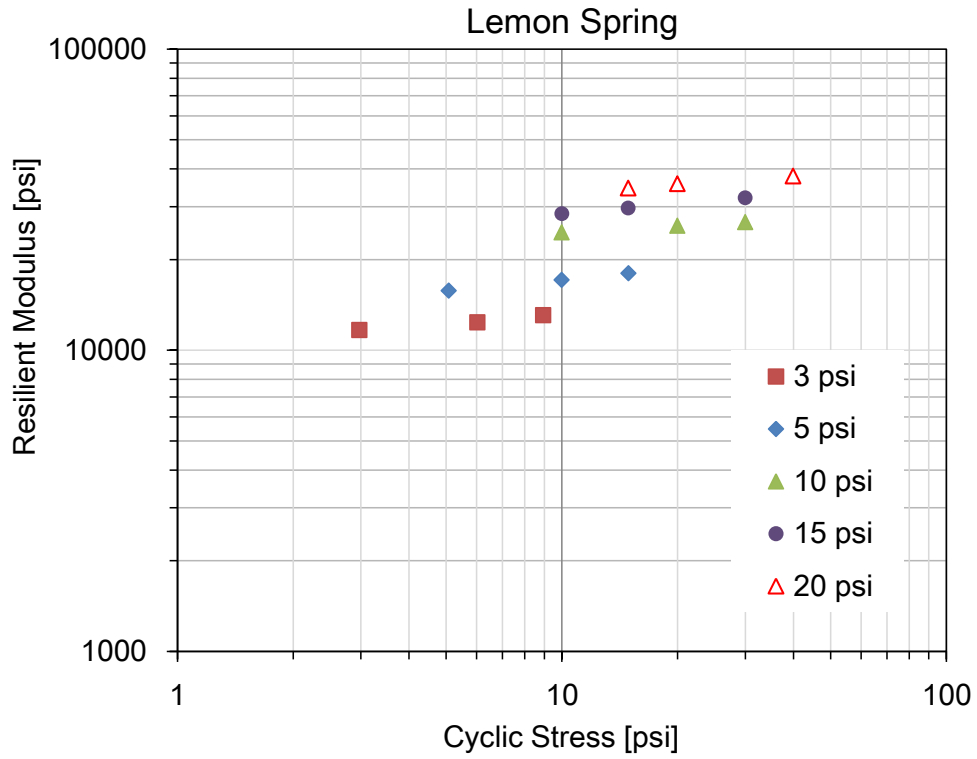


**Figure E.1 (Cont'd)** Resilient Modulus results for the fifteen aggregate materials at the source gradations (Results are for the average of two samples)

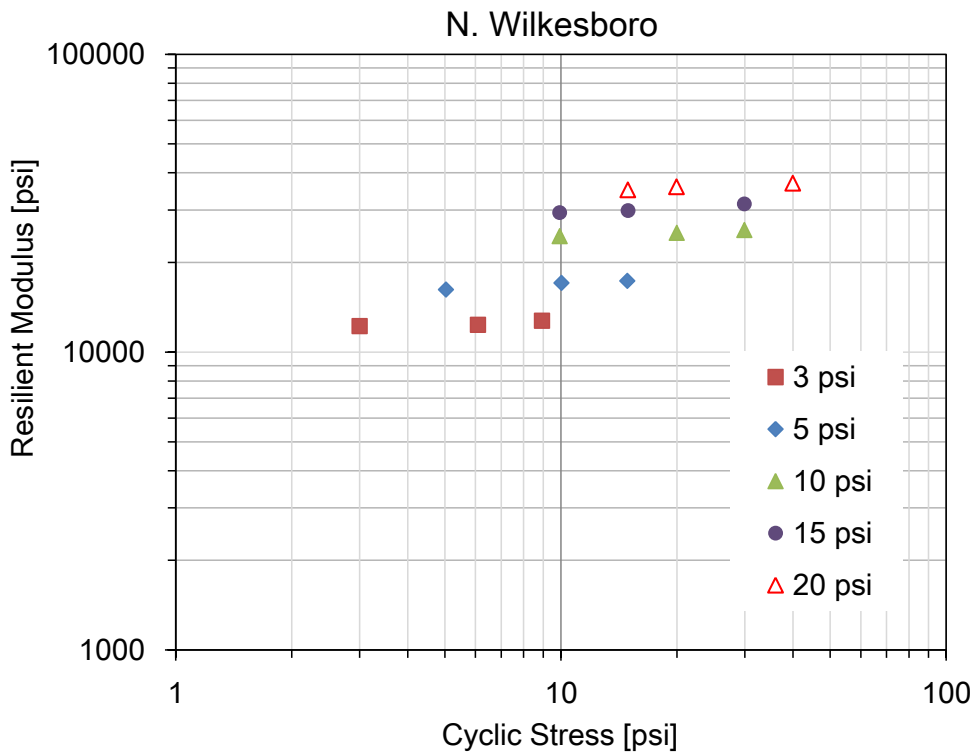
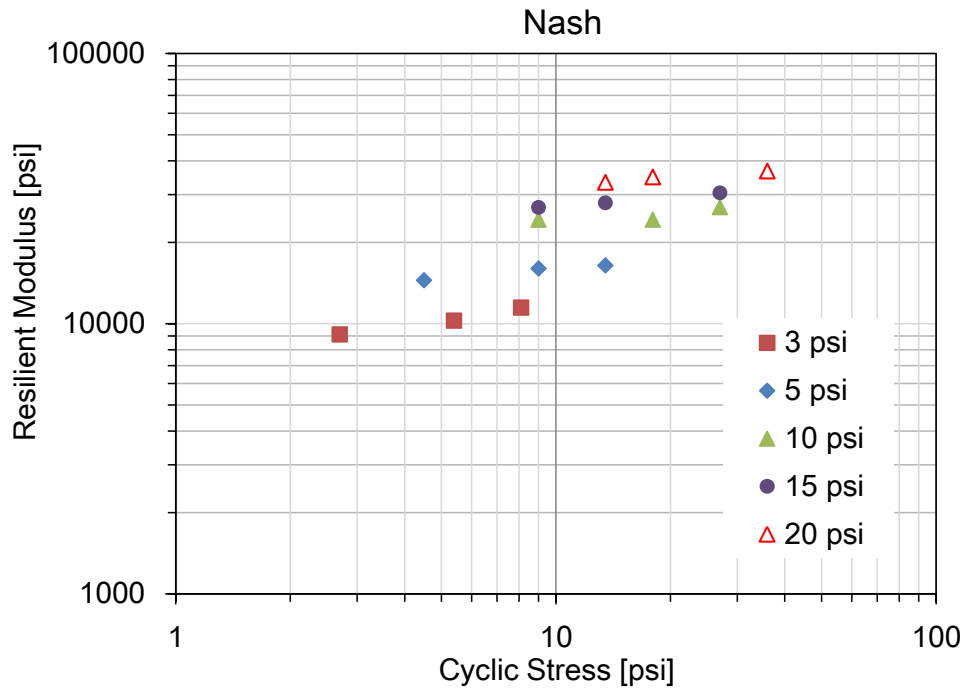


**Figure E.1 (Cont'd)** Resilient Modulus results for the fifteen aggregate materials at the source gradations (Results are for the average of two samples)

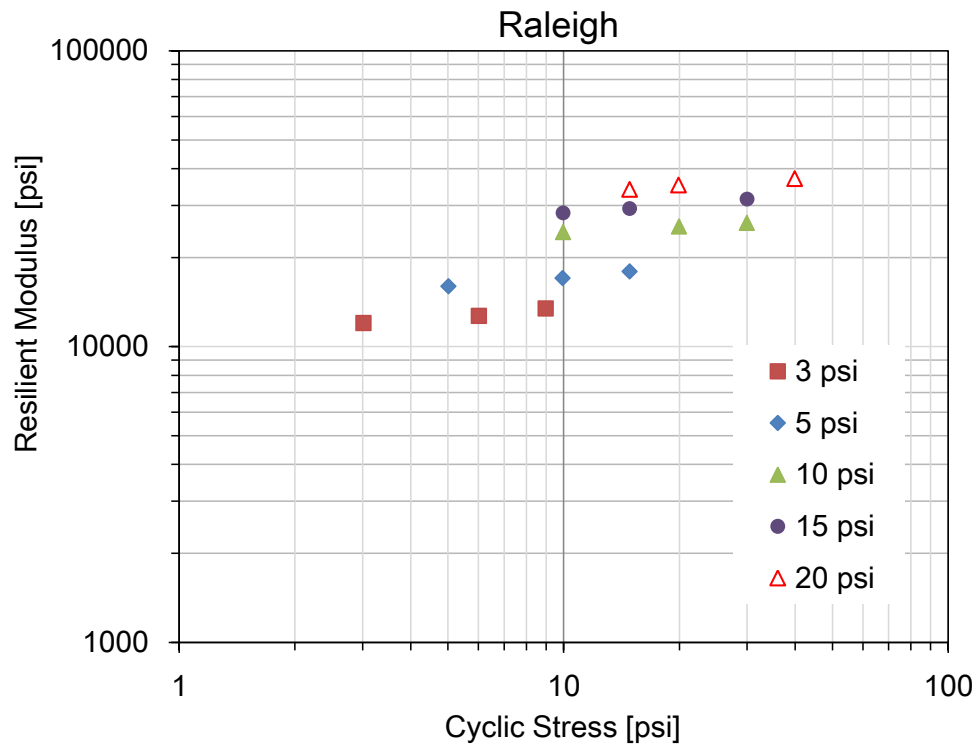
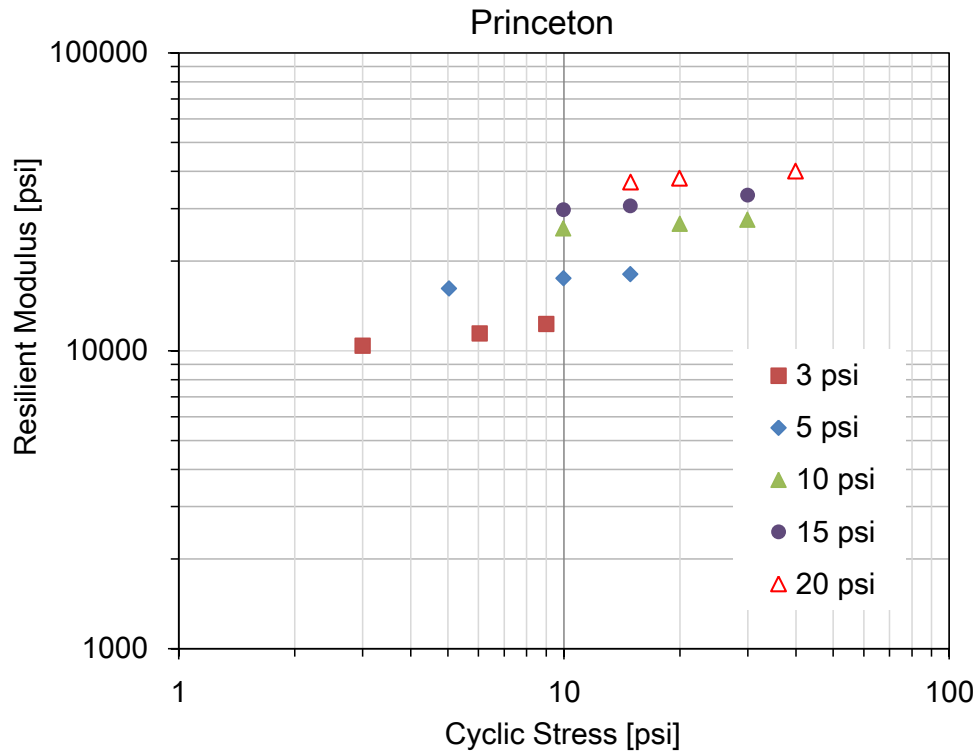


**Figure E.1 (Cont'd)** Resilient Modulus results for the fifteen aggregate materials at the source gradations (Results are for the average of two samples)

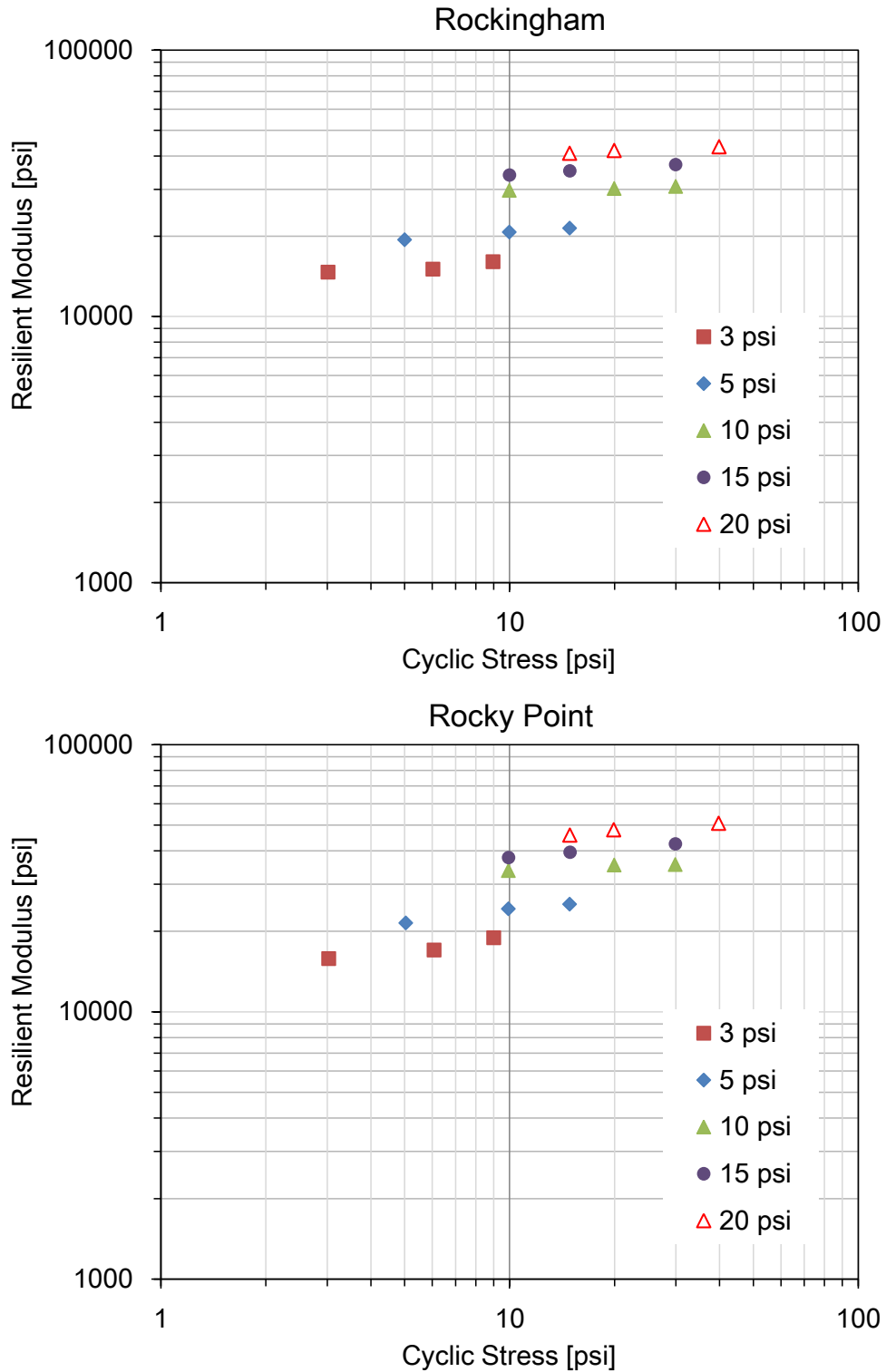


**Figure E.1 (Cont'd)** Resilient Modulus results for the fifteen aggregate materials at the source gradations (Results are for the average of two samples)

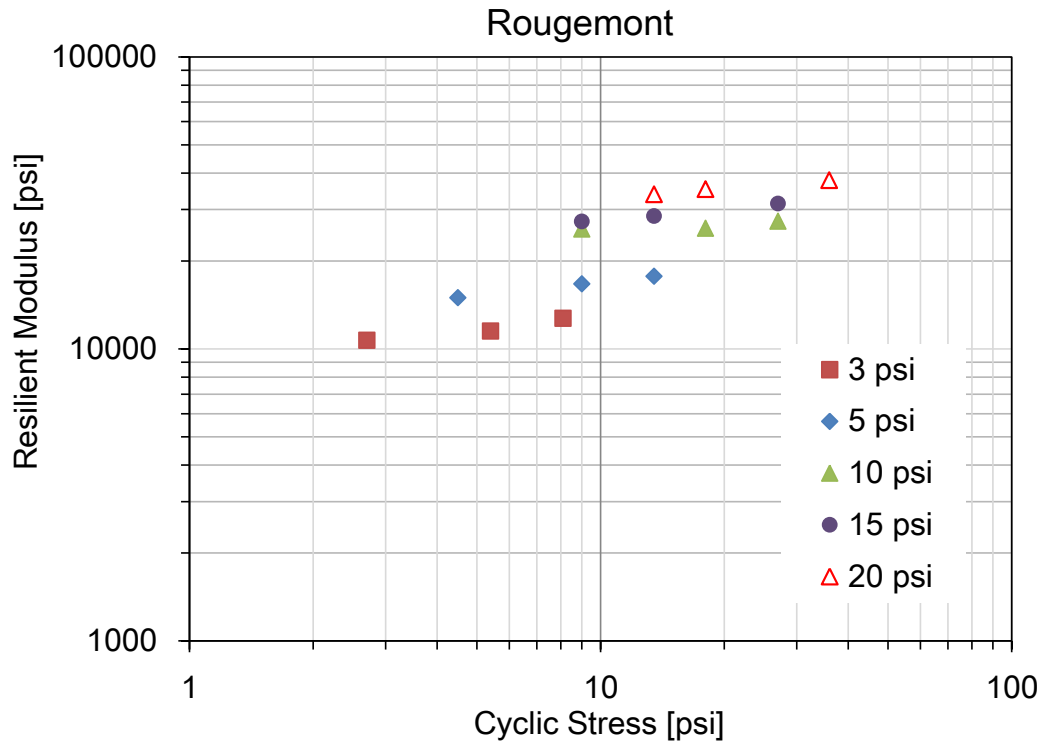


**Figure E.1 (Cont'd)** Resilient Modulus results for the fifteen aggregate materials at the source gradations (Results are for the average of two samples)

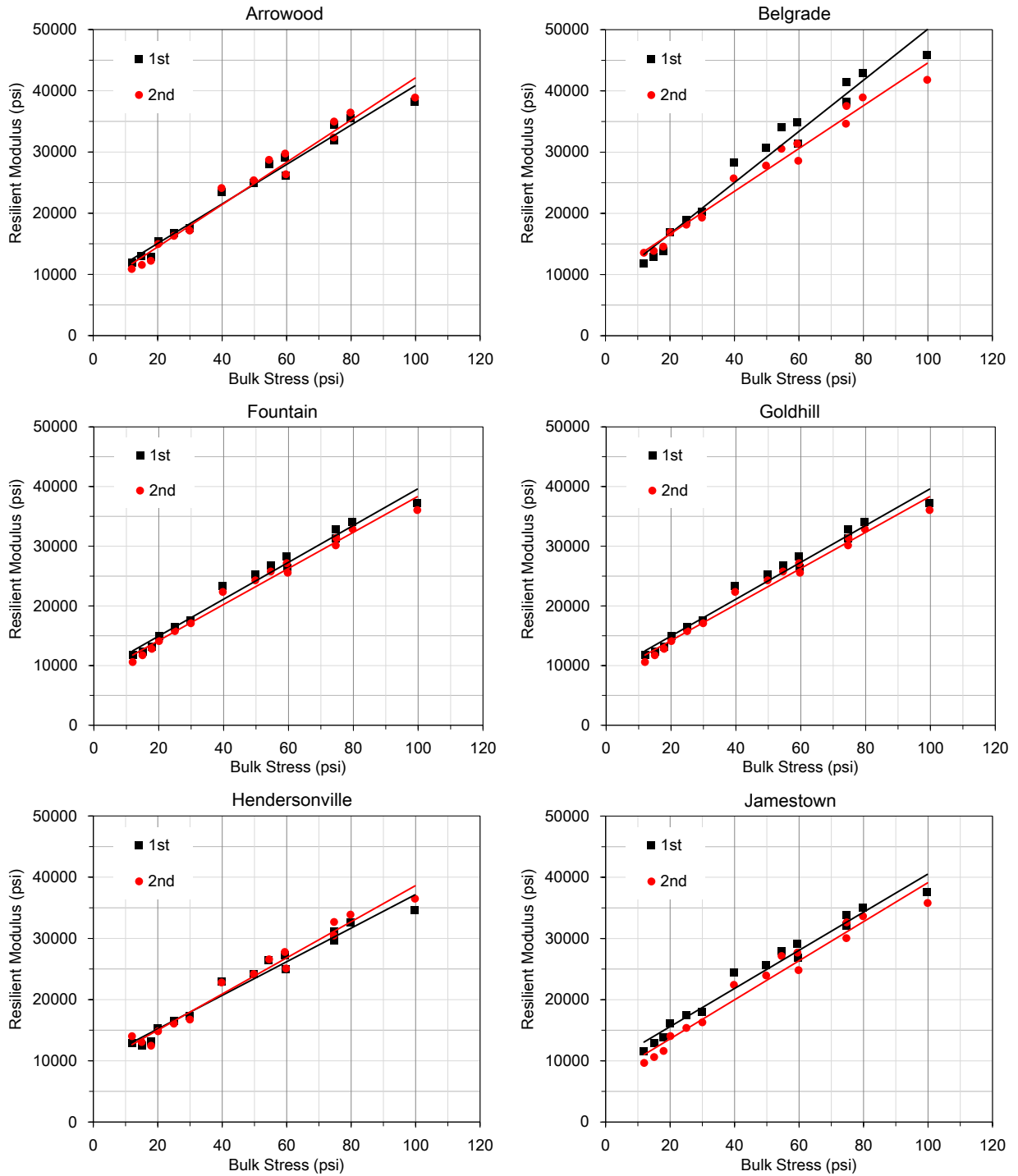


**Figure E.2** Resilient Modulus results showing two replicas for each aggregate material at the source gradation

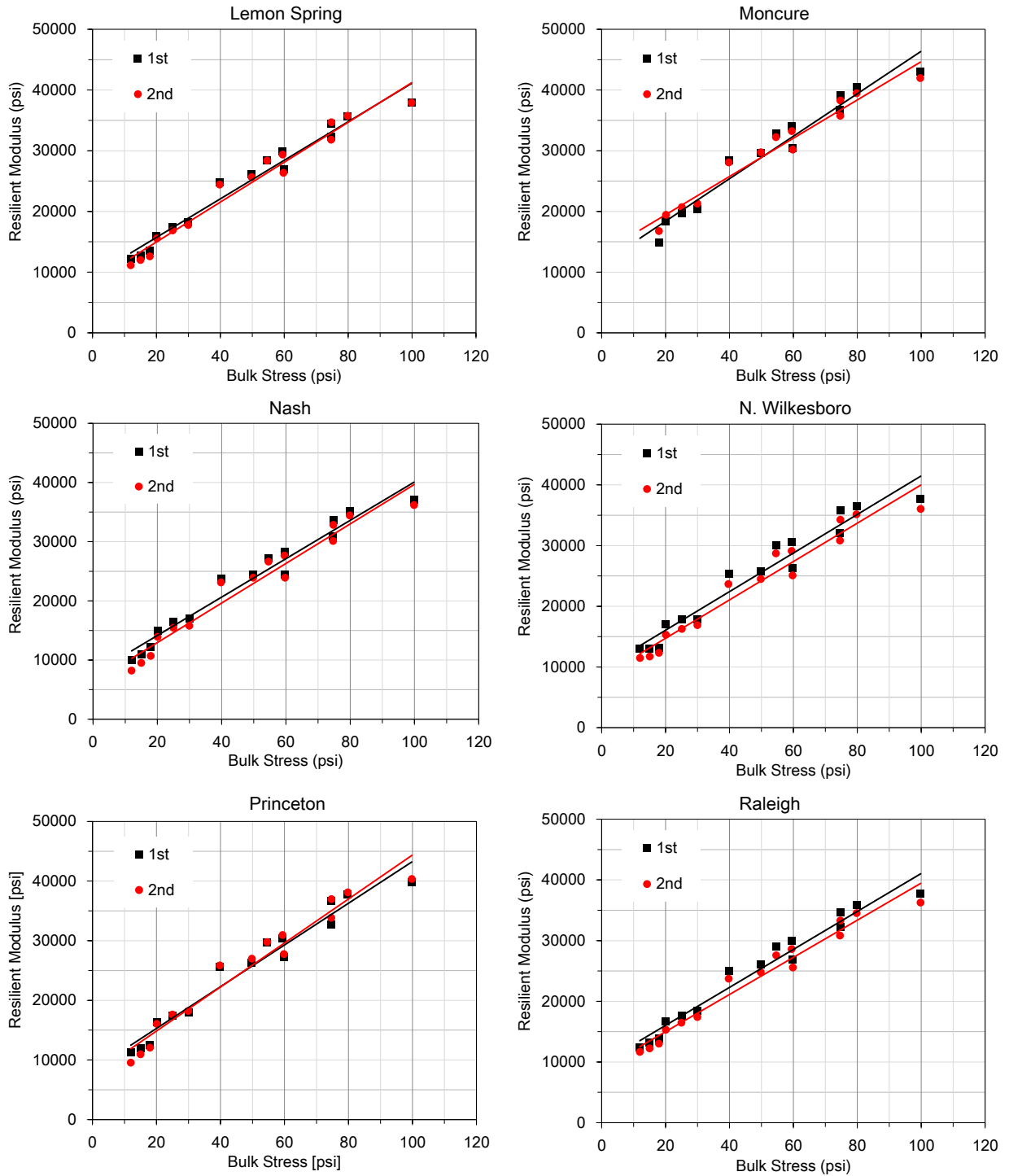


**Figure E.2 (Cont'd)** Resilient Modulus results showing two replicas for each aggregate material at the source gradation

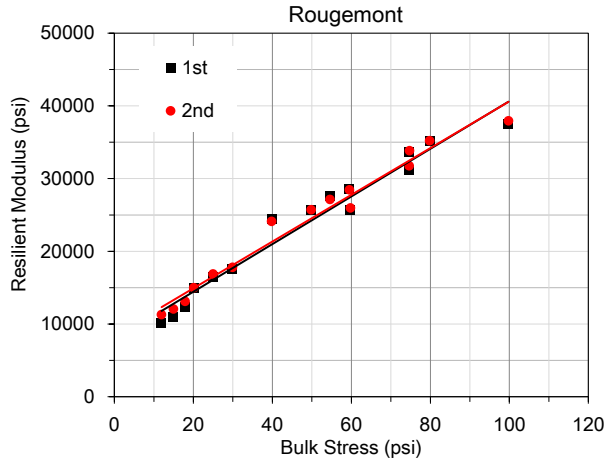
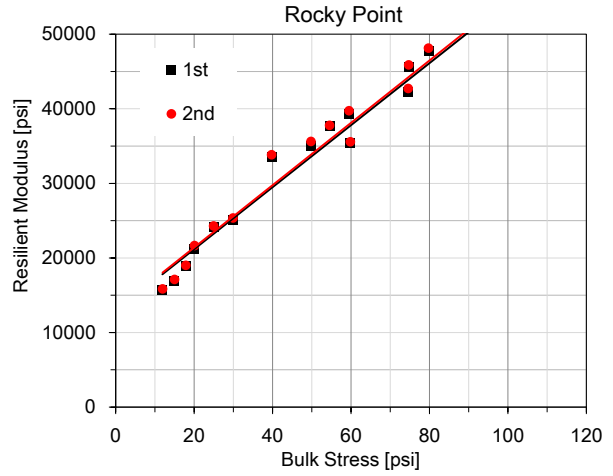
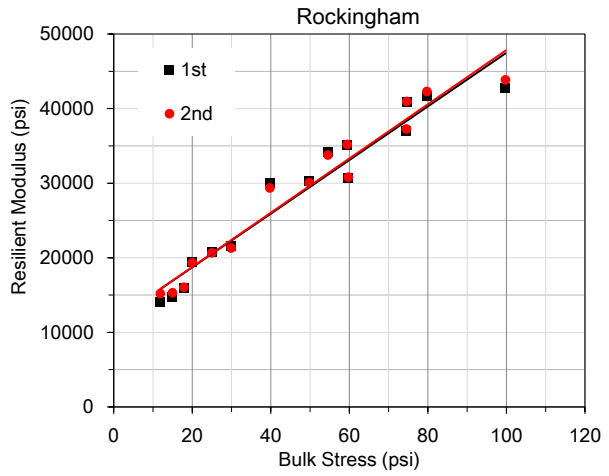


**Figure E.2 (Cont'd)** Resilient Modulus results showing two replicas for each aggregate material at the source gradation

## APPENDIX F Material Properties for Stepwise Regression Analysis

**Table F.1** Compiled data for the material properties (gradation, PI, compaction, particle shape, and shear strength properties) for all tests

Material	Gradation Properties													
	Cu	Cc	D10 (mm)	D30 (mm)	D50 (mm)	D60 (mm)	P <sub>38.1</sub> mm (%)	P <sub>25.4</sub> mm (%)	P <sub>12.7</sub> mm (%)	P <sub>4.75</sub> mm (%)	P <sub>2</sub> mm (%)	P <sub>0.425</sub> mm (%)	P <sub>0.075</sub> mm (%)	P <sub>0.075</sub> /log(Cu)
Arrowood _SG	47.80	2.17	0.234	2.381	7.245	11.17 8	100	93.45	62.8	40.18	27.34	12.8	4.46	2.66
Belgrade _SG	70.17	2.75	0.145	2.010	6.246	10.15 3	100	88	65	44	30	19	5	2.71
Fountain _SG	84.21	1.32	0.095	1.000	4.900	8.000	100	94.17	68.84	48.37	36.47	19.87	5.98	3.11
Goldhill _SG	24.00	1.04	0.200	1.000	3.000	4.800	100	95.25	77.59	58.73	40.61	12.15	1.51	1.09
Hendersonville _SG	152.4 2	2.25	0.066	1.223	6.046	10.05 9	100	89.39	64.78	45.38	33.24	23.02	11.7	5.36
Hendersonville (5.5%)	152.4 2	2.25	0.066	1.223	6.046	10.05 9	100	89.39	64.78	45.38	33.24	23.02	11.7	5.36
Jamestown _SG	37.93	2.98	0.248	2.637	6.952	9.412	100	90	68	39	26	13	4.7	2.98
Lemon Spring _SG	43.60	1.76	0.272	2.378	7.419	11.84 1	100	93	63	40	28	13	4.5	2.74
Moncure _SG	31.38	1.35	0.460	2.991	9.635	14.43 3	100	91	55	37	24	10	4	2.67
Nash County _SG	75.00	0.78	0.076	0.580	3.200	5.700	100	93.95	74.3	54.88	41.47	24.75	10.46	5.58
N. Wilkesboro _SG	111.7 2	3.33	0.104	2.008	7.628	11.62 2	100	92	62	40	29	20	8	3.91
Princeton _SG	71.58	2.82	0.142	2.016	6.323	10.16 3	100	88	65	44	30	19	5	2.70
Raleigh _SG	76.91	2.48	0.144	1.987	7.386	11.06 3	100	93	63	40	30	19	5	2.65
Rockingham _SG	81.18	0.74	0.109	0.843	3.768	8.841	100	85	63	53	42	21	7	3.67
Rocky Point _SG	123.2 3	3.05	0.111	2.151	9.374	13.68 0	100	88	56	38	29	21	6	2.87
Rougemont _SG	66.67	2.45	0.180	2.300	7.400	12.00 0	100	93.33	62.59	39.42	26.98	11.59	2.64	1.45
Arrowood _EG	94.74	1.55	0.095	1.150	5.900	9.000	100	92	68	45	35	22	8	4.05
Belgrade _EG	94.74	1.55	0.095	1.150	5.900	9.000	100	92	68	45	35	22	8	4.05
Fountain _EG	94.74	1.55	0.095	1.150	5.900	9.000	100	92	68	45	35	22	8	4.05
Franklin _EG	94.74	1.55	0.095	1.150	5.900	9.000	100	92	68	45	35	22	8	4.05
Goldhill _EG	94.74	1.55	0.095	1.150	5.900	9.000	100	92	68	45	35	22	8	4.05
Hendersonville _EG	94.74	1.55	0.095	1.150	5.900	9.000	100	92	68	45	35	22	8	4.05

Jamestown_EG	94.74	1.55	0.095	1.150	5.900	9.000	100	92	68	45	35	22	8	4.05
Lemon Spring_EG	94.74	1.55	0.095	1.150	5.900	9.000	100	92	68	45	35	22	8	4.05
Moncure_EG	94.74	1.55	0.095	1.150	5.900	9.000	100	92	68	45	35	22	8	4.05
Nash County_EG	94.74	1.55	0.095	1.150	5.900	9.000	100	92	68	45	35	22	8	4.05
N. Wilkesboro_EG	94.74	1.55	0.095	1.150	5.900	9.000	100	92	68	45	35	22	8	4.05
Princeton_EG	94.74	1.55	0.095	1.150	5.900	9.000	100	92	68	45	35	22	8	4.05
Raleigh_EG	94.74	1.55	0.095	1.150	5.900	9.000	100	92	68	45	35	22	8	4.05
Rockingham_EG	94.74	1.55	0.095	1.150	5.900	9.000	100	92	68	45	35	22	8	4.05
Rocky Point_EG	94.74	1.55	0.095	1.150	5.900	9.000	100	92	68	45	35	22	8	4.05
Rougemont_EG	94.74	1.55	0.095	1.150	5.900	9.000	100	92	68	45	35	22	8	4.05

**Table F.1 (Cont'd):** Compiled data for the material properties (gradation, PI, compaction, particle shape, and shear strength properties) for all tests

Material	Compaction Properties					Shear Strength Properties			Plasticity Index	Shape Properties		
	Achieved Water content (%)	OMC (%)	Achieved MC / OMC	Max dry density (pcf)	MDD <sup>2</sup> /P <sub>0.425</sub>	Friction Angle	Secant friction angle	Cohesion (kPa)		AI	STI	FER
Arrowood_SG	5	5.4	0.93	158.9	1972.59	35.4	47.7	24	0	408	2.216	2.549
Belgrade_SG	6.59	6.8	0.97	134.5	952.12	50.6	60.4	49.2	0	558	1.883	1.859
Fountain_SG	4.83	6.1	0.79	142.4	1020.52	39.4	56.9	55.1	0	444	2.393	2.834
Goldhill_SG	5.87	5.87	1.00	141.6	1650.25	40.3	56.2	48.9	6	464	2.226	2.375
Hendersonville_SG	4.5	6.1	0.74	143.3	892.05	23.6	50.5	60.4	0	490	2.678	2.504
Hendersonville (5.5%)	4.4	5.5	0.80	143.3	892.05	57.8	50.7	0	0	490	2.678	2.504
Jamestown_SG	5.11	5.9	0.87	142.7	1566.41	30.4	53.5	61.4	0	434	1.951	2.287
Lemon Spring_SG	4.81	5.2	0.93	145.4	1626.24	41.5	63.4	121.6	0	424	1.773	2.456
Moncure_SG	4.7	5.6	0.84	150	2250.00	54.4	62.9	40.7	0	438	1.685	2.194
Nash County_SG	5.37	5.7	0.94	143.6	833.17	40	50.8	21.4	0	405	1.908	2.567
N. Wilkesboro_SG	4.83	4.9	0.99	145.3	1055.60	46.7	55.8	31.1	0	416	1.997	2.643
Princeton_SG	4.6	5.6	0.82	145.7	1117.29	40	49.2	20.2	0	462	2.348	2.392
Raleigh_SG	5.1	6.4	0.80	141.5	1053.80	48.6	47	0	0	414	2.36	2.739
Rockingham_SG	5.03	5.4	0.93	140.5	940.01	37.4	51.5	29	0	488	2.139	1.99
Rocky Point_SG	5.59	6	0.93	139.6	928.01	44.1	64.3	93.2	0	511	1.933	1.974
Rougemont_SG	4.82	6	0.80	144.7	1806.57	48.1	55.8	13.1	0	516	2.746	2.573
Arrowood_EG	3.9	4.2	0.93	153.5	1071.01	50.2	65.2	85.1	0	408	2.216	2.549
Belgrade_EG	6.9	7.4	0.93	131.3	783.62	41.8	42.5	6.5	0	558	1.883	1.859
Fountain_EG	4.3	6.1	0.70	141.2	906.25	39.3	66.9	139.4	0	444	2.393	2.834
Franklin_EG	4.2	4.7	0.89	151.5	1043.28	34.1	51.1	39.9	0	394	1.753	2.315
Goldhill_EG	6	6.4	0.94	142.2	919.13	37.7	50.5	43.6	6	464	2.226	2.375
Hendersonville_EG	4.7	5.5	0.85	139.3	882.02	45.3	59.4	59.4	0	490	2.678	2.504

Jamestown_EG	5	5.8	0.86	141.6	911.39	41.2	49.4	23.3	0	434	1.951	2.287
Lemon Spring_EG	5.2	5.5	0.95	140.9	902.40	41.4	46.6	11.3	0	424	1.773	2.456
Moncure_EG	4.8	5.2	0.92	148.2	998.33	50.6	47.1	1.1	0	438	1.685	2.194
Nash County_EG	5.1	5.7	0.89	142.3	920.42	41.4	51.2	19.1	0	405	1.908	2.567
N. Wilkesboro_EG	4.8	5	0.96	142.5	923.01	46	58	48	0	416	1.997	2.643
Princeton_EG	4.4	5.1	0.86	141.3	907.53	49.1	45.3	7.1	0	462	2.348	2.392
Raleigh_EG	5.2	6.1	0.85	139.6	885.83	42.3	51.1	17.9	0	414	2.36	2.739
Rockingham_EG	5.1	6.1	0.84	141.4	908.82	41.7	54.3	35.7	0	488	2.139	1.99
Rocky Point_EG	5.7	5.9	0.97	134.7	824.73	44.9	42.4	2.4	0	511	1.933	1.974
Rougemont_EG	5.1	6.1	0.84	144	942.55	48.8	51.3	3.7	0	516	2.746	2.573

### APPENDIX G Comparison of Forced and Stepwise Regression Results

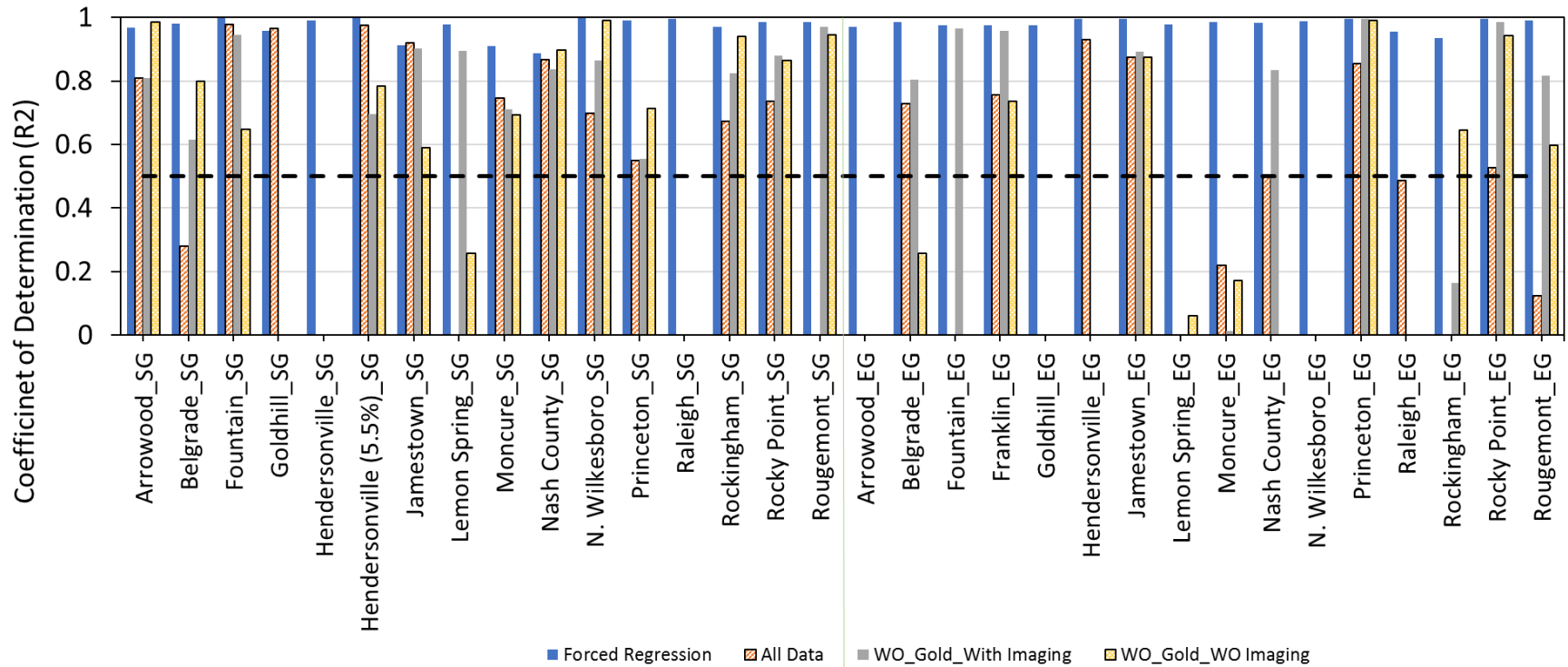
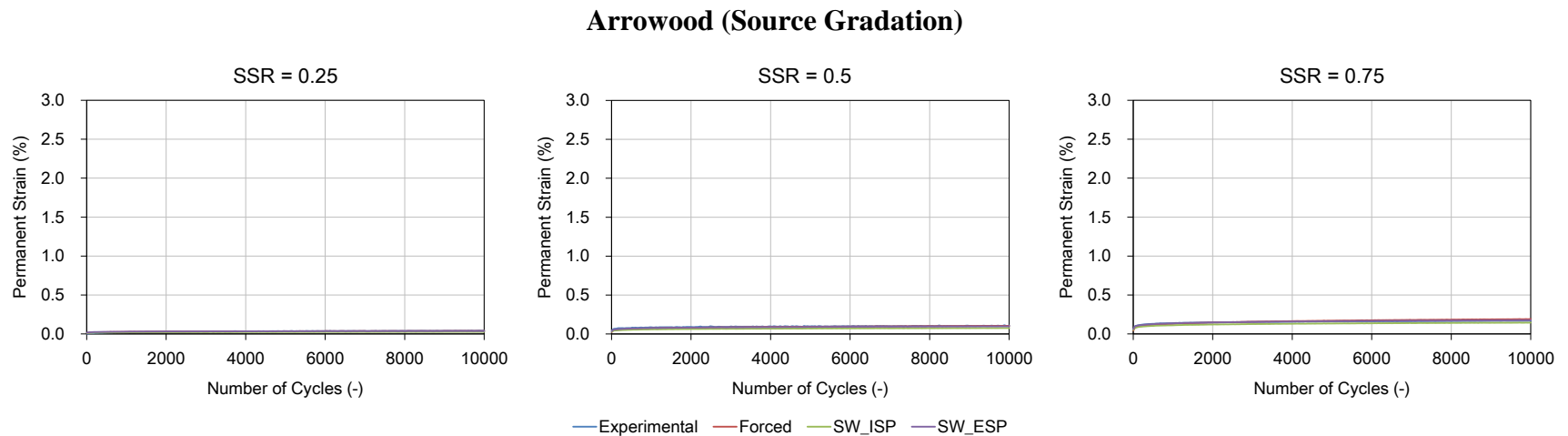


**Figure G.1** Coefficient of determination ( $R^2$ ) obtained for all 32 materials using forced regression, stepwise regression with all 32 tests (All data), stepwise regression excluding Goldhill and including shape properties (WO\_Gold\_With Imaging), and stepwise regression excluding Goldhill and excluding shape properties (WO\_Gold\_WO Imaging)

## APPENDIX H Permanent Deformation Predictions with Forced Regression and Stepwise Regression (Excluding Goldhill)



### Arrowood (Engineered Gradation)

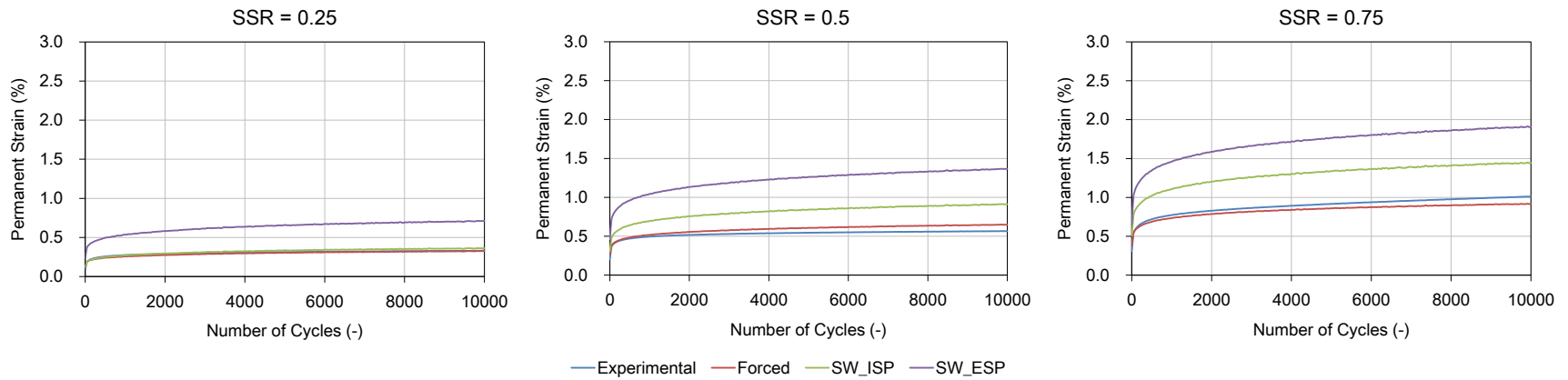
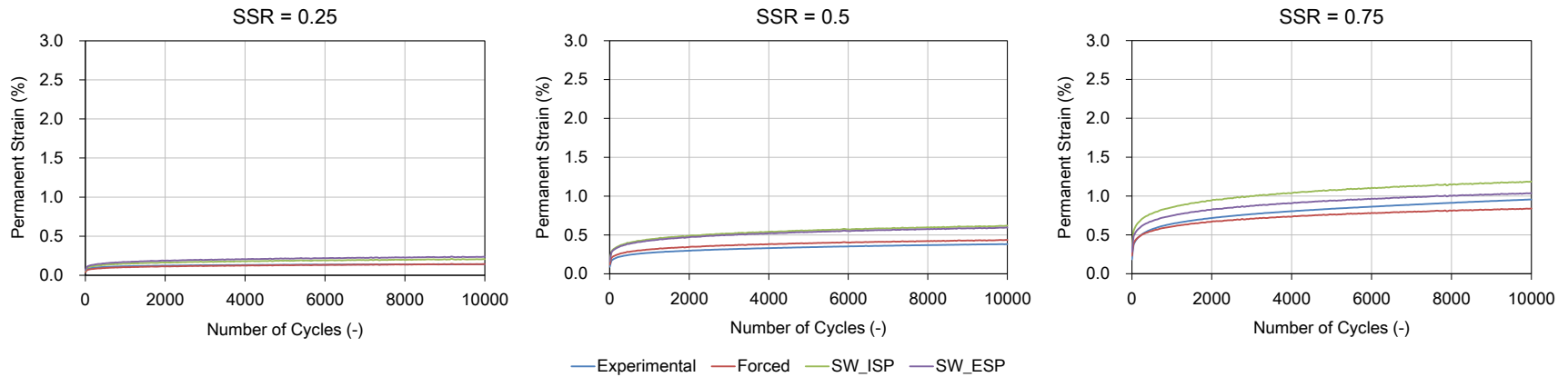


**Figure H.1** Curves for Permanent strain accumulations for Arrowood at SG and EG at different SSR values  
 Experimental results (blue), prediction using forced regression (red), prediction using stepwise regression including and excluding shape properties (green and purple, respectively)

**Belgrade (Source Gradation)**



**Belgrade (Engineered Gradation)**

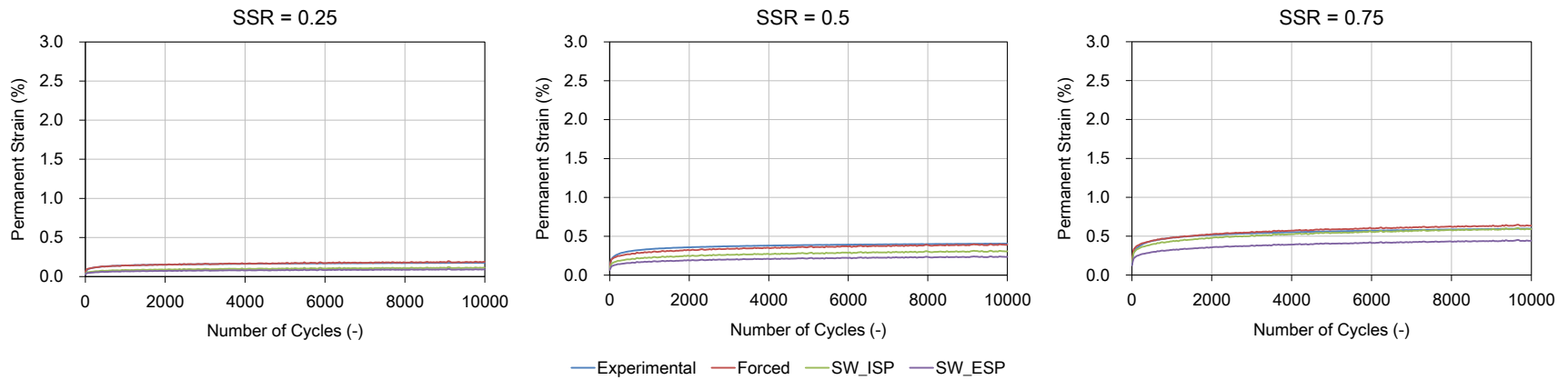
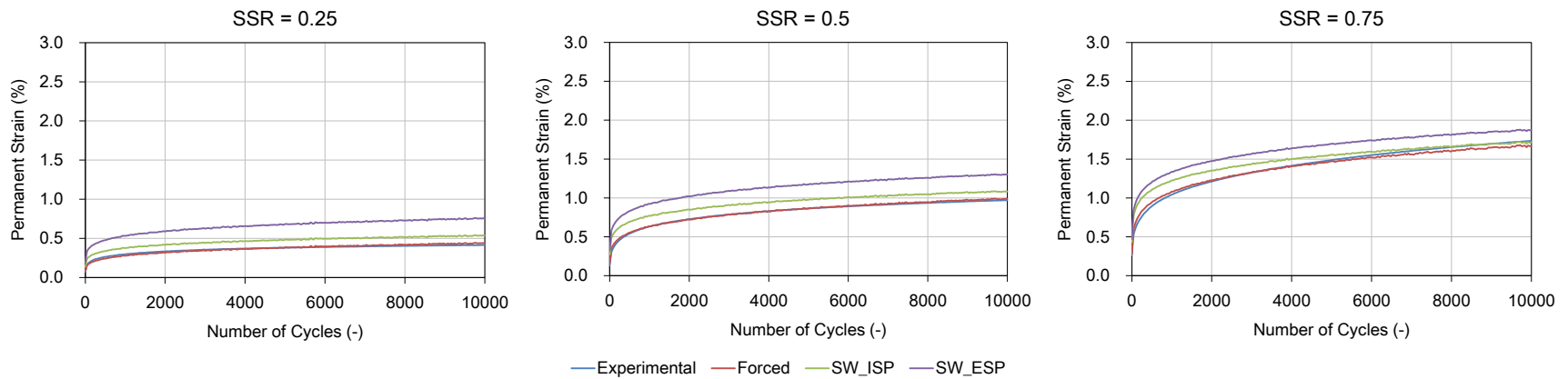


**Figure H.2** Curves for Permanent strain accumulations for Belgrade at SG and EG at different SSR values  
 Experimental results (blue), prediction using forced regression (red), prediction using stepwise regression including and excluding shape properties (green and purple, respectively)

**Fountain (Source Gradation)**



**Fountain (Engineered Gradation)**

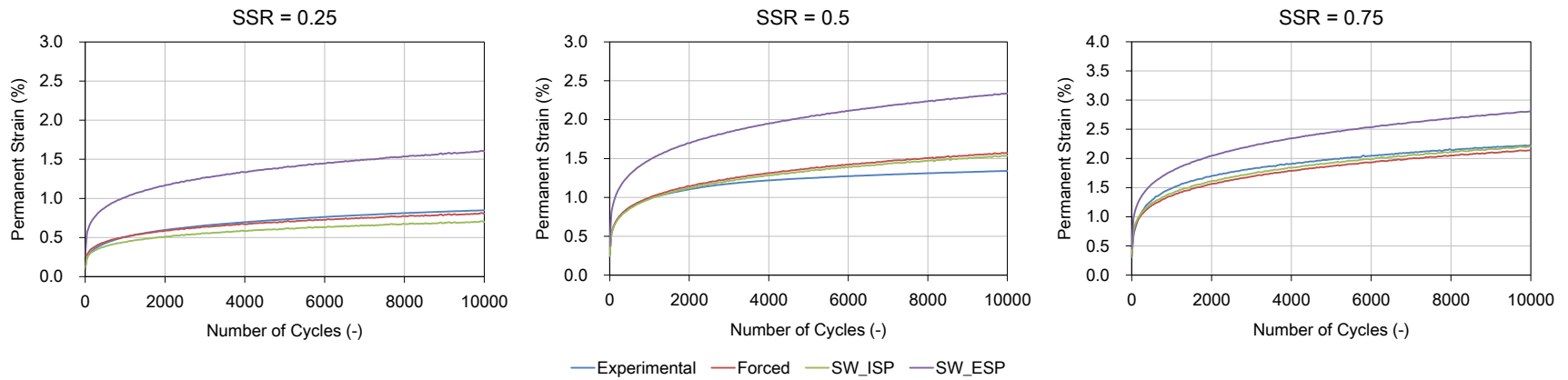
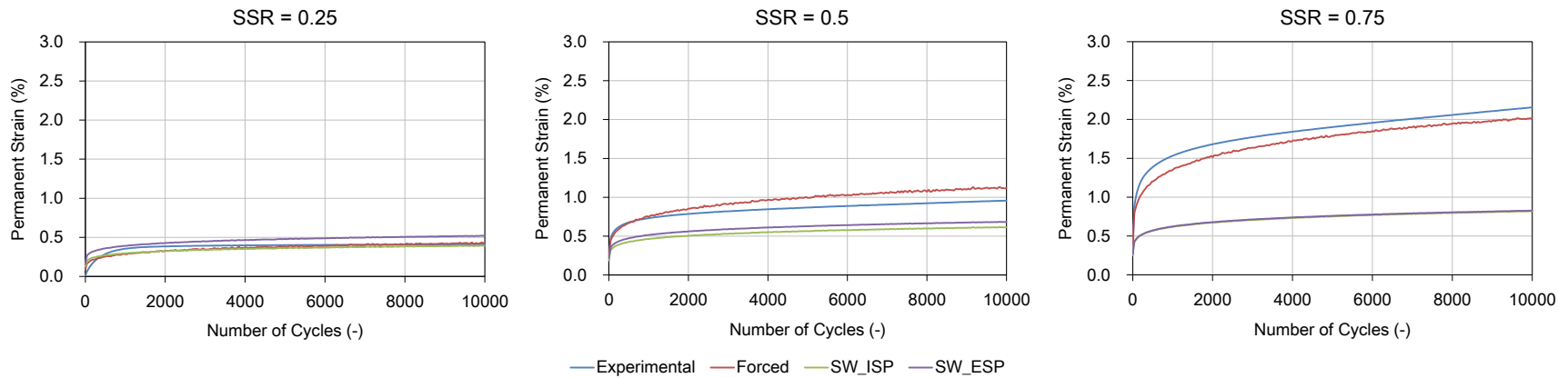


**Figure H.3** Curves for Permanent strain accumulations for Fountain at SG and EG at different SSR values  
 Experimental results (blue), prediction using forced regression (red), prediction using stepwise regression including and excluding shape properties (green and purple, respectively)

Note: y-axis scale of Foundtain at EG and SSR=0.75 is different from others

### Goldhill (Source Gradation)



### Goldhill (Engineered Gradation)

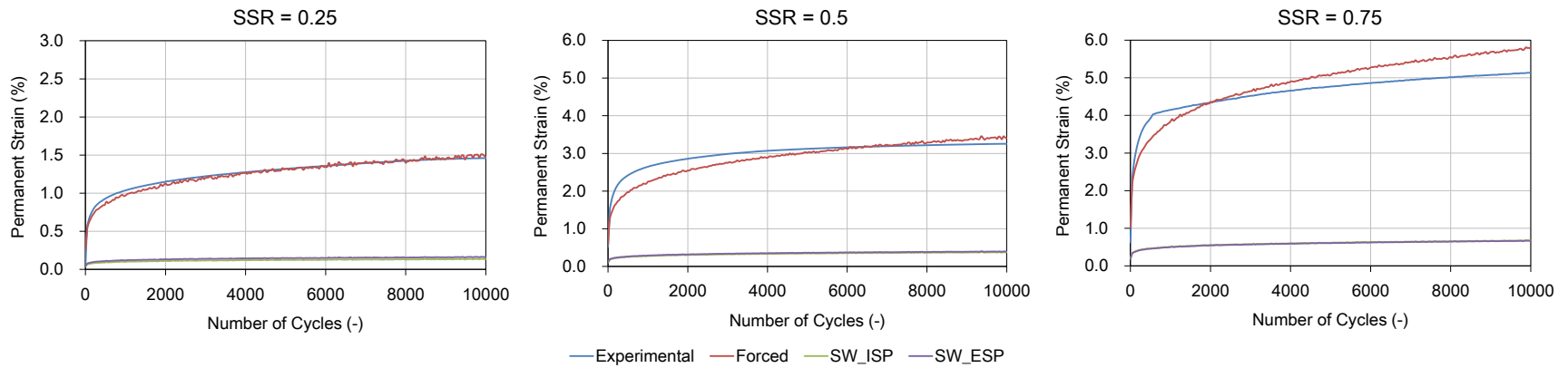
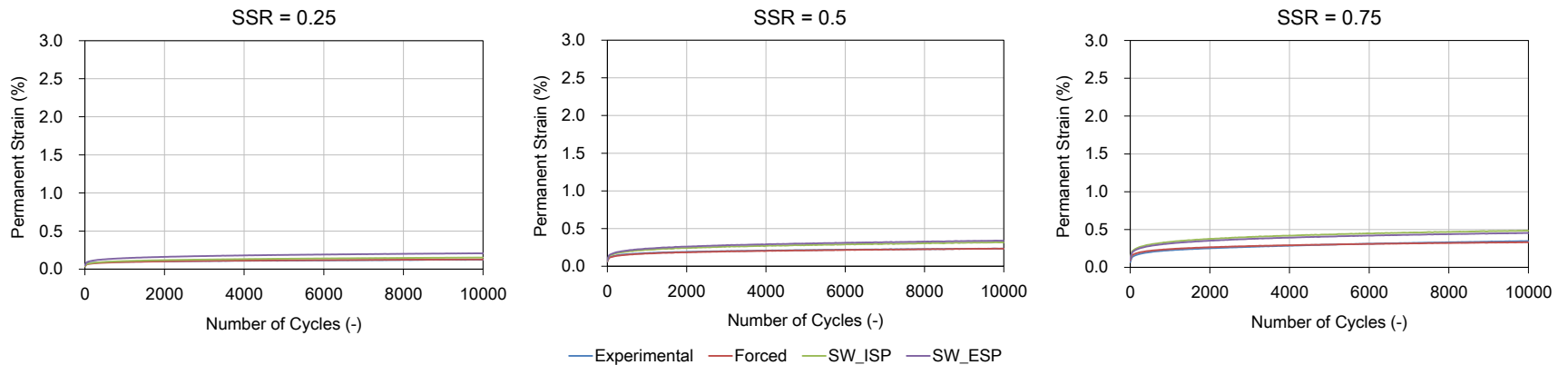


**Figure H.4** Curves for Permanent strain accumulations for Goldhill at SG and EG at different SSR values  
 Experimental results (blue), prediction using forced regression (red), prediction using stepwise regression including and excluding shape properties (green and purple, respectively)

Note: y-axis scales of Goldhill at EG and SSR=0.5 & 0.75 are different from others

### Hendersonville (Source Gradation\_OMC)



### Hendersonville (Engineered Gradation)

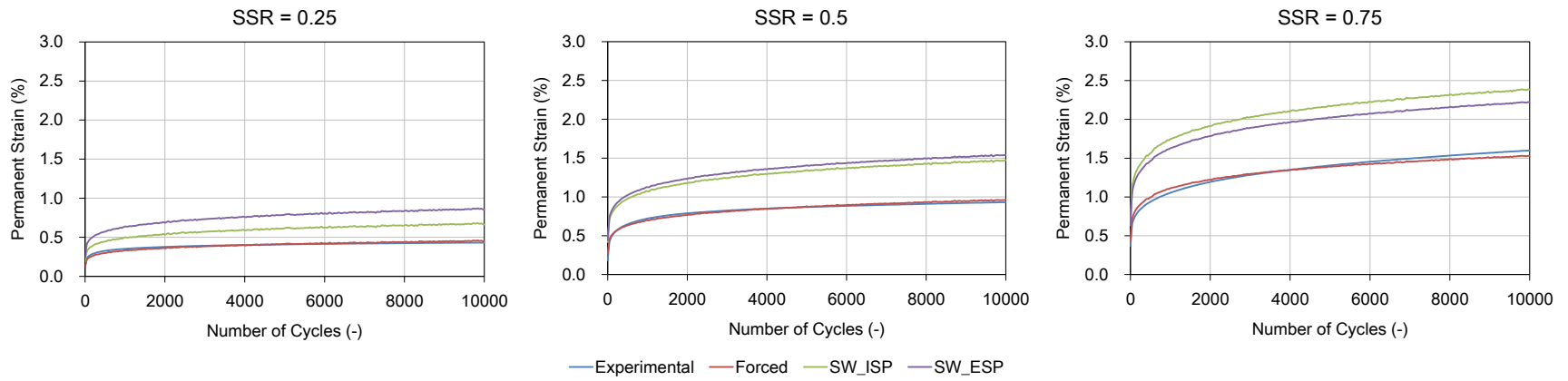
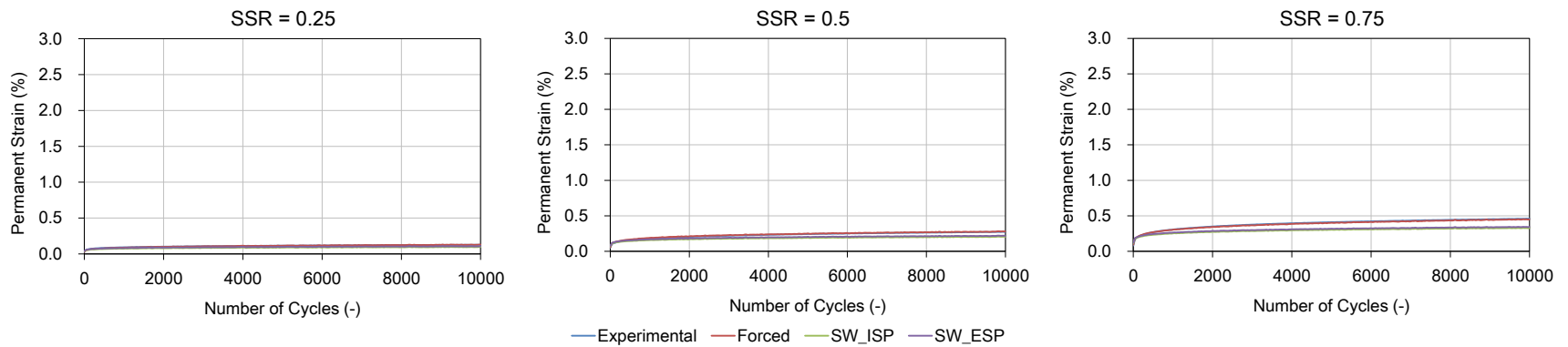


**Figure H.5** Curves for Permanent strain accumulations for Hendersonville at SG and EG at different SSR values  
 Experimental results (blue), prediction using forced regression (red), prediction using stepwise regression including and excluding shape properties (green and purple, respectively)

**Hendersonville (Source Gradation\_w=5.5%)**



**Franklin (Engineered Gradation)**

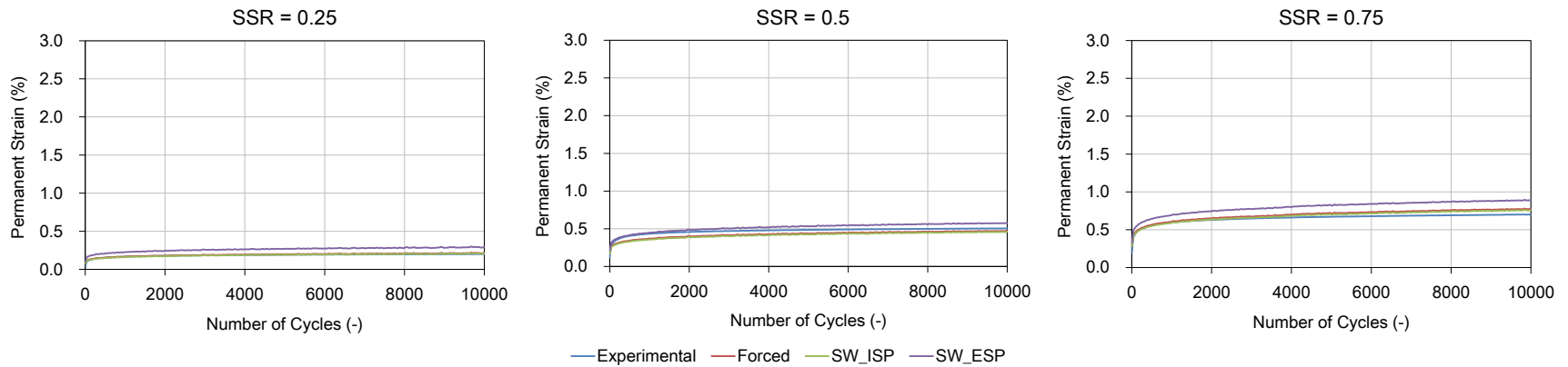
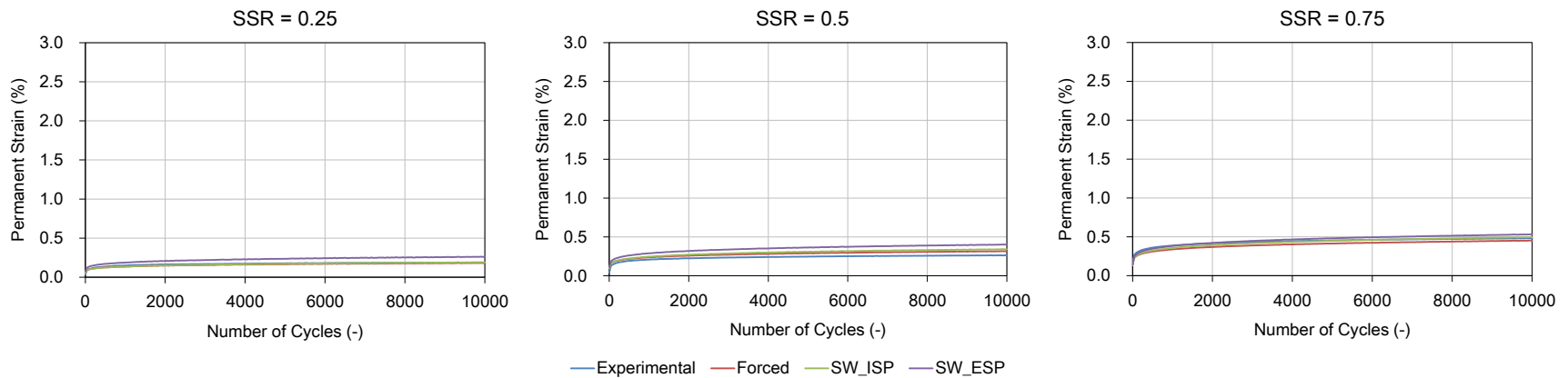


**Figure H.6** Curves for Permanent strain accumulations for Hendersonville at SG and Franklin at EG at different SSR values. Experimental results (blue), prediction using forced regression (red), prediction using stepwise regression including and excluding shape properties (green and purple, respectively)

### Jamestown (Source Gradation)



### Jamestown (Engineered Gradation)

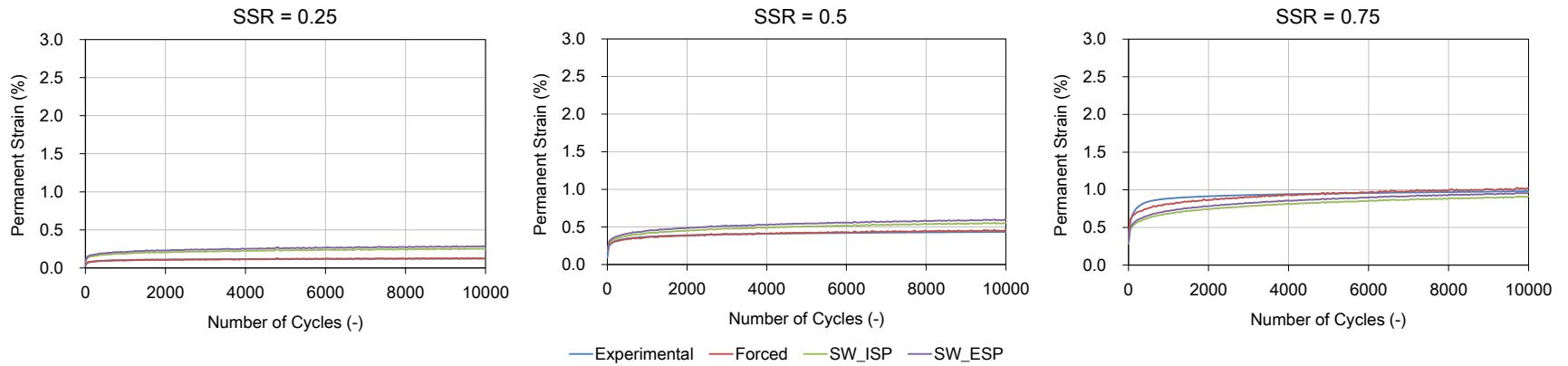
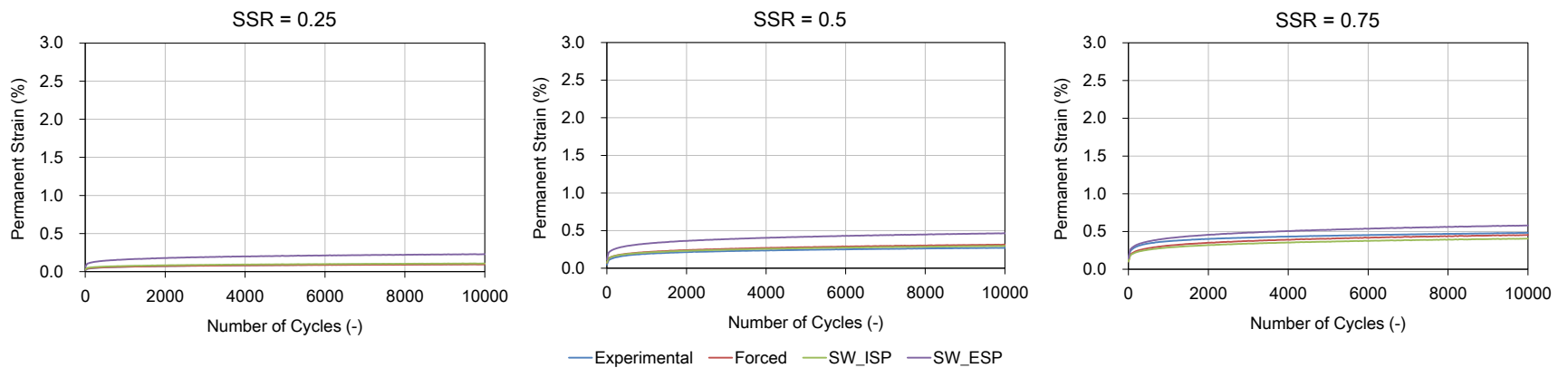


**Figure H.7** Curves for Permanent strain accumulations for Jamestown at SG and EG at different SSR values  
Experimental results (blue), prediction using forced regression (red), prediction using stepwise regression including and excluding shape properties (green and purple, respectively)

### Lemon Spring (Source Gradation)



### Lemon Spring (Engineered Gradation)

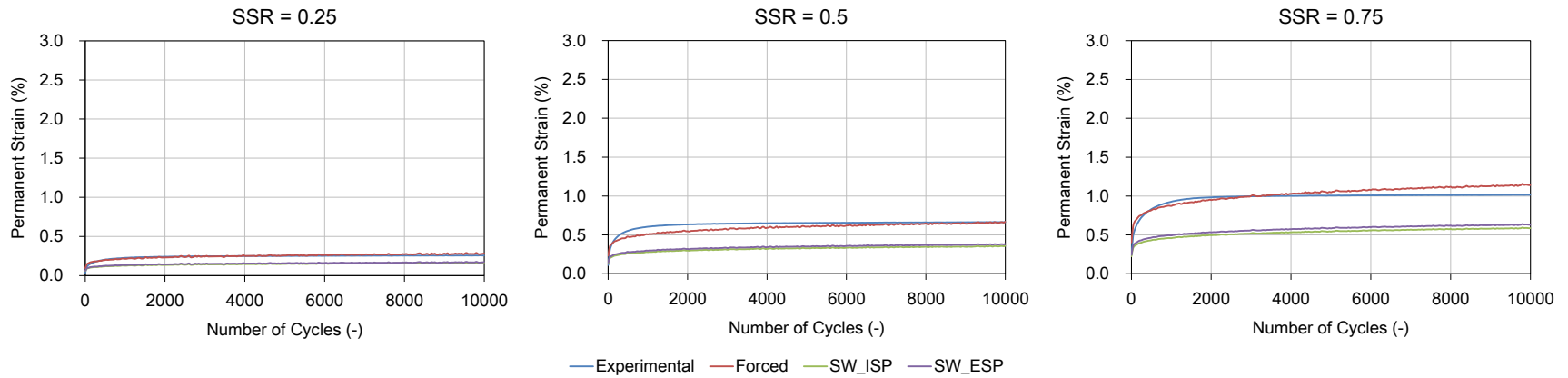
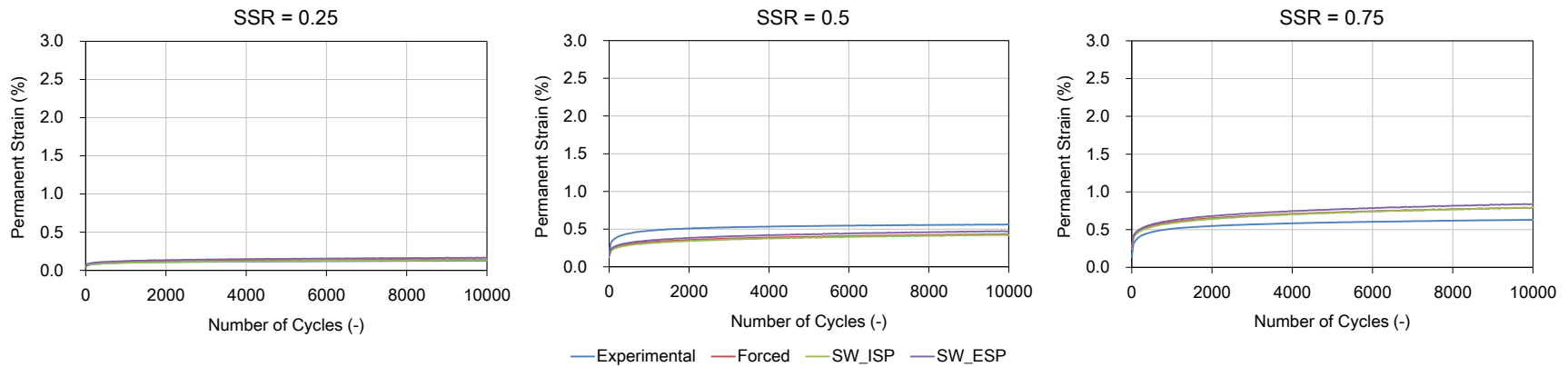


**Figure H.8** Curves for Permanent strain accumulations for Lemon Spring at SG and EG at different SSR values  
 Experimental results (blue), prediction using forced regression (red), prediction using stepwise regression including and excluding shape properties (green and purple, respectively)

### Moncure (Source Gradation)



### Moncure (Engineered Gradation)

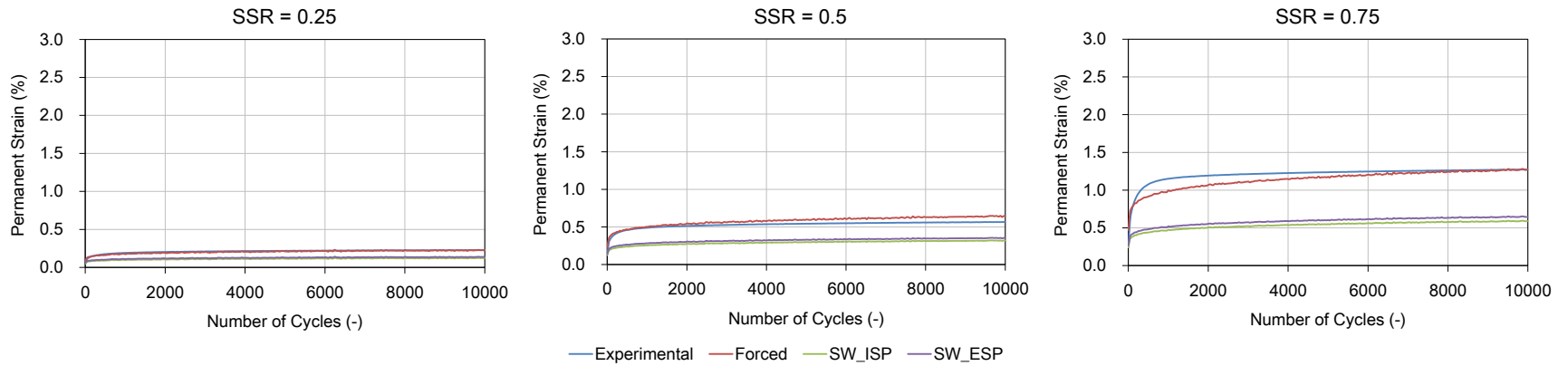
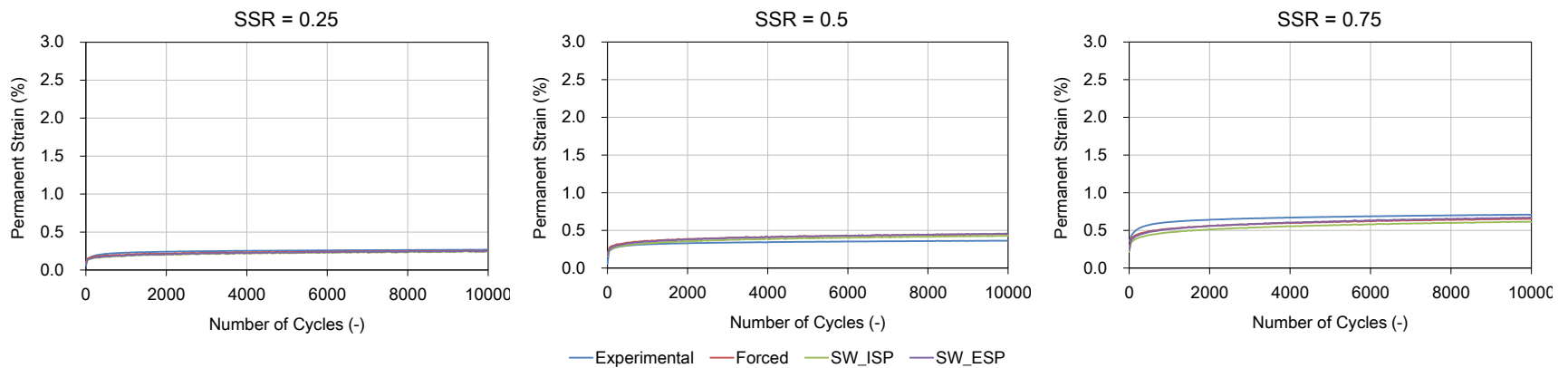


**Figure H.9** Curves for Permanent strain accumulations for Moncure at SG and EG at different SSR values  
 Experimental results (blue), prediction using forced regression (red), prediction using stepwise regression including and excluding shape properties (green and purple, respectively)

### Nash County (Source Gradation)



### Nash County (Engineered Gradation)

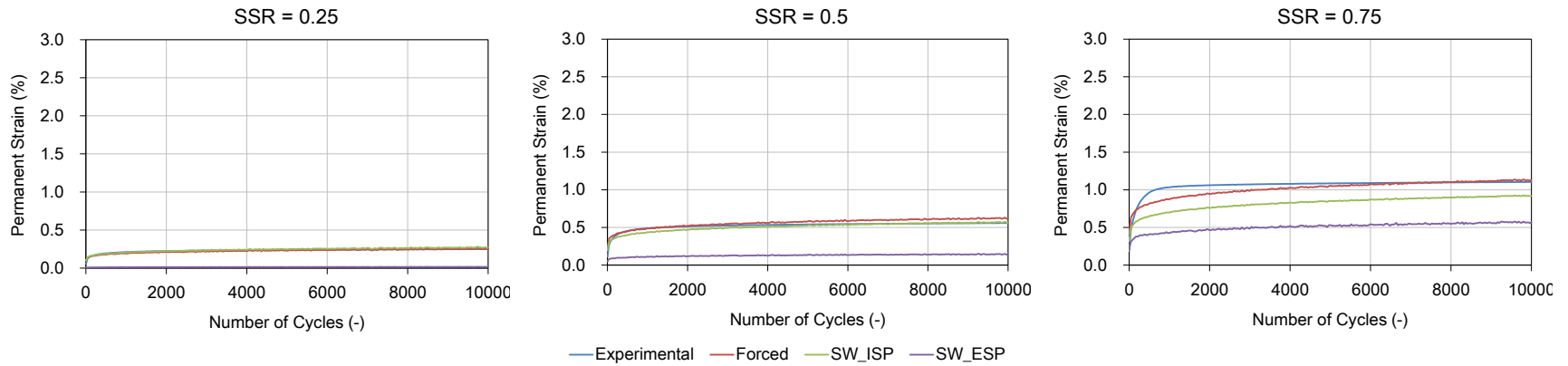
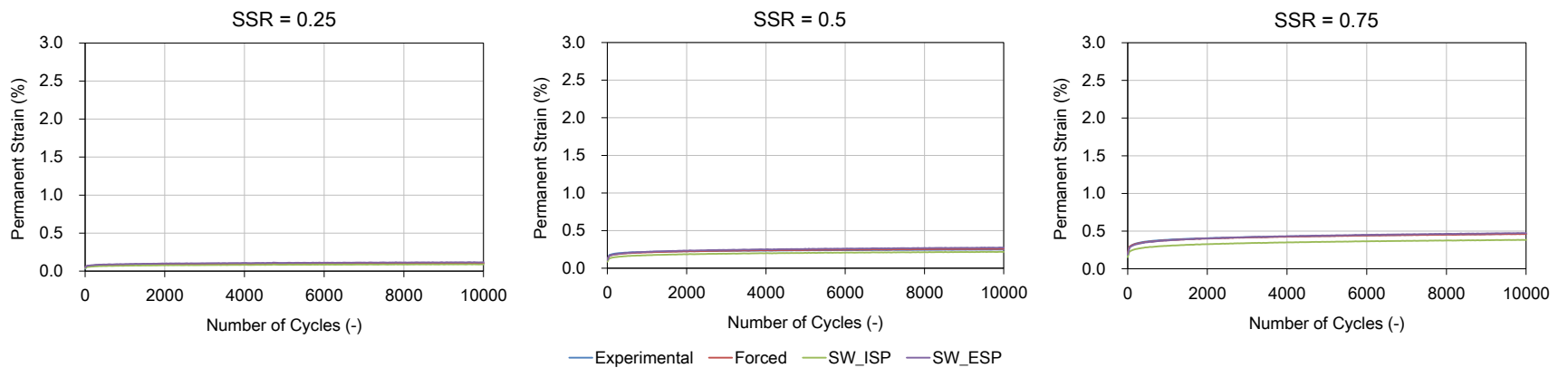


**Figure H.10** Curves for Permanent strain accumulations for Nash County at SG and EG at different SSR values  
 Experimental results (blue), prediction using forced regression (red), prediction using stepwise regression including and excluding shape properties (green and purple, respectively)

### N. Wilkesboro (Source Gradation)



### N. Wilkesboro (Engineered Gradation)

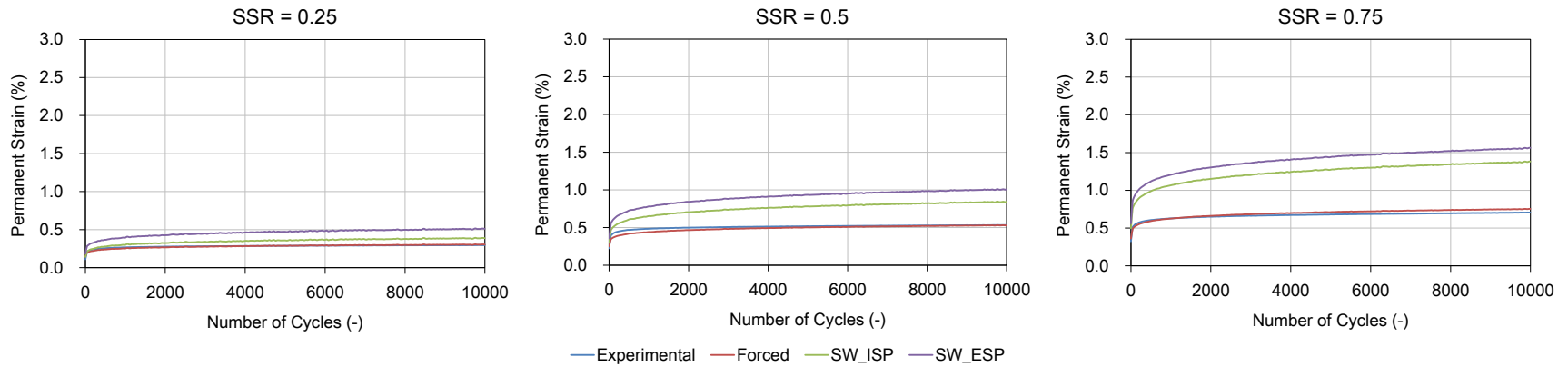
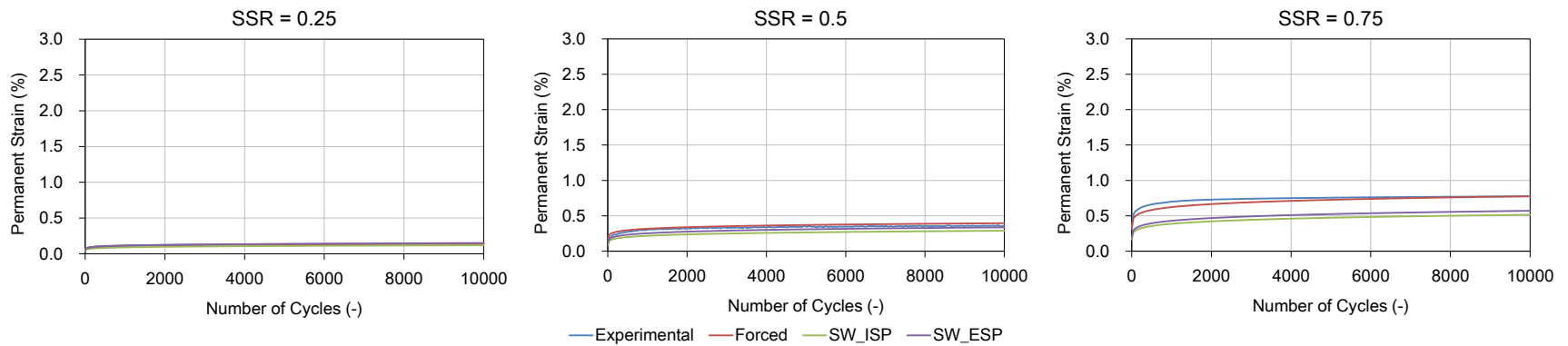


**Figure H.11** Curves for Permanent strain accumulations for N. Wilkesboro at SG and EG at different SSR values  
 Experimental results (blue), prediction using forced regression (red), prediction using stepwise regression including and excluding shape properties (green and purple, respectively)

### Princeton (Source Gradation)



### Princeton (Engineered Gradation)

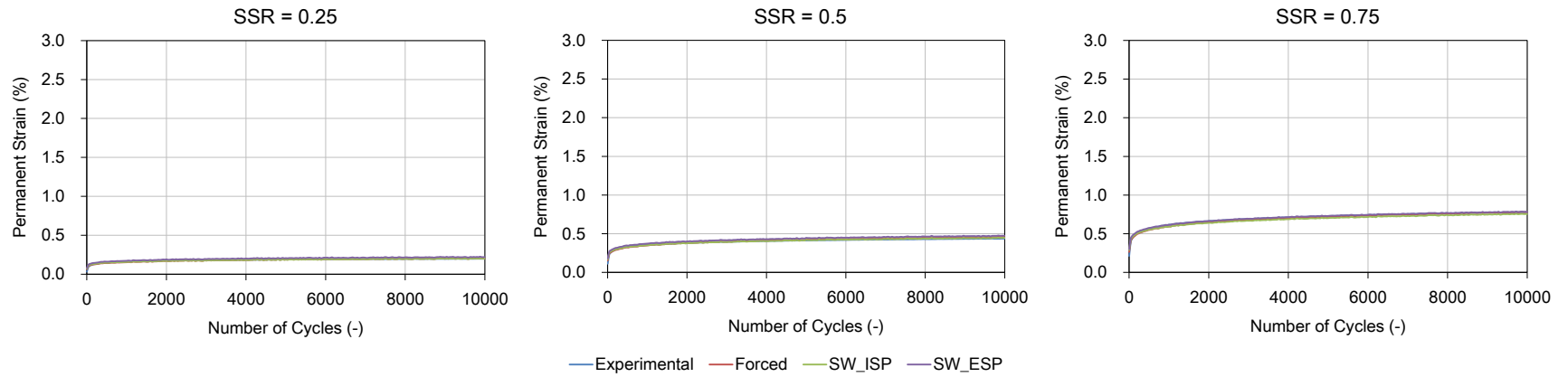


**Figure H.12** Curves for Permanent strain accumulations for Princeton at SG and EG at different SSR values  
Experimental results (blue), prediction using forced regression (red), prediction using stepwise regression including and excluding shape properties (green and purple, respectively)

### Raleigh (Source Gradation)

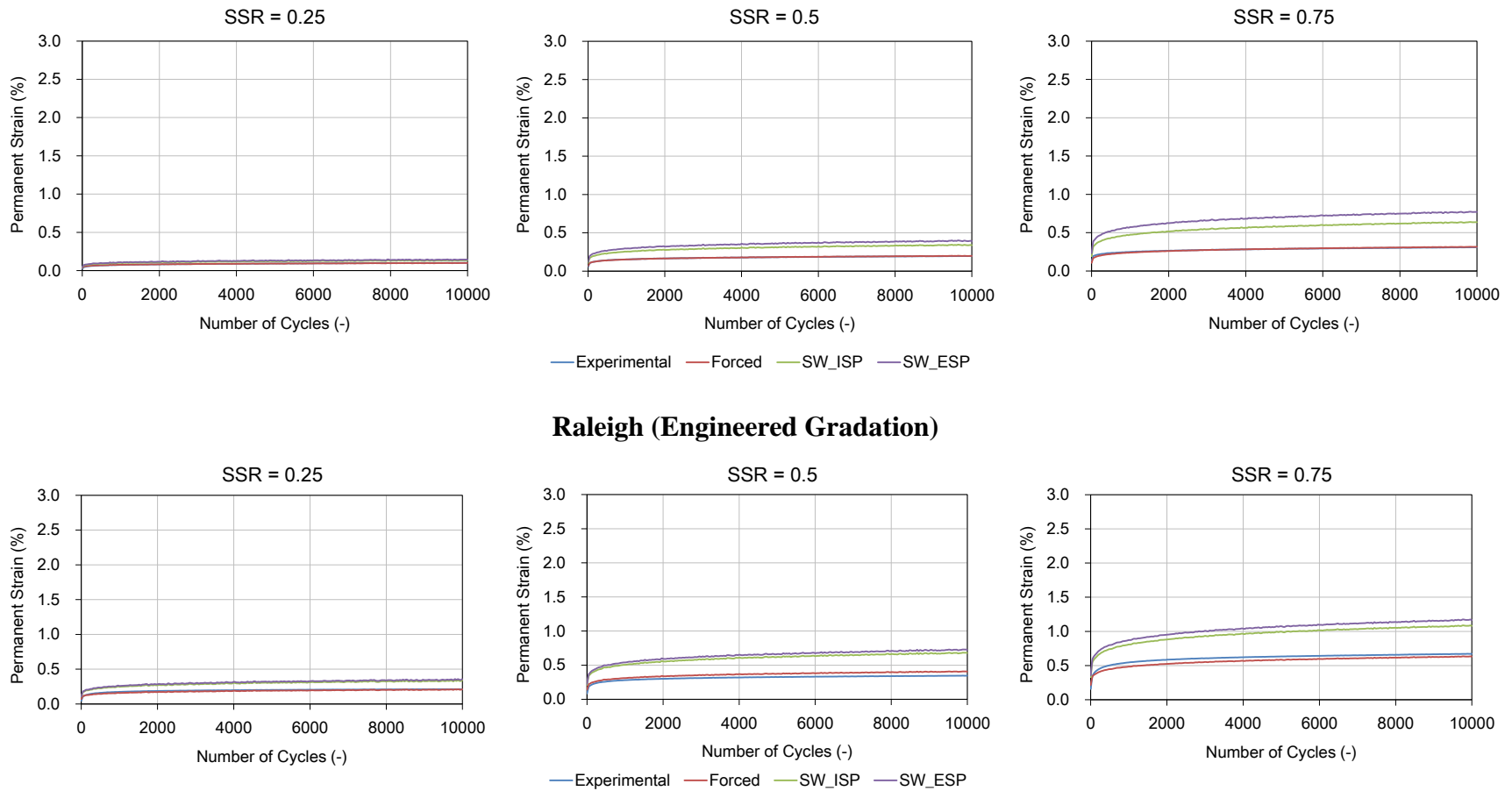
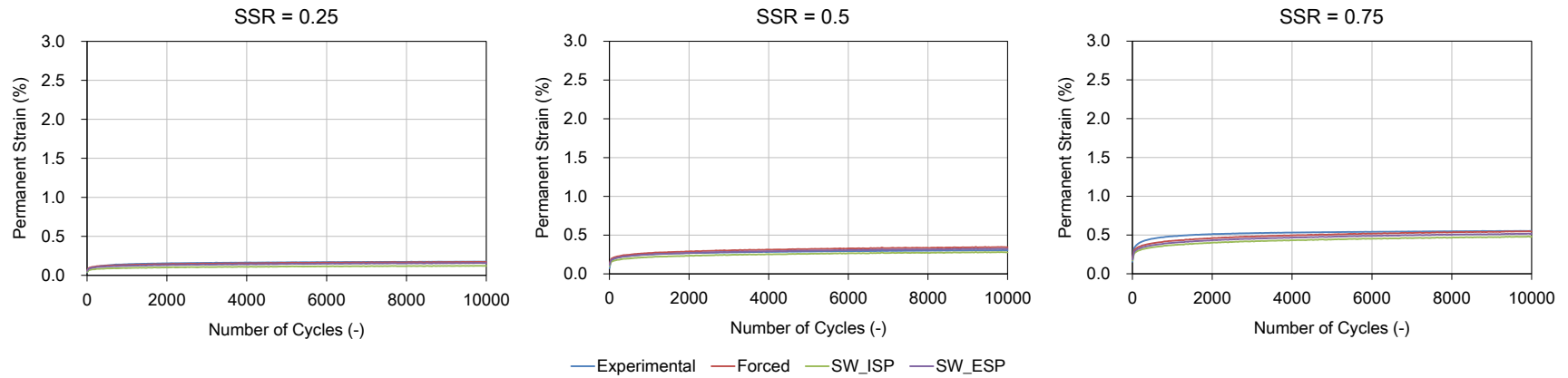


**Figure H.13** Curves for Permanent strain accumulations for Raleigh at SG and EG at different SSR values  
 Experimental results (blue), prediction using forced regression (red), prediction using stepwise regression including and excluding shape properties (green and purple, respectively)

### Rockingham (Source Gradation)



### Rockingham (Engineered Gradation)

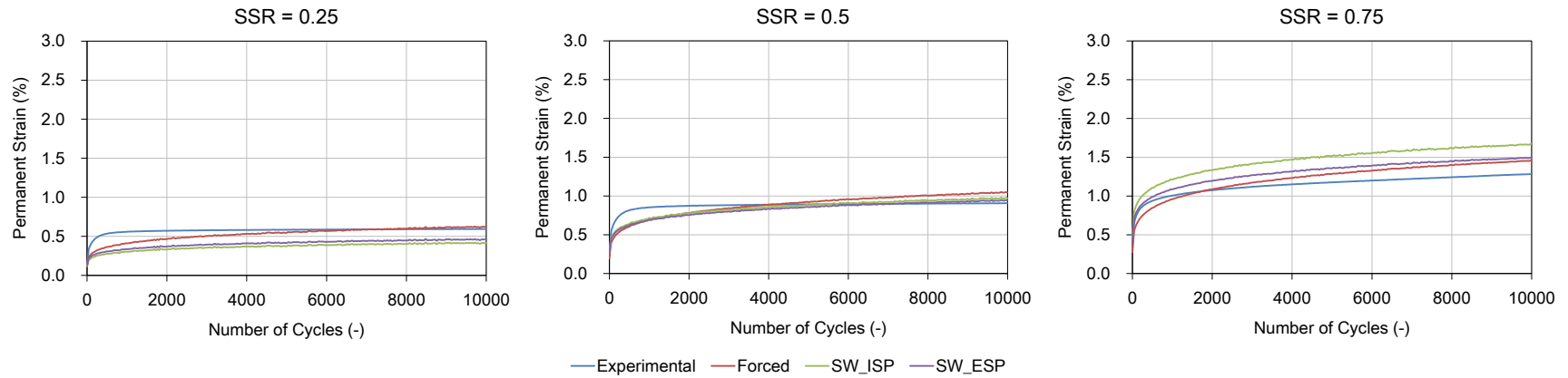
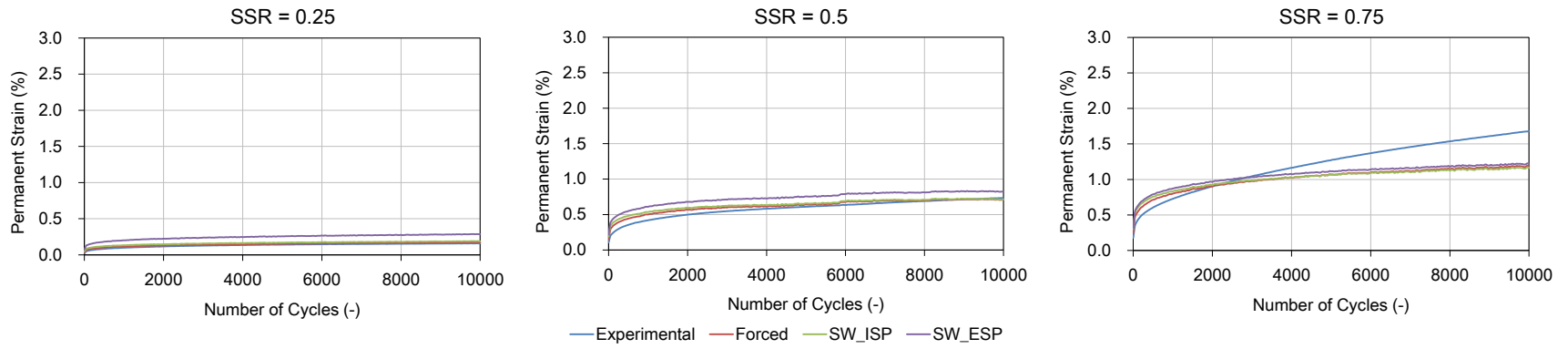


**Figure H.14** Curves for Permanent strain accumulations for Rockingham at SG and EG at different SSR values  
Experimental results (blue), prediction using forced regression (red), prediction using stepwise regression including and excluding shape properties (green and purple, respectively)

### Rocky Point (Source Gradation)



### Rocky Point (Engineered Gradation)

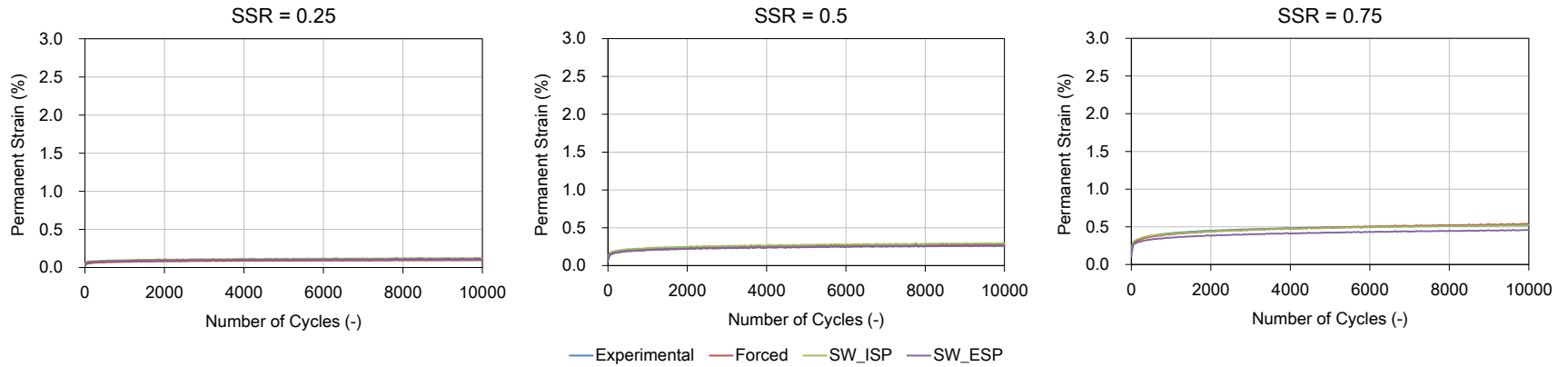
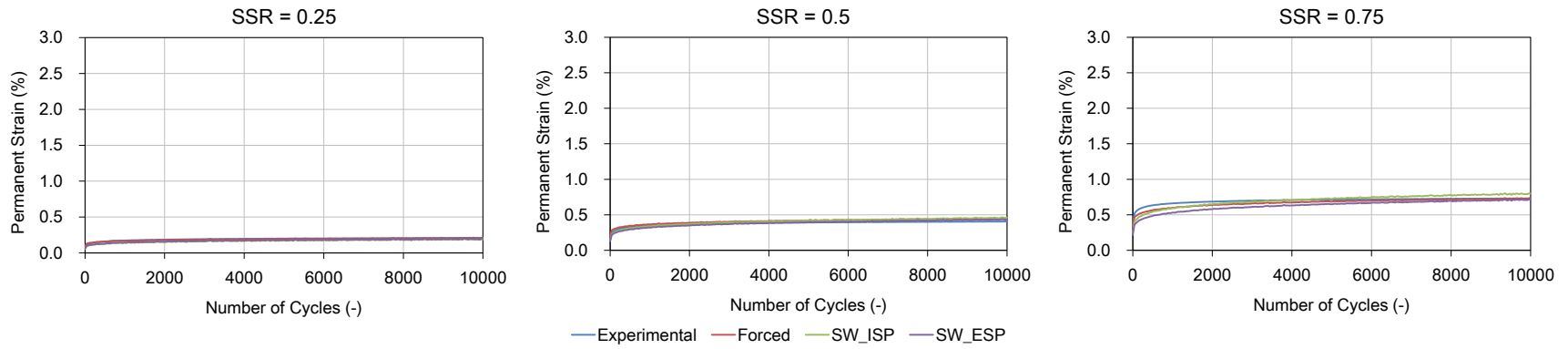


**Figure H.15** Curves for Permanent strain accumulations for Rocky Point at SG and EG at different SSR values  
Experimental results (blue), prediction using forced regression (red), prediction using stepwise regression including and excluding shape properties (green and purple, respectively)

### Rougemont (Source Gradation)



### Rougemont (Engineered Gradation)

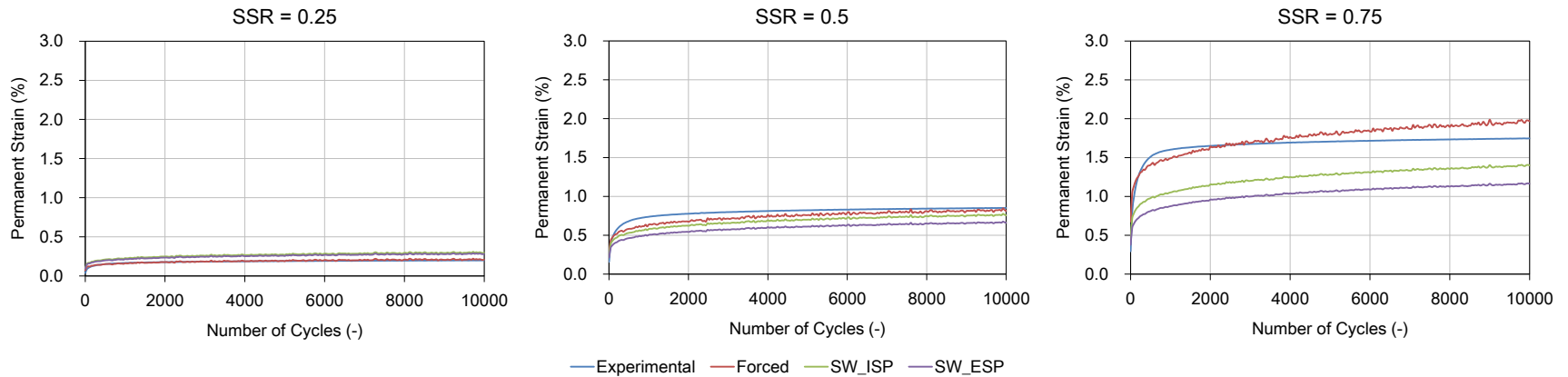


**Figure H.16** Curves for Permanent strain accumulations for Rougemont at SG and EG at different SSR values  
Experimental results (blue), prediction using forced regression (red), prediction using stepwise regression including and excluding shape properties (green and purple, respectively)